NASA CR 72741
PWA FR-3840

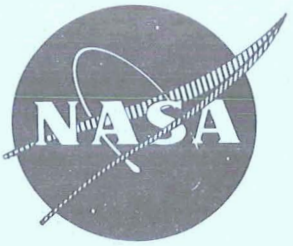

SINGLE-STAGE EXPERIMENTAL EVALUATION OF COMPRESSOR BLADING WITH SLOTS AND VORTEX GENERATORS

PART III -DATA AND PERFORMANCE FOR STAGE 4

By
J. A. Brent

Prepared For
National Aeronautics and Space Administration
Contract NAS3-10481

Pratt & Whitney Aircraft DIVISION OF UNITED AIRCRAFT CORPORATION
FLORIDA RESEARCH AND DEVELOPMENT CENTER

Requests for copies of this report should be referred to:

National Aeronautics and Space Administration
Scientific and Technical Information Facility
P.O. Box 33
College Park, Md. 20740

NASA CR 72741
PWA FR-3840

SINGLE-STAGE EXPERIMENTAL EVALUATION OF COMPRESSOR BLADING WITH SLOTS AND VORTEX GENERATORS

PART III -DATA AND PERFORMANCE FOR STAGE 4

By
J. A. Brent

29 DECEMBER 1970

Prepared For
National Aeronautics and Space Administration

Contract NAS3-10481

Technical Management
NASA Lewis Research Center
Cleveland, Ohio

NASA Program Manager: L. Joseph Herrig
Fluid System Components Division

Pratt & Whitney Aircraft DIVISION OF UNITED AIRCRAFT CORPORATION
FLORIDA RESEARCH AND DEVELOPMENT CENTER

ABSTRACT

Stage 4 of a series of highly loaded stages was tested without slots and with slots and/or vortex generators to determine the extent that these devices could extend the stable operating range of an 0.8 hub/tip ratio subsonic axial flow compressor stage. At design equivalent rotor speed, pressure ratio and efficiency of slotted stage 4 both with and without vortex generators were lower than the results obtained with the unslotted stage. The addition of vortex generators upstream of the rotor and between the rotor and stator of a stage comprised of unslotted rotor 4 and slotted stator 4 produced a 10% increase in stage stall margin at design speed. The peak pressure ratio remained about the same both with and without vortex generators, whereas, the addition of vortex generators resulted in a slight increase in peak efficiency.

CONTENTS

CONTENTS (Continued)

SINGLE STAGE EXPERIMENTAL EVALUATION OF COMPRESSOR BLADING WITH SLOTS AND VORTEX GENERATORS

PART III - DATA AND PERFORMANCE FOR STAGE 4

J. A. Brent

PRATT & WHITNEY AIRCRAFT
FLORIDA RESEARCH AND DEVELOPMENT CENTER

SUMMARY

A 0.8 hub/tip ratio single stage subsonic compressor was designed and tested without slots and/or vortex generators to determine the extent that these devices could extend the stable operating range of axial flow compressors. The stage was designed with zero rotor prewhirl, axial discharge flow, and constant exit total pressure across the span. The design velocity diagrams and predicted performance were based on the assumption that the rotor and stator blade element losses would be reduced by the addition of slots and vortex generators. Since the assumed reduction in wall losses did not completely compensate for the increased losses that have been observed in highly-loaded blade rows, increased blade camber was required near the walls to achieve a uniform stage exit total pressure profile. The rotor and stator blading were designed with 65-series airfoil sections. Blade aspect ratios, solidities, and maximum thickness distributions were generally consistent with design practice for compressor middle stages.

The predicted and measured performance for the four configurations tested are summarized in table 1. All of the configurations failed to achieve their predicted rotor and stage pressure ratio and efficiency at design equivalent rotor speed and corrected flow conditions. At design equivalent rotor speed the pressure ratio and efficiency of slotted stage 4, both with and without vortex generators, were lower than the values obtained with the unslotted stage.

Table 1. Summary of Predicted and Measured Performance

Configuration	Predicted Performance For Design Equivalent Rotor Speed and Corrected Flow*				Measured Performance at Design Equivalent Rotor Speed and Corrected Flow**				Measured Peak Efficiency and Corresponding Pressure Ratio at Design Equivalent Rotor Speed			
	Rotor		Stage		Rotor		Stage		Rotor		Stage	
	η_{ad}	PR	η_{ad}	PR	η_{ad}	PR	η_{ad}	PR	η_{ad}	PR	η_{ad}	PR
Unslotted Rotor 4 - Unslotted Stator 4	0.868	1.335	0.781	1.305	0.858	1.298	0.730	1.254	0.874	1.324	0.748	1.274
Slotted Rotor 4 - Slotted Stator 4	0.895	1.349	0.838	1.324	0.800	1.258	0.665	1.210	0.857	1.318	0.740	1.271
Slotted Rotor 4 - Slotted Stator 4 With Vortex Generators Ahead of the Rotor	0.895	1.349	0.838	1.324	0.795	1.254	0.650	1.203	0.862	1.317	0.747	1.279
Unslotted Rotor 4 - Stator 4 With Vortex Generators Ahead of the Rotor and Between the Rotor and Stator	0.895	1.349	0.838	1.324	0.865	1.300	0.723	1.247	0.882	1.326	0.769	1.281

* The predicted performance for the Rotor 4 - Stator 4 configuration is based on the rotor and stator blade element loss data of Reference 4 through 9. The predicted performance for the remaining configurations is based on the assumption that slots and vortex generators would reduce the blade element losses below the level of the data of References 4 through 9.

** Design equivalent rotor tip speed and corrected flow are 757 ft/sec and 110 lb/sec, respectively.

The addition of the rotor inlet vortex generators to the slotted stage produced slight improvement in the rotor tip region losses with little change in the losses at the hub. The addition of vortex generators upstream of the rotor and between the rotor and stator of a stage consisting of unslotted rotor 4 and slotted stator 4 produced a 10% increase in stage stall margin at design speed. The peak pressure ratio remained about the same both with and without vortex generators.

INTRODUCTION

Experience with highly-loaded axial-flow compressors has shown that the region of the flowpath most critical to achieving high performance is that area adjacent to the walls. In the wall region of these stages the flow is predominantly three-dimensional, whereas, at midspan the flow is more nearly two-dimensional. The three-dimensional aspects of the flow result in a marked reduction in adiabatic efficiency and associated low total pressure ratio and flow near the wall. Because these factors generally represent a conversion of kinetic energy into internal energy at an increase in entropy, the diffusion limits for a conventional blade row are encountered near the wall, and stall or compressor surge is induced by flow separation in these regions. Further, the wall diffusion limits prevent the utilization of the full loading capacity of the midstream portion of the blade, since the reduction in flow near the walls causes an increase in the midspan velocity with a resultant decrease in midspan loading. These factors indicate that advanced compressor design concepts for the increase of allowable stage loading and stable, low-loss operating range should be concerned with the problem of three-dimensional flow near the walls.

Previous attempts to increase allowable stage loading limits by means of slotted blading under NASA Contract NAS3-7603 (Reference 1) indicated good performance for the blade midspan regions, but poor performance near the walls. The relative effectiveness of the slots at midspan and their ineffectiveness near the wall was attributed to the chordal placement of the slots and their inability to sufficiently reduce the three-dimensional flows in the wall region. To attain the full potential of highly loaded blading, methods must be developed to reduce the three-dimensional (i.e., secondary) flow losses in this region. A single stage

experimental investigation was initiated with the following three approaches for the improvement of blade element in the wall region.

1. Add blade-end slots and secondary flow fences to Stage 3 of Contract NAS3-7603.

2. Design and test two new stages, designated 4 and 5, with relatively high work input (blade camber) near the walls to compensate for the high losses.

3. Evaluate blade slots and wall vortex generators added to stages 4 and 5 to reduce the wall losses.

Experimental results obtained with Stage 3 modified with blade-end slots and secondary flow fences, including discussion of the design modifications, are presented in Reference 2. Discussion of the aerodynamic and mechanical design of Stages 4 and 5 is presented in Reference 3. This report presents the data and performance obtained with the following Stage 4 configurations:

1. Unslotted Rotor 4 - Unslotted Stator 4 (baseline configuration)

2. Slotted Rotor 4 - Slotted Stator 4

3. Slotted Rotor 4 - Slotted Stator 4 with vortex generators ahead of the rotor.

4. Unslotted Rotor 4 - Slotted Stator 4 with vortex generators ahead of the rotor and between the rotor and stator.

During the last test (Item 4 above) one-third of the stator inlet vortex generators separated from the wall, and because the time at which the separation occurred could not be determined, their influence on stator performance could not be evaluated.

DESIGN SUMMARY

Blading Design

An important premise for the Stage 4 blading design was the assumption that slots and vortex generators would reduce the rotor and stator blade element losses below the levels of loss that were established as a function of loading from the data of References 4 through 9. Additionally, it was specified that the rotor inlet and stator exit velocities were to be axial, and that the stator exit total pressure was to be constant across the span. A design rotor tip velocity

of 757 ft per sec provided the desired tip inlet relative Mach No. of approximately 0.8.

The design velocity diagrams were calculated by means of a computer program which solves the continuity, energy, and radial equilibrium equations for an axisymmetric flow. Radial gradients of enthalpy and entropy were included in the calculation, and the influence of wall and streamline curvature on the radial distribution of static pressure was taken into account.

Rotor and stator design velocity diagrams were selected in accordance with the foregoing assumptions, design requirements, and calculation procedure. NACA Series 65 blade sections with A = 1.0 meanlines (Reference 10) were selected for the rotor and stator blading to be consistent with the blading used under the Contract NAS3-7603 program (Reference 1). Other blade geometry variables such as chord length, aspect ratio, solidity, and maximum thickness were the same as, or very similar to, those for the Reference 1 blading. (Slight departures in aspect ratio and hub/tip ratio resulted from the wall convergence at the rotor and stator tips that was provided to limit the diffusion factors.)

Design incidence (minimum loss) and deviation angles were calculated using the appropriate equations in Reference 11. For the rotor, 2 deg were subtracted from the calculated incidence angles in accordance with the minimum loss incidence results obtained under the Reference 1 program.

Rotor and stator design velocity diagram data, blade element geometry data, and predicted performance for Stage 4, designed on the assumption that the losses would be reduced due to slots and vortex generators, are presented in tables B-1 and B-2 of Appendix B. Symbols and performance variables are defined in Appendix A. Details of the Stage 4 blading aerodynamic and mechanical design are presented in Reference 3.

Design Predictions Without Slots and Vortex Generators

Velocity diagrams and overall performance were calculated for the Stage 4 blading without assuming reduced losses due to slots and vortex generators to provide comparative data for test results obtained with the baseline stage. The results of these calculations, are presented in tables B-3 and B-4 of Appendix B. These results are based on the assumptions that the rotor and stator deviation angles would be the same both with and without slots and that the unslotted stator blade elements would be operating close to minimum loss. The former assumption is consistent with the results obtained in Reference 1.

Slot Design

Four factors were considered for the selection of rotor and stator slot configurations:

1. Spanwise extent
2. Chordal location
3. Number
4. Geometry

Spanwise extent, chordal location, and the number of slots were based on the Stage 4 unslotted (baseline) test results obtained at near design point operating conditions. Slot geometry was based on the results of a two dimensional potential flow analysis. Slot design details are given in Reference 3; a brief description of the slot design is given below for convenience.

The estimated stalled regions on the rotor and stator suction surfaces at near design operating conditions are illustrated in figure 1. The spanwise extent of the stalled regions was estimated on the basis of the axial velocity and loss coefficient distributions shown in the figure. The shape of the stalled regions generally conforms to secondary flow patterns that have been observed on cascade airfoils. The maximum spanwise extent of the slots was selected to cover the spanwise extent of the stalled regions on the suction surfaces. The chordal location of the slots was selected such that all of the slot flow would enter the suction surface flow ahead of the estimated flow separation line. Because of the larger radial flow gradients indicated by the axial velocity distribution for the rotor (as opposed to those indicated for the stator) two rows of slots were specified for the rotor. The upstream row, of lesser spanwise extent, is intended to move the starting point of the stalled region beyond the downstream row. Chordal location and spanwise extent for the rotor and stator slots are summarized below.

Rotor and Stator Slot Location

	Chordal Location On Suction Surface (Percent Chord)	Spanwise Extent (Percent from Tip)
Rotor	20	0-20 ; 80-100
	45	0-30 ; 70-100
Stator	20	0-30 ; 80-100

Slot geometry was evaluated on the basis of calculated pressure coefficient distributions for the airfoil section at 85% span from the tip of Stator 4. Two-

dimensional, steady, incompressible, and inviscid potential flow was assumed for these calculations. The 85% span section was selected as being representative of both the rotor and stator section geometry near the wall. Slot geometries for the rotor hub and tip and the stator tip sections were made geometrically similar to the configuration selected for the stator at 85% span. Final slot geometry and locations are shown for several spanwise sections for the rotor in figures 2a and 2b, and for the stator in figure 3.

Vortex Generator Design

Based on the development of severe secondary flows in both the rotor and stator blade rows, as indicated by the baseline test results, it was concluded that vortex generators should be designed for the inner and outer walls of both blade rows. The vortex generators are intended, by means of turbulent mixing, to induce high momentum air from the mainstream into the wall boundary layer flow and low momentum air from the wall region into the mainstream flow, thus helping to unload the blades in the wall region and load the midspan region. Vortex generator design criteria presented in References 12 and 13, were used as a guideline for the design of these wall vortex generators. The vortex generators for the rotor were located approximately 20 boundary layer thicknesses upstream of the rotor leading edge positioned symmetrically in pairs to produce counter-rotating vortices. A boundary layer thickness of 0.41 in. was determined from rotor inlet total pressure traverse data obtained during the unslotted Stage 4 test. Vortex generator height was set equal to 1.1 boundary layer thicknesses, and they were equally spaced 2.7 heights apart at 25% chord. The chord length was set equal to approximately twice the height. Based on the above criteria, a chord of 0.91 in. was desired. Sixty-five series airfoil stock with a 0.983 in. chord was available, and was used to expedite fabrication. The resulting configuration is shown in figures 4a and 4b. The strip stock had a maximum thickness-to-chord ratio of 9%, and a camber (based on an equivalent circular arc meanline) of 25 deg. To produce the maximum lift-drag ratio, an angle of attack of 14 deg was selected.

Design of the stator vortex generators was not straight-forward since no clearly defined boundary layer exists downstream of the rotor, and the upstream distance from a "separation" point (such as the stalled regions on the stator vanes) for placement of the generators was limited. A pseudo boundary layer thickness was therefore defined as one-twentieth of the maximum distance

available for generator placement upstream of the stator mid-chord. Thus, with the vortex generator height set at 1.1 boundary layer thicknesses, the required distance for turbulent mixing is provided between the generators and the "separation" point (stator mid-chord, in this case). One pair of counter-rotating vortex generators was provided for each stator vane passage. These vortex generators were fabricated from 0.020 in. sheet stock because of their small size. They were cambered 20 deg and installed at an angle of attack of 10 deg. The chord angle was determined from the stator inlet air angles measured during the testing of slotted Stage 4 with vortex generators ahead of the rotor. The resulting configuration is shown in figure 4c.

TEST EQUIPMENT

Facility

The compressor test facility is shown schematically in figure 5. The compressor is driven by a single-stage turbine, powered by exhaust gases from a J75 slave engine, with compressor speed controlled by means of the engine throttle. The slave engine exhaust gas is also used to power an ejector for compressor wall boundary layer suction. Air enters the compressor test rig through a 103-ft. long combined inlet duct, plenum and bellmouth inlet, and is exhausted through an exit diffuser to the atmosphere. The inlet duct contains a flow measuring orifice designed and installed in accordance with ASME standards. An area contraction ratio from plenum to compressor inlet of approximately 10:1 provides near stagnation conditions in the plenum. The inlet duct and plenum were mounted on a track and can be rolled away from the compressor rig inlet to facilitate configuration changes.

Compressor Test Rig

A schematic of the single-stage compressor rig is shown in figure 6, and the flowpath dimensions are given in figure 7. The hub-tip ratio at the rotor inlet is 0.789, the test section has a constant hub diameter of 32.85 in., and the outer wall converges from a dia of 41.14 in. at the rotor leading edge to 39.99 in. at the stator exit. (Outer wall convergence was provided at the rotor and stator tips to control diffusion factor). Rotor bearing loads are transmitted to the rig support through struts located in the inlet and exhaust case assemblies. The inlet struts are sufficiently far upstream so their wakes are dissipated ahead of the rotor. The stage design specifications of zero rotor prewhirl and

axial discharge flow eliminated the need for inlet and exit guide vanes. Flow-rate was varied with a set of motor driven throttle vanes located in the exhaust case.

Porous walls were installed for boundary layer suction at the rotor tip and the stator hub and tip as shown in figure 8. The porous wall was 0.060 in. thick and had 0.066-in. dia holes on 0.187-in. centers, providing an 11% open area.

Instrumentation

Instrumentation was provided to obtain overall and blade element performance data for each blade row. The locations of axial instrumentation stations are indicated in figure 7. Axial and circumferential locations of the instrumentation are shown in figure 9.

Airflow was measured with the ASME standard thin plate orifice located in the inlet duct. Rotor speed was measured with an electromagnetic sensor mounted adjacent to a 60-tooth gear on the rotor shaft. Gear tooth passing frequency was displayed as rpm on a digital counter. Rotor rpm was also recorded on magnetic tape. Inlet total temperature was measured in the inlet plenum by means of five Kiel-type total temperature probes; inlet total pressure was measured in the inlet plenum by means of five Kiel-type total pressure probes. Six equally spaced static pressure taps were located on both the inner and outer walls upstream of the rotor (station 0). From a rig calibration over a wide range of weight flows, a correlation between bellmouth and orifice measured weight flow was derived and used to check subsequent weight flow measurements.

Stage exit total temperature was measured at nine radial positions at each of four circumferential locations using shielded thermocouples installed in radial rakes at Stations 2A and 3. The stage exit temperature distributions measured with these radial rakes were used for rotor performance calculations. Redundant total temperature measurements at Stations 1, 2, and 2A, were provided by means of thermocouples in the 20-deg wedge traverse probes located at each of these stations. One 20-deg wedge traverse probe was provided at Station 1 to measure rotor inlet total pressure and air angle. Two 20-deg wedge traverse probes were located at Station 2 (rotor exit) for total pressure and air angle measurement; rotor exit total pressure was also measured at five radial positions at one circumferential location with a Kiel-head rake. Three sets of circumferential total pressure rakes were installed at Station 2A (stator exit)

for total pressure measurement. One set had circumferential rakes located at 5, 30, and 85% span; the second set had rakes at 15, 50, and 95% span; and the third set had rakes at 10, 70, and 90% span. Two 20-deg wedge probes were located at Station 2A for the measurement of stator exit air angle.

Static pressures at Stations 1, 2, and 2A were measured by means of 8-deg wedge traverse probes. Four inner wall and four outer wall static pressure taps, approximately equally spaced, were located at each of these axial stations. The pressure taps ahead of and behind the stator were located on extensions of the mid-channel streamlines. Stations 2 and 2A also had four inner and four outer wall taps installed across a vane gap to measure the static pressure variation across the gap. Twenty static pressure taps were equally spaced between 20 and 83% chord at 10 and 90% span on the suction surfaces of two stator blades, as shown in figure 10, for the baseline test.

Total pressure and temperature radial rakes are shown in figure 11. A typical circumferential total pressure rake is shown in figure 12. Twenty-deg and 8-deg wedge traverse probes are shown in figure 13.

Steady-state pressure data were measured with a multi-channel pressure transducer scanning system that includes automatic data recording on computer cards. Steady-state temperature measurements were also automatically recorded on computer cards by a multi-channel scanning system in conjunction with a temperature reference oven and a digital voltmeter. Traverse and transient pressure data were recorded on magnetic tape at up to 600 samples per minute per channel.

Two static pressure taps, located in the plenum, two outer wall static pressure taps at Station 0, and the total pressure radial rake at Station 2A (188° in figure 9), were close-coupled to transducers for transient recording during operation into and out of stall. A high response pressure transducer, mounted in a total pressure probe at 10% span from the tip behind the rotor, was used to detect the initiation of rotating stall. The transducer output was recorded on magnetic tape and correlated in time with the transient recording of bellmouth static and stage exit total pressures.

Five rotor blades were each instrumented with three strain gages. These strain gage outputs were displayed on oscilloscopes and visually monitored during tests. Gage locations were determined in bench vibration tests with the aid of stress-coat and the selected locations were verified by a fatigue test.

PROCEDURES

Test Procedures

Wall Bleed Flow Selection

Provisions were available for wall boundary layer bleed at the rotor tip and stator hub and tip. Since the rotor and stator bleed flows were independently controlled, the rotor bleed flow was selected prior to determining the stator bleed flow. With the baseline compressor stage operating at near design conditions, total pressures at 5% span from the tip downstream of the rotor, and 5 and 95% span downstream of the stator, were monitored as the rotor and then the stator bleed flows were varied between zero and maximum. The maximum bleed flow (limited by the perforated shroud effective flow areas) provided the largest improvement in the observed total pressures and was therefore selected for both the rotor and stator. With the exception of several points where the bleed flow was intentionally reduced the maximum bleed flow setting was maintained throughout the Stage 4 test program.

Performance Tests

Overall and blade element performance data were obtained at 50, 70, 90, 100, and 110% of design equivalent rotor speed for the unslotted baseline configuration, and 70 and 100% of design equivalent rotor speed for the slotted configuration and the two configurations with vortex generators. Six data points were recorded at each speed to define stage performance between maximum obtainable flow and near stall. The near stall point was determined on the basis of flow, stage exit pressure, and blade stresses monitored on oscilloscopes. At each test point traverse surveys were followed by the recording of fixed pressure and temperature instrumentation data with the traverse probes withdrawn. Blade stresses were monitored during steady-state and stall transient operation at all rotor speeds.

The influence of wall boundary layer bleed flow on performance was evaluated at design equivalent rotor speed for all configurations except the unslotted (baseline) configuration. Overall and blade element data were recorded with reduced bleed flow for two data points at design equivalent rotor speed. One point was at near stall flow and the other at a flow approximately 5 lb per sec greater than the stall flow.

Transient measurements of bellmouth static pressure, rotor speed, and stator exit total pressure were recorded ten times per sec to define stall characteristics as the stage was operated into and out of stall. The output from a high response pressure transducer, mounted in a total pressure probe behind the rotor, was also recorded and correlated in time with the other transient measurements to detect the initiation of rotating stall. A typical plot of the transient data is compared with an oscillograph record of the transducer signal in figure 14.

Data Reduction Procedures

Data reduction was accomplished in two steps. The first step involved the use of two computer programs to (1) convert millivolt readings to appropriate engineering units, and (2) provide an array (tabulated and plotted) of pressure, temperature and air angle data at each axial station. Conversion of data to absolute values, appropriate Mach number corrections, and correction of pressures and temperatures to NASA standard day conditions were performed in the second computer program.

The second step in the data reduction procedure involved the calculation of overall and blade element performance variables for the rotor and stator blades. The array of data provided in step 1 above was analyzed for the selection of radial distributions of pressure, temperature, and air angle at each axial station for input into the overall and blade element performance computer program. Stator exit total temperatures were used for the calculation of rotor blade element data and rotor efficiency.

Pressure ratios were calculated for the rotor, and the rotor-stator (stage). The rotor and stator exit total pressures were weighted according to local mass flow to obtain average values. The stator wake total pressures at each radial measuring station were mass averaged using the local total pressure in the wake and the 8-deg wedge probe static pressure to define local Mach No. Mass flux was then obtained from the relationship

$$\bar{m} = \frac{W\sqrt{T}}{PA} = \sqrt{\frac{\gamma g}{R}} M \left[1 + \frac{\gamma - 1}{2} M^2\right]^{1/2} \frac{p}{P}$$

where T is measured total temperature and A is the flow area associated with each total pressure tube. With the radial distribution of total pressure and mass flux calculated, the total pressures were mass averaged in the radial direction.

Behind the rotor, the selected radial distribution of total pressure was mass flow averaged using the 8-deg wedge probe static pressure and stator exit radial temperature distribution to define weight flow. Wall static pressure data at each station was used to check the 8-deg wedge probe data. In addition to the four equally-spaced static pressure taps in the outer wall at Stations 2 and 2A, four taps were spaced across one stator gap to check the static pressure gradient associated with stator leading edges and/or wakes. These wall static pressures are compared with the 8-deg wedge probe data extrapolated to the wall, for the baseline configuration in figure 15. The extrapolated pressures agree favorably with the wall static pressures.

Performance and velocity diagram calculations were performed for each blade row along design streamlines that pass through 5, 10, 15, 30, 50, 70, 85, 90, and 95% span at the rotor exit instrumentation station. The measured static pressures were used in conjunction with measured total pressures, total temperatures, and flow angles to define velocity distributions at each axial station. The performance and velocity diagram data were calculated directly from the measurements obtained at the instrumentation stations. Translation of these measurements to the blade-row leading and trailing edges was not considered necessary because, with the small wall convergence, the data at the instrumentation stations very nearly approximates that at the leading and trailing edges.

Stall Transient Data

Bellmouth static pressure at incipient stall was determined from plots similar to the one shown in figure 14, and the corresponding weight flow was determined from the correlation of bellmouth static pressure and orifice flow shown in figure 16. Stage exit total pressures, also obtained from plots similar to the one shown in figure 14, were arithmetically averaged to obtain the general shape of the pressure ratio-flow characteristic up to the point of incipient stall. The steady-state data were extrapolated to the stall flow using the shape of the transient data curve as a guide line. Incipient stall points were determined in this manner for each rotor speed.

PRESENTATION OF DATA

The data are presented and discussed separately for each of the four configurations. A summary comparison of performance for the four configurations

follows the presentation of data. The order of presentation is outlined below for convenience to the reader.

Unslotted Rotor 4 - Unslotted Stator 4

Overall Performance
Blade Element Performance

Slotted Rotor 4 - Slotted Stator 4

Overall Performance
Blade Element Performance

Slotted Rotor 4 - Slotted Stator 4 With Vortex Generators Ahead of the Rotor

Overall Performance
Blade Element Performance

Unslotted Rotor 4 - Slotted Stator 4 With Vortex Generators Ahead of the Rotor and Between the Rotor and Stator

Overall Performance
Blade Element Performance

The data for the baseline (unslotted) blading are compared to predicted performance without the assumed improvement in wall losses. The data for the configurations with slots and/or vortex generators are compared to the predicted performance assuming that the losses would be reduced due to slots and vortex generators. Definitions of the symbols and performance variables are presented in Appendix A.

Unslotted Rotor 4 - Unslotted Stator 4

Overall Performance

Overall performance data are presented in terms of pressure ratio and adiabatic efficiency as functions of corrected weight flow ($W\sqrt{\theta}/\delta$) and equivalent rotor speed ($N/\sqrt{\theta}$) for the rotor and stage, respectively, in figures 17 and 18. The solid symbol on the stall line is the stall point determined from the transient data. Overall performance and bleed flow data for the steady-state data points are presented in table A-1 of Reference 14.

The rotor achieved an efficiency of 85.8% and a pressure ratio of 1.298 at design equivalent rotor speed and corrected flow (110 lb/sec) compared with respective predicted values (without slots and vortex generators) of 86.8% and 1.335. Stage efficiency and pressure ratio were 73.0% and 1.254 at design

equivalent rotor speed and corrected flow (figure 18) relative to predicted values of 78.1% and 1.305.

Rotor Blade Element Performance

Blade element performance and velocity diagram data are tabulated in table B-1 of Reference 14 for each of the nine design streamline locations. Rotor diffusion factor, deviation angle, and loss coefficient are shown as functions of incidence angle in figures 19a through 19i. At the design incidence angle for design speed the total pressure losses are slightly higher than the predicted values (without slots and vortex generators) at all locations except 30% span from the tip where the loss is equal to the predicted value. The greatest departures from the predicted loss occurred at 90 and 95% span. Deviation angles larger than design values from 70 to 95% span and from 5 to 15% span combined with increased midspan axial velocity, associated with the high hub region losses, resulted in lower than design diffusion factors between 30 and 90% span. The diffusion factors within 10% span from either wall are larger than the predicted values since the reduction in axial velocity in this region was sufficient to offset the reduction in loading caused by the large rotor deviation angles.

Loss parameter versus diffusion factor is presented in figures 20a through 20e for 10, 30, 50, 70, and 90% span. Correlations of the minimum loss data of References 4 through 9 that were used to predict the performance of Stage 4 without slots and vortex generators are included in the figures for comparison with the data. For design equivalent rotor speed, the loss parameter values that correspond to the minimum loss coefficients in figure 19 at 10 and 30% span are slightly below the correlation curve, whereas at 50, 70, and 90% span they are above the correlation curve.

Stator Blade Element Performance

The stator inlet Mach No. and air angle distributions for design equivalent rotor speed are shown in figure 21. The predicted distributions (without slots and vortex generators) are included for comparison and, as indicated, the test data for near design equivalent weight flow (108.68 lb/sec) agrees closely with these values across the span.

Blade element performance and velocity diagram data are tabulated in table B-1 of Reference 14 for each of the nine design streamline locations. Stator diffusion factor, deviation angle, and loss coefficient are presented as functions of incidence angle in figures 22a through 22i. The diffusion factors are

lower than the indicated predicted values across the entire span, primarily because of the relatively large deviation angles seen in the figures and the associated high exit tangential velocities. The stator losses at design incidence angle are less than the predicted values (without slots and vortex generators) from 50 to 95% span and larger than the predicted values from 0 to 30% span.

Loss parameter is shown as a function of diffusion factor in figures 23a through 23e for 10, 30, 50, 70, and 90% span. Correlations of the minimum loss data of References 4 through 9 that were used to predict the performance of Stator 4 without slots and vortex generators are included for comparison with the test data. For design equivalent rotor speed, the loss parameter values corresponding to the minimum loss coefficient in figure 22 are above the correlation curves for 10 and 30% span and they are on or below the correlation curves for 50, 70 and 90% span.

Pressure coefficient distributions for the stator suction surface at 10 and 90% span from the tip are shown in figures 24 and 25. The data are shown for design equivalent rotor speed at incidence angles corresponding to maximum attainable flow and near stage stall flow and three flows between these limits. The pressure distribution that corresponds to near minimum loss and the predicted static pressure rise are indicated on each figure.

Although the shapes of the hub and tip static pressure distributions are similar at minimum loss, the high tip deviation angle (approximately 8 deg larger than predicted relative to a 3 deg difference for the hub-figures 22b and h), combined with the apparent trend toward a constant static pressure coefficient at 70% chord for the tip section, indicates that the tip section apparently separated prior to the hub-section. The measured static pressure rise from Station 2 to Station 2A for the near minimum loss incidence angles are also shown on the figures for comparison with the data and predicted performance. These results indicate that the predicted pressure rise was achieved as the result of axial diffusion downstream of the vane row and not because of stator turning.

Slotted Rotor 4 - Slotted Stator 4

Overall Performance

Overall performance data are presented in terms of pressure ratio and adiabatic efficiency as functions of corrected weight flow ($W\sqrt{\theta}/\delta$) and equivalent

rotor speed ($N/\sqrt{\theta}$) for the slotted rotor and slotted stage, respectively, in figures 26 and 27. The solid symbol on the stall line is the stall point determined from the transient data. Also shown in these figures is the effect of boundary layer bleed flow on overall performance. Overall performance and bleed flow data for the steady-state data points are presented in table A-1 of Reference 14.

The rotor achieved an efficiency of 80% and a pressure ratio of 1.258 at design equivalent rotor speed and corrected flow (110 lb/sec) compared with respective design values of 89.5% and 1.349. Stage efficiency and pressure ratio were 66.5% and 1.21 (figure 27), respectively, at design equivalent rotor speed and corrected flow compared to respective design values of 83.8% and 1.324. As indicated in figures 26 and 27, reducing the boundary layer bleed flow resulted in a lower stall flow with reduced rotor and stage pressure ratio and efficiency.

Rotor Blade Element Performance

Blade element performance and velocity diagram data are tabulated in table B-2 of Reference 14 for each of the nine design streamline locations. Rotor diffusion factor, deviation angle, and loss coefficient are shown as functions of incidence angle in figures 28a through 28i. The losses in the hub and tip regions (15% span from either wall) are extremely high relative to predicted values for all incidence angles; the loss coefficients in these regions are between 0.25 and 0.45. At design incidence angle the losses from 30 to 70% span are also larger than design. Larger than design deviation angles from 5 through 90% span, combined with increased midspan axial velocity associated with the high wall losses, resulted in lower than design diffusion factors from 30 to 90% span. Between 5 and 15% span the diffusion factors are greater than or equal to design because the reduction in axial velocity in this region was sufficient to offset the reduction in loading caused by the large rotor deviation angles.

The effect of rotor tip bleed flow on blade element performance is also indicated in figures 28a through 28i. Reducing the bleed flow resulted in significantly greater losses and diffusion factors for the outer 30% span. The deviation angles from 5 to 15% span are also substantially higher with reduced bleed flow. These increases do not appear to be normal extensions of the blade element loss, deviation angle and diffusion factor characteristics at the tip with bleed flow, and are apparently associated with increased secondary flow. The

increase in axial velocity from 50 to 100% span associated with the high tip losses resulted in reduced loading and losses for the hub region.

Loss parameter versus diffusion factor is presented in figures 29a through 29e for 10, 30, 50, 70, and 90% span. Correlation curves for the minimum loss data of References 4 through 9 and the slotted Stage 4 predicted performance curves are included on the figures for comparison with the data. The predicted performance curves are more optimistic than the data correlation curves because of the expected reduction in losses with slots and wall vortex generators. For design equivalent rotor speed the minimum loss parameter values are above the predicted performance and data correlation curves at all span locations.

Stator Blade Element Performance

The stator inlet Mach Number and air angle distributions for design equivalent rotor speed are shown in figure 30. The stator midspan region (approximately 30 to 70% span) was operating with less than design incidence over the entire flow range. Design incidence near the wall (15% span from either wall) occurred at approximately design flow (110 lb/sec). As indicated in figure 30, the Mach No. are higher than predicted for the midspan region and lower near the tip for all flow conditions.

Blade element performance and velocity diagram data are tabulated in table B-2 of Reference 14 for each of the nine design streamline locations. Stator diffusion factor, deviation angle, and loss coefficient are plotted as functions of incidence angle in figures 31a through 31i. At design incidence angle the diffusion factors are less than the predicted values from 5 to 30% span and from 85 to 95% span regions. At 50 and 70% span design incidence was not obtained and the maximum diffusion factor was less than predicted. Larger than design deviation angles across the entire span are primarily responsible for the low diffusion factors. The minimum loss coefficients were equal to or less than the predicted values except at the tip (5, 10, and 30% span); but they did not occur at the design incidence angles.

The effect of bleed flow on stator performance for design equivalent rotor speed is also indicated in figures 31a through 31i. Reducing the stator bleed produced a noticeable increase in loss coefficient at the stator hub. However, decreasing the stator bleed flow had little effect on the stator tip. The change to large positive incidence angles seen at the stator tip without bleed

flow and the associated loss increase is attributed to the large reduction in stator inlet axial velocity caused by the increased rotor tip losses without bleed.

Loss parameter is shown as a function of diffusion factor in figures 32a through 32e for 10, 30, 50, 70, and 90% span. Correlation curves for the minimum loss data of References 4 through 9, and the slotted Stage 4 predicted performance curves are included in the figures for comparison with the data. The predicted performance curves are more optimistic than the data correlation curves because of the expected improvement in losses from slots and vortex generators. For design equivalent rotor speed, the loss parameter values at 50, 70, and 90% span from the tip, that correspond to the minimum loss coefficients in figure 31, are approximately on or below the predicted performance curves. At the other span location, the loss parameter values that correspond to the minimum loss coefficients are above the predicted performance and data correlation curves.

Slotted Rotor 4 - Slotted Stator 4 with Vortex Generators Ahead of the Rotor

Overall Performance

Overall performance data are presented in terms of pressure ratio and adiabatic efficiency as functions of corrected weight flow ($W\sqrt{\theta}/\delta$) and equivalent rotor speed ($N/\sqrt{\theta}$) for the rotor and stage in figures 33 and 34. The solid symbol on the stall line is the stall point determined from the transient data. Also shown in these figures is the effect of boundary layer bleed flow on overall performance. Overall performance and bleed flow data for the steady-state points are presented in table A-3 of Reference 14.

The slotted rotor achieved an efficiency of 79.5% and a pressure ratio of 1.254 at design equivalent rotor speed and corrected flow (110 lb/sec), compared with respective design values of 89.5% and 1.349. Stage efficiency and pressure ratio were 65.0% and 1.203, respectively, at design equivalent rotor speed and corrected flow conditions compared with respective design values of 83.8% and 1.324. As indicated in figures 33 and 34, reducing the wall boundary layer bleed flow resulted in a lower stall flow with reduced rotor and stage pressure ratio and efficiency.

Rotor Blade Element Performance

Blade element performance and velocity diagram data are tabulated in table B-3 of Reference 14 for each of the nine design streamline locations. Rotor diffusion factor, deviation angle, and loss coefficient are shown as functions of incidence angle in figures 35a through 35i. The losses in the hub and tip regions (15% from either wall) are high relative to the predicted values for all incidence angles, with loss coefficients of 0.25 or larger. The losses at 30% span are also greater than the predicted values for all incidence angles, with loss coefficients of 0.13 to 0.20 relative to the predicted value of 0.095. At design incidence angle the losses at 50 and 70% span are approximately equal to the predicted values. Deviation angles near the hub and tip (15% span from either wall) at design incidence angles are 5 to 9 deg greater than the design values, whereas near the middle of the flowpath (30 to 70% span) they are within 2 deg of design. Between 30 and 70% span the diffusion factors are less than predicted because of the increased midspan axial velocities associated with the high wall losses. Near the wall (15% span from either wall) the diffusion factors are approximately equal to or greater than the predicted values since the reduction in diffusion factor associated with the high deviation angles was offset by the effect of the low axial velocities in these regions.

The effect of rotor tip bleed flow on blade element performance is also indicated in figures 35a through 35i. With reduced bleed flow the losses and diffusion factors are significantly greater from 5 to 30% span. Moreover, the deviation angles for the 5 to 15% span region are substantially higher with reduced bleed flow. These increases do not appear to be normal extensions of the blade element loss, deviation angle and diffusion factor characteristics at the tip with bleed flow, and are apparently associated with increased secondary flows. In the hub region, the increase in axial velocity associated with the high tip losses, unloaded the blades and reduced the losses from 70 to 95% span.

Loss parameter is shown as a function of diffusion factor in figures 36a through 36e for 10, 30, 50, 70, and 90% span. Correlation curves for the minimum loss data of References 4 through 9, and the slotted Stage 4 predicted performance curves are included for comparison with the data. The predicted performance curves are more optimistic than the data correlation curves because of the expected reduction in losses with slots and vortex generators. For design equivalent rotor speed, the loss parameter values at 10, 30, 70, and 90% span

that correspond to the minimum loss coefficients in figure 35 are above the predicted performance and correlation curves. At midspan the loss parameter that corresponds to the minimum loss coefficient in figure 35e is approximately on the predicted performance curve.

Stator Blade Element Performance

The stator inlet Mach No. and air angle distributions for design equivalent rotor speed are shown in figure 37. As seen in the figure, the hub and tip region data indicate operation over a wide range of incidence angles both above and below the design incidence, whereas the data for 30, 50, and 70% span indicate operation primarily below design incidence. As indicated in figure 37, the Mach No. for all flow conditions were close to the predicted values across the entire span.

Blade element performance and velocity diagram data are tabulated in table B-3 of Reference 14 for each of the nine design streamline locations. Stator diffusion factor, deviation angle, and loss coefficient are presented as functions of incidence angle in figures 38a through 38i. The diffusion factors are slightly lower than the indicated predicted values across the entire span, primarily because of the relatively large deviation angles seen in the figures and the associated high exit tangential velocities. Stator losses are high relative to the indicated predicted values from 5 to 30% span and from 85 to 95% span. At 50 and 70% span the losses are slightly less than the predicted values.

The effect of bleed flow on stator performance is indicated in figures 38a through 38i. Reducing the stator bleed produced a noticeable increase in the loss coefficient at the stator hub. However, decreasing the stator bleed flow had little effect on the stator tip. The change to large positive incidence angles at the stator tip without bleed flow and the associated loss increase is attributed to the large reduction in stator inlet axial velocity caused by the increased rotor tip losses without bleed.

Loss parameter is shown as a function of diffusion factor in figures 39a through 39e for 10, 30, 50, 70, and 90% span. Correlation curves for the minimum loss data of References 4 through 9, and the slotted Stage 4 predicted performance curves are included on the figures for comparison with the data. The predicted performance curves are more optimistic than the data correlation curves because of the expected improvement in losses from slots and vortex generators.

For design equivalent rotor speed, the loss parameter values at 50, 70, and 90% span that correspond to the minimum loss coefficients in figure 38 are lower than the predicted performance curves. At the other span locations (10 and 30% span) the loss parameter values are above the correlation curves.

Unslotted Rotor 4 - Slotted Stator 4 With Vortex Generators Ahead of the Rotor and Between the Rotor and Stator

During the testing of this configuration approximately one-third of the stator inlet vortex generators separated from the wall. Since the time at which the separation occurred could not be determined and since the relationship of the remaining vortex generators to the instrumentation locations was such that sufficient pressure, temperature, and air angle data was not available for vane passages with vortex generators, the influence of the stator inlet vortex generators on stator performance could not be evaluated. However, the slotted stator performance data is included in this report for the reader's convenience. Because of their small size, the effect of the non-uniform distribution of the remaining stator inlet vortex generators on rotor performance is considered negligible. Therefore, the performance results for the rotor with inlet vortex generators are considered valid.

Overall Performance

Overall performance data are presented in terms of pressure ratio and adiabatic efficiency as functions of corrected weight flow ($W\sqrt{\theta}/\delta$) and equivalent rotor speed ($N/\sqrt{\theta}$) for the rotor and stage in figures 40 and 41. The solid symbol on the stall line is the stall point determined from the transient data. Also shown in the figures is the effect of boundary layer bleed flow on overall performance. Overall performance and bleed flow data for the steady-state data points are presented in table A-4 of Reference 14.

The rotor achieved an efficiency of 86.5% and a pressure ratio of 1.30 at design equivalent rotor speed and corrected flow (110 lb/sec) compared with respective design values of 89.5% and 1.349. Stage efficiency and pressure ratio were 72.3% and 1.247 at design equivalent rotor speed and correct flow conditions compared to respective design values of 83.8% and 1.324. As indicated in figures 40 and 41, reducing the boundary layer bleed flow resulted in a lower stall flow with reduced rotor and stage pressure ratio and efficiency.

Rotor Blade Element Performance

Blade element performance and velocity diagram data are tabulated in table B-4 of Reference 14 for each of the nine design streamline locations. Rotor diffusion factor, deviation angle, and loss coefficient are shown as functions of incidence angle in figures 42a through 42i. The losses in the hub and tip regions (15% span from either wall) are high relative to the predicted values. Larger than design deviation angles from 5 through 15% span and 70 through 95% span combined with increased midspan axial velocity associated with the high wall losses resulted in lower than design diffusion factors from 30 to 95% span. From 5 to 15% span the diffusion factors are greater than the predicted values because the reduction in axial velocity in this region was sufficient to offset the reduction in loading associated with the large rotor deviation angles.

The effect of rotor-tip bleed flow on the blade element performance is indicated in figures 42a through 42i. With reduced bleed flow the losses and diffusion factors are larger from 5 to 15% span. The deviation angles from 5 to 15% span are also substantially higher with reduced bleed flow. These increases do not appear to be normal extensions of the blade element loss, deviation angle and diffusion factor characteristics at the tip with bleed flow, and are apparently associated with increased secondary flows. The increase in axial velocity from 50 to 95% span associated with the high tip losses reduced the loading and losses for the hub region.

Loss paramter versus diffusion factor is presented in figures 43a through 43e for 10, 30, 50, 70, and 90% span. Correlation curves for the minimum loss data of References 4 through 9 and the slotted Stage 4 predicted performance curves are included for comparison with the data. The predicted performance curves are more optimistic than the data correlation curves because of the expected reduction in losses with slots and vortex generators. For design equivalent rotor speed, the loss parameter values that correspond to the minimum loss coefficients in figure 42 and 30 at 50% span are on or below the predicted performance curves, whereas at 70 and 90% span they are above the data correlation curves. At 10% span the loss parameter value that corresponds to the minimum loss coefficient in figure 42b is between the data correlation and predicted performance curves.

Stator Blade Element Performance

As previously stated, approximately one-third of the stator inlet vortex generators were lost during the test program. The non-uniform distribution of the remaining vortex generators and their location relative to the instrumentation precluded their evaluation. However, the stator blade element data are presented for general information purposes.

The stator inlet Mach No and air angle distributions for design equivalent rotor speed are shown in figure 44. The predicted distributions (with slots and vortex generators) are included for comparison, and with the exception of the tip Mach No. are seen to be within the range of test data. For design flow the stator was operating with less than design incidence angle from 15 to 85% span and approximately design incidence at the hub. The tip sections (5 and 10% span) were operating with higher than design incidence angle at design flow.

Blade element performance and velocity diagram data are tabulated in table B-4 Reference 14 for each of the nine design streamline locations. Stator diffusion factor, deviation angle, and loss coefficient are plotted as functions of incidence angle in figures 45a and 45i. The losses are higher than the predicted values from 5 to 15% and from 70 to 95% span. At 30 and 50% span from the tip the losses are slightly less than predicted. The diffusion factors are less than the predicted values across the span primarily because of the larger than design deviation angles seen in the figures and the associated high exit tangential velocities.

The effect of bleed flow on stator performance is also indicated in figures 45a through 45i. Reducing the stator bleed flow produced a noticeable increase in the loss coefficient at the stator hub. However, decreasing the stator bleed flow had little effect on the stator tip losses. The change to large positive incidence angles seen at the stator tip without bleed flow is attributed to the large reduction in stator inlet axial velocity caused by the increased rotor tip losses without bleed.

Loss parameter versus diffusion factor is presented in figures 46a through 46e for 10, 30, 50, 70, and 90% span. Correlation curves for the minimum loss data of References 4 through 9 and the slotted Stage 4 predicted performance curves are included for comparison with the data. The predicted performance curves and more optimistic than the data correlation curves because of the expected reduction in losses with slots and vortex generators.

For design equivalent rotor speed, the loss parameter values corresponding to the minimum loss coefficients in figure 45 at 10 and 70% span are on or above the predicted predicted performance and correlation curves, while at 50 and 90% span they are below the predicted performance curves. At 30% span the loss parameter value that corresponds to the minimum loss coefficient in figure 45d is approximately on the predicted performance curve.

SUMMARY AND COMPARISON OF PERFORMANCE

This section provides a summary and a comparison of the overall and blade element performance that was presented for individual stage configurations in preceding sections.

Performance Summary

The several stage 4 configurations tested exhibited generally poor pressure ratios and efficiencies compared to the predicted values. The low rotor total pressure ratios are attributed to reduced rotor work input due to increased midspan axial velocity (associated with the losses near the walls), and larger than design deviation angles near the walls. The low rotor efficiencies result primarily from the high losses near the walls. High stator losses resulted in poor stage efficiency. The stator tip losses were particularly high compared to the predicted losses for the tip region.

Reducing the wall boundary layer bleed flow in the rotor and stator altered the rotor and stage pressure ratio and efficiency and changed the pressure ratio-flow characteristic at constant rotor speed. The cause of this result is believed to be a redistribution of the flow brought about by increased secondary flow and higher losses in the rotor tip region.

Performance Comparisons

The operating characteristics (pressure ratio-flow) for the 4 configurations are compared for both the rotor and stage in figure 47. The corresponding efficiencies are compared in figure 48. Since it is of interest to note the range and stall margin obtained with each configuration, the stall limit lines are included on figures 47 and 48. As discussed in the Data Reduction Procedures, the stall limit line was determined by calculating the incipient stall flow from the transient recording of bellmouth static pressure and extrapolating the steady-state pressure ratio-flow characteristic to the stall flow. To provide a quantitative criterion for evaluating the stability

range of each configuration, the stall margin (percentage by which the pressure ratio divided by the flow at stall exceeds that quantity at the design point) was calculated for both the rotor and stage and is presented in table A-5 of Reference 14 for each configuration.

With the exception of the minimum flow data at 70% of design equivalent rotor speed, the pressure ratio and efficiency of slotted stage 4 were lower than those of the baseline configuration. At design corrected rotor speed, the slots caused a shift in the pressure ratio-flow characteristic toward lower flow. At 70% design corrected rotor speed, the maximum flow for the slotted stage was less than the maximum flow for the baseline stage, but the stall flows were approximately the same. The addition of vortex generators ahead of the slotted rotor resulted in slightly higher peak rotor and stage efficiencies, but the efficiencies were still substantially less than the baseline configuration at design equivalent rotor speed.

The addition of vortex generators ahead of the rotor and between the rotor and stator of a stage comprised of unslotted rotor 4 and slotted stator 4 resulted in approximately a 10% increase stall margin, relative to the baseline configuration, at design speed without a reduction in peak pressure ratio. As shown in figure 48, the increase in surge margin was also accompanied by higher peak rotor and stage efficiencies. The maximum flow was reduced somewhat from that of the unslotted stage. At the higher flows the pressure ratio was slightly less than the unslotted baseline stage, but the reductions in pressure ratio and efficiency were significantly less than that observed with the slotted stage. Since the surge line is approximately the same for the slotted stage both with and without rotor inlet vortex generators, one might conclude that the stator inlet vortex generators were responsible for the gain in surge margin for the unslotted rotor and slotted stator stage. Since the loss of approximately 30% of the stator inlet vortex generators precluded their evaluation and since the stage was not tested without the stator inlet vortex generators, the individual effects of the rotor and stator inlet vortex generator cannot be separated. However, the increase in surge margin can be partially attributed to the rotor inlet vortex generators since they unloaded the rotor blade end regions and reduced the losses at high incidence angles allowing the midspan loading to increase prior to stall. The increase in midspan loading was accompanied by operation at higher incidence angles and consequently lower flows before reaching a stalled condition.

Composite plots of rotor loss coefficient, deviation angle, and diffusion factor are presented as a function of incidence angle for the four configurations at the hub, mean and tip in figures 49a through 49c. As previously stated, the rotor slots increased the wall losses and tip deviation angles while the addition of vortex generators upstream of the unslotted rotor reduced the wall loading and losses at the higher incidence angles. The midspan losses and hub deviation angles were also reduced by the addition of the vortex generators ahead of the unslotted rotor. The addition of vortex generators ahead of the slotted rotor produced a slight reduction in rotor tip losses relative to the slotted rotor results, with little change at the hub.

The same blade element performance variables are presented for the stator hub, mean and tip sections in figures 50a through 50c. The slots lowered the stator hub loading and slightly reduced the losses, but the reductions in losses were not significant enough to affect the stage performance. The effect of the stator inlet vortex generators on stator performance could not be evaluated because approximately one-third of the vortex generators separated from the wall during the test program.

REFERENCES

1. Rockenbach, R. W., "Single Stage Experimental Evaluation of Slotted Rotor and Stator Blading, Part IX - Final Report," NASA CR-54553, PWA FR-2289, 26 September 1968.

2. Rockenbach, R. W. and J. A. Brent, "Single Stage Experimental Evaluation of Compressor Blading with Slots and Wall Flow Fences," NASA CR-72635, PWA FR-3597.

3. Rockenbach, R. W., J. A. Brent, and B. A. Jones, "Single Stage Experimental Evaluation of Compressor Blading with Slots and Vortex Generators, Part I - Design of Stages 4 and 5," NASA CR-72626, PWA FR-3461.

4. Linder, C. G., and B. A. Jones, "Single Stage Experimental Evaluation of Slotted Rotor and Stator Blading, Part III - Data and Performance for Slotted Rotor 1," NASA CR-54546, PWA FR-2110, February 1967.

5. Linder, C. G., and B. A. Jones, "Single Stage Experimental Evaluation of Slotted Rotor and Stator Blading, Part IV - Data and Performance for Slotted Rotor 2," NASA CR-54547, PWA FR-2111, February 1967.

6. Linder, C. G., and B. A. Jones, "Single Stage Experimental Evaluation of Slotted Rotor and Stator Blading, Part V - Data and Performance for Slotted Rotor 3 - Slotted Stator 2," NASA CR-54547, PWA FR-2285, August 1967.

7. Linder, C. G., and B. A. Jones, "Single Stage Experimental Evaluation of Slotted Rotor and Stator Blading, Part VI - Data and Performance for Slotted Stator 1," NASA CR-54549, PWA FR-2286, July 1967.

8. Linder, C. G., and B. A. Jones, "Single Stage Experimental Evaluation of Slotted Rotor and Stator Blading, Part VII - Data and Performance for Slotted Stator 2," NASA CR-54550, PWA FR-2287, September 1967.

9. Linder, C. G., and B. A. Jones, "Single Stage Experimental Evaluation of Slotted Rotor and Stator Blading, Part VIII - Data and Performance for Slotted Stator 3," NASA CR-54551, PWA FR-2288, October 1967.

10. Abbott, Ira H., and Albert, E. Von Doenhoff, "Theory of Wing Sections," Dover Publications, Inc., June 1959.

11. Aerodynamic Design of Axial Flow Compressors (Revised), NASA SP-36, 1965.

12. Taylor, H. D., "Application of Vortex Generator Mixing Principle to Diffusers - Concluding Report." United Aircraft Research Department Report R-15064-5, December 1948.

13. Brown, A. C., H. F. Nawrocki, and P. N. Paley, "Subsonic Diffusers Designed Integrally with Vortex Generators," Journal of Aircraft, Vol. 5, No. 3, May-June, 1968, pp. 221-229.

14. Brent, J. A., "Single Stage Experimental Evaluation of Compressor Blading With Slots and Vortex Generators, Part IV - Supplemental Data for Stage 4," NASA CR-72778, PWA FR-4135, November 1970.

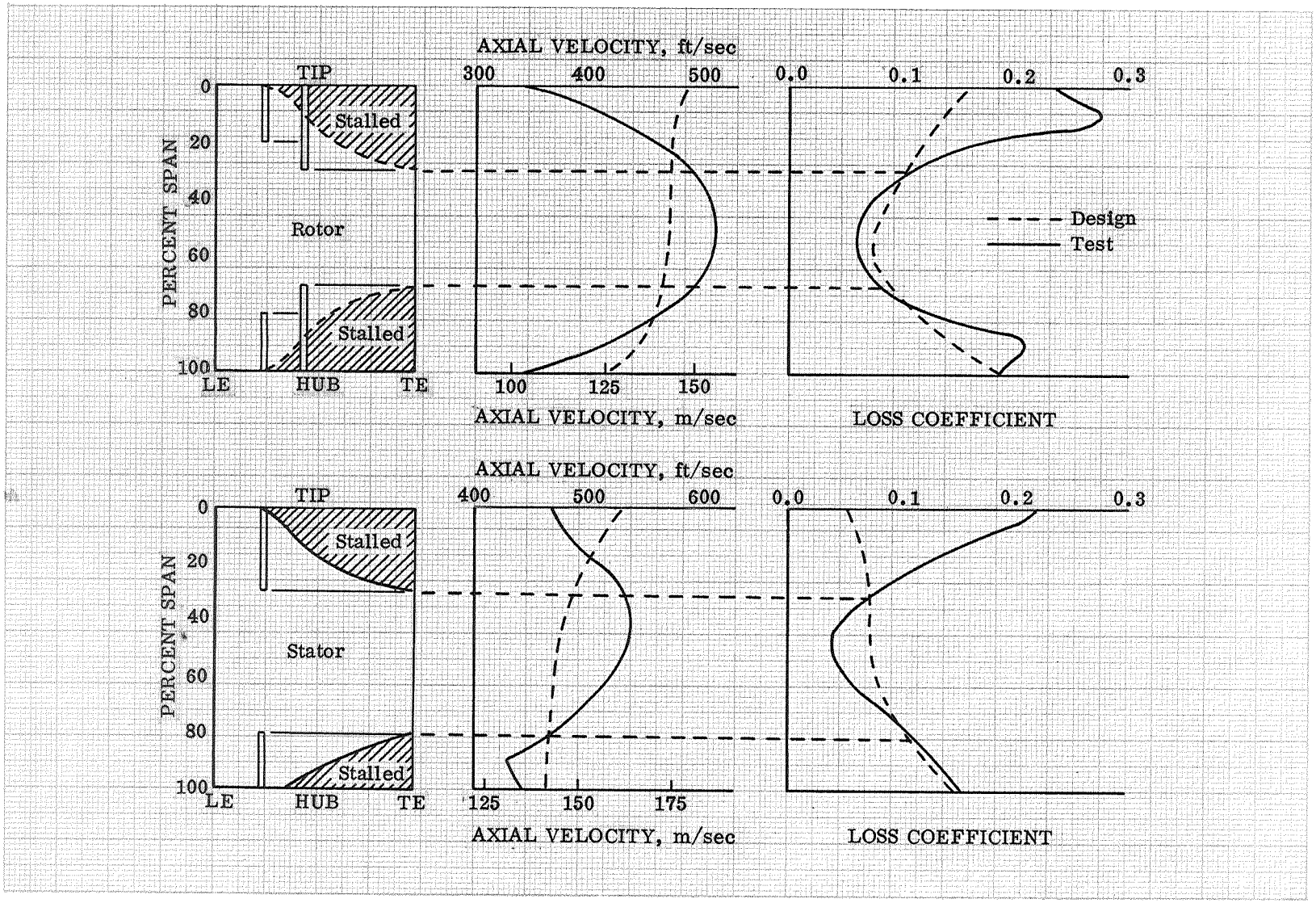

Figure 1. Stage 4 Baseline Test Results

DF 78788

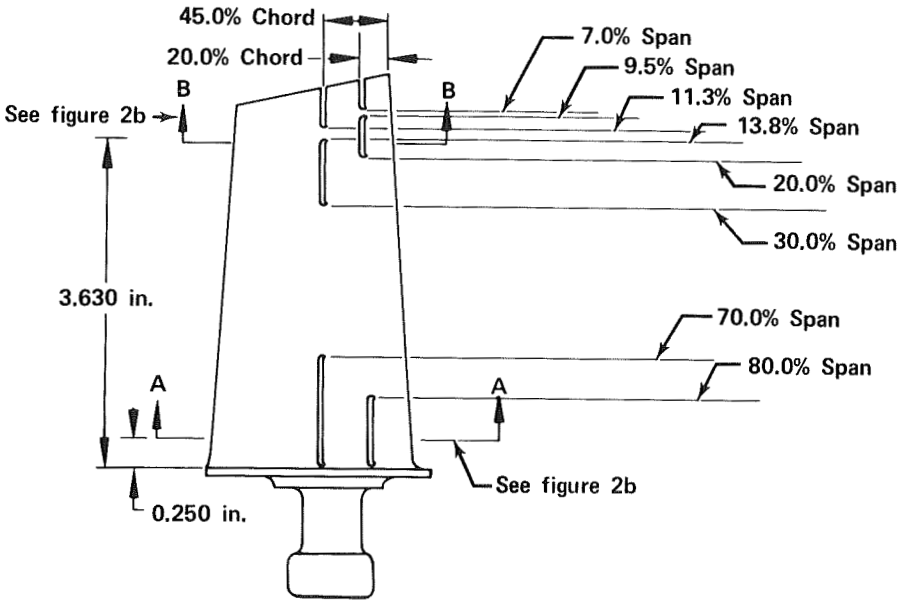

Figure 2a. Rotor 4 Slot Locations on Suction Surface FD 47259

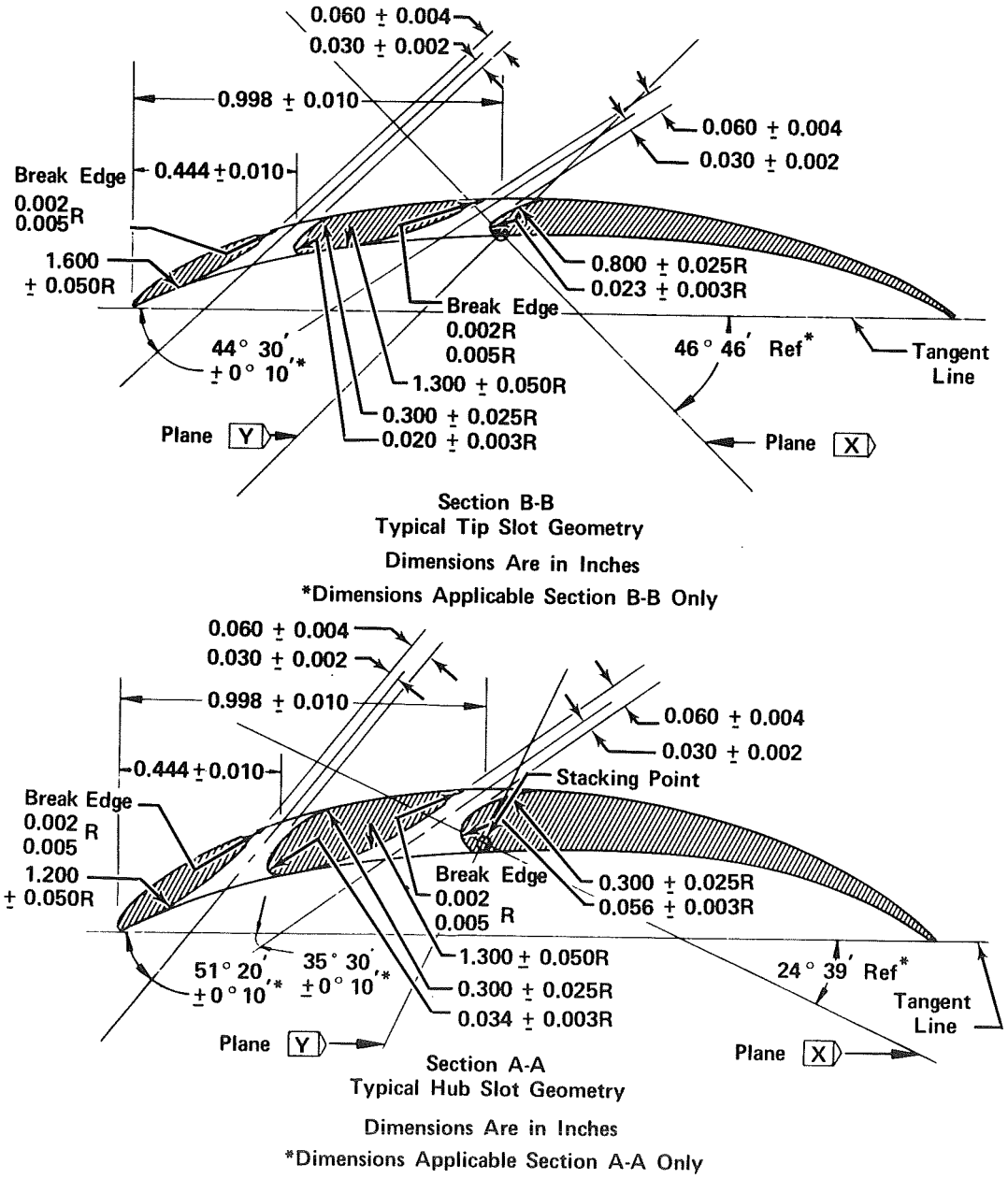

Figure 2b. Rotor 4 Slot Configuration FD 38124

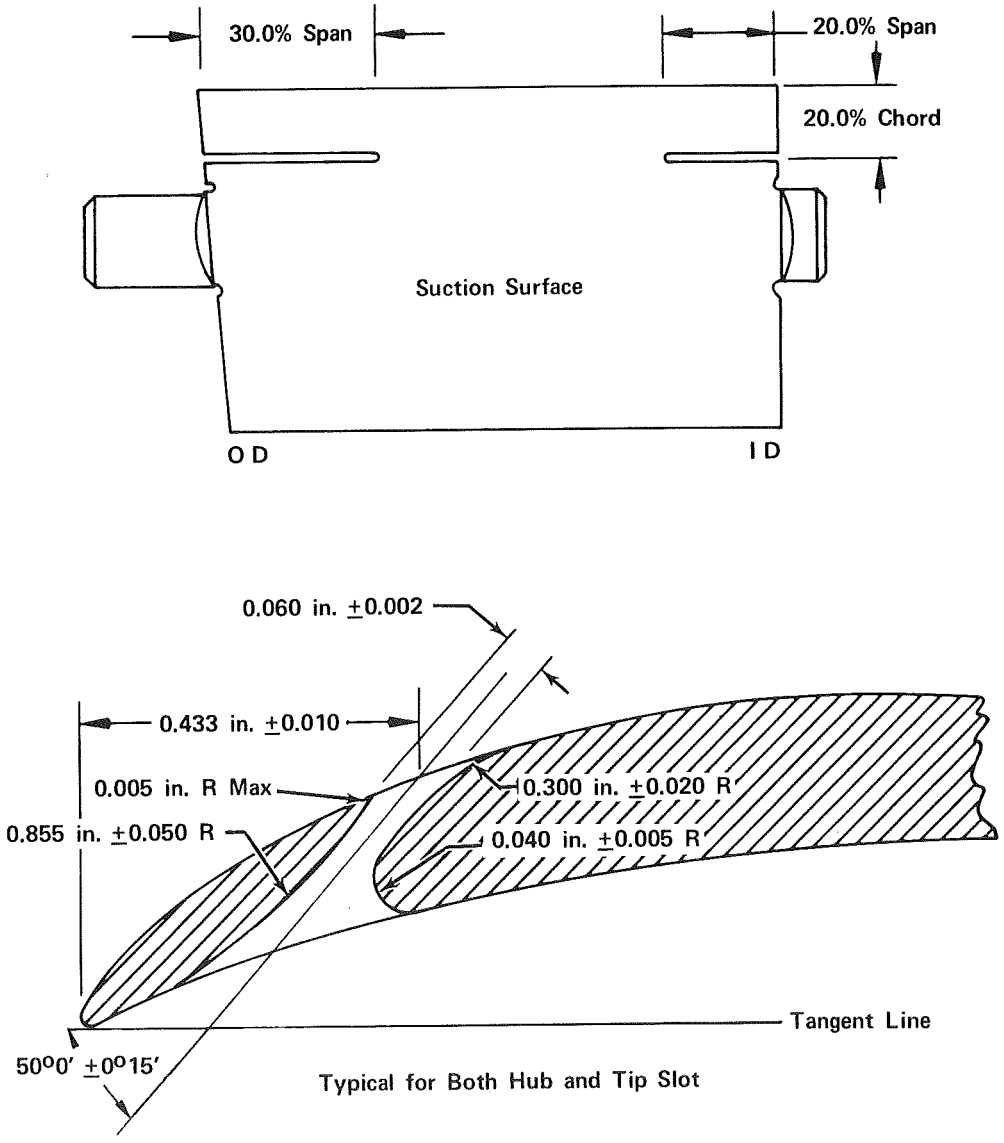

Figure 3. Stator 4 Slot Configuration FD 38120A

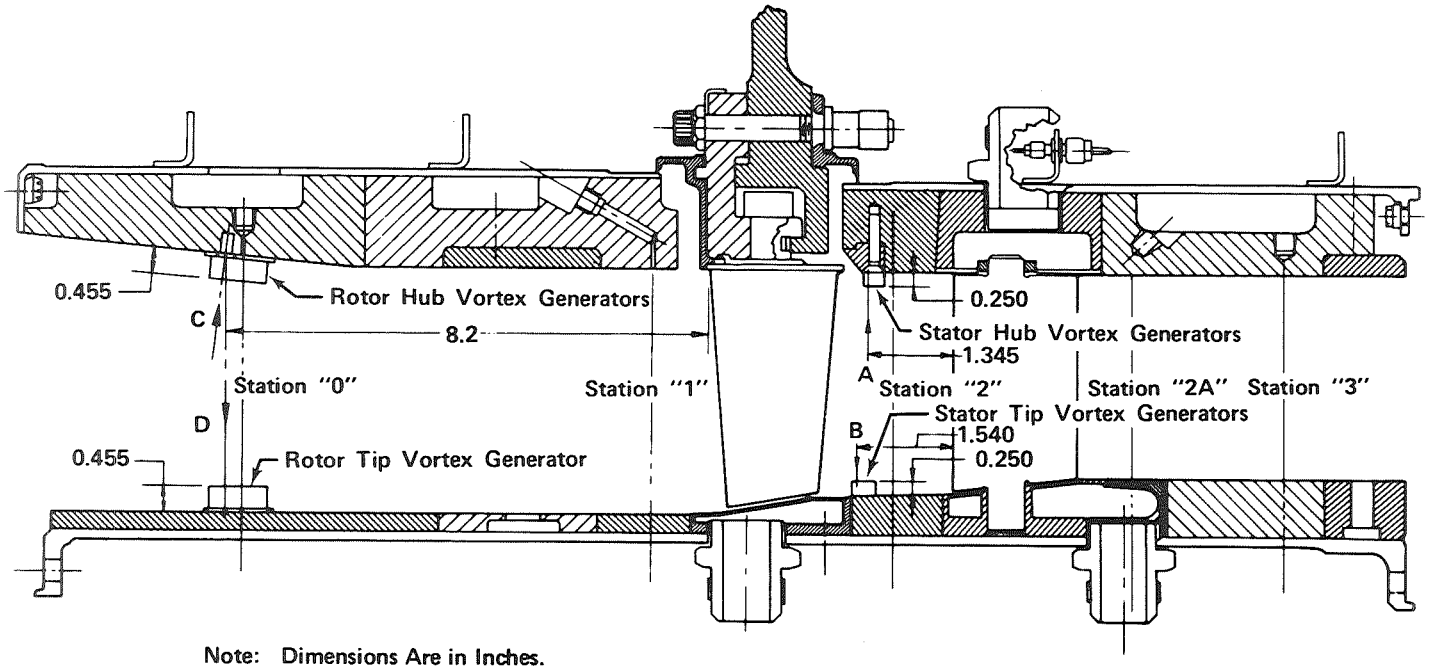

Figure 4a. Vortex Generator Locations

FD 38119A

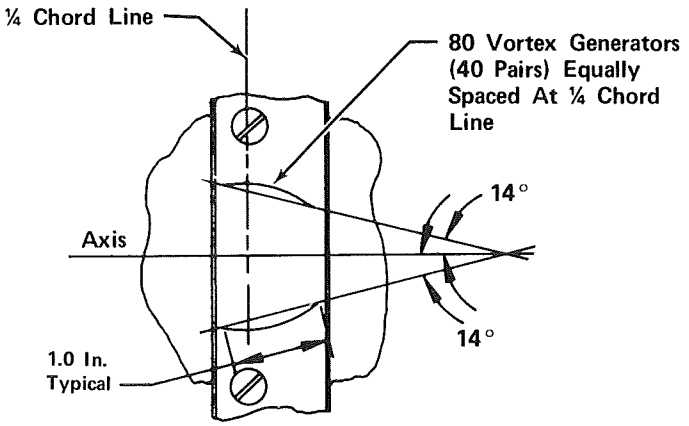

Inner Diameter
View C

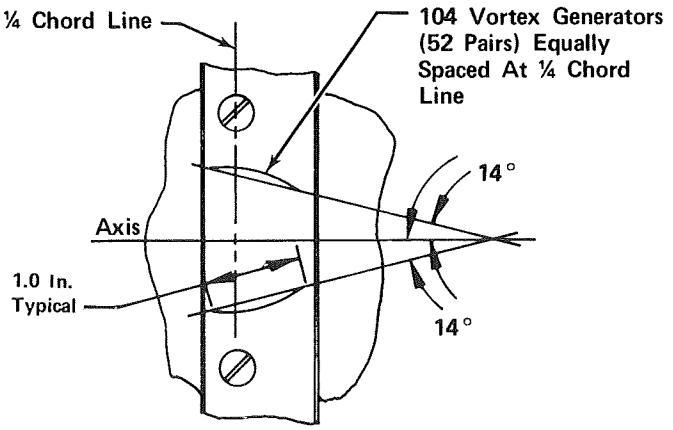

Outer Diameter
View D

Figure 4b. Rotor Vortex Generator Design FD 38118A

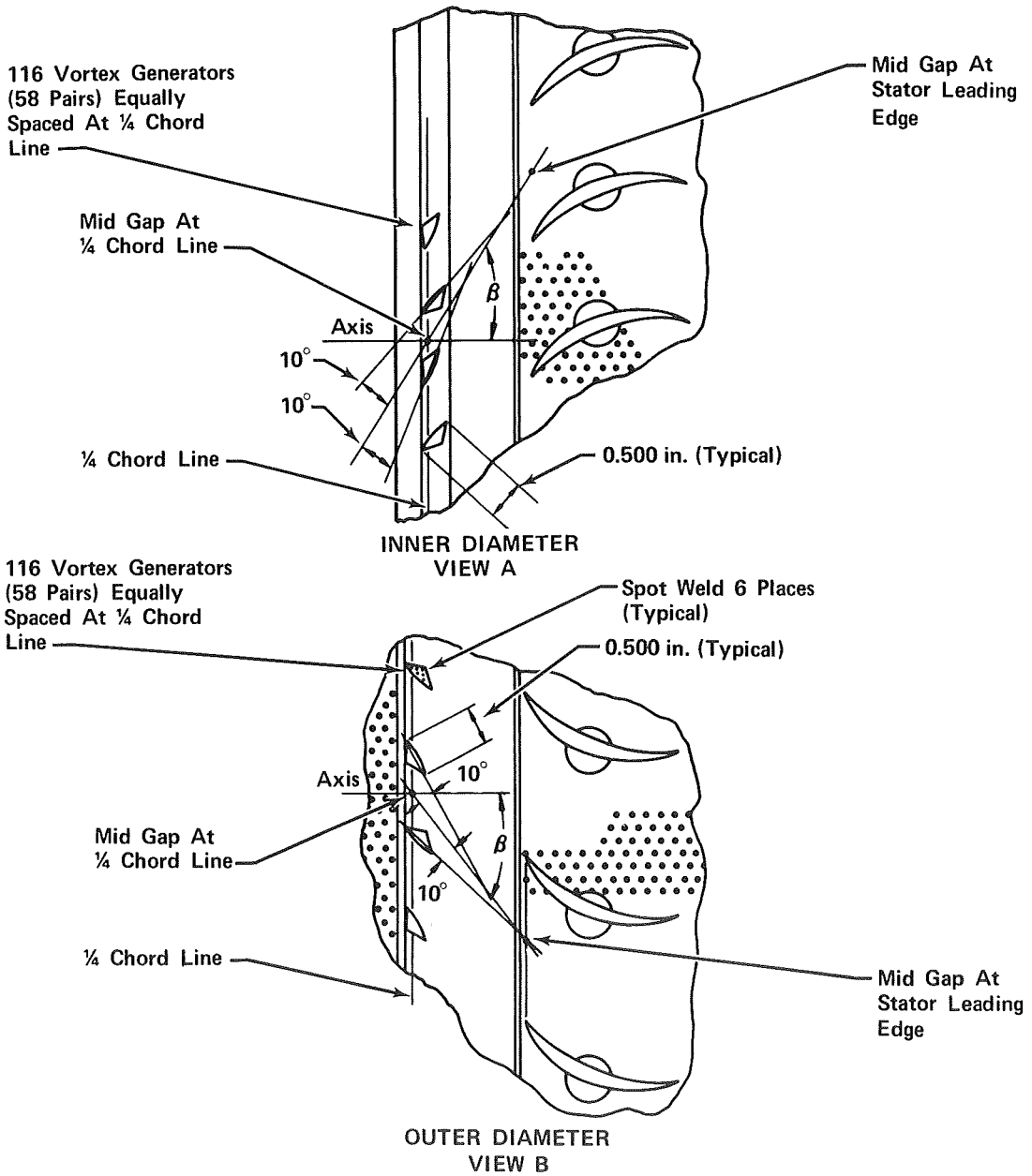

Figure 4c. Stator Vortex Generator Design FD 38117A

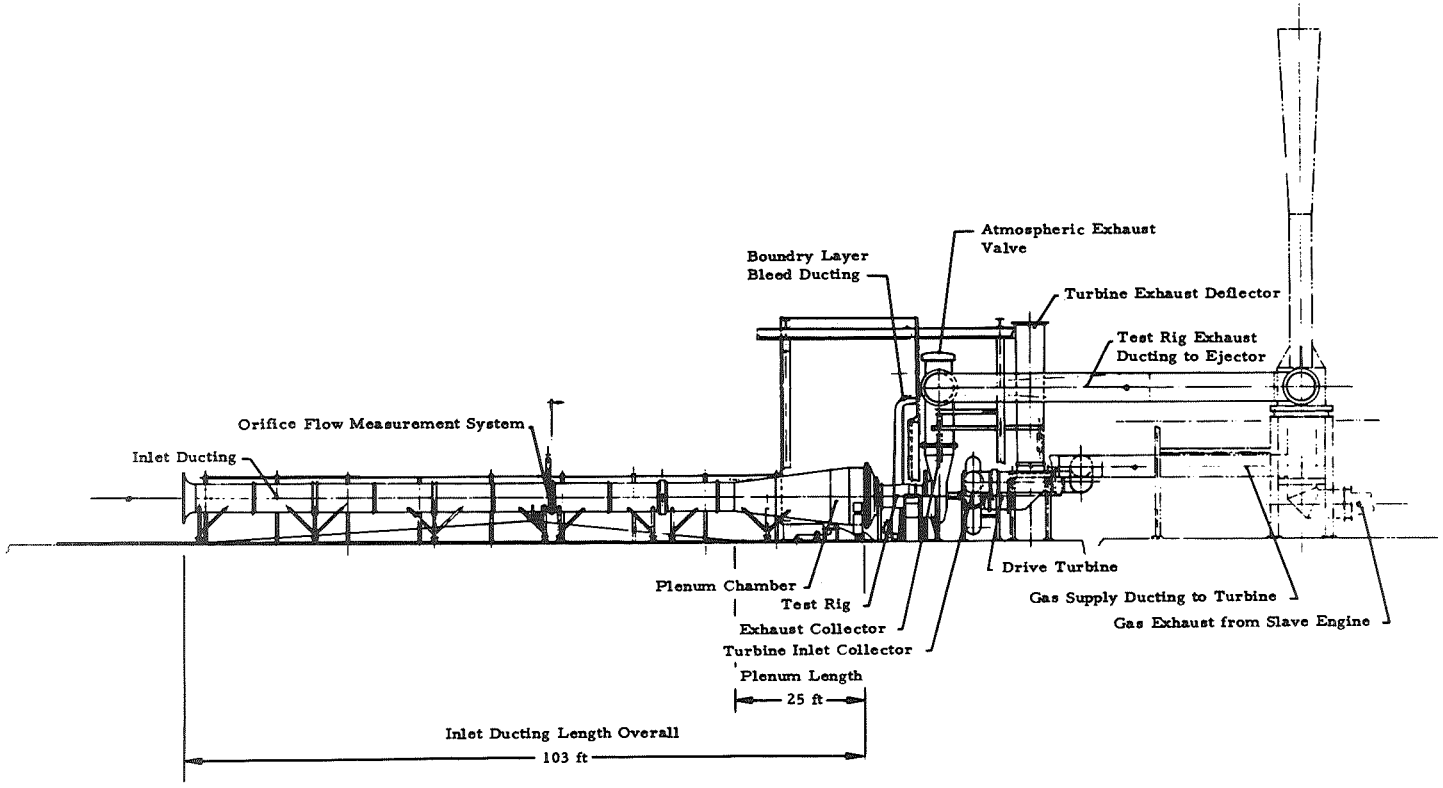

Figure 5. Compressor Research Facility

FD 10891B

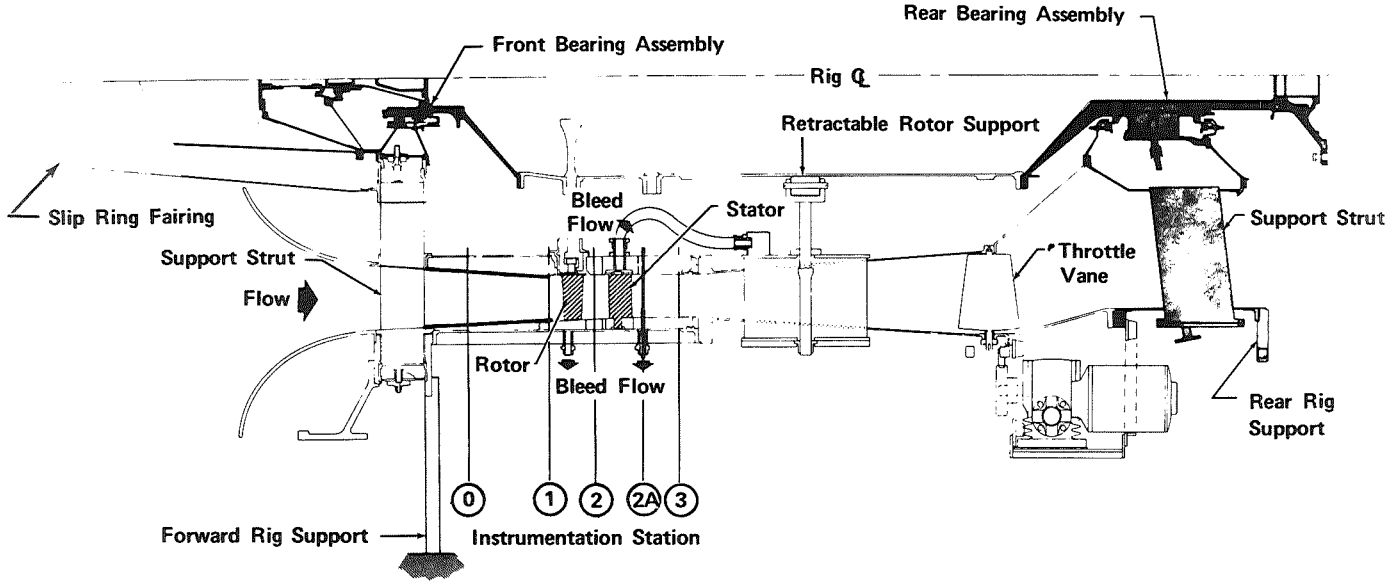

Figure 6. Single Stage Compressor Rig

FD 14681B

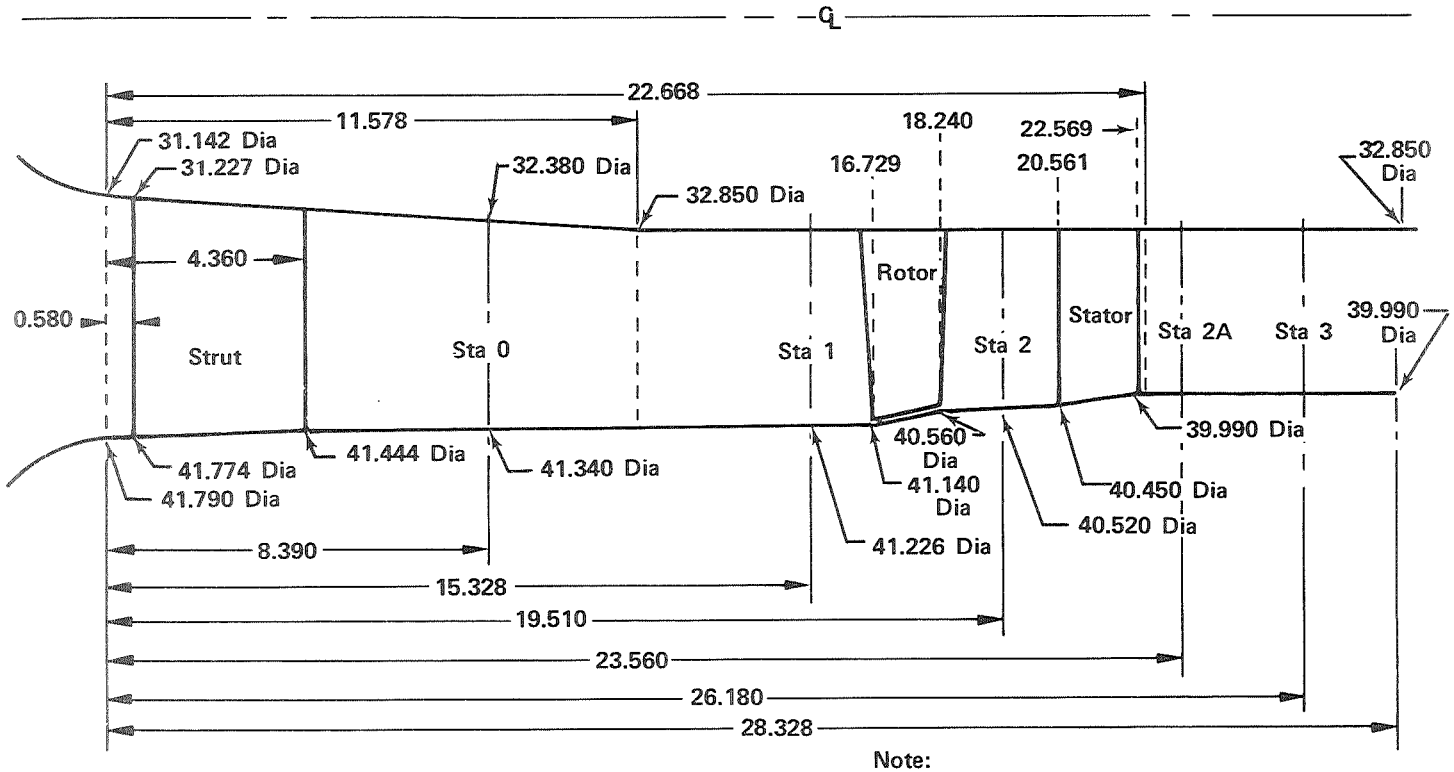

Figure 7. Flowpath Dimensions

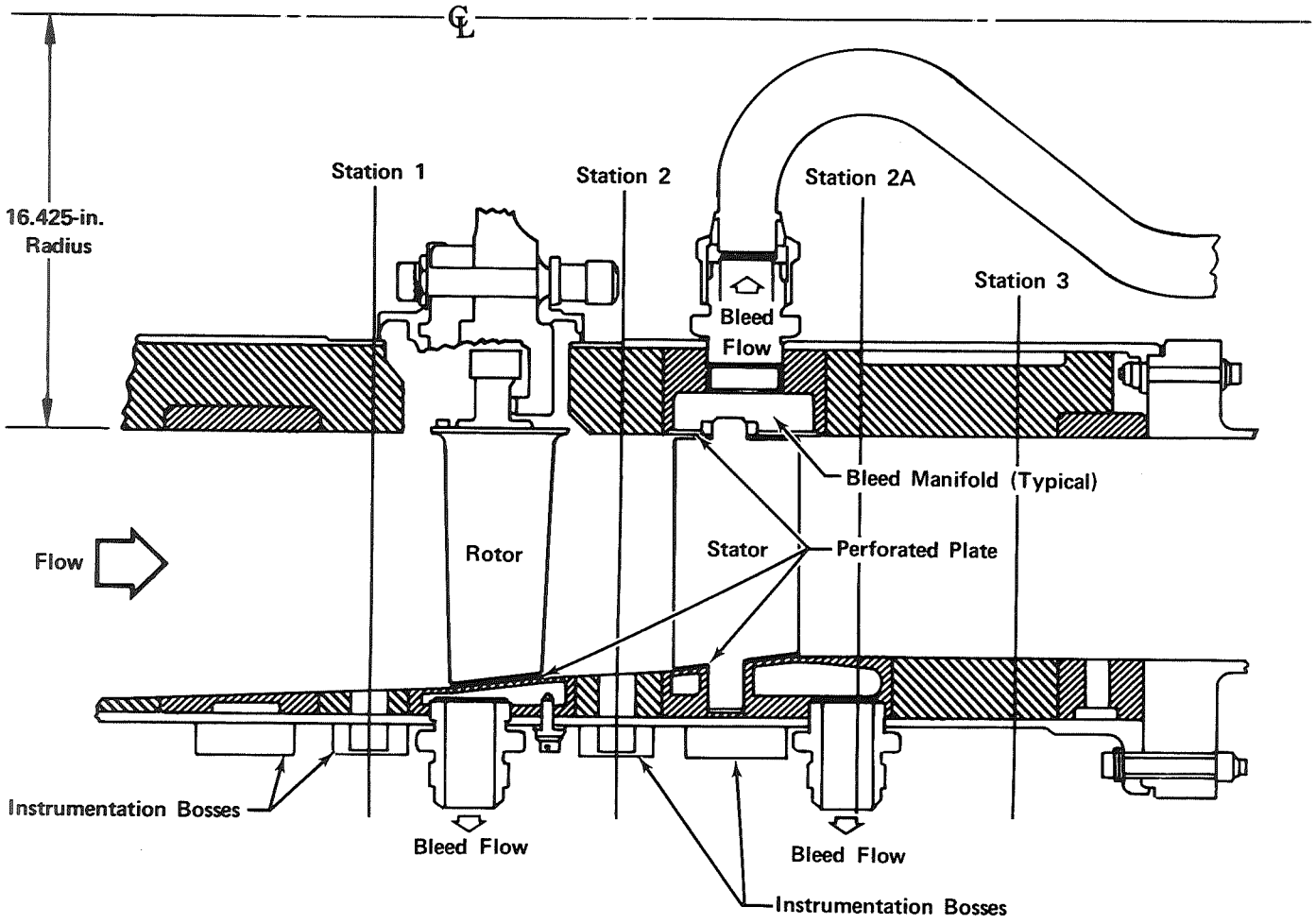

Figure 8. Boundary Layer Bleed System

FD 34363

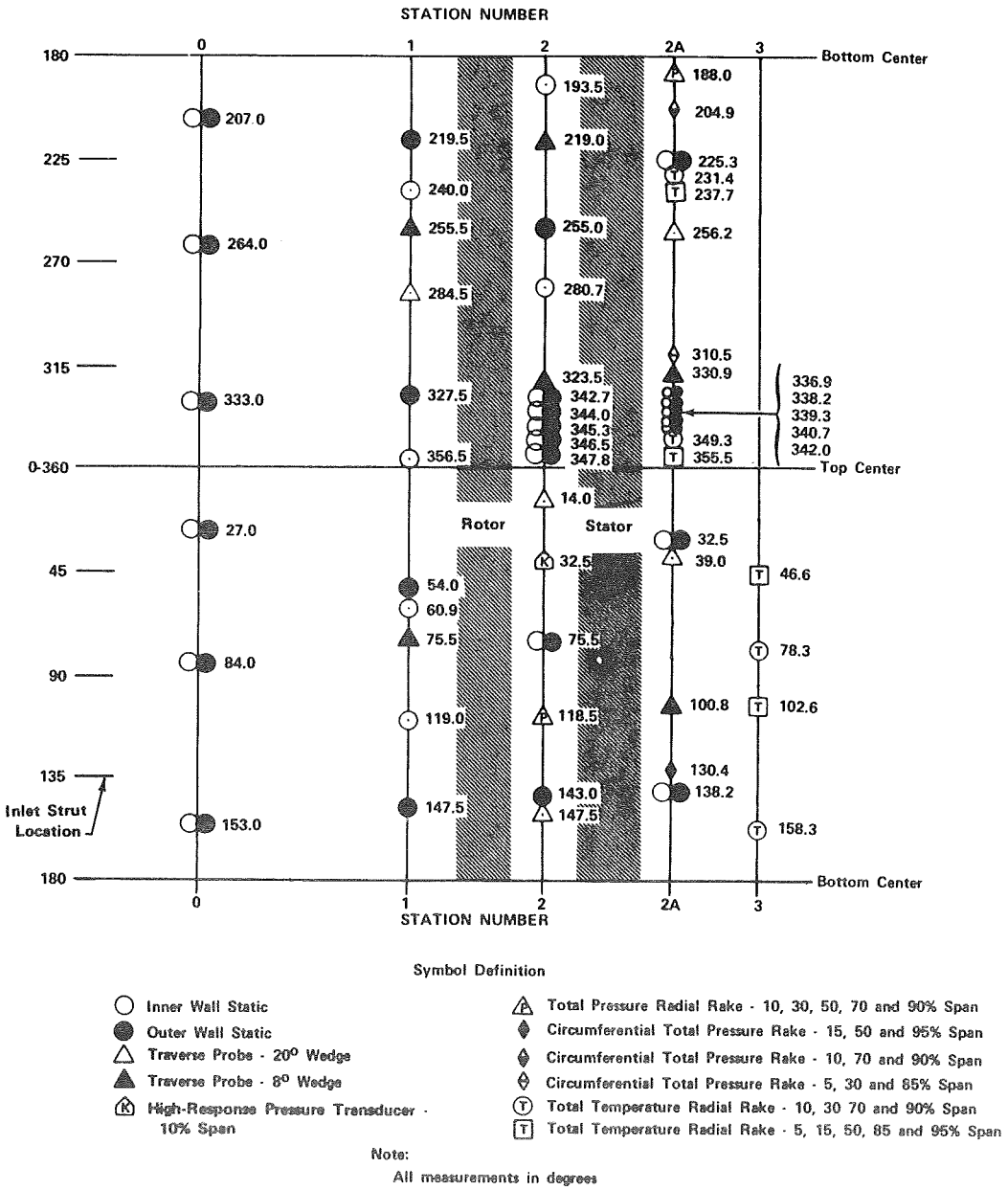

Figure 9. Instrumentation Layout

FD 34366A

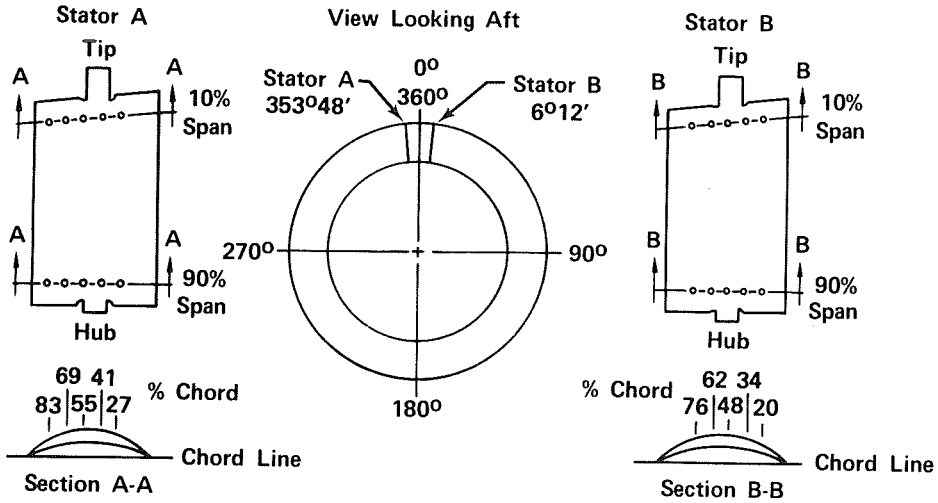

Figure 10. Stator Static Pressure Instrumentation FD 34362

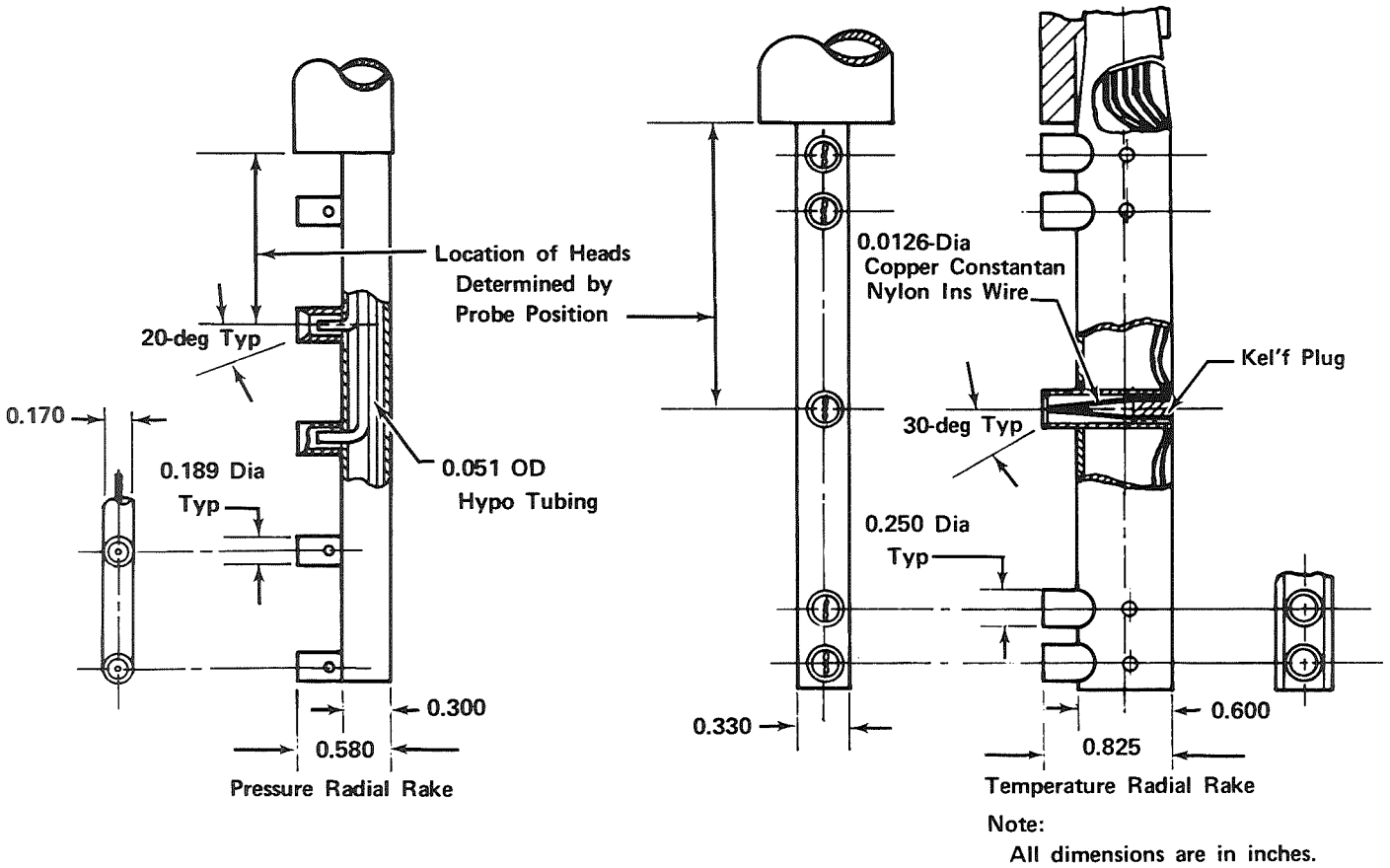

Figure 11. Total Pressure and Temperature Rakes

FD 34361

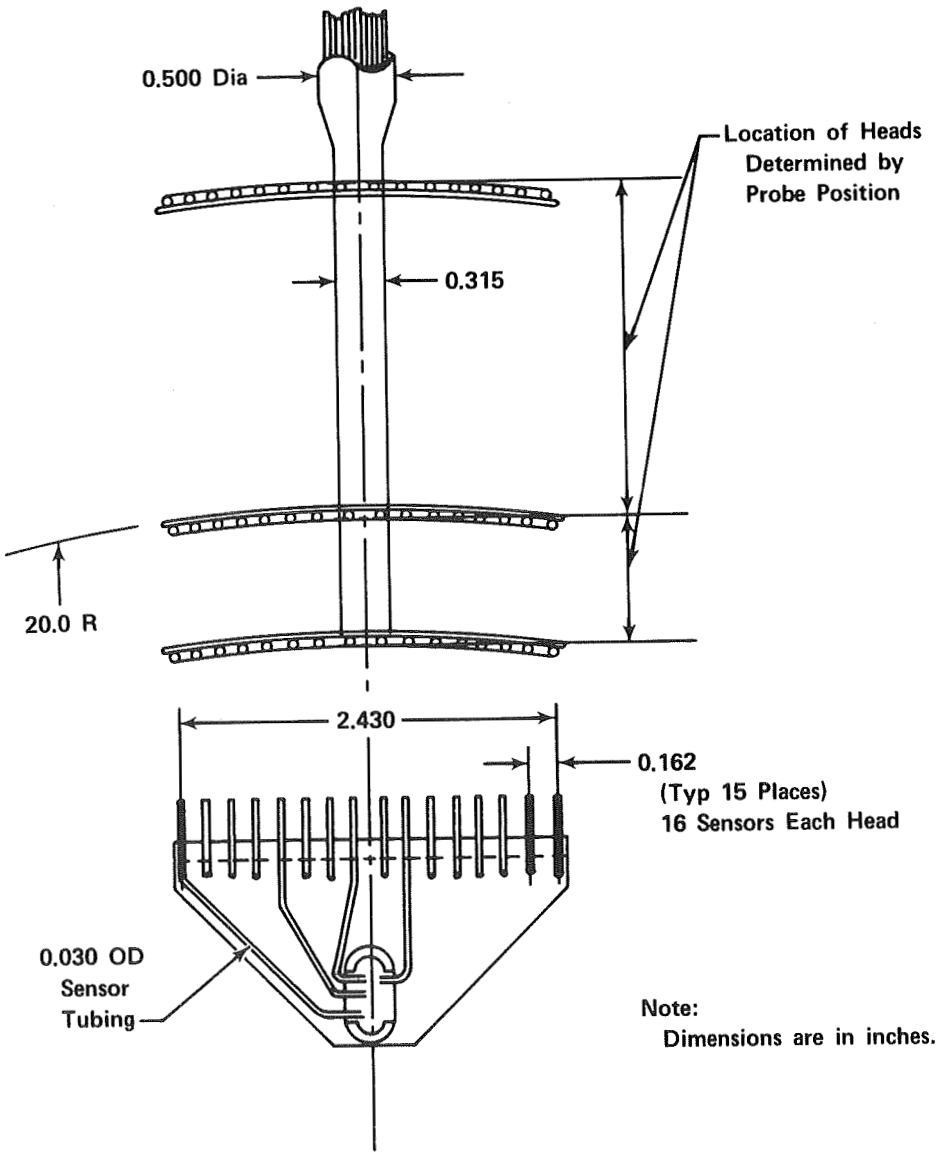

Figure 12. Circumferential Total Pressure Rake FD 34365

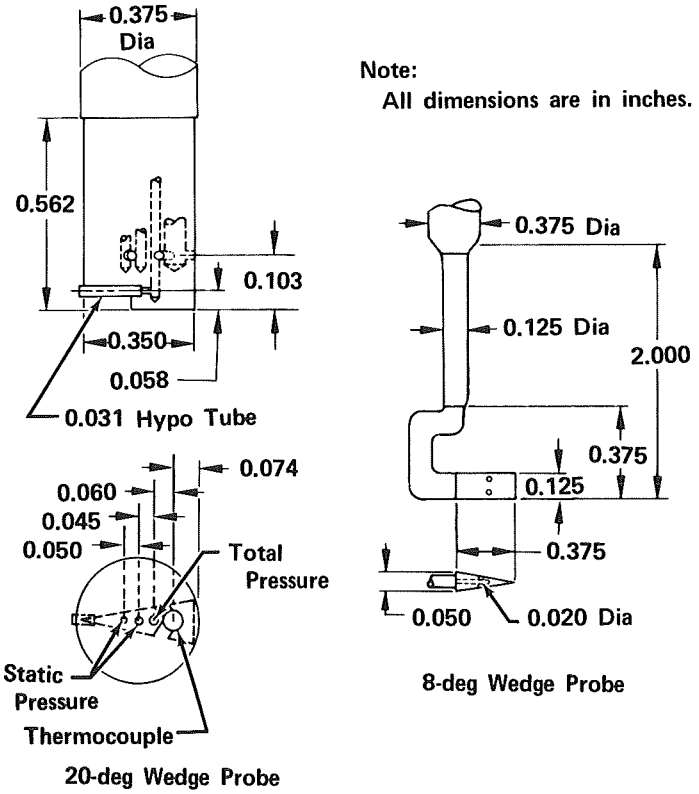

Figure 13. Wedge Traverse Probes FD 18483B

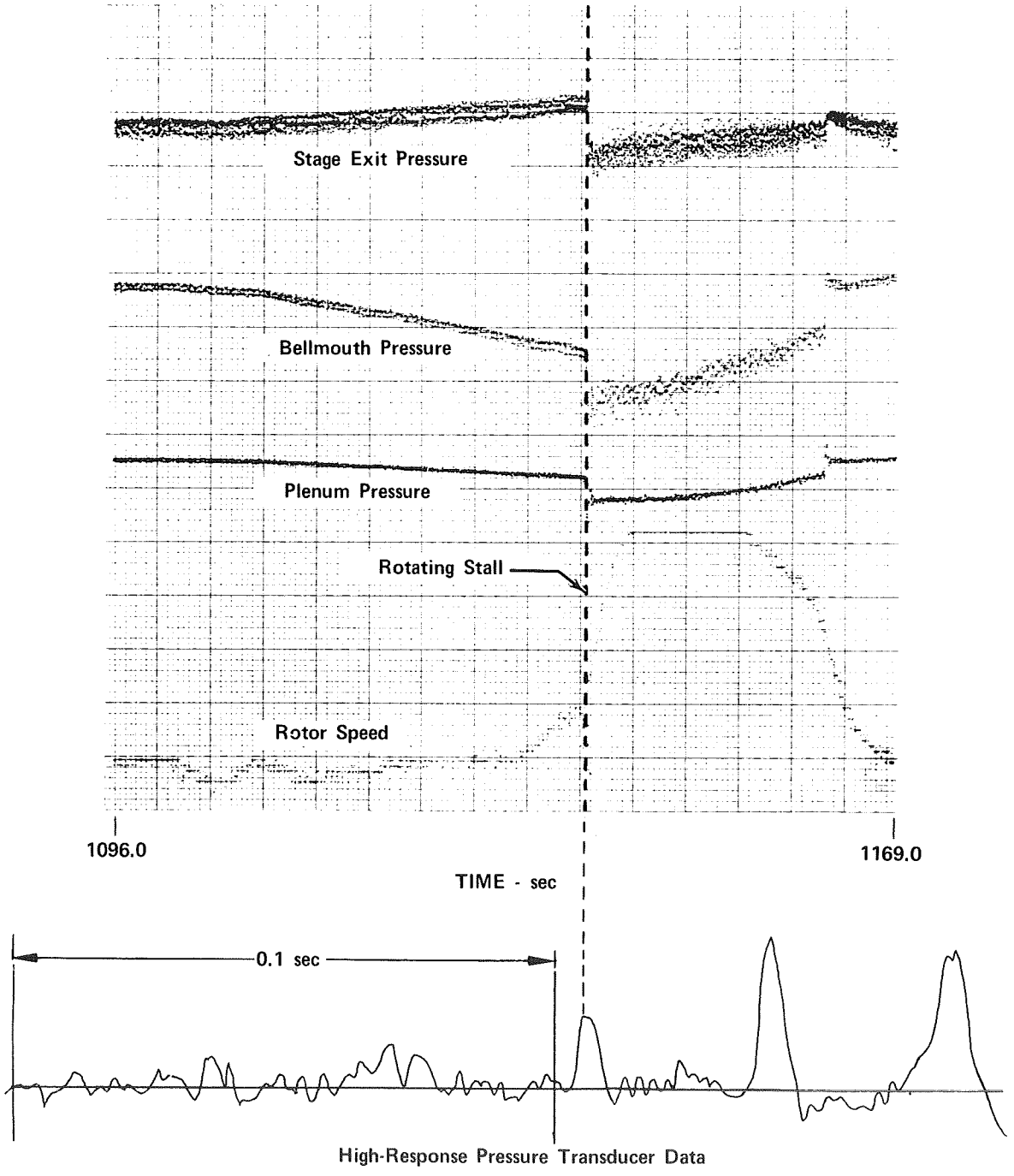

Figure 14. Typical Stall Transient Data FD 47258

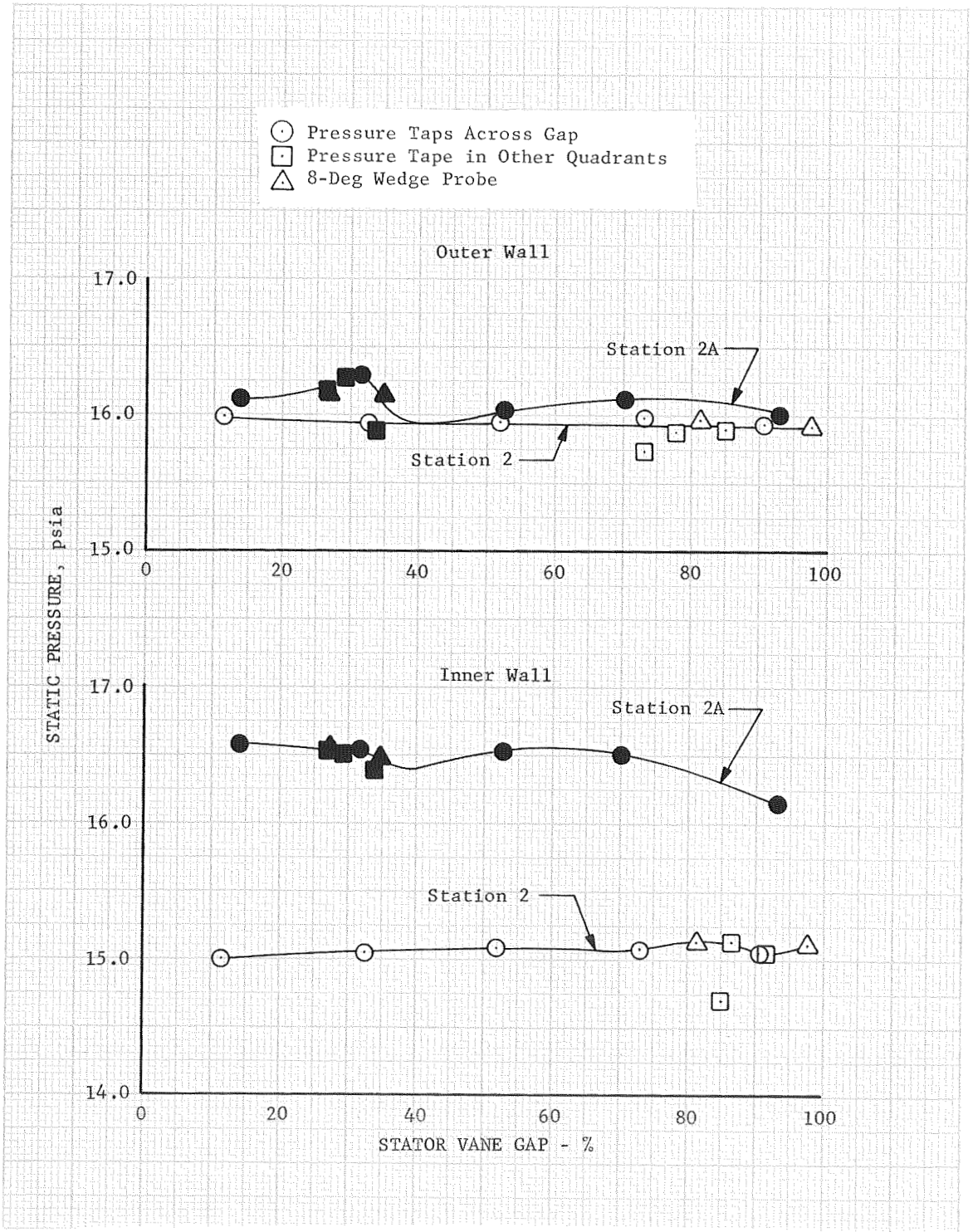

Figure 15. Comparison of Stator Inlet and Exit Wall Static Pressures at Near Design Flow

DF 83415

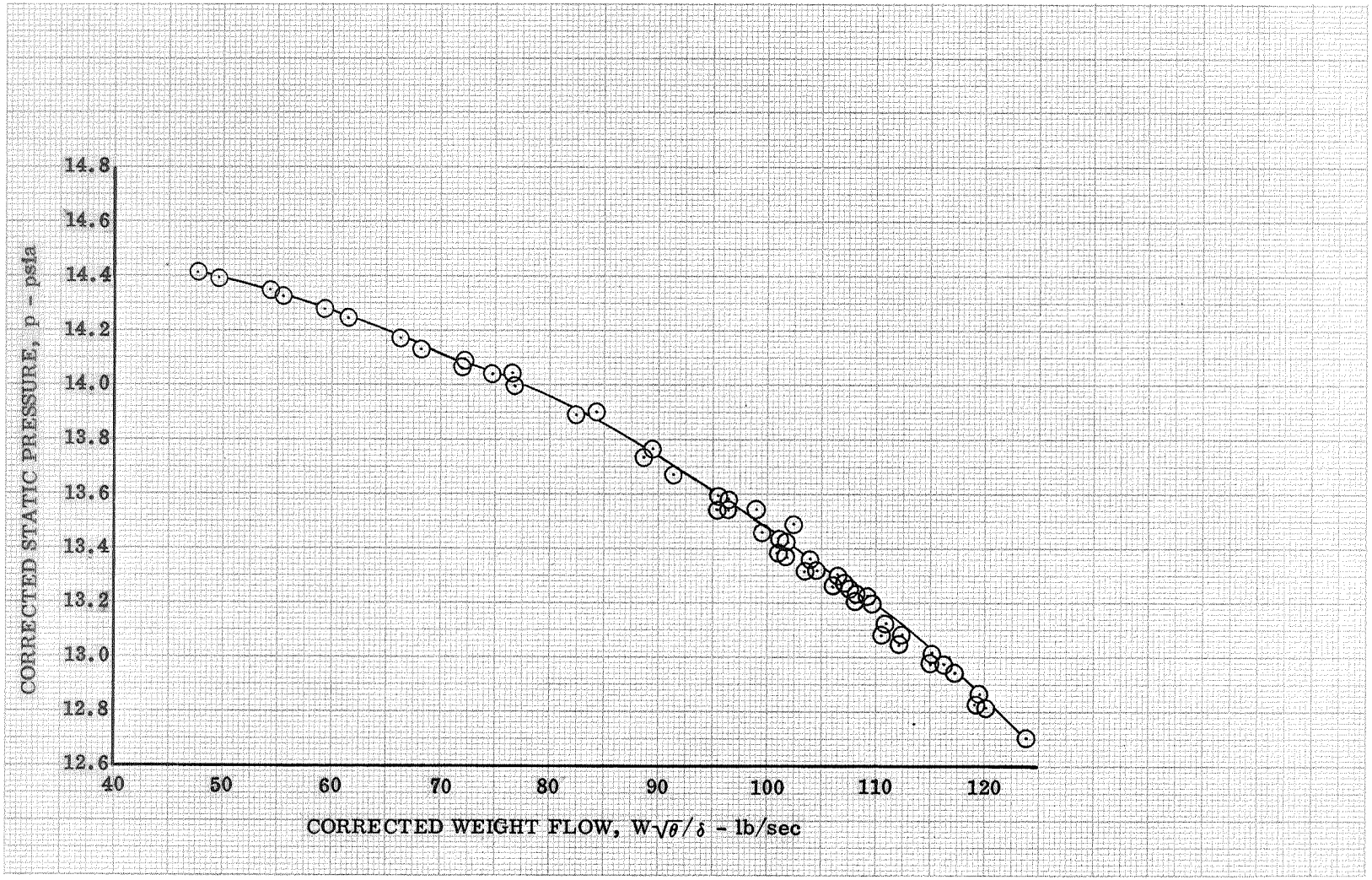

Figure 16. Station O Corrected Static Pressure vs Corrected Weight Flow

DF 77017

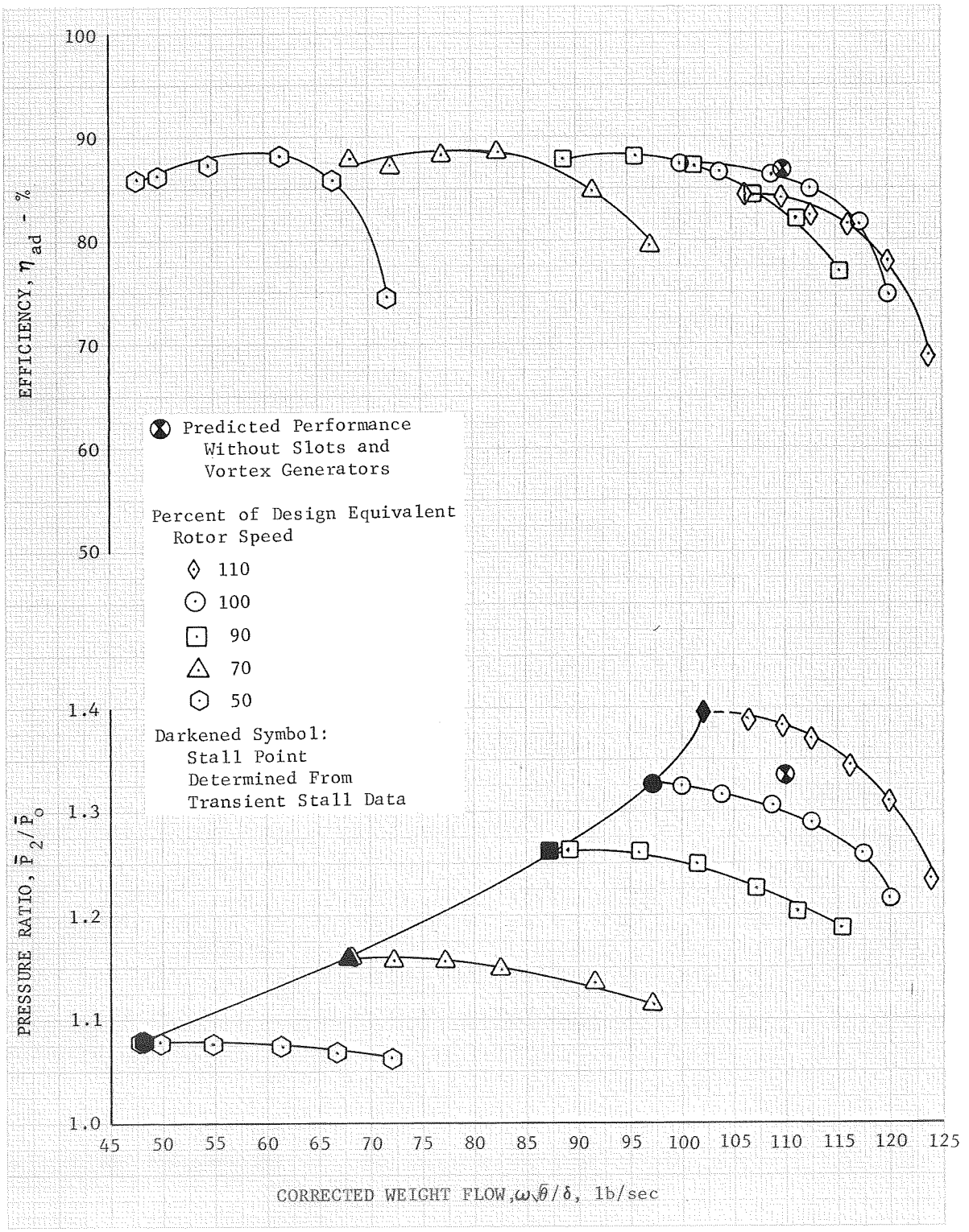

Figure 17. Overall Performance of Unslotted Rotor DF 83381

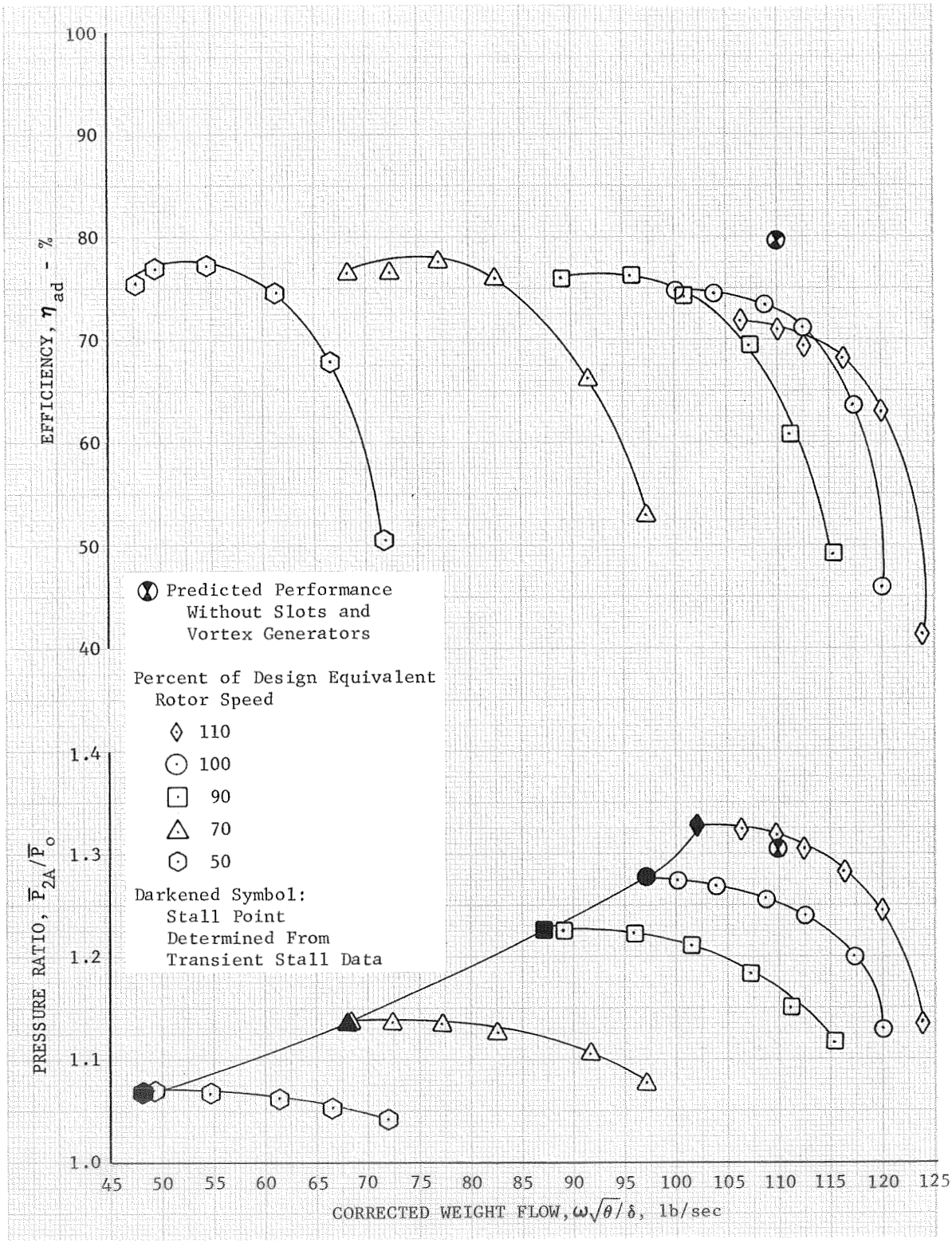

Figure 18. Overall Performance of Unslotted Stage 4 DF 83382

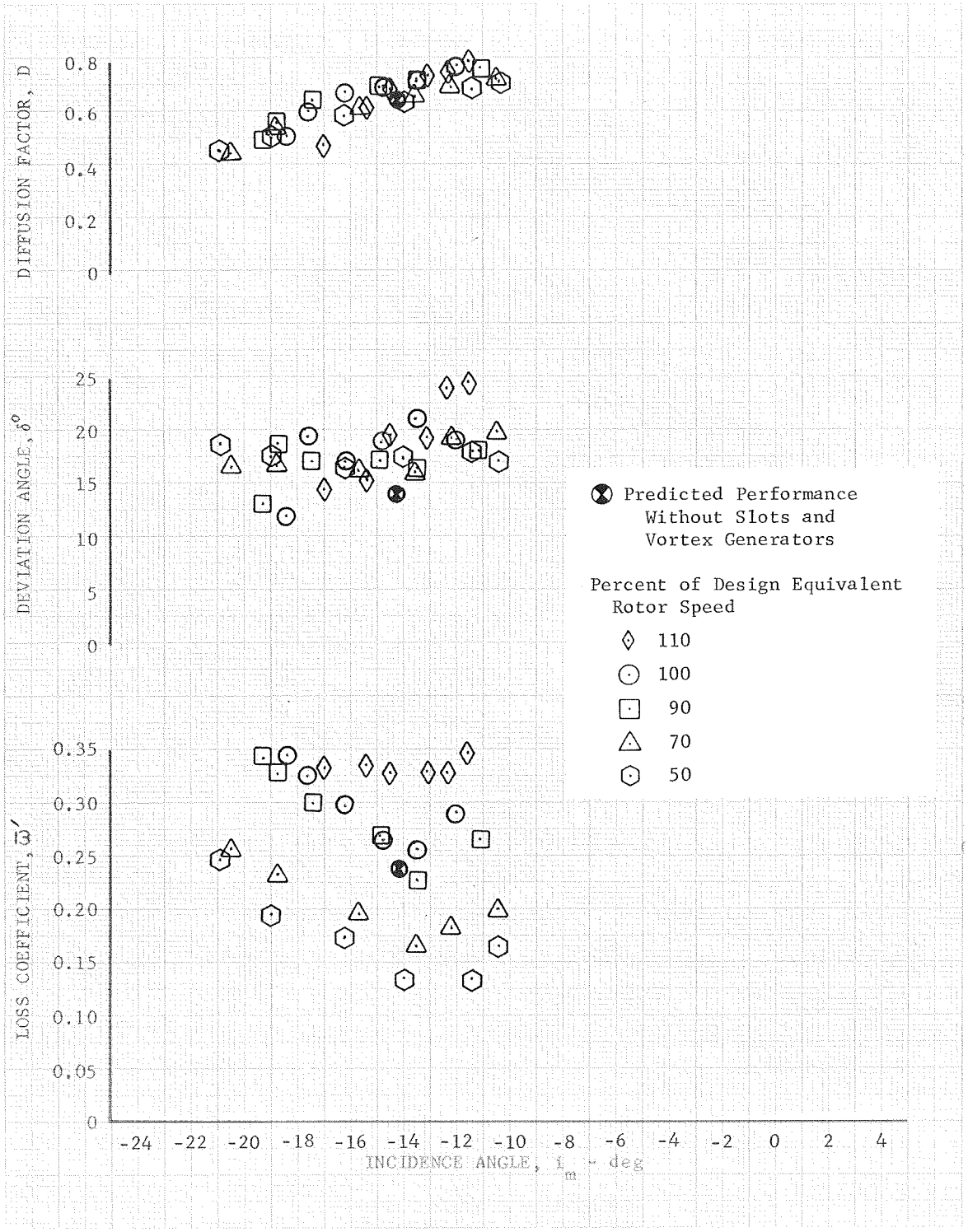

Figure 19a. Unslotted Rotor 4 Blade Element Performance, 5% Span From Tip

DF 83383

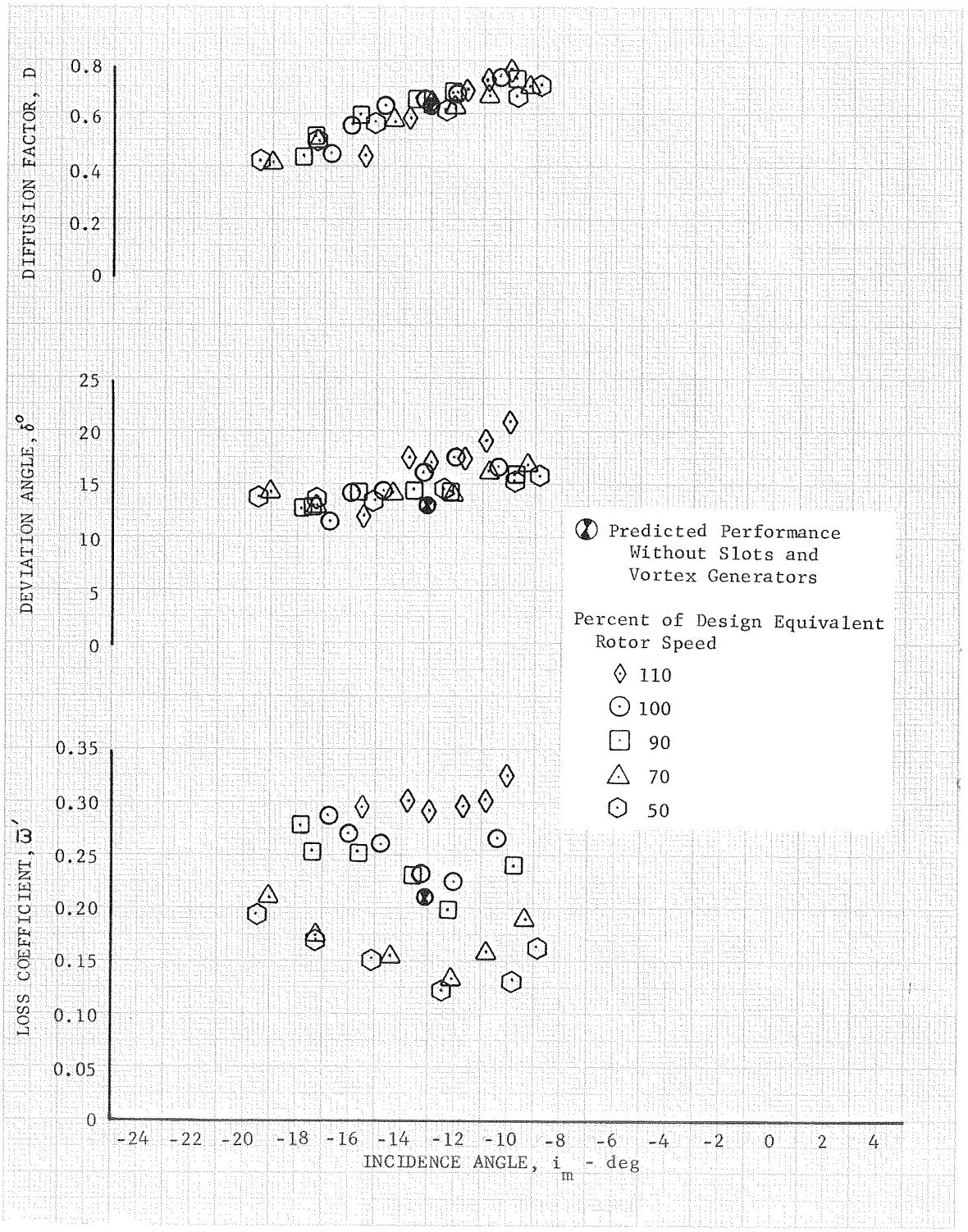

Figure 19b. Unslotted Rotor 4 Blade Element Performance, 10% Span From Tip

DF 83384

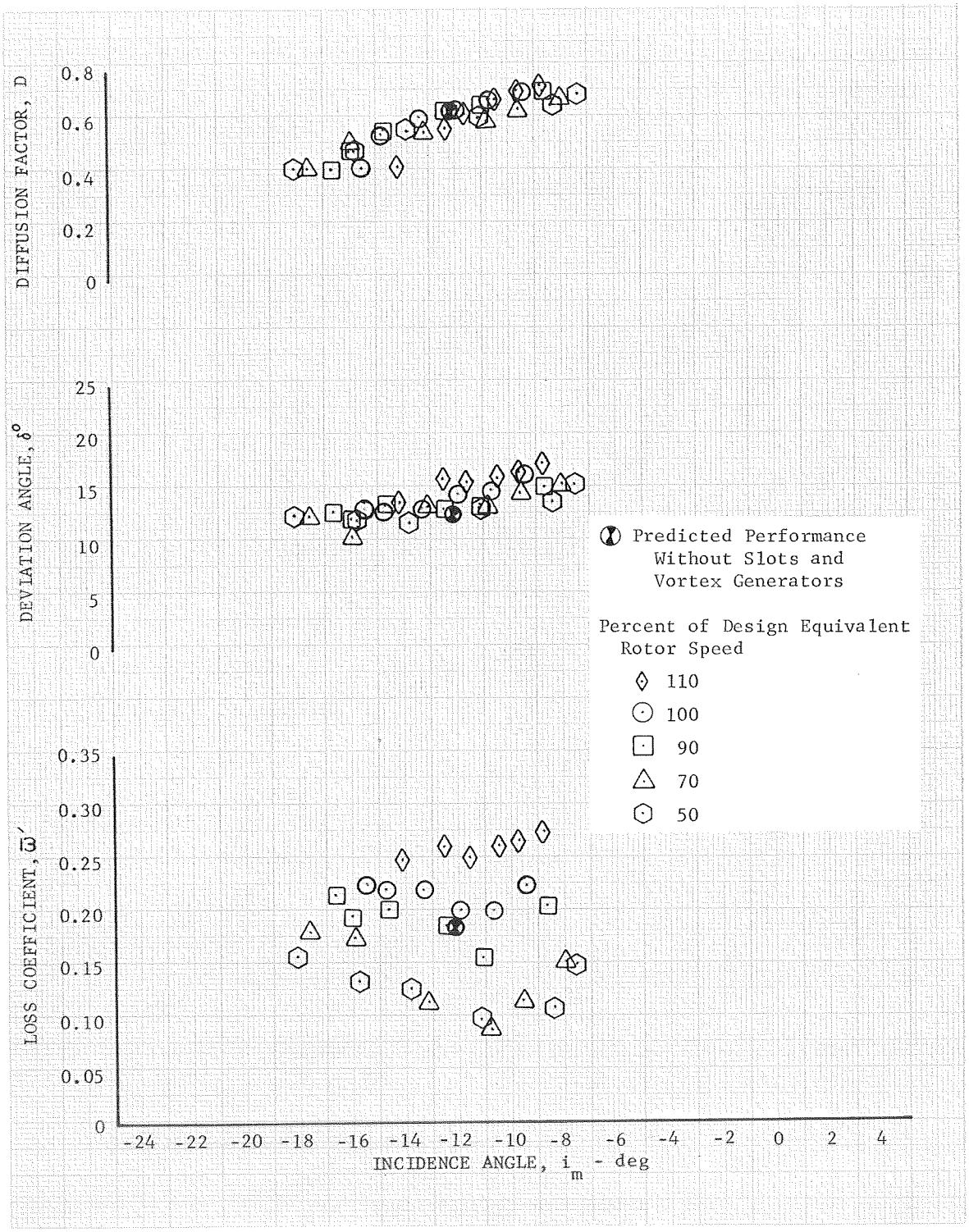

Figure 19c. Unslotted Rotor 4 Blade Element Performance, 15% Span From Tip

DF 83385

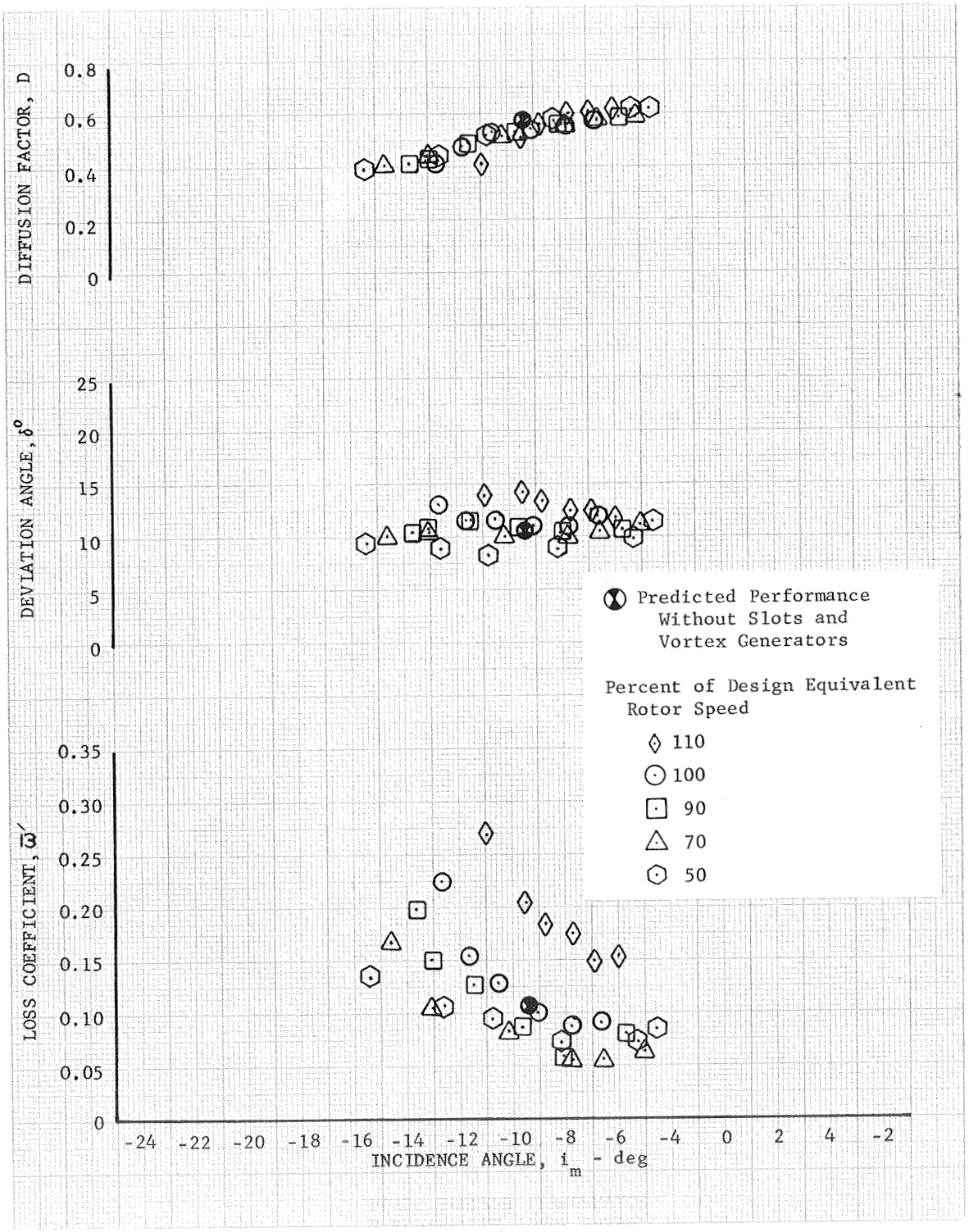

Figure 19d. Unslotted Rotor 4 Blade Element Performance, 30% Span From Tip

DF 83386

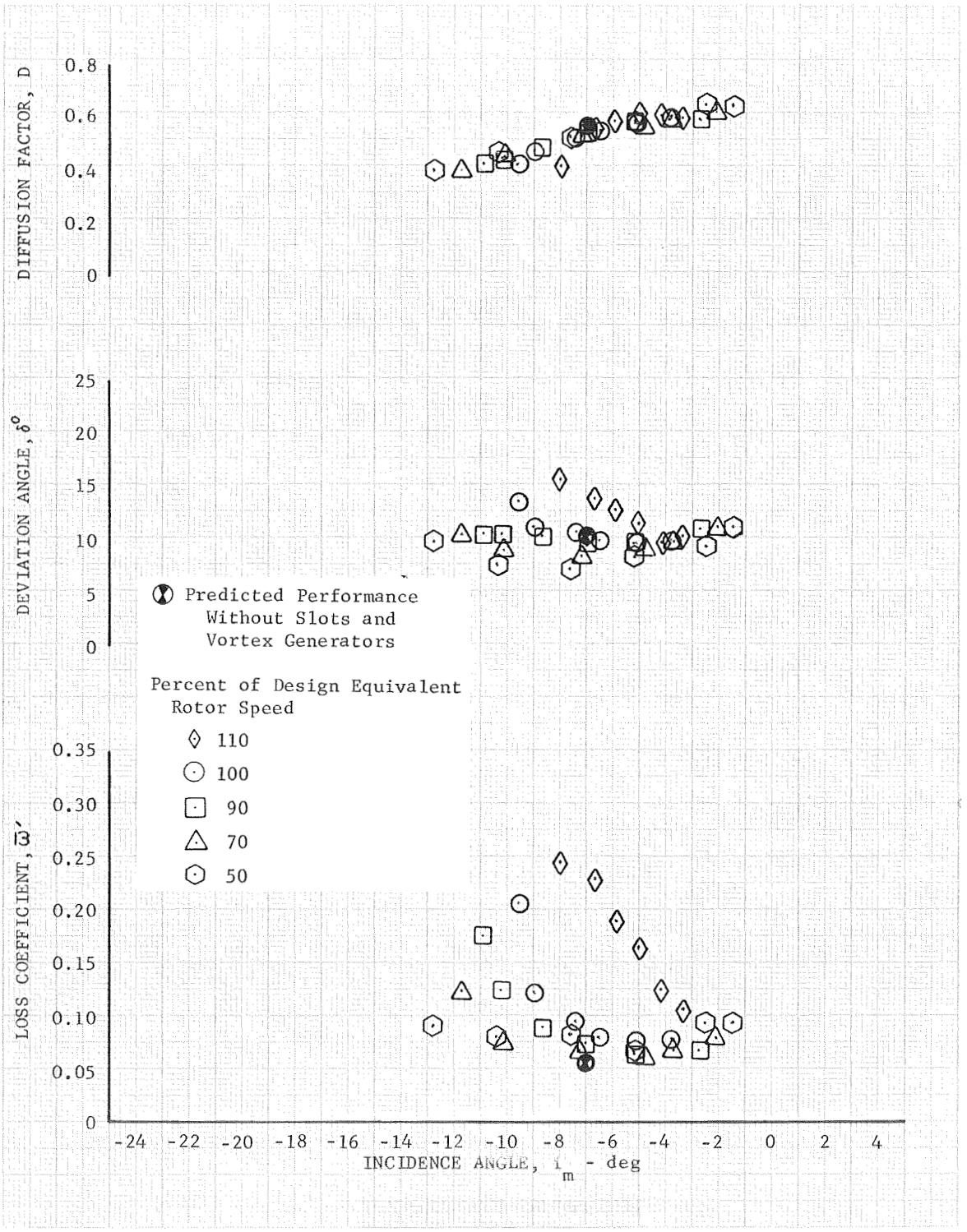

Figure 19e. Unslotted Rotor 4 Blade Element Performance, 50% Span From Tip

DF 83387

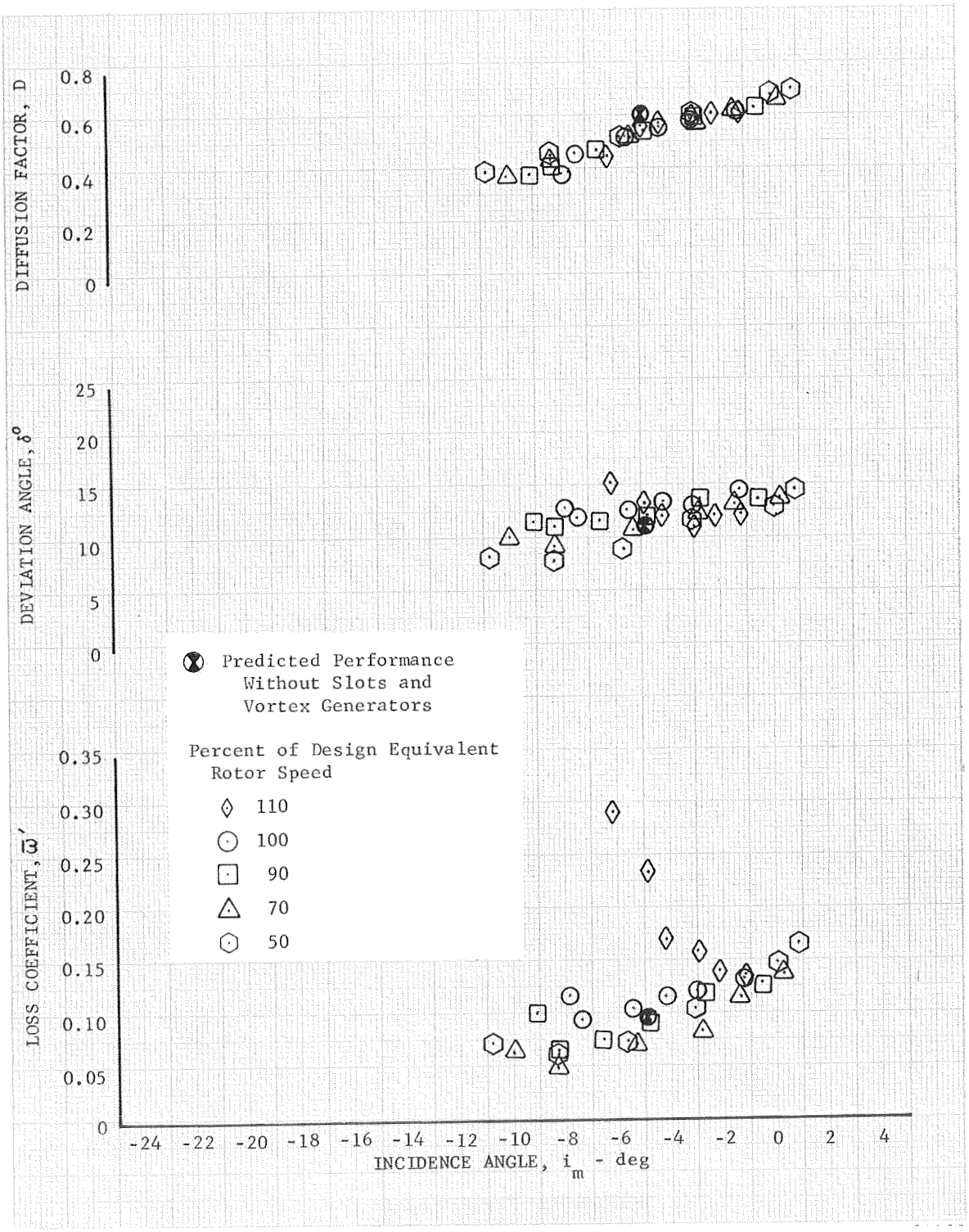

Figure 19f. Unslotted Rotor 4 Blade Element Performance, 70% Span From Tip

DF 83388

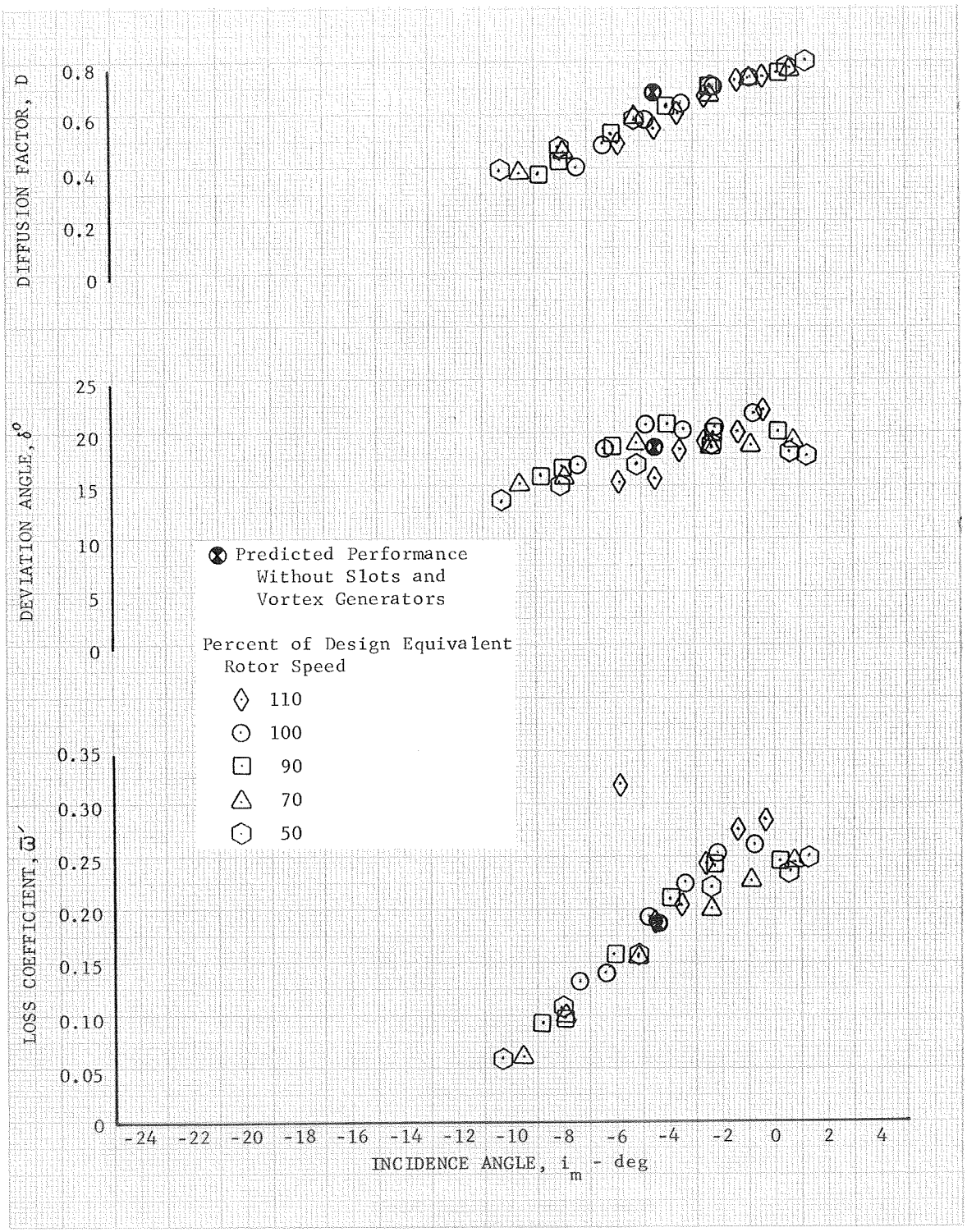

Figure 19g. Unslotted Rotor 4 Blade Element Performance, 85% Span From Tip

DF 83389

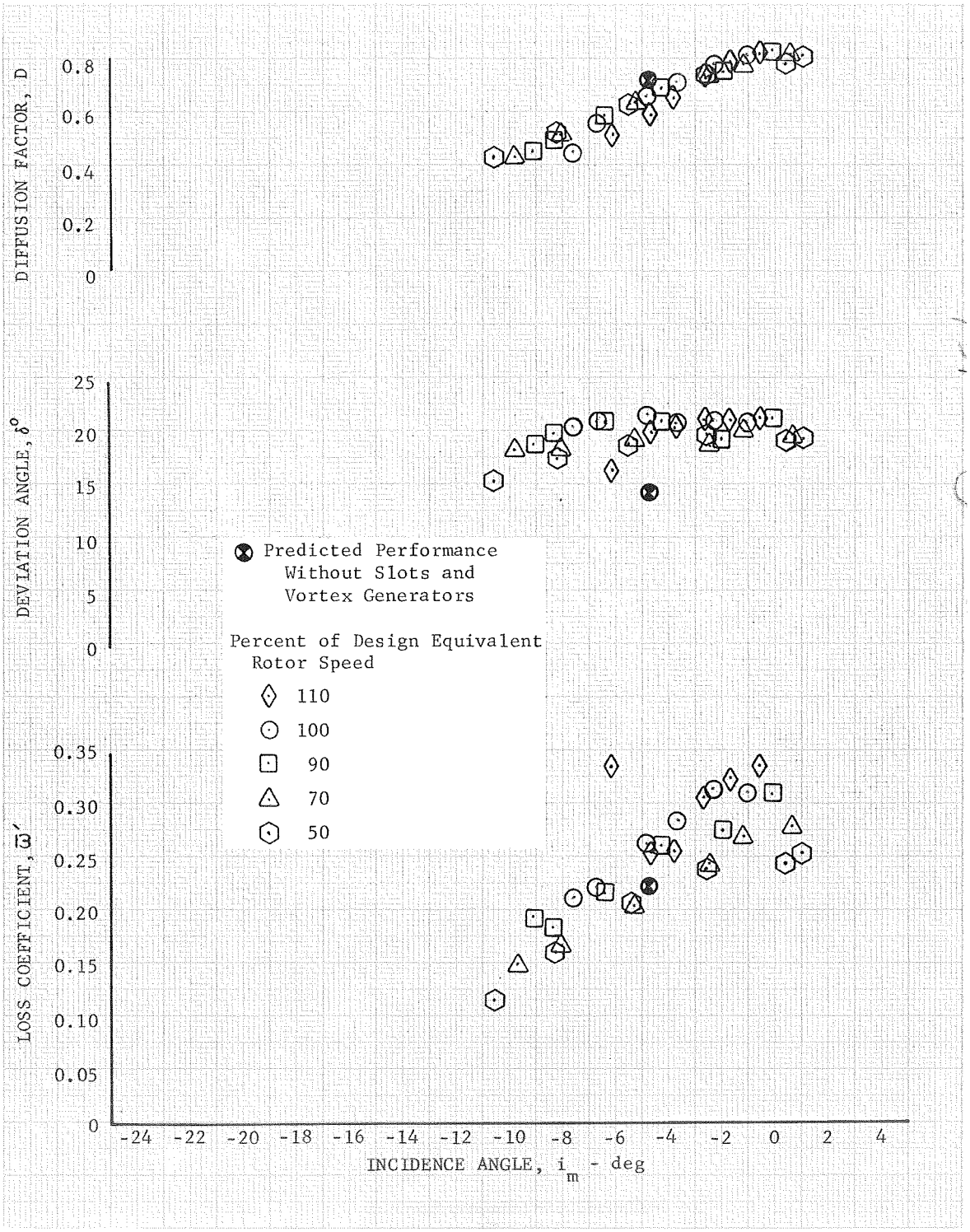

Figure 19h. Unslotted Rotor 4 Blade Element Performance, 90% Span From Tip

DF 83390

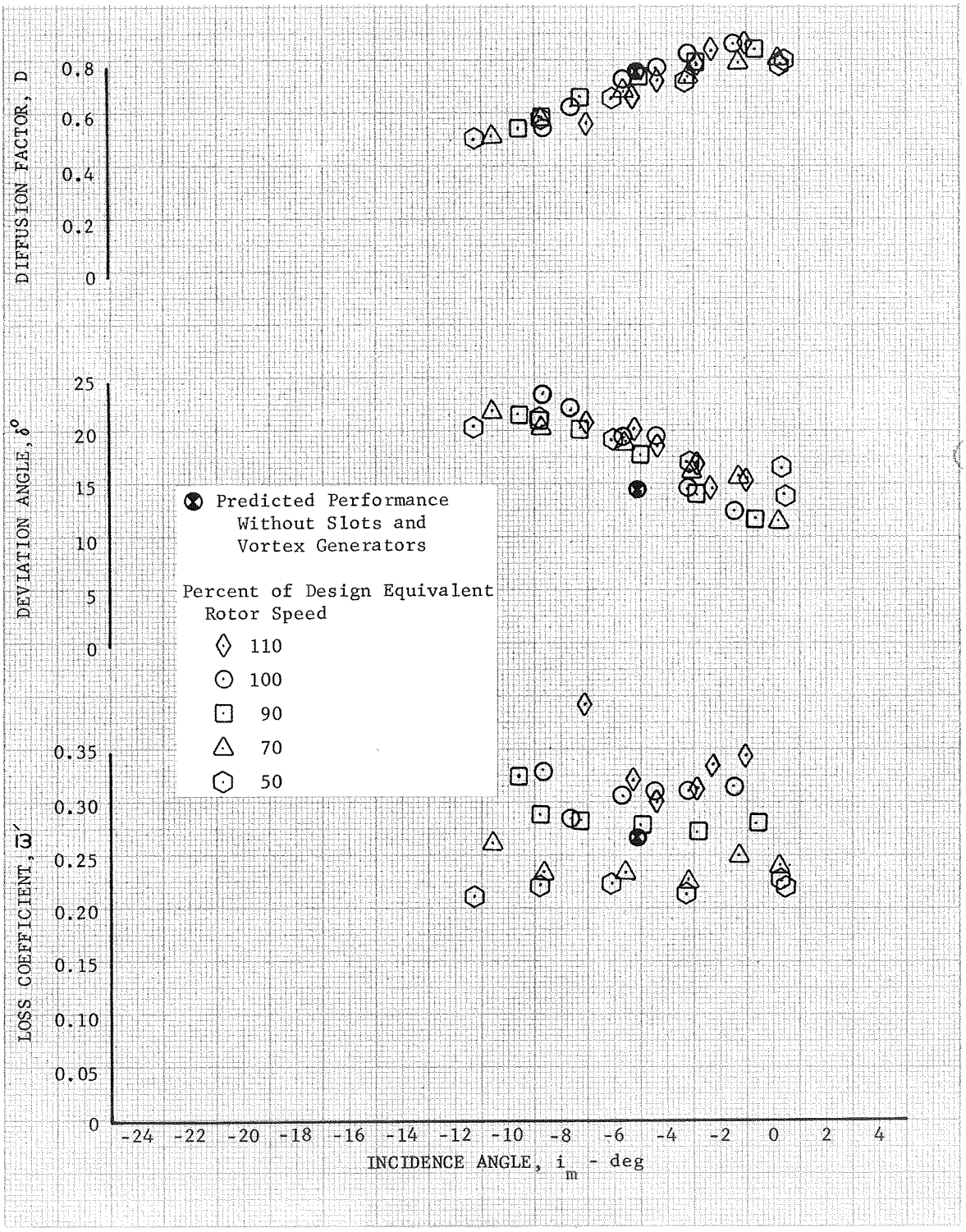

Figure 19i. Unslotted Rotor 4 Blade Element Performance, 95% Span From Tip

DF 83391

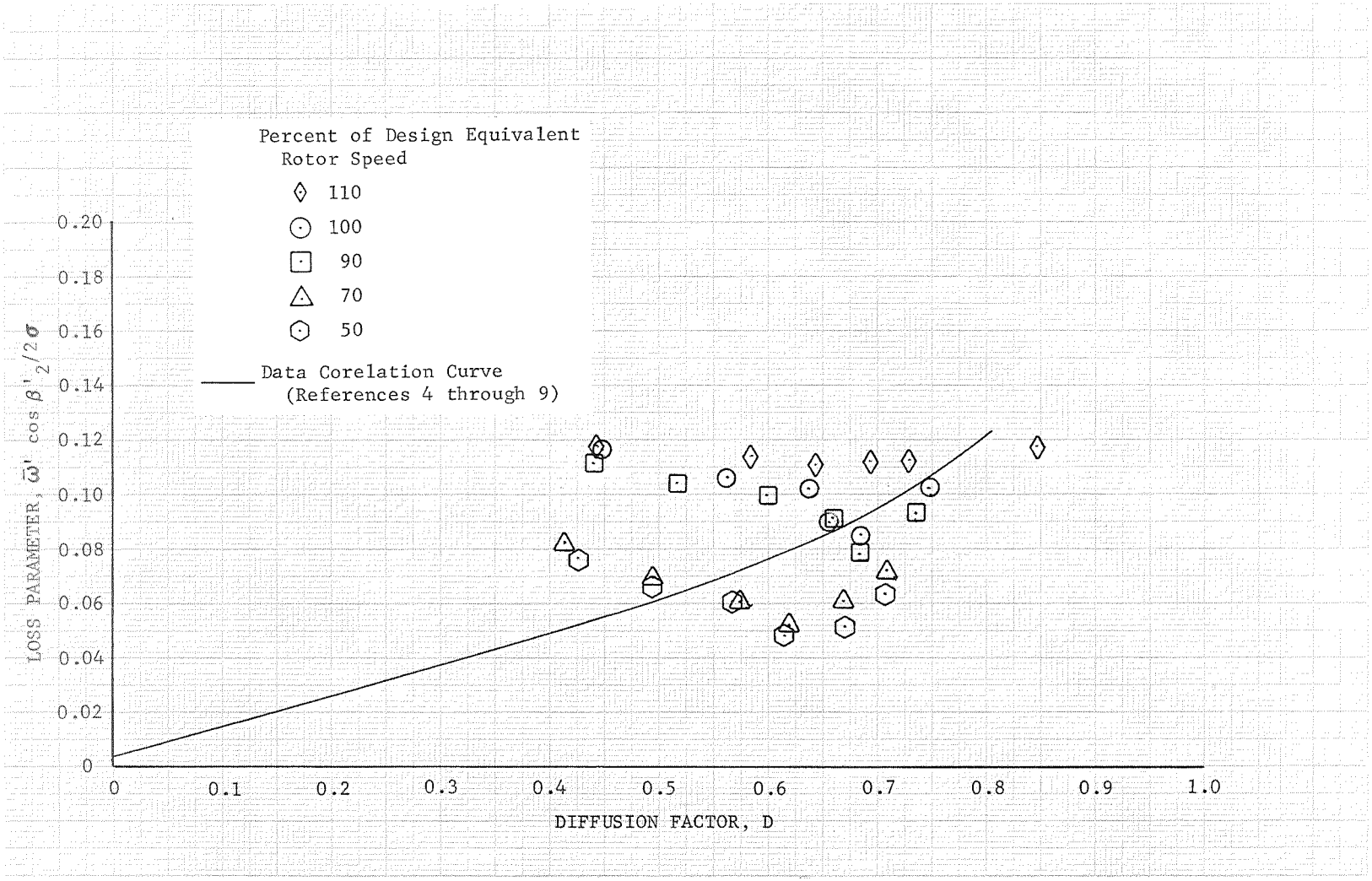

Figure 20a. Rotor 4 Loss Parameter vs Diffusion Factor, 10% Span From Tip

DF 83392

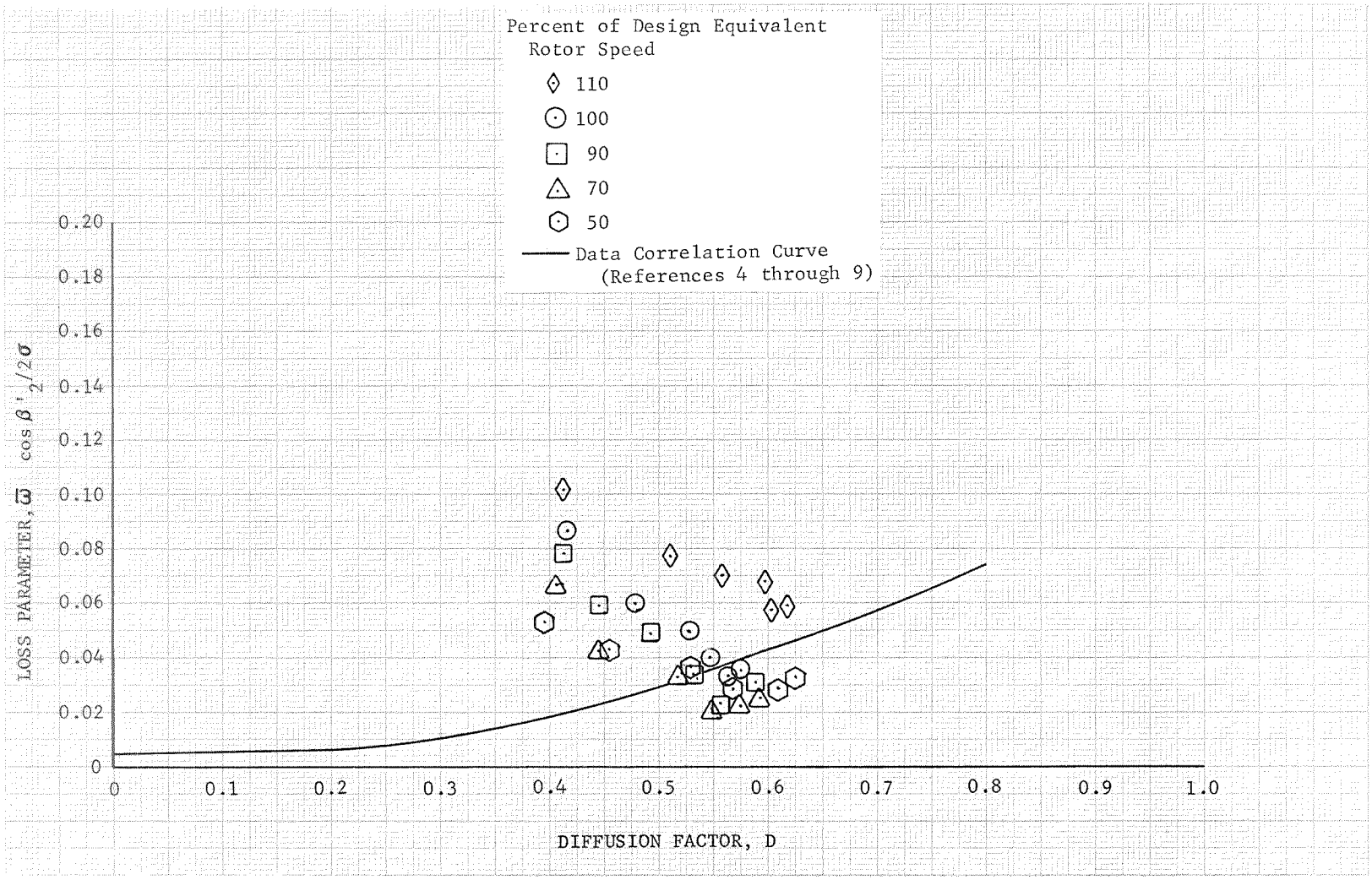

Figure 20b. Rotor 4 Loss Parameter vs Diffusion Factor, 30% Span From Tip

DF 83393

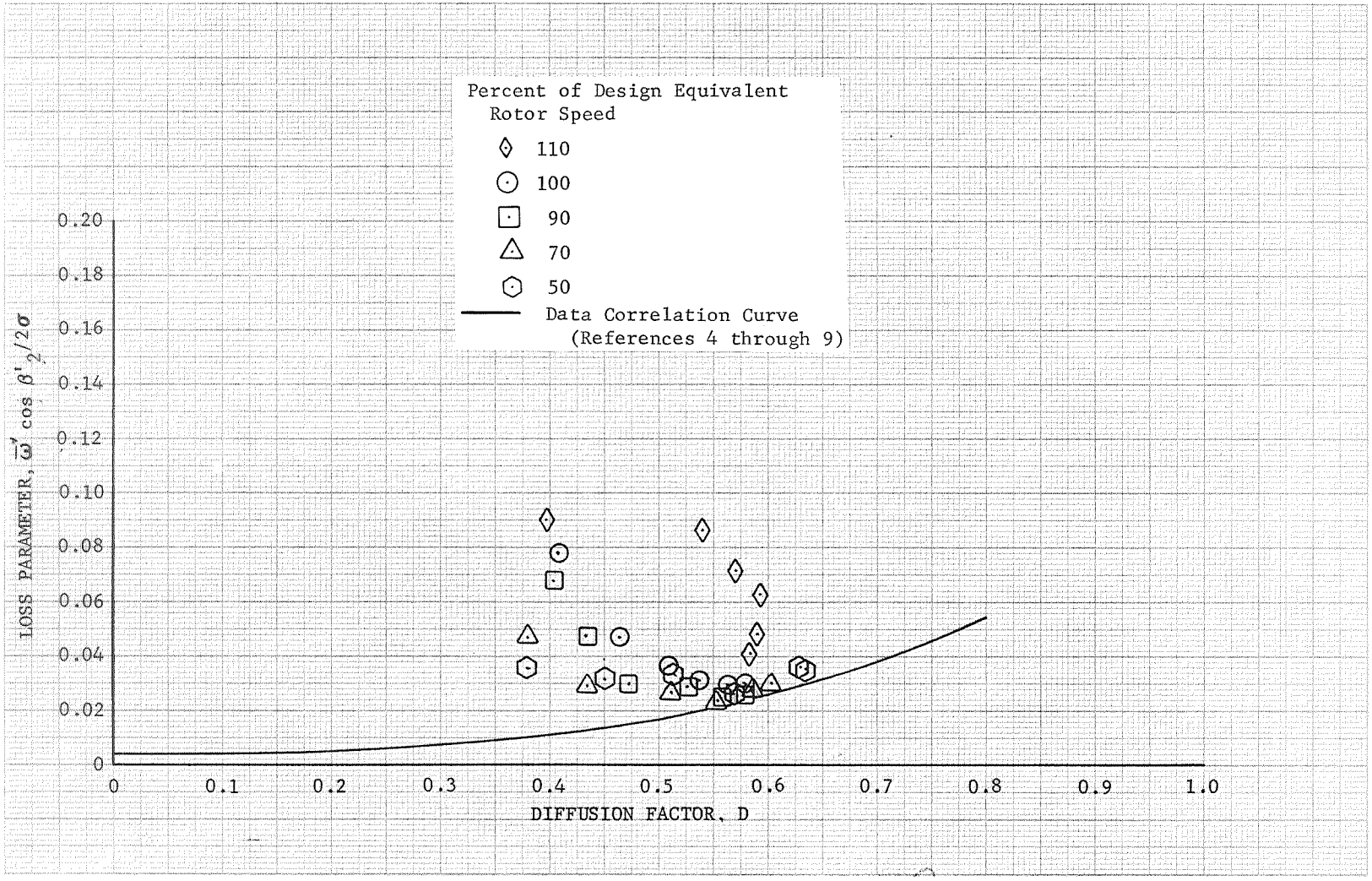

Figure 20c. Rotor 4 Loss Parameter vs Diffusion Factor, 50% Span From Tip

DF 83394

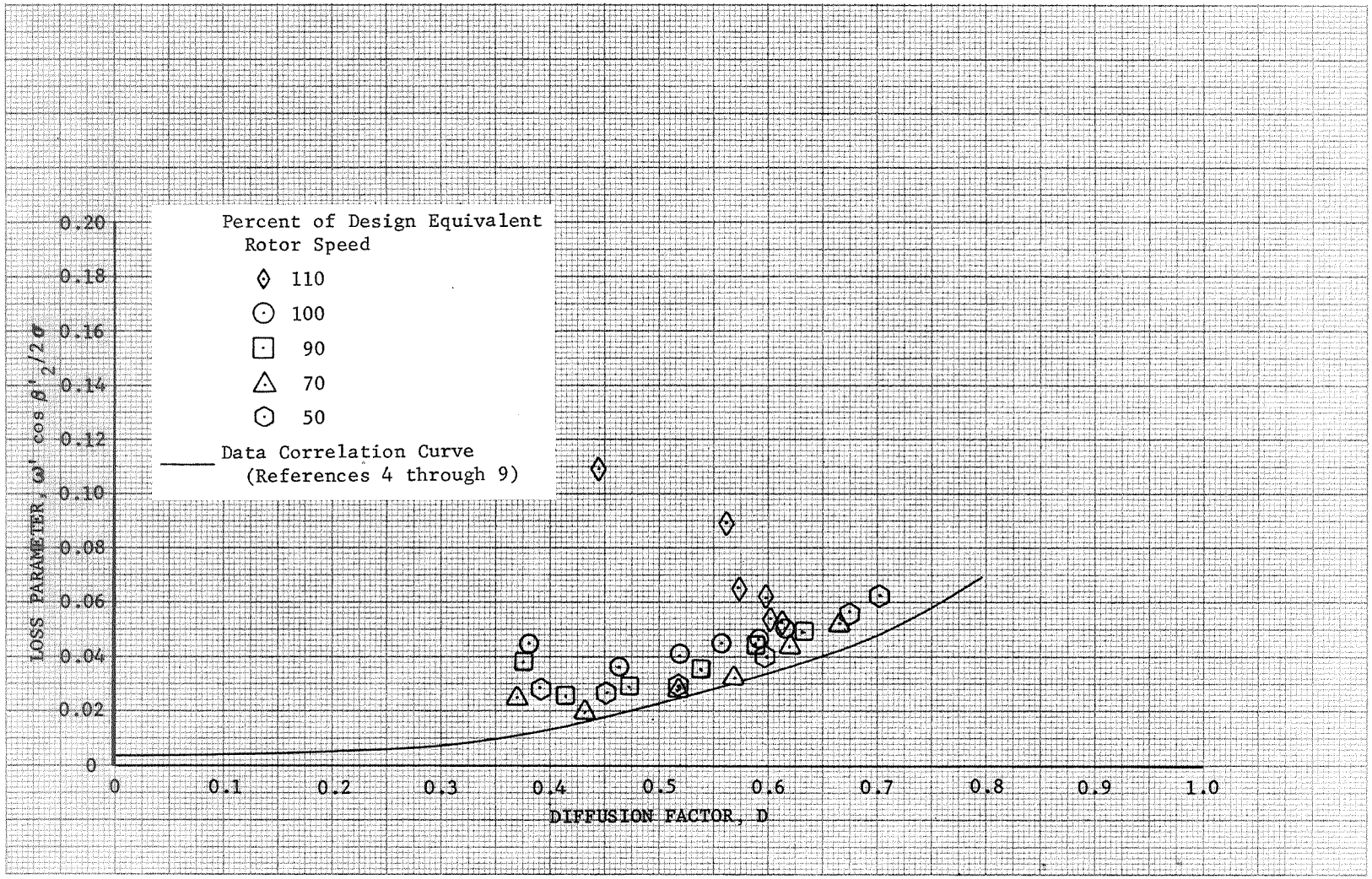

Figure 20d. Rotor 4 Loss Parameter vs Diffusion Factor, 70% Span From Tip

DF 83395

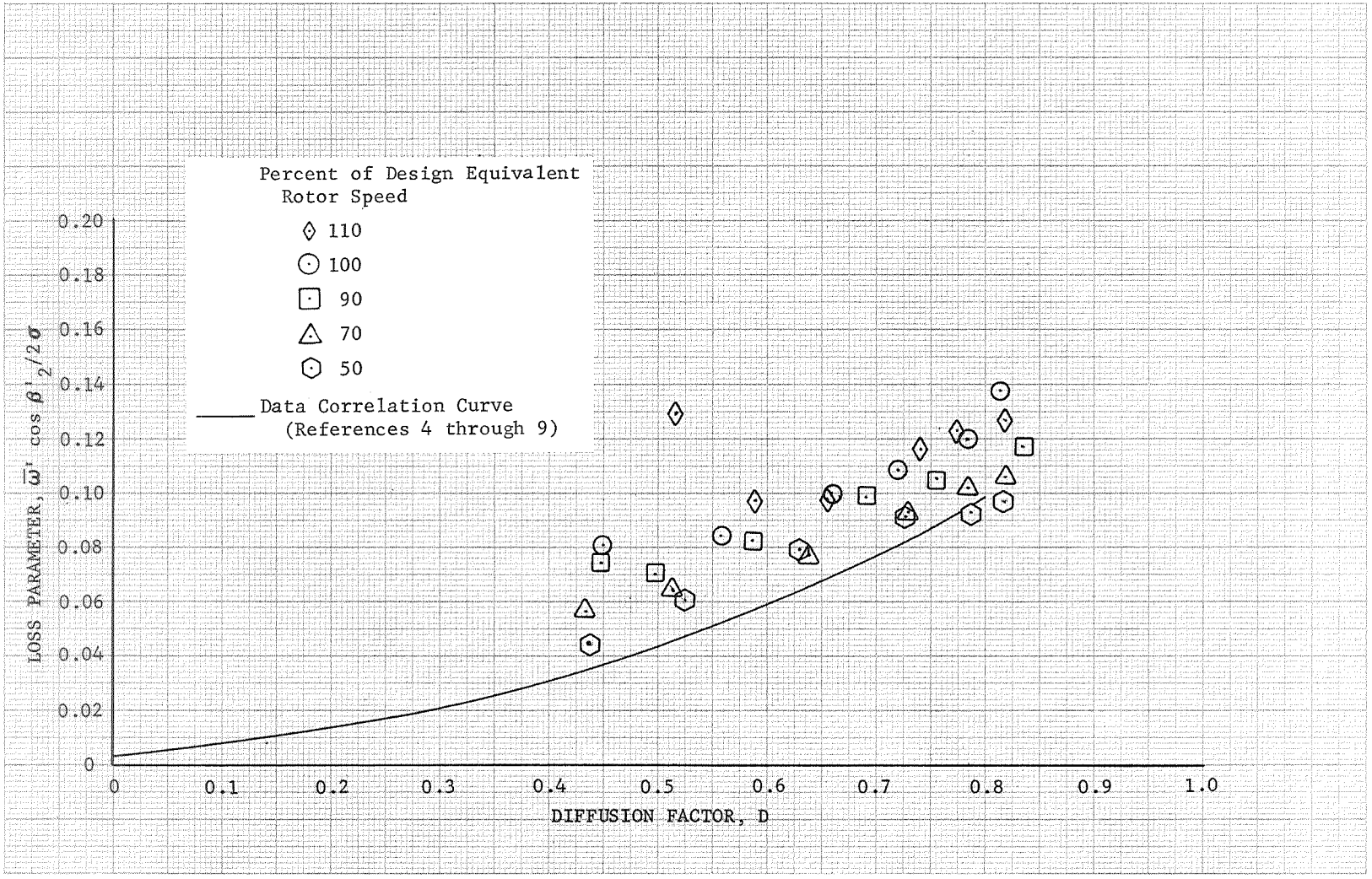

Figure 20e. Rotor 4 Loss Parameter vs Diffusion Factor, 90% Span From Tip

DF 83396

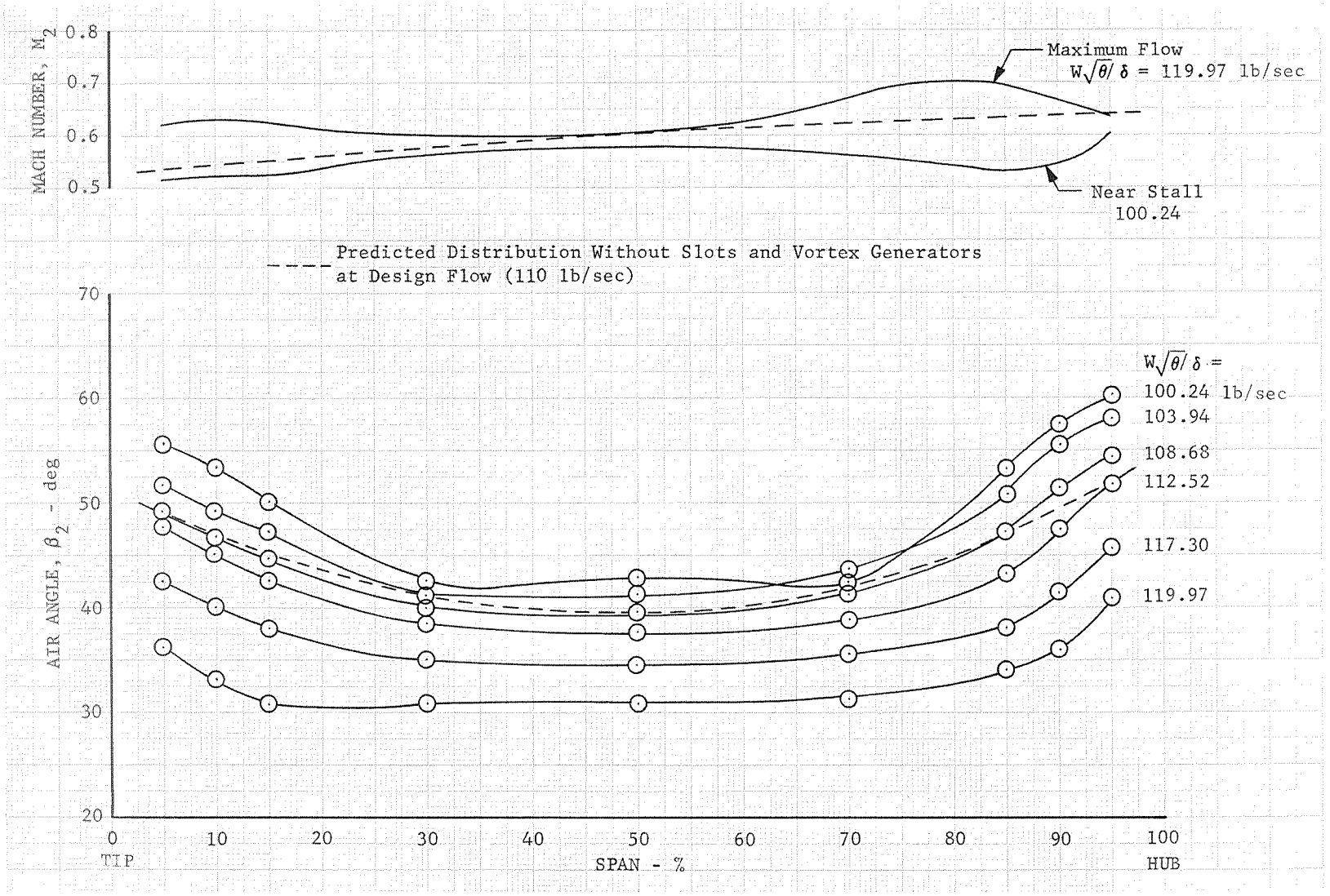

Figure 21. Stator 4 Inlet Air Angle and Mach No. Distribution Design Environment Rotor Speed DF 83413

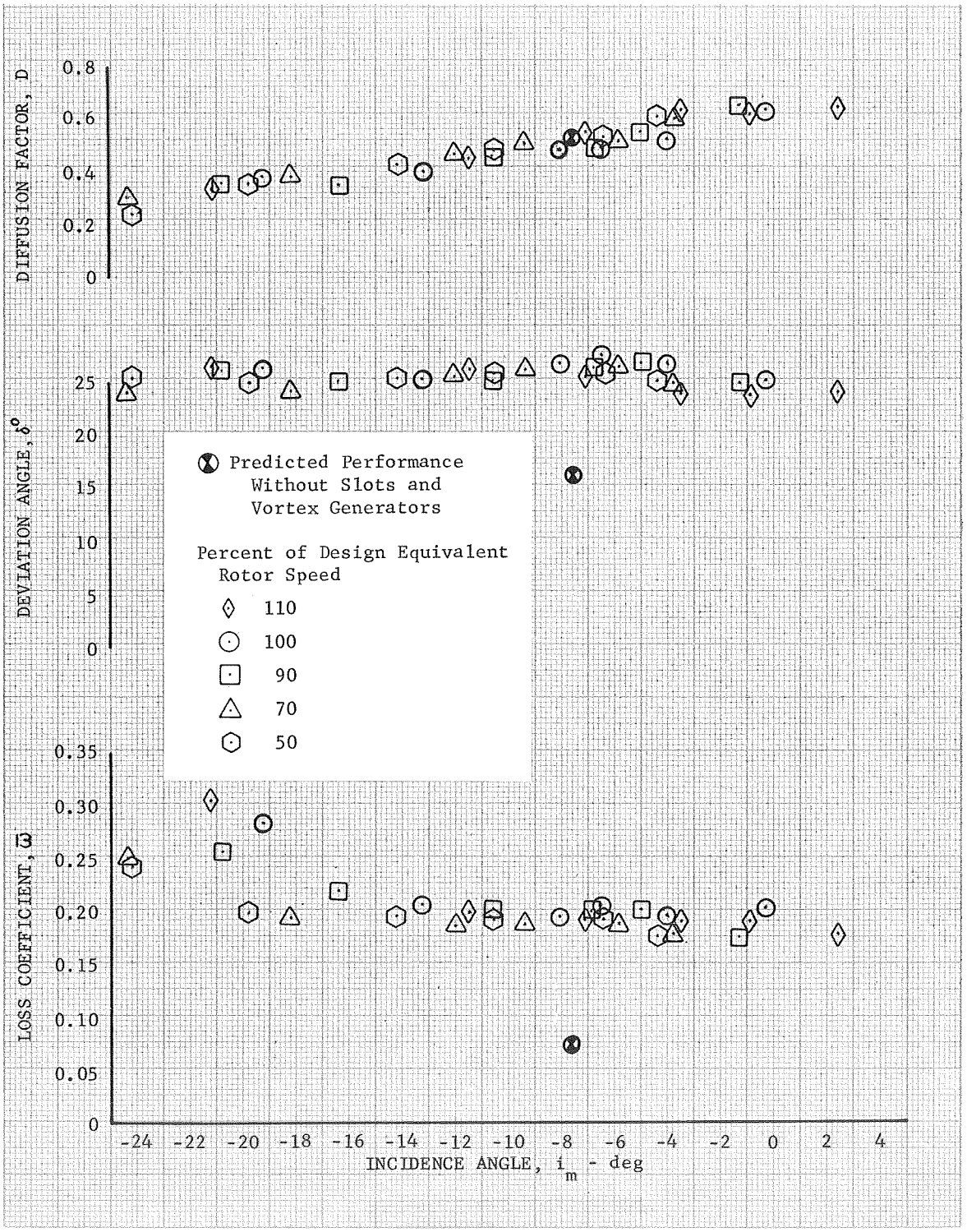

Figure 22a. Unslotted Stator 4 Blade Element Performance, 5% Span From Tip

DF 83397

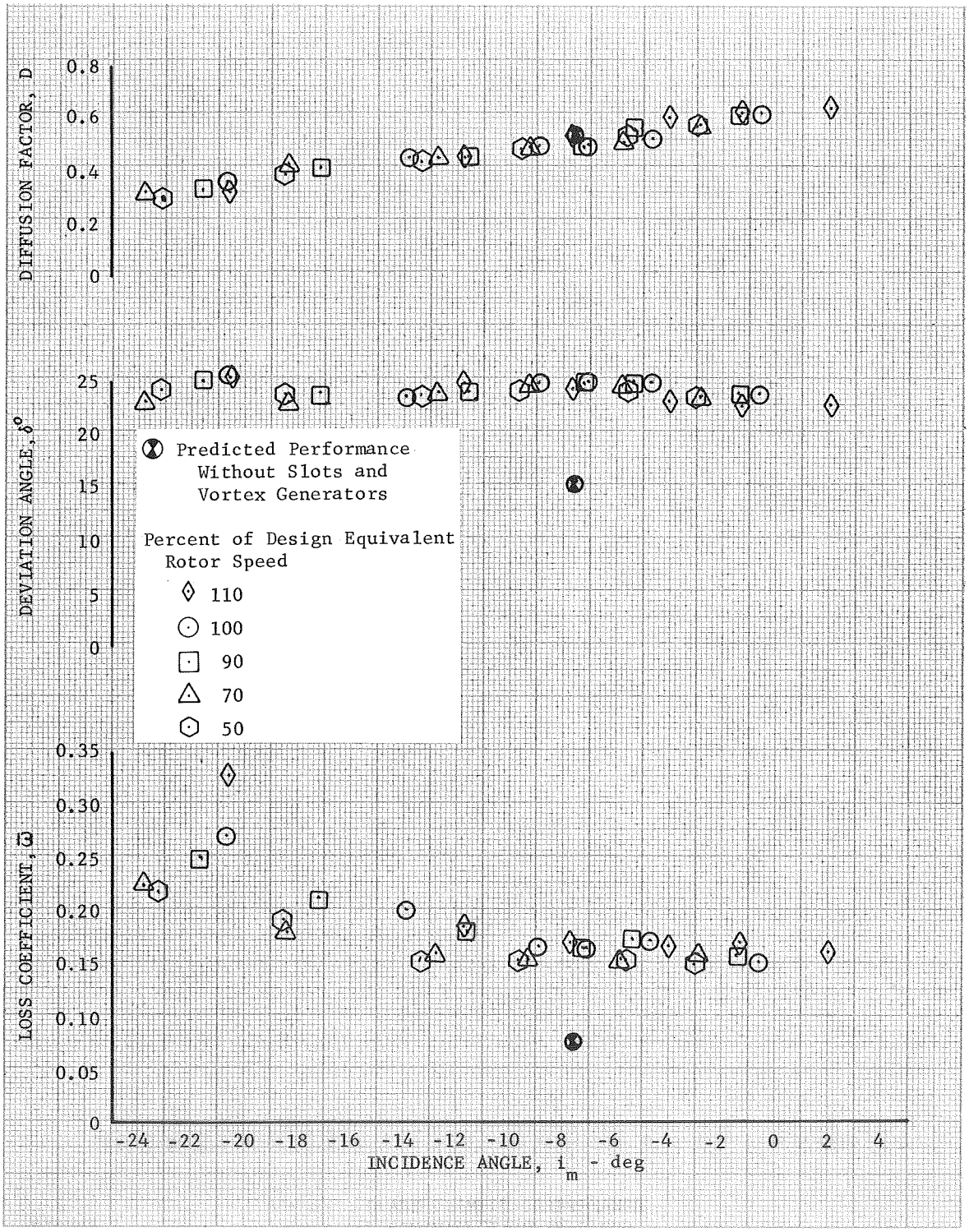

Figure 22b. Unslotted Stator 4 Blade Element Performance, 10% Span From Tip

DF 83398

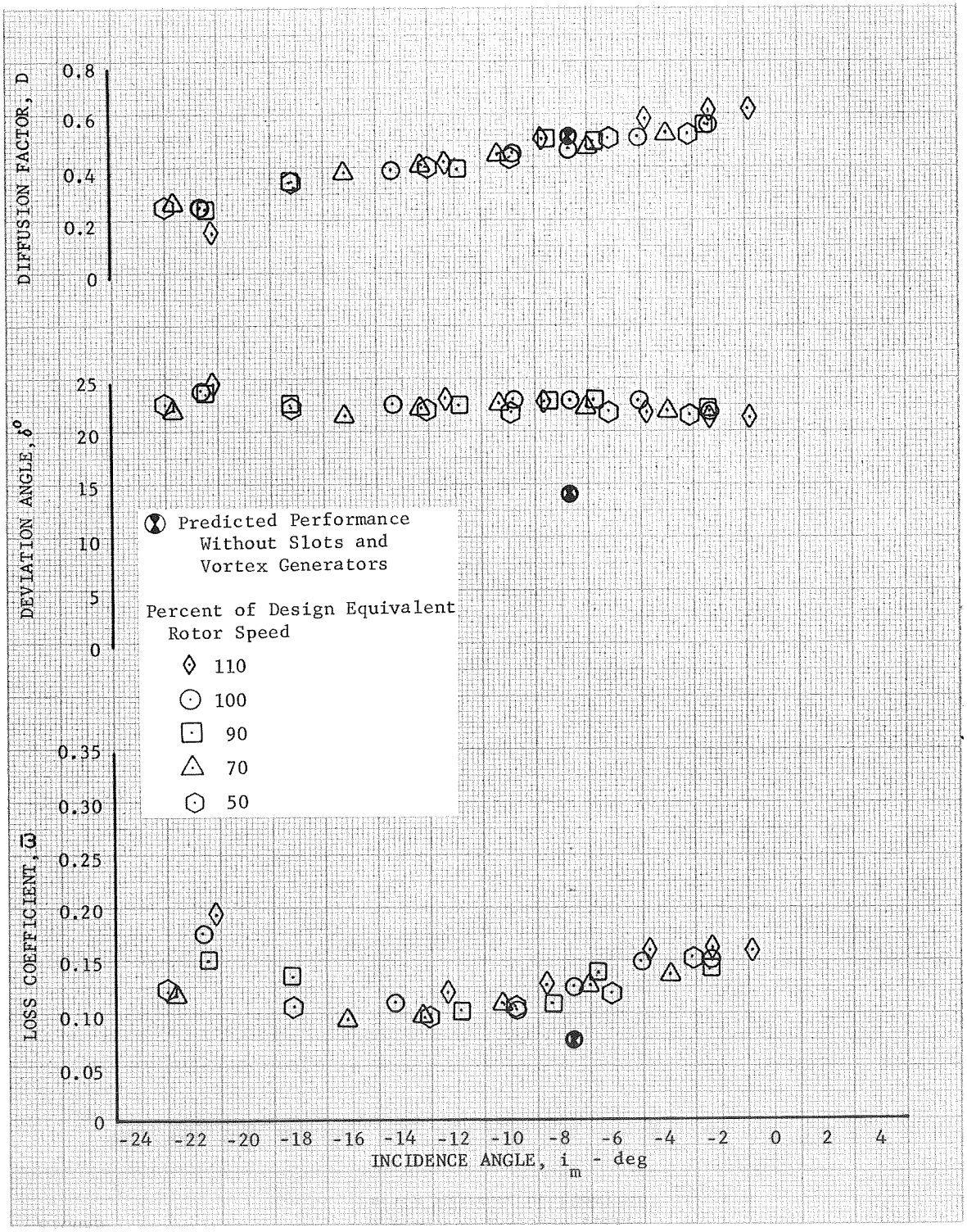

Figure 22c. Unslotted Stator 4 Blade Element Performance, 15% Span From Tip DF 83399

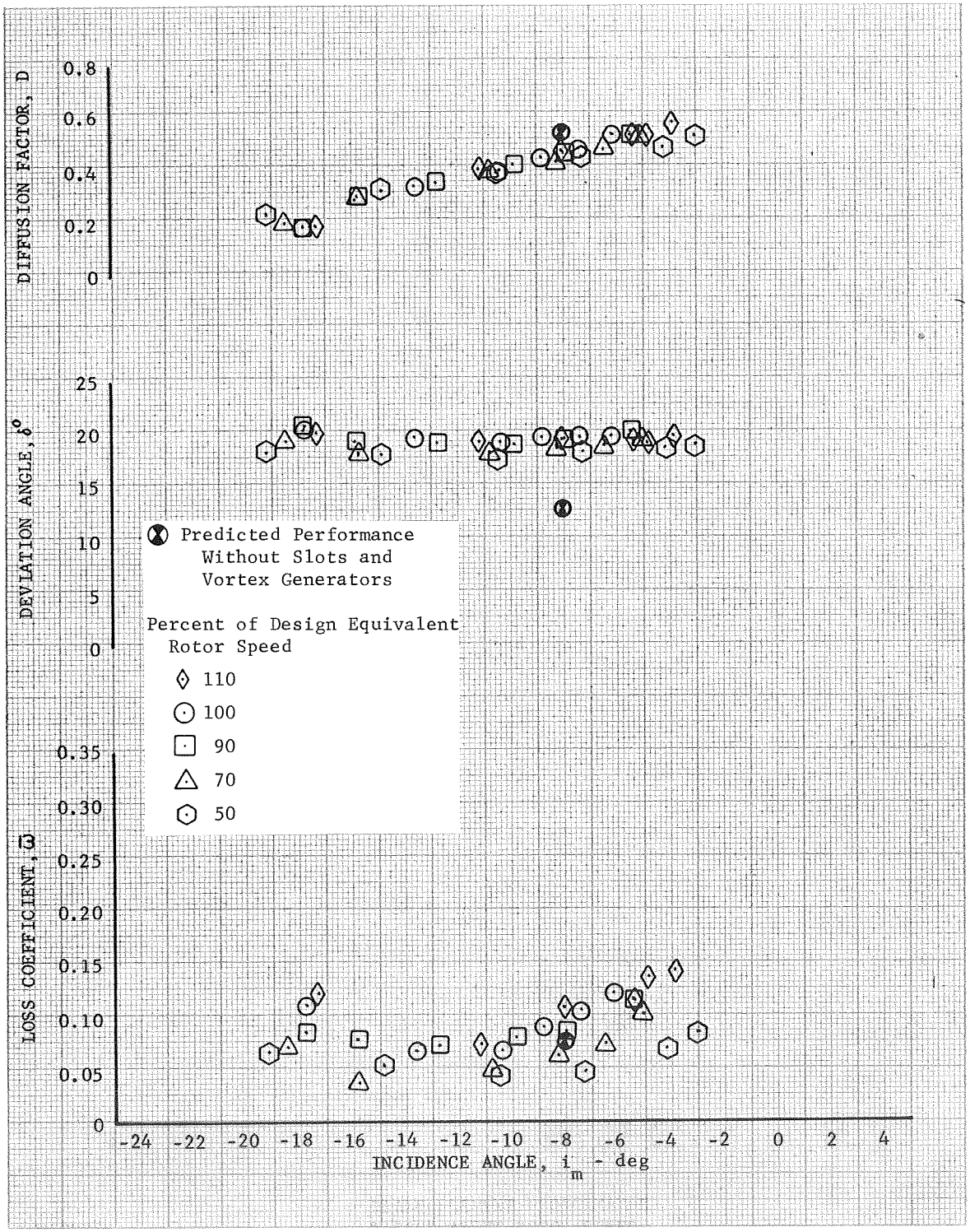

Figure 22d. Unslotted Stator 4 Blade Element Performance, 30% Span From Tip

DF 83400

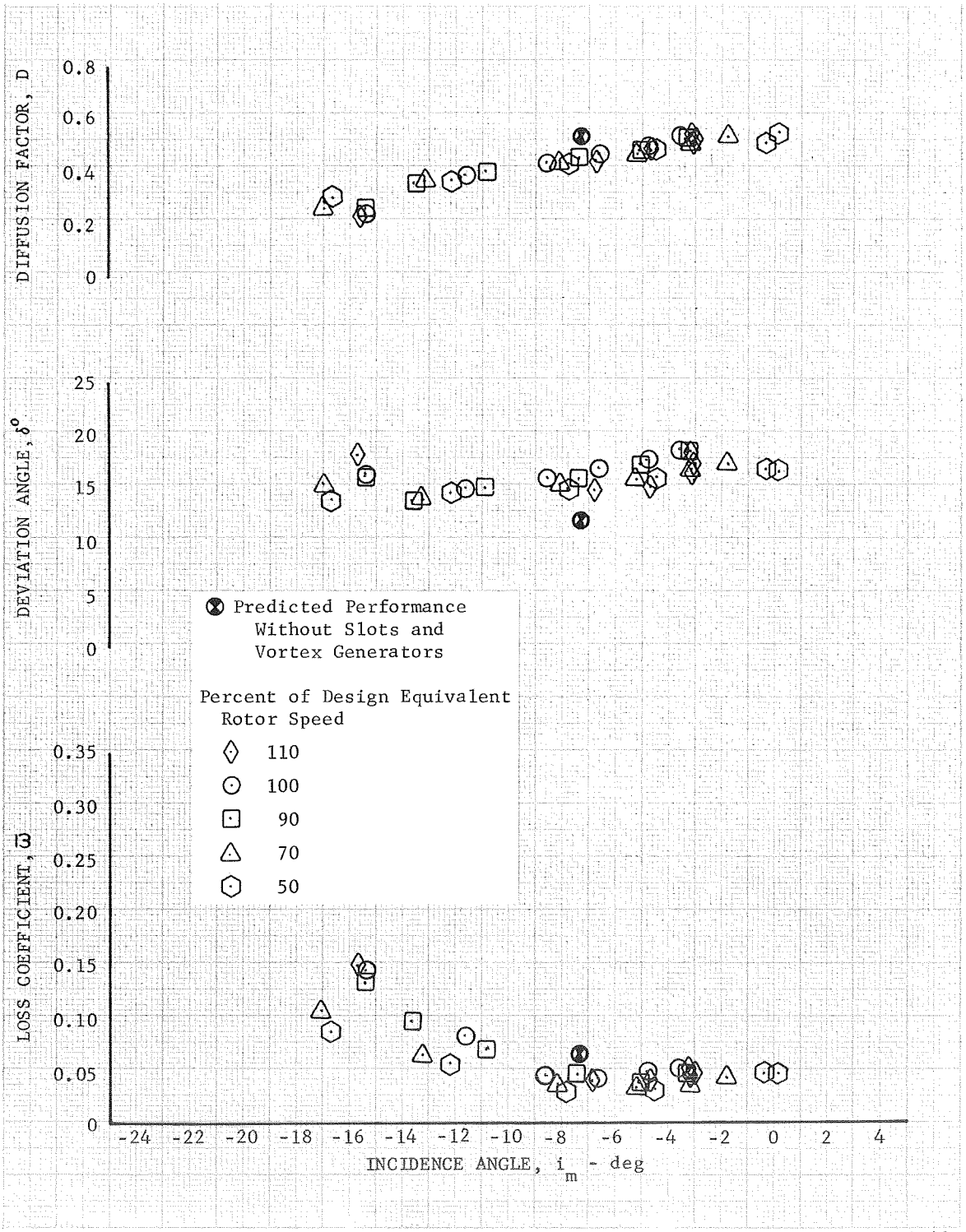

Figure 22e. Unslotted Stator 4 Blade Element Performance, 50% Span From Tip DF 83401

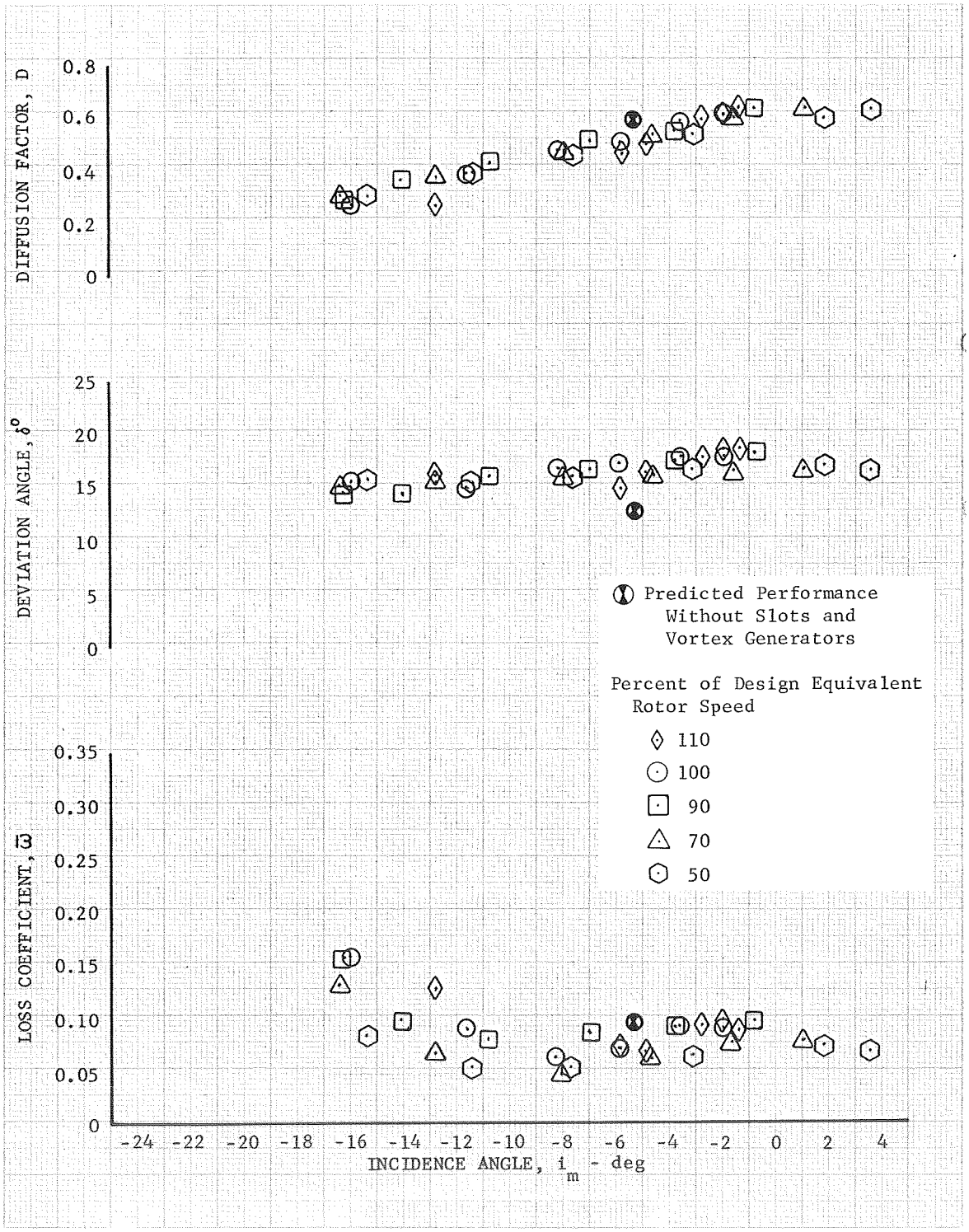

Figure 22f. Unslotted Stator 4 Blade Element Performance, 70% Span From Tip

DF 83402

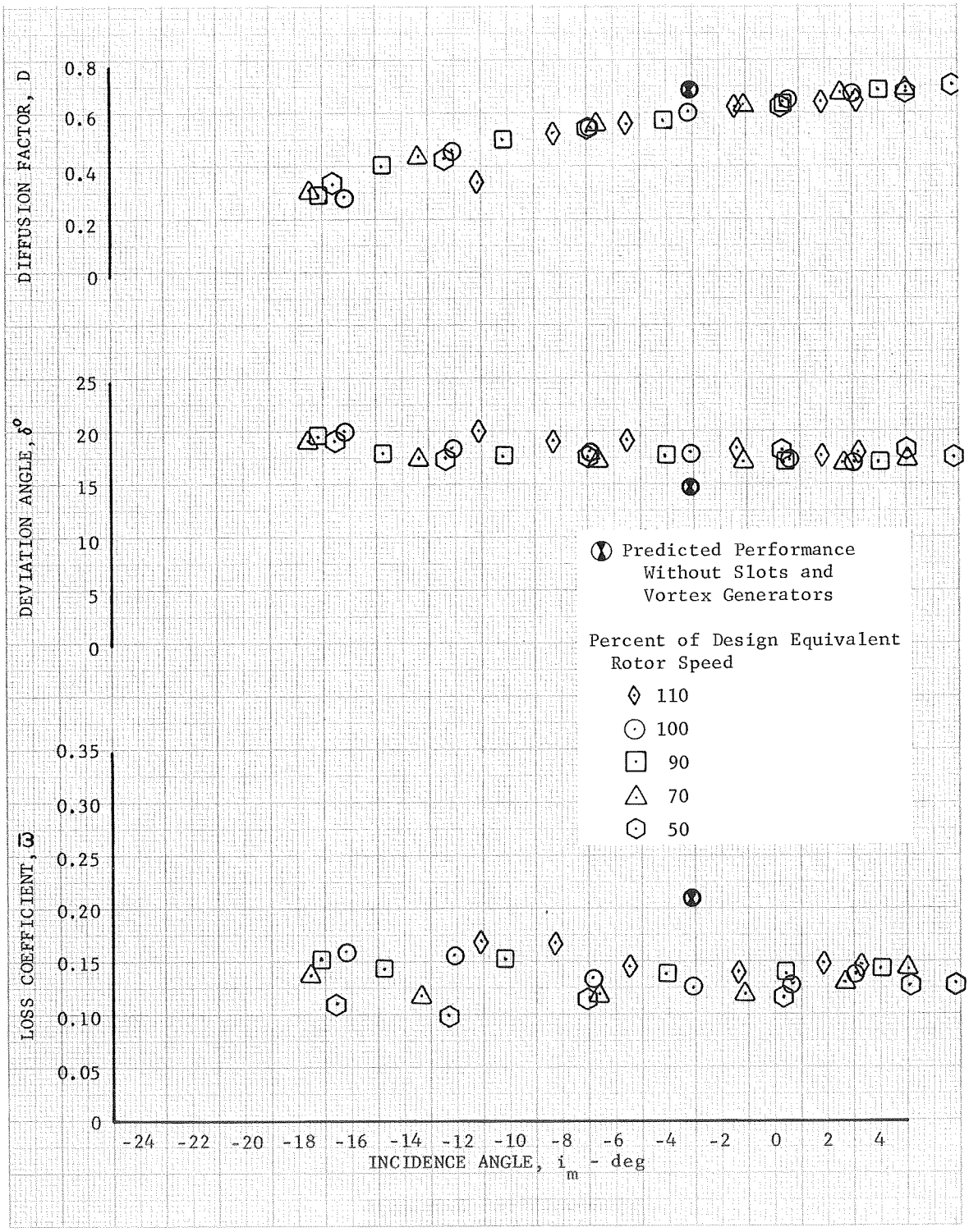

Figure 22g. Unslotted Stator 4 Blade Element Performance, 85% Span From Tip DF 83403

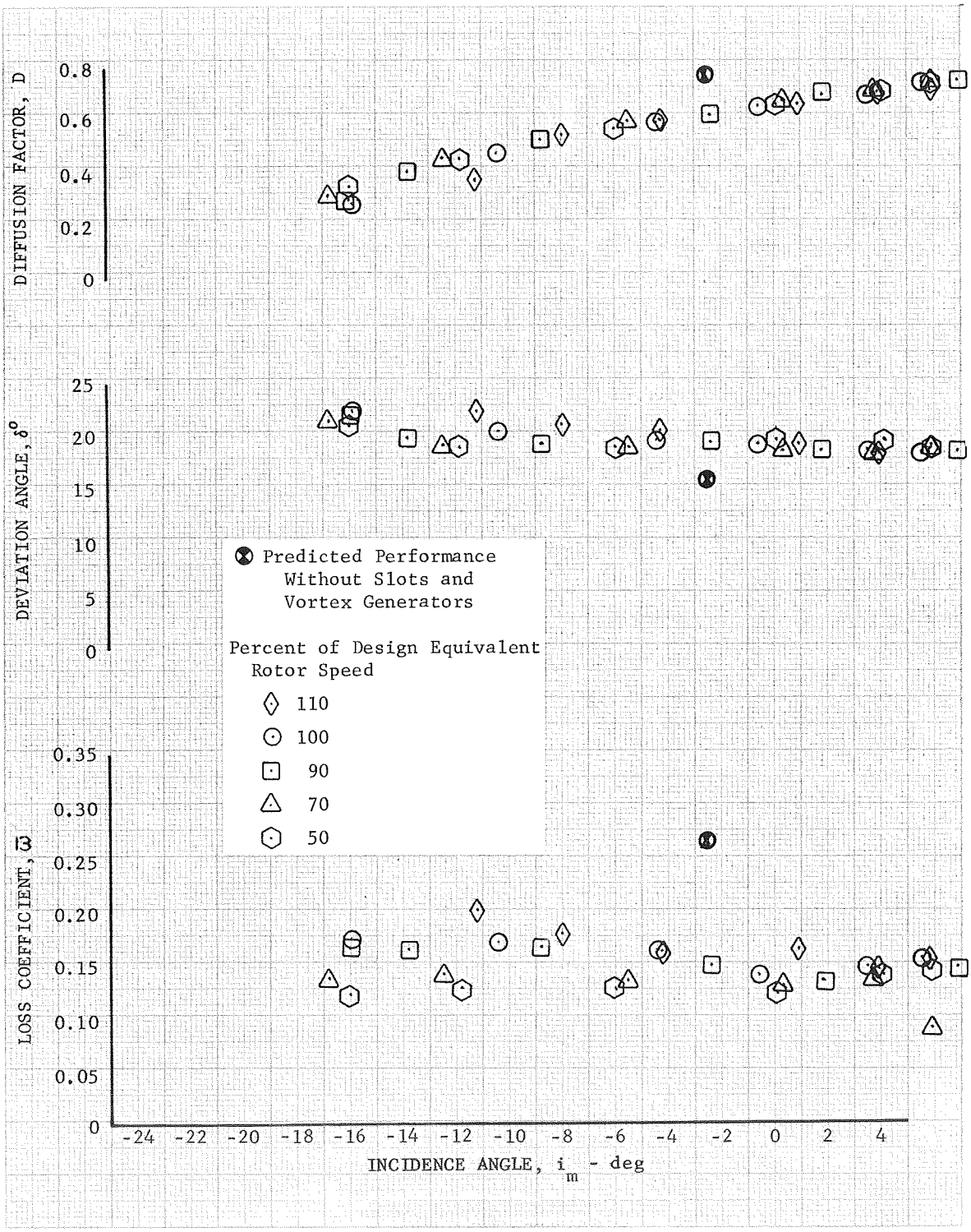

Figure 22h. Unslotted Stator 4 Blade Element Performance, 90% Span From Tip DF 83404

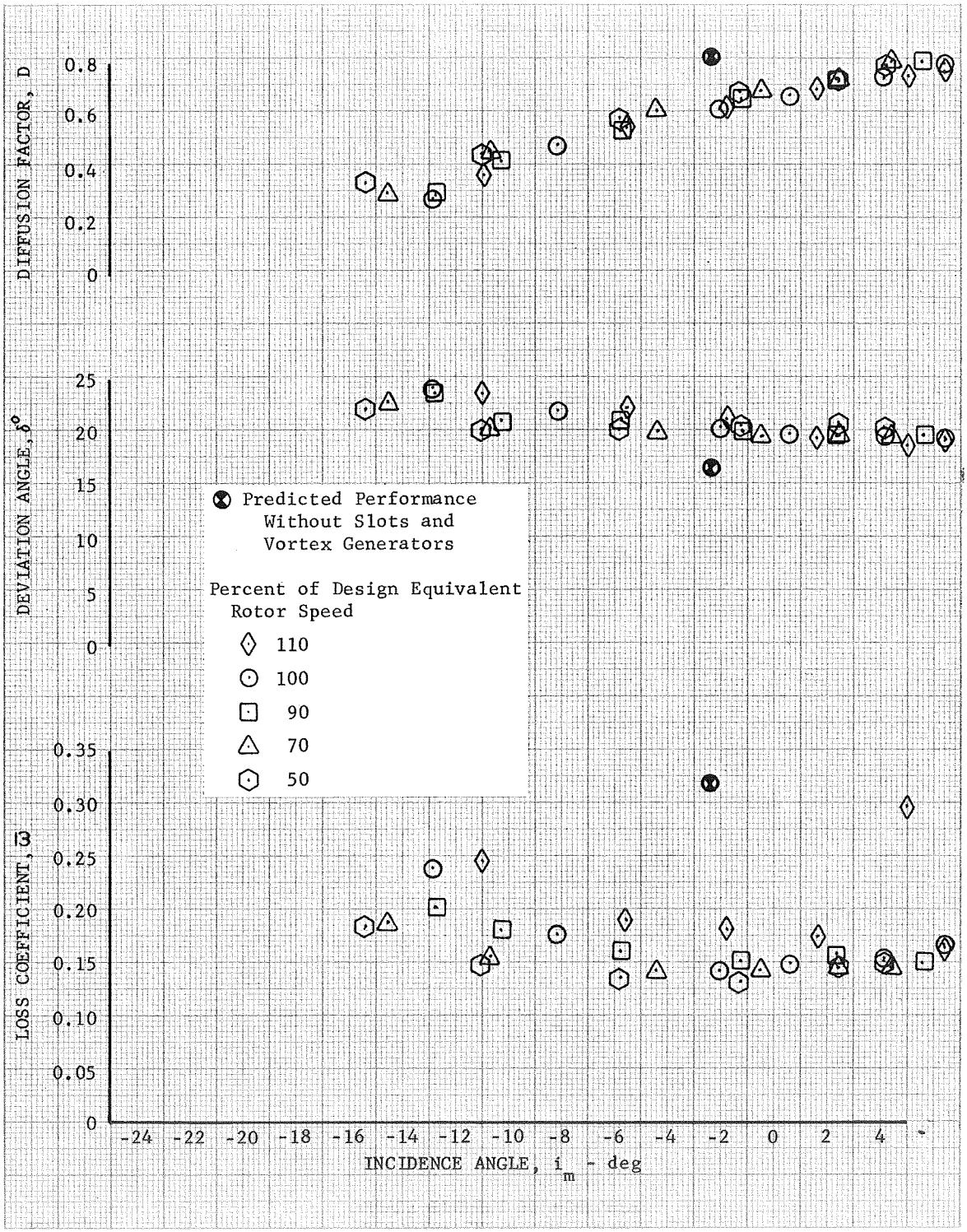

Figure 22i. Unslotted Stator 4 Blade Element Performance, 95% Span From Tip

DF 83405

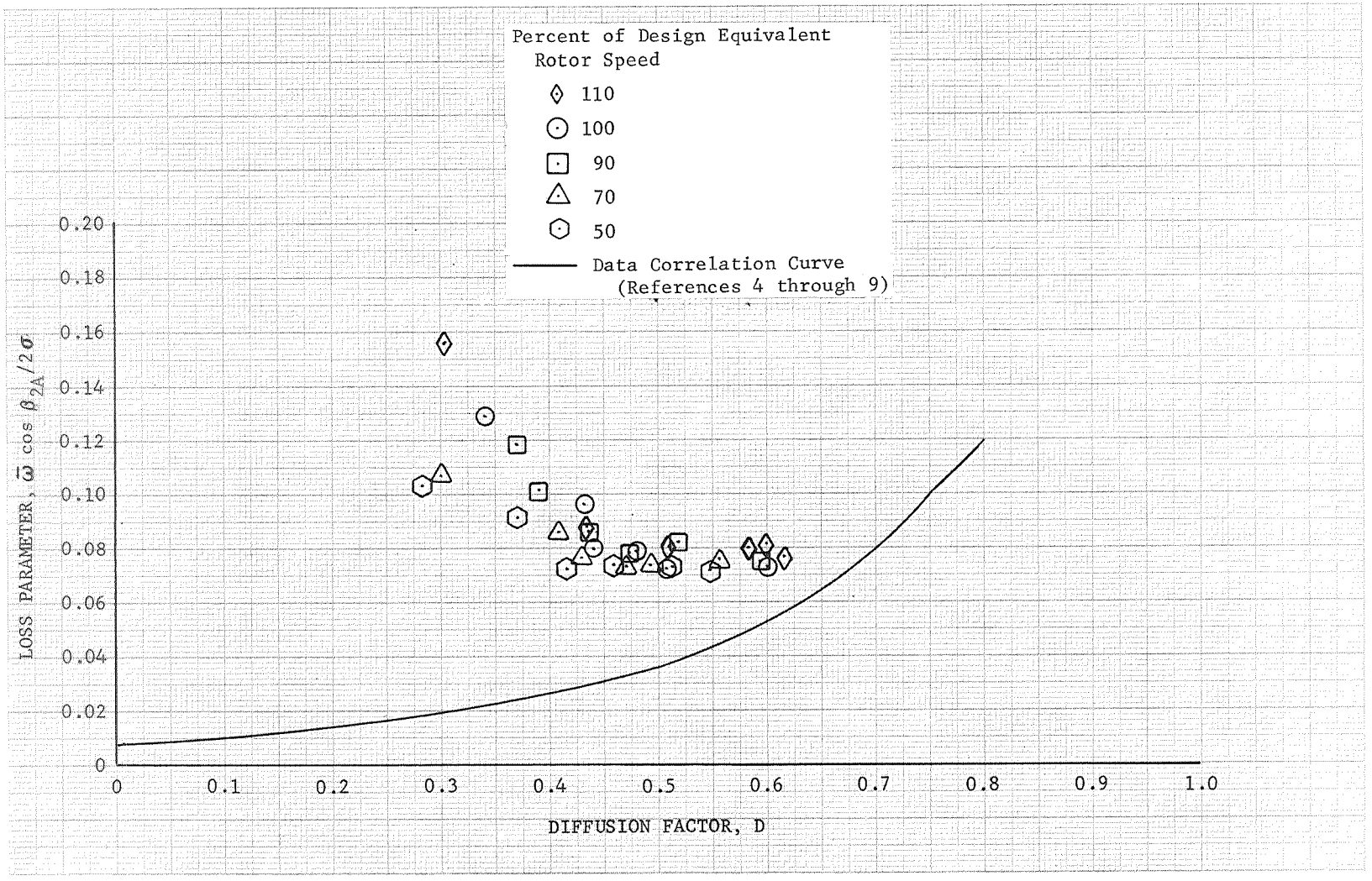

Figure 23a. Stator 4 Loss Parameter vs Diffusion Factor, 10% Span From Tip

DF 83406

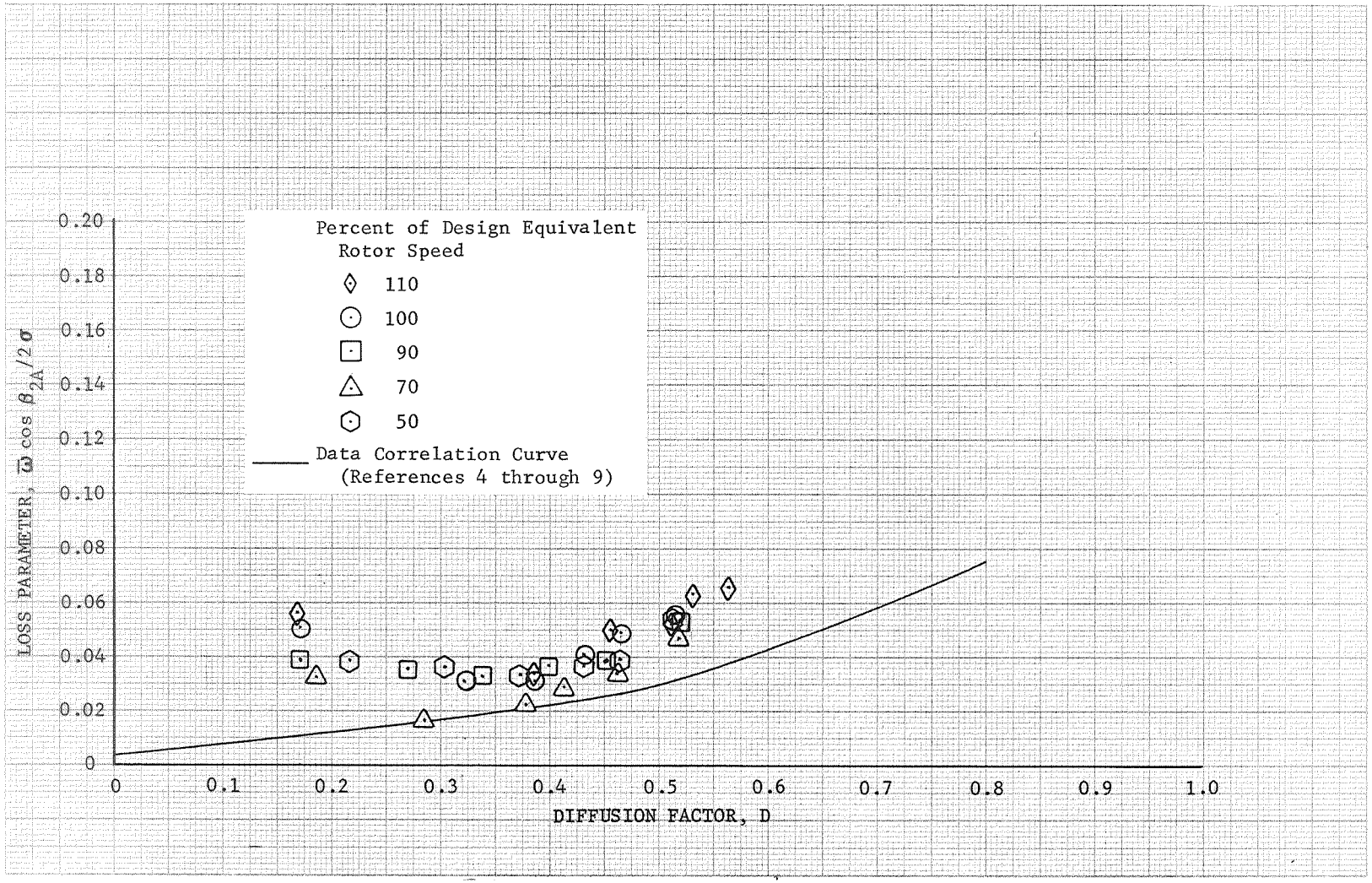

Figure 23b. Stator 4 Loss Parameter vs Diffusion Factor, 30% Span From Tip DF 83407

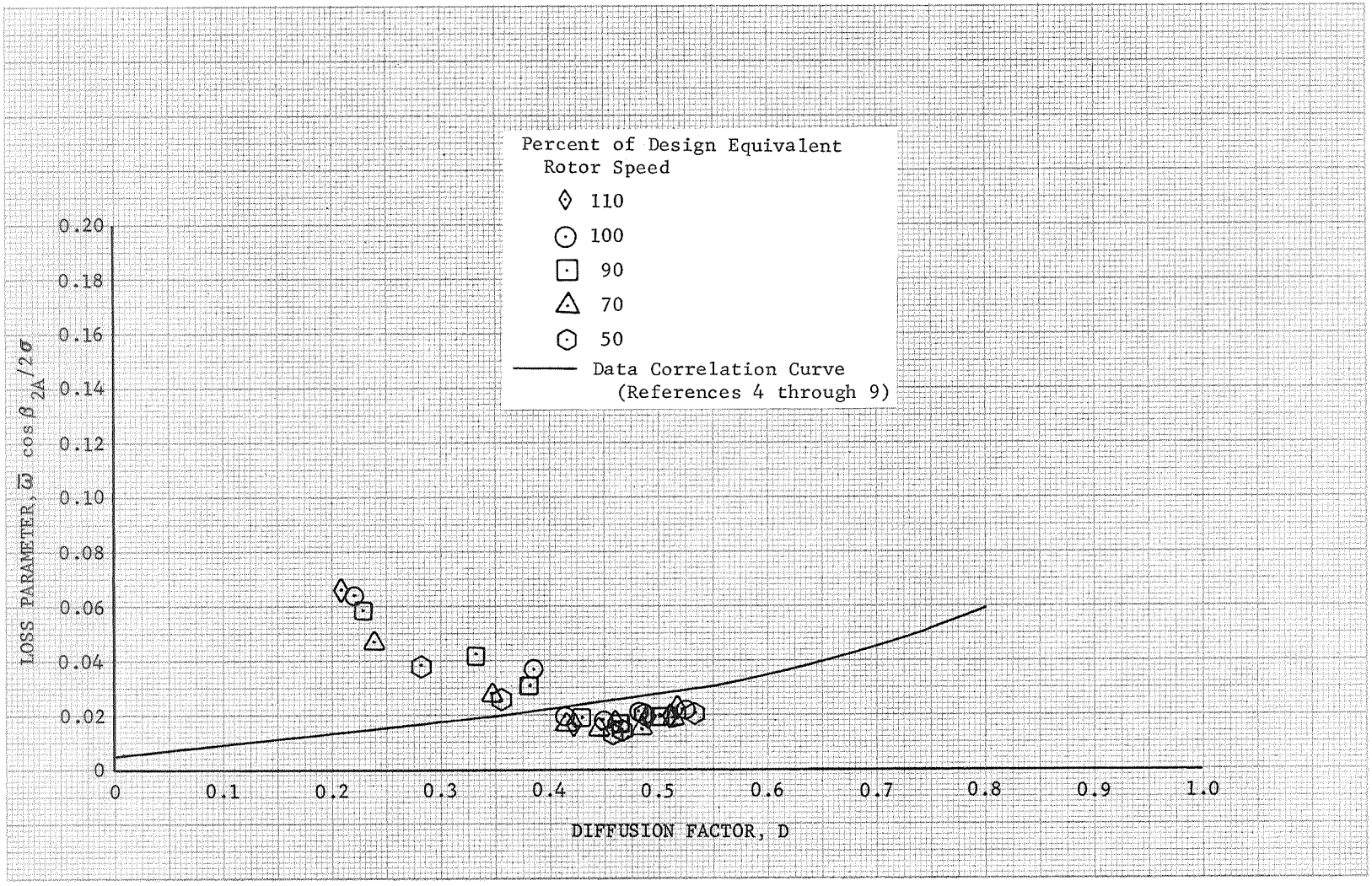

Figure 23c. Stator 4 Loss Parameter vs Diffusion Factor, 50% Span From Tip

DF 83408

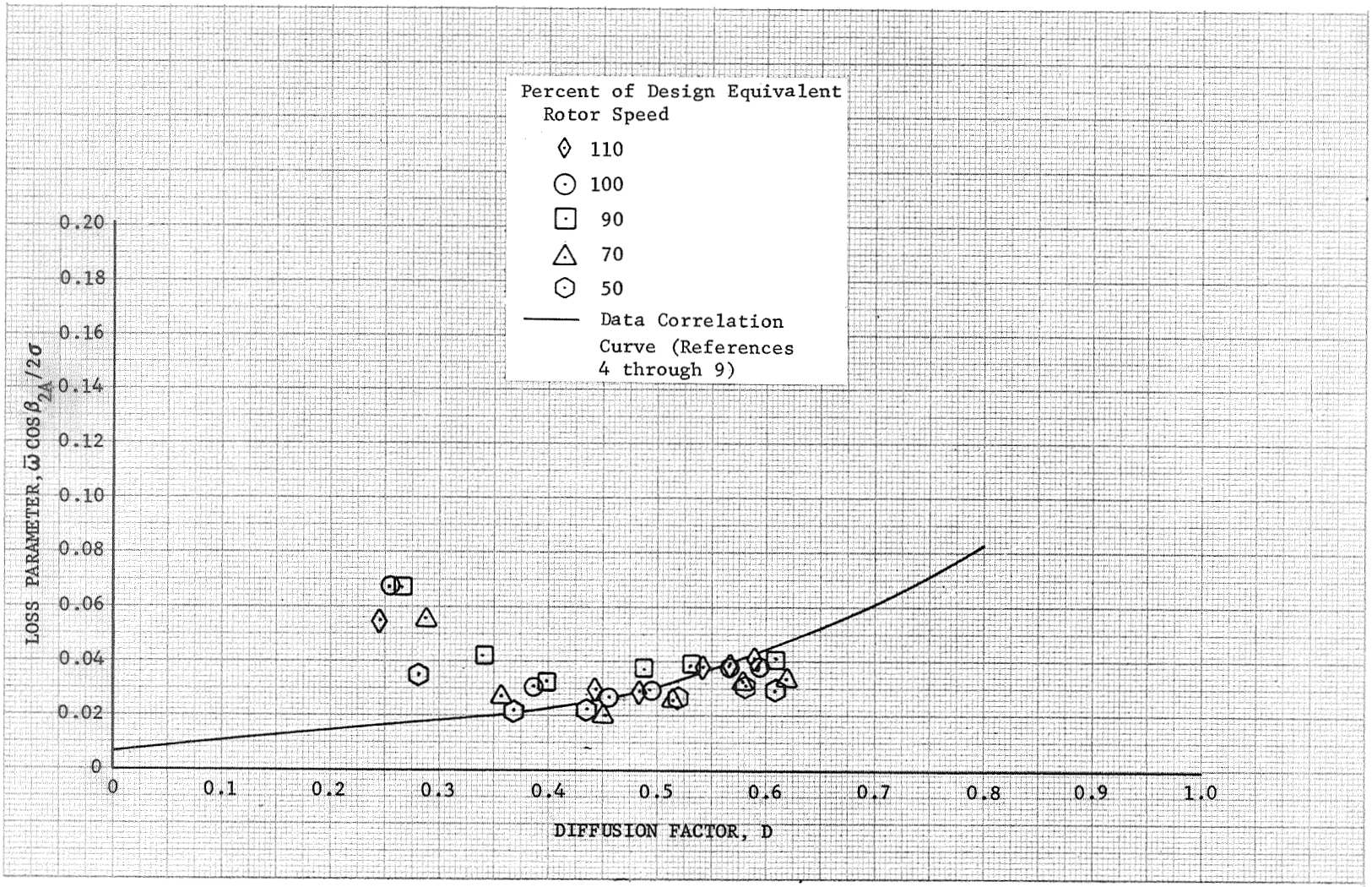

Figure 23d. Stator 4 Loss Parameter vs Diffusion Factor, 70% Span From Tip

DF 83409

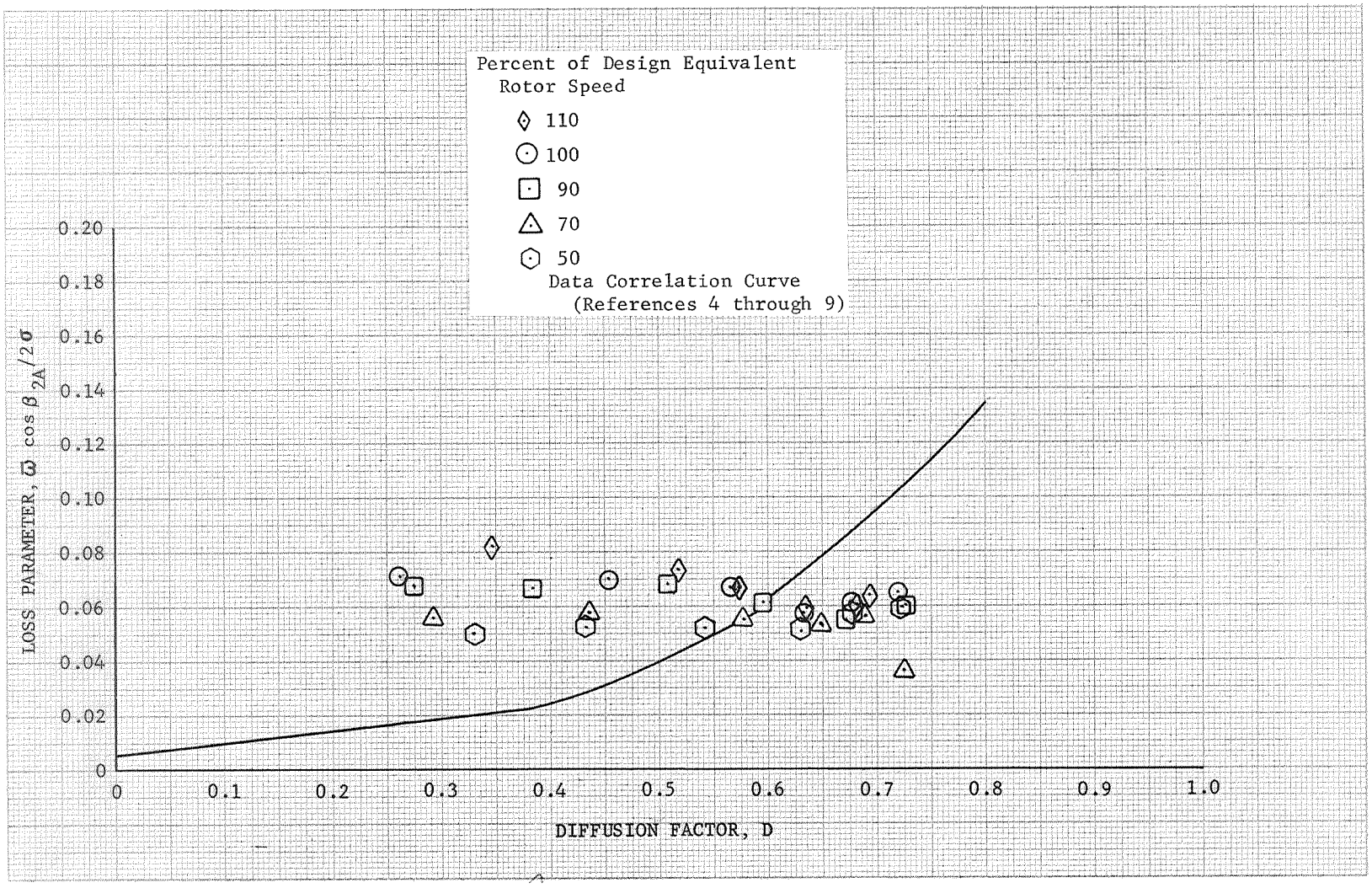

Figure 23e. Stator 4 Loss Parameter vs Diffusion Factor, 90% Span From Tip

DF 83410

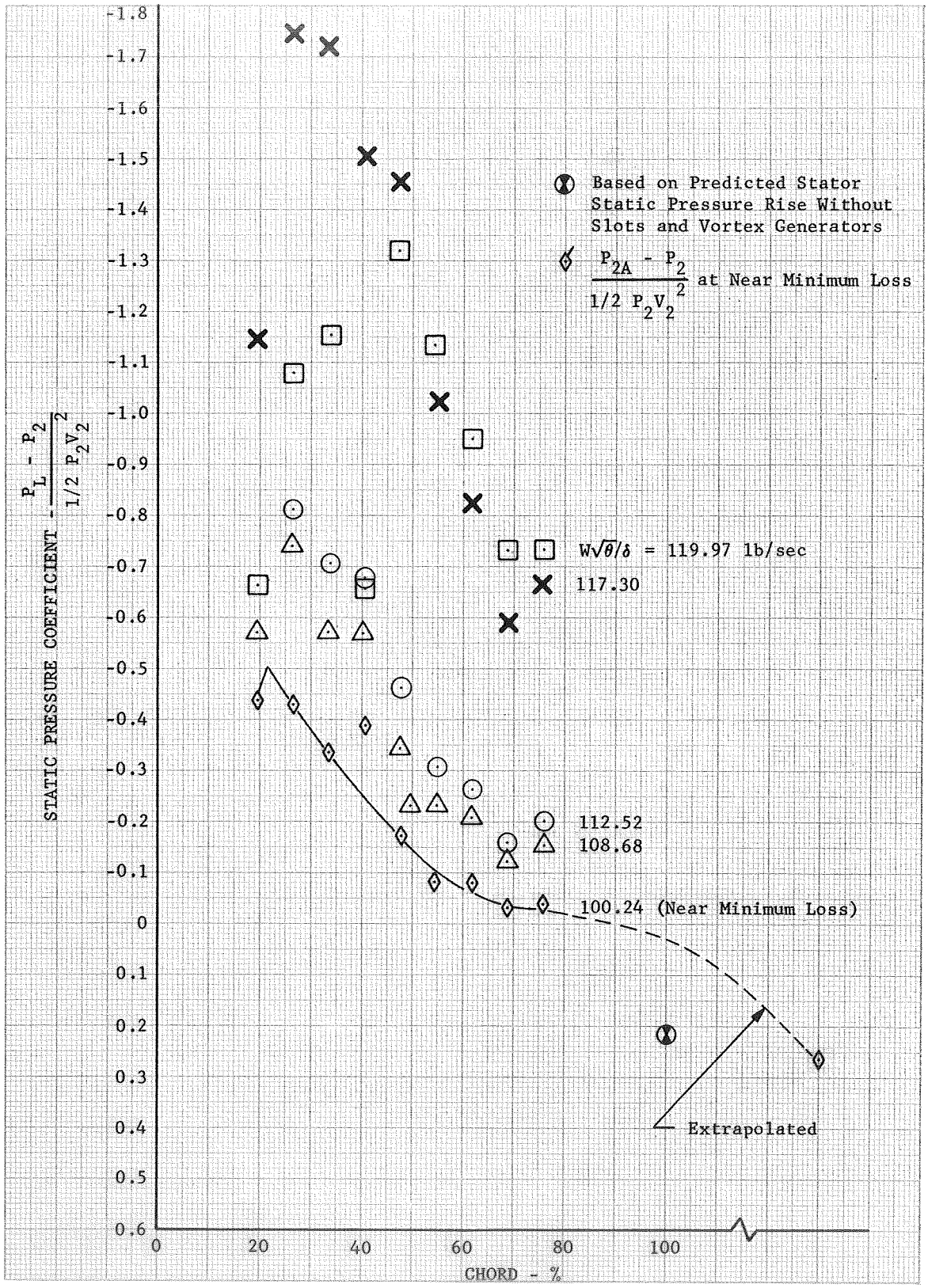

Figure 24. Unslotted Stator 4 Static Pressure Coefficient, 100% Design Equivalent Rotor Speed-10% Span

DF 83416

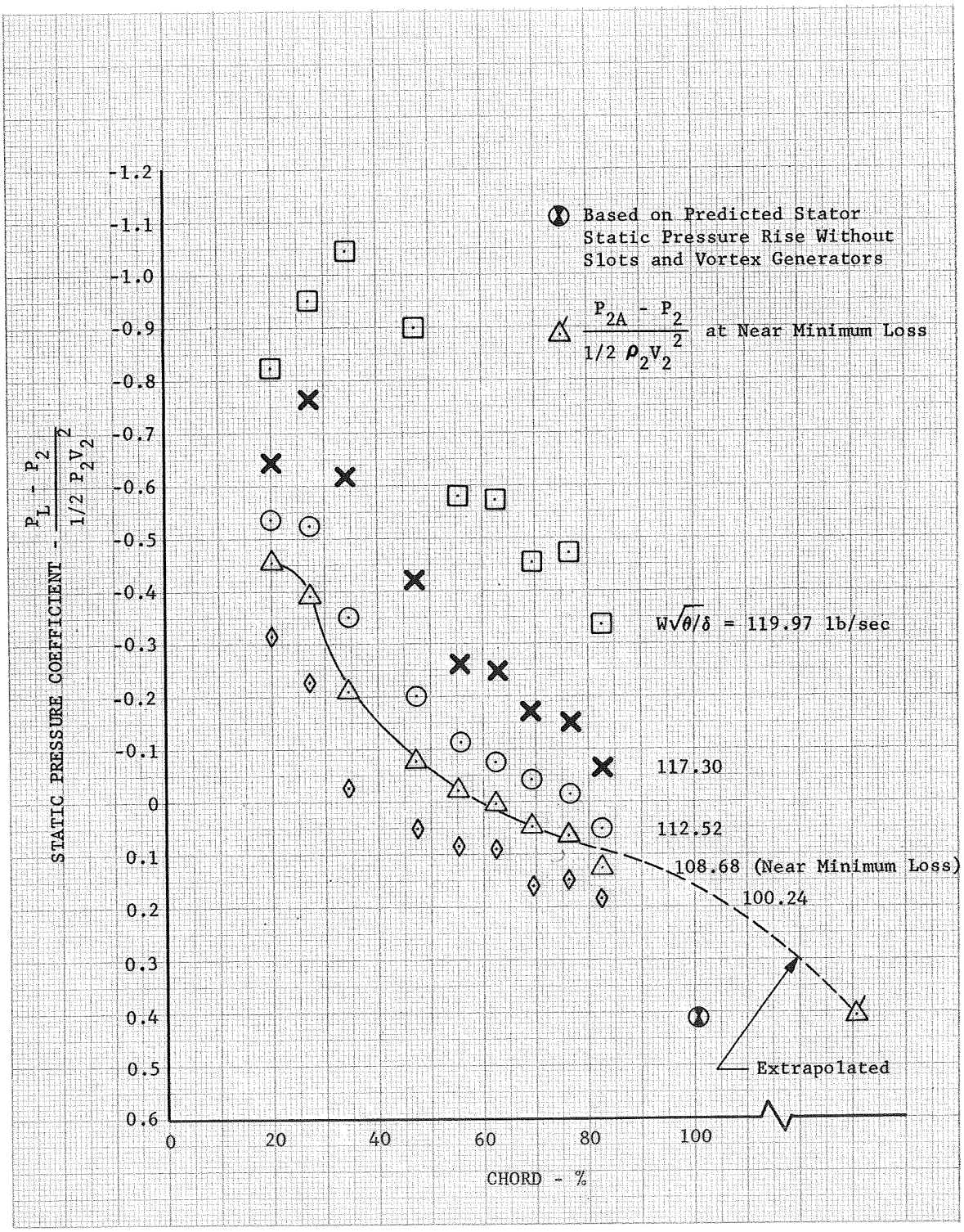

Figure 25. Unslotted Stator 4 Static Pressure Coefficient, 100% Design Equivalent Rotor Speed-90% Span

DF 83417

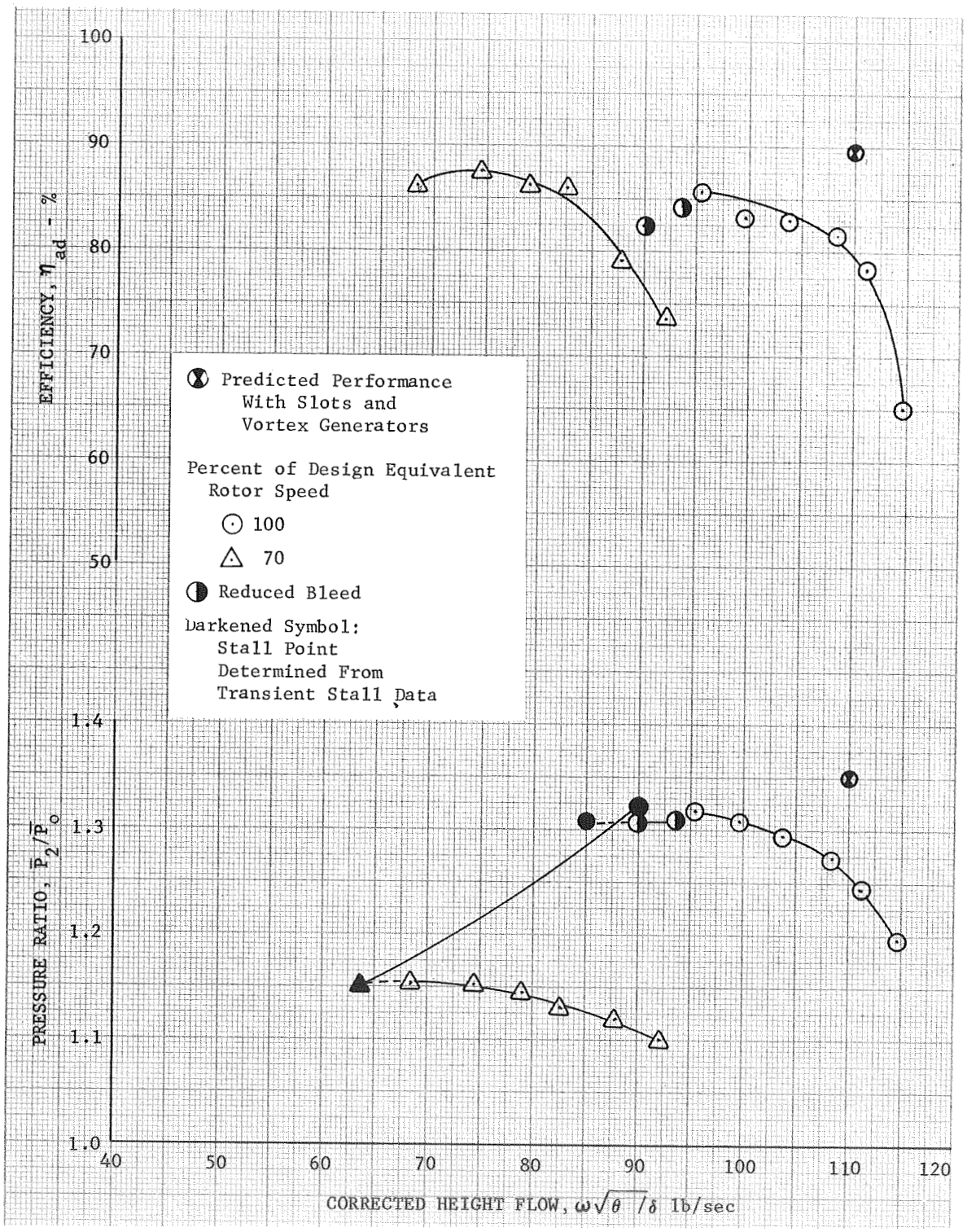

Figure 26. Overall Performance, Slotted Rotor 4 DF 83411

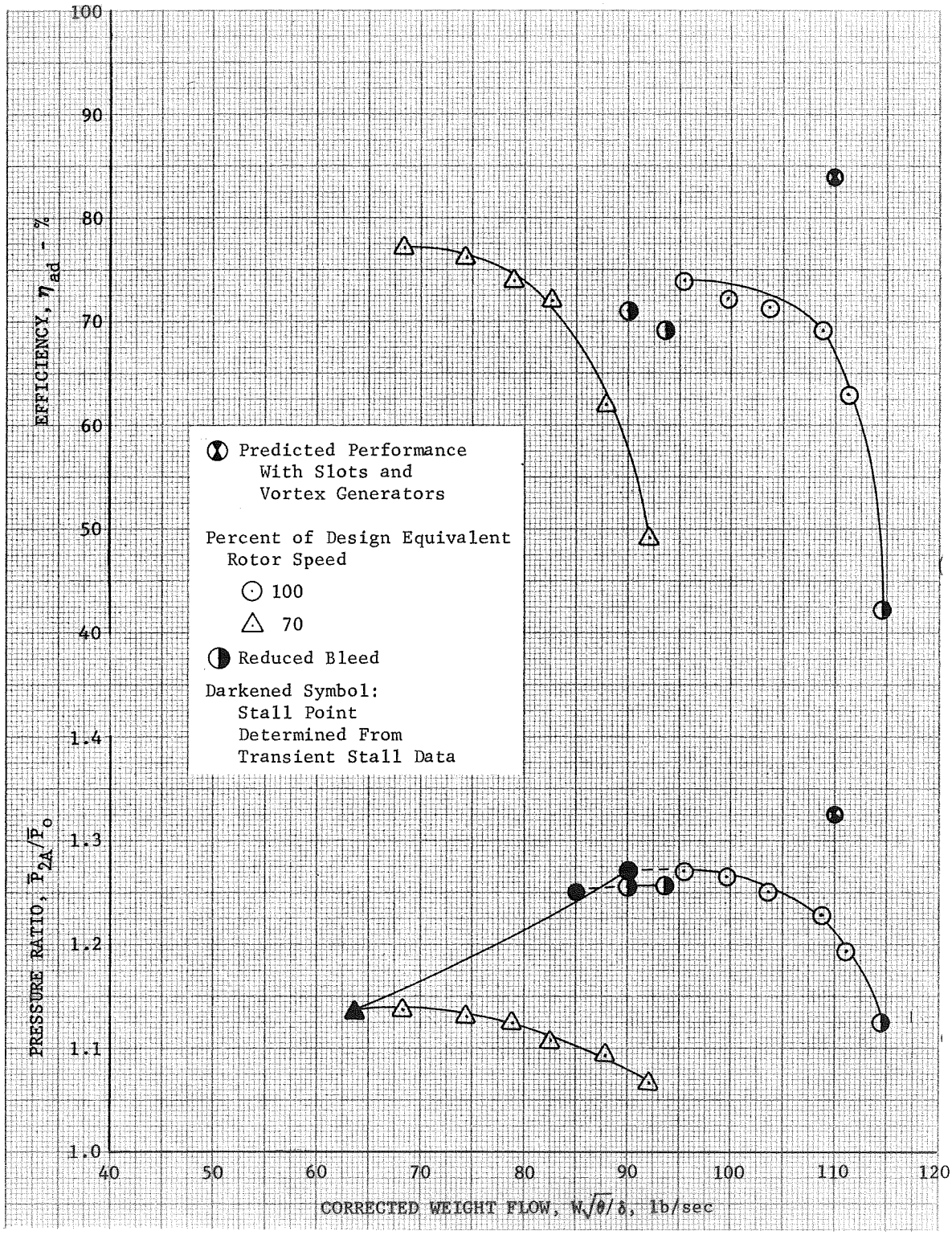

Figure 27. Overall Performance, Slotted Stage 4 DF 83412

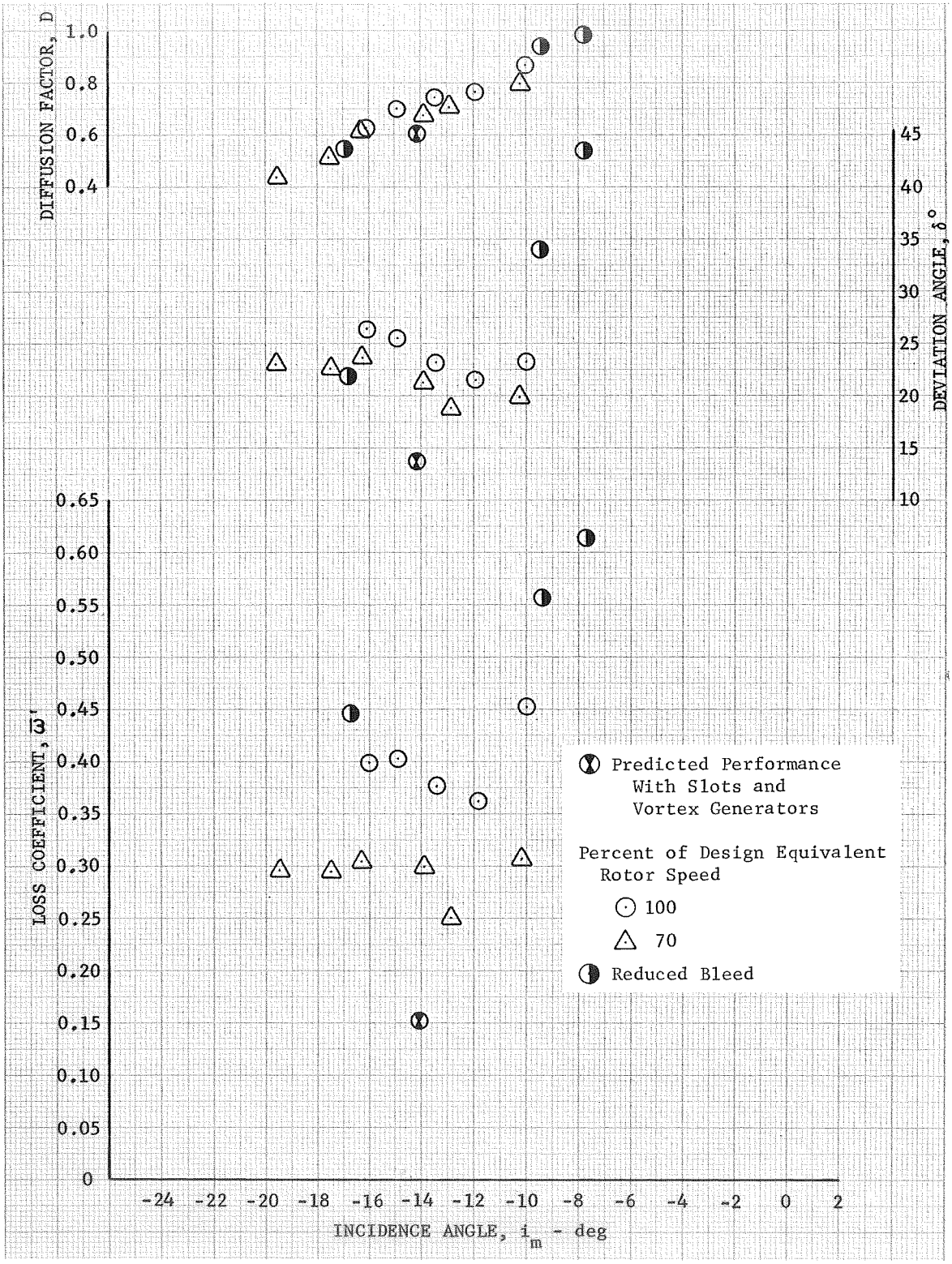

Figure 28a. Slotted Rotor 4 Blade Element Performance, 5% Span From Tip

DF 83418

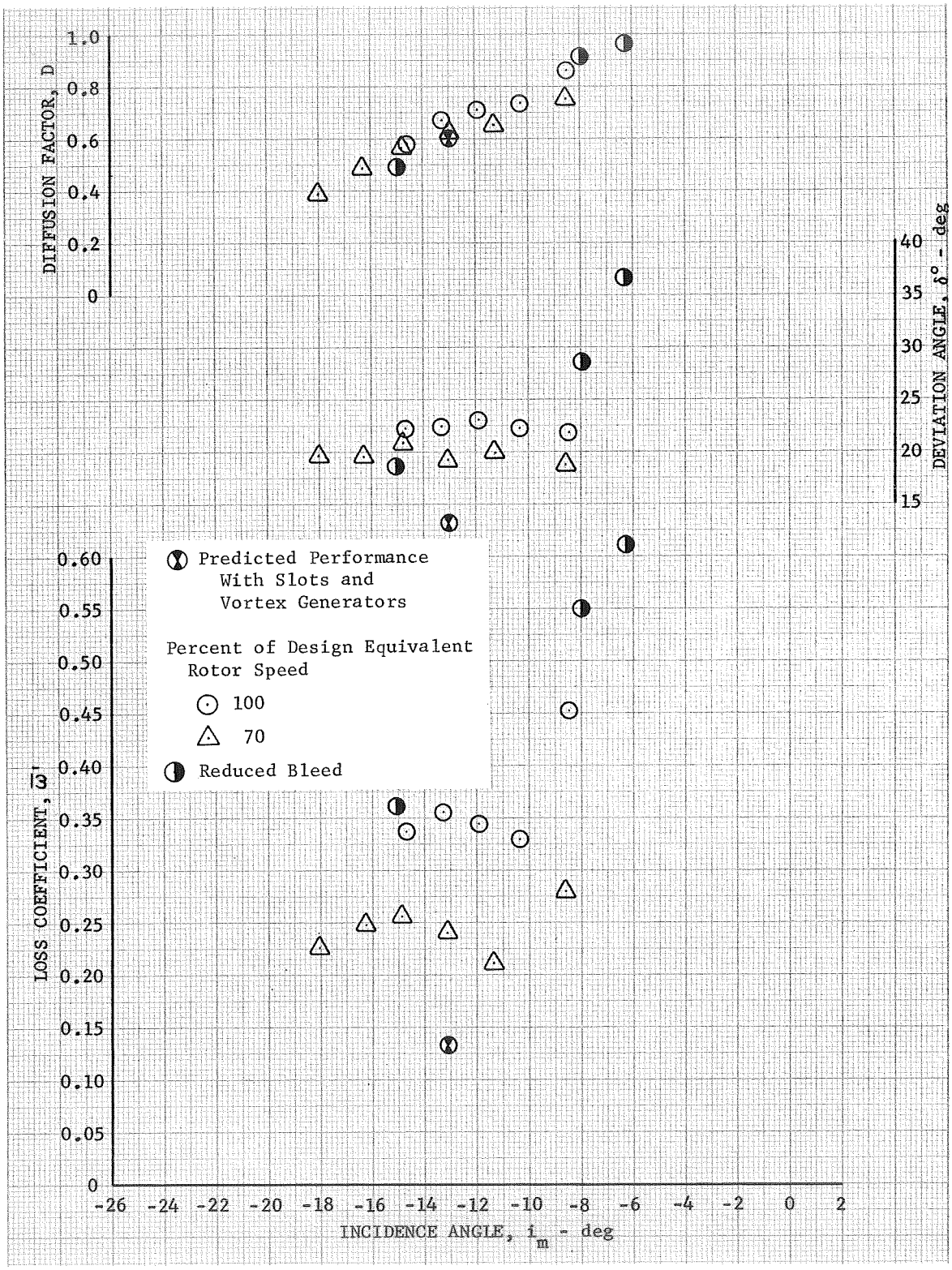

Figure 28b. Slotted Rotor 4 Blade Element Performance, 10% Span From Tip

DF 83419

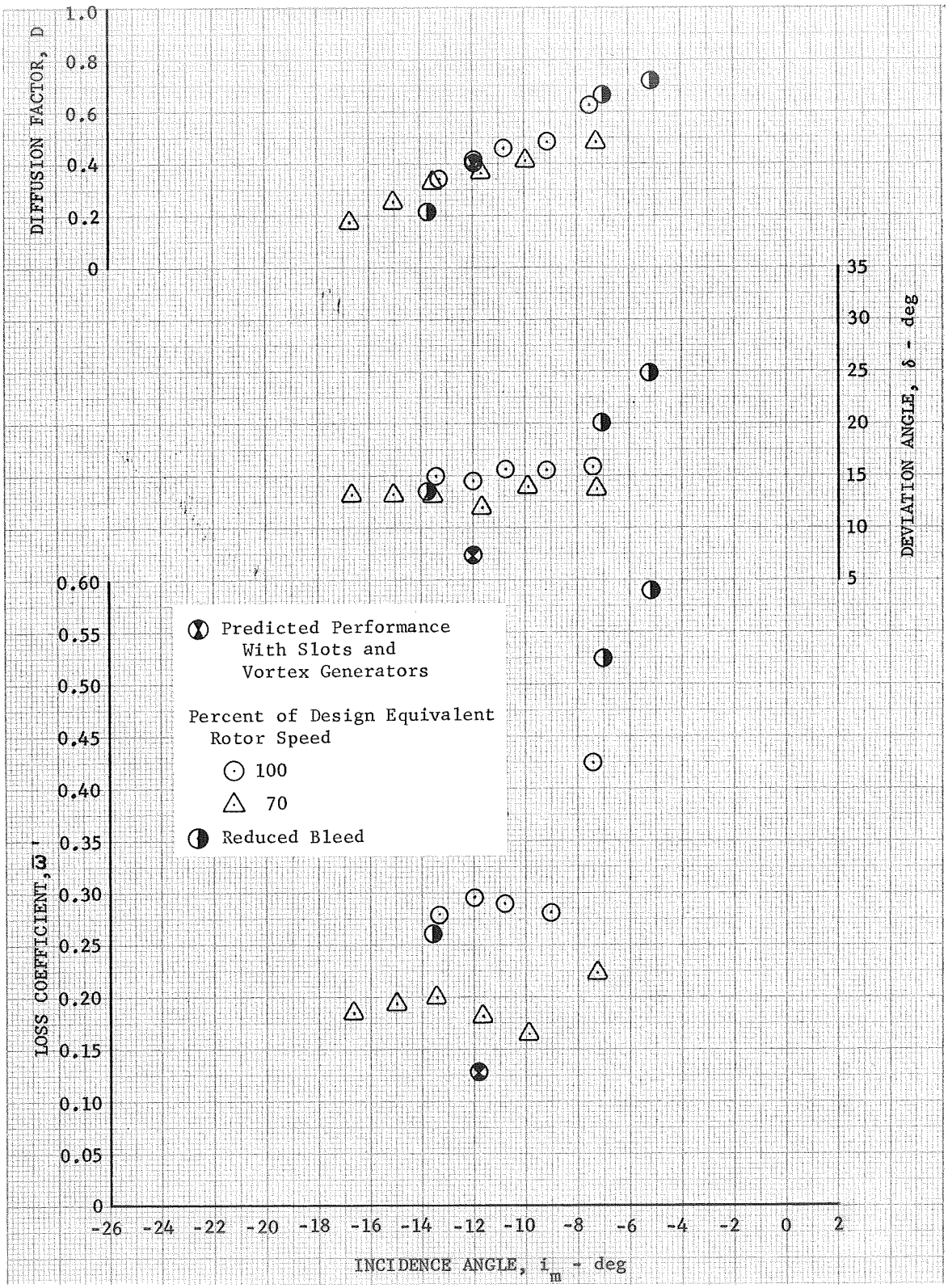

Figure 28c. Slotted Rotor 4 Blade Element Performance, 15% Span From Tip DF 83420

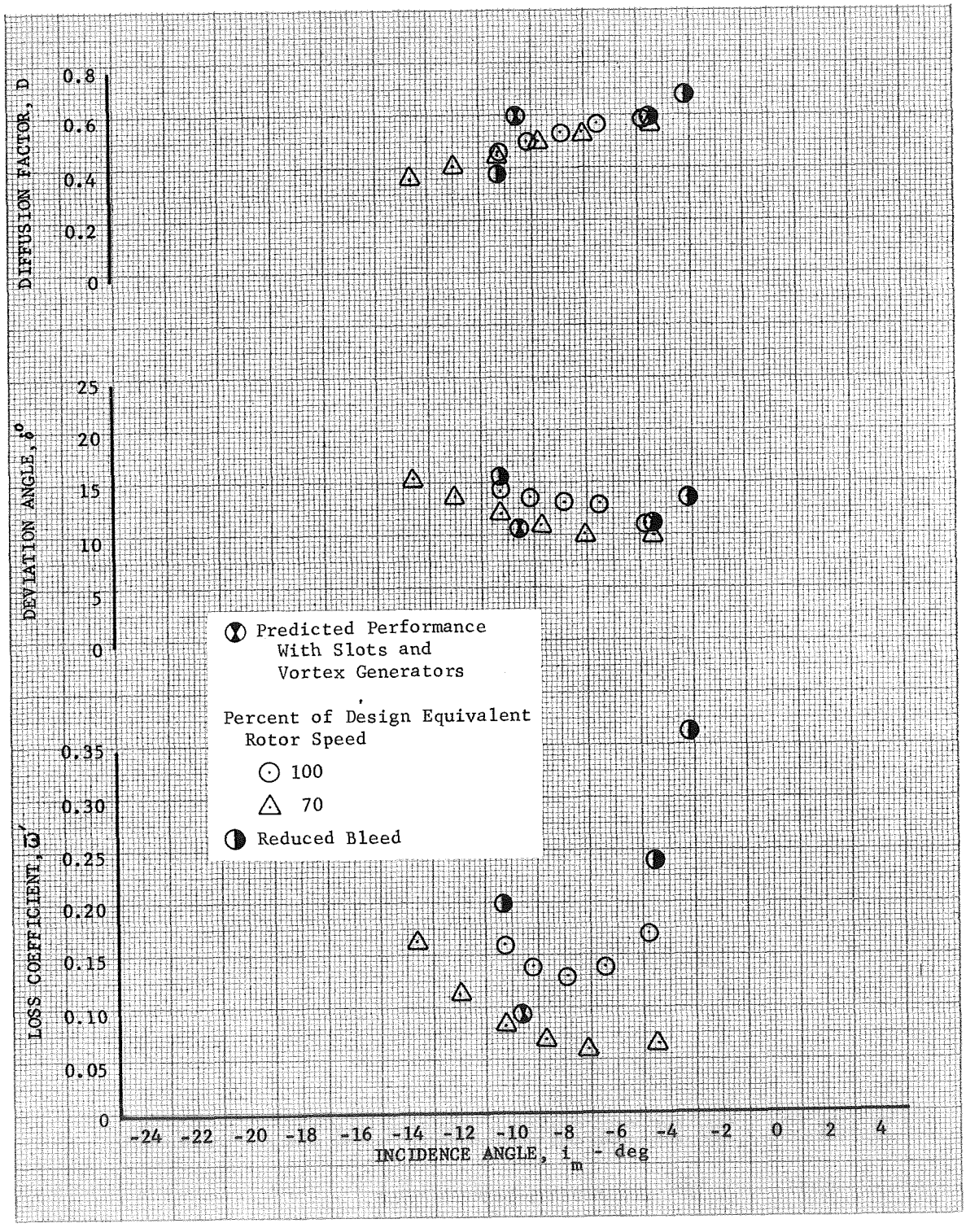

Figure 28d. Slotted Rotor 4 Blade Element Performance, 30% Span From Tip

DF 83414

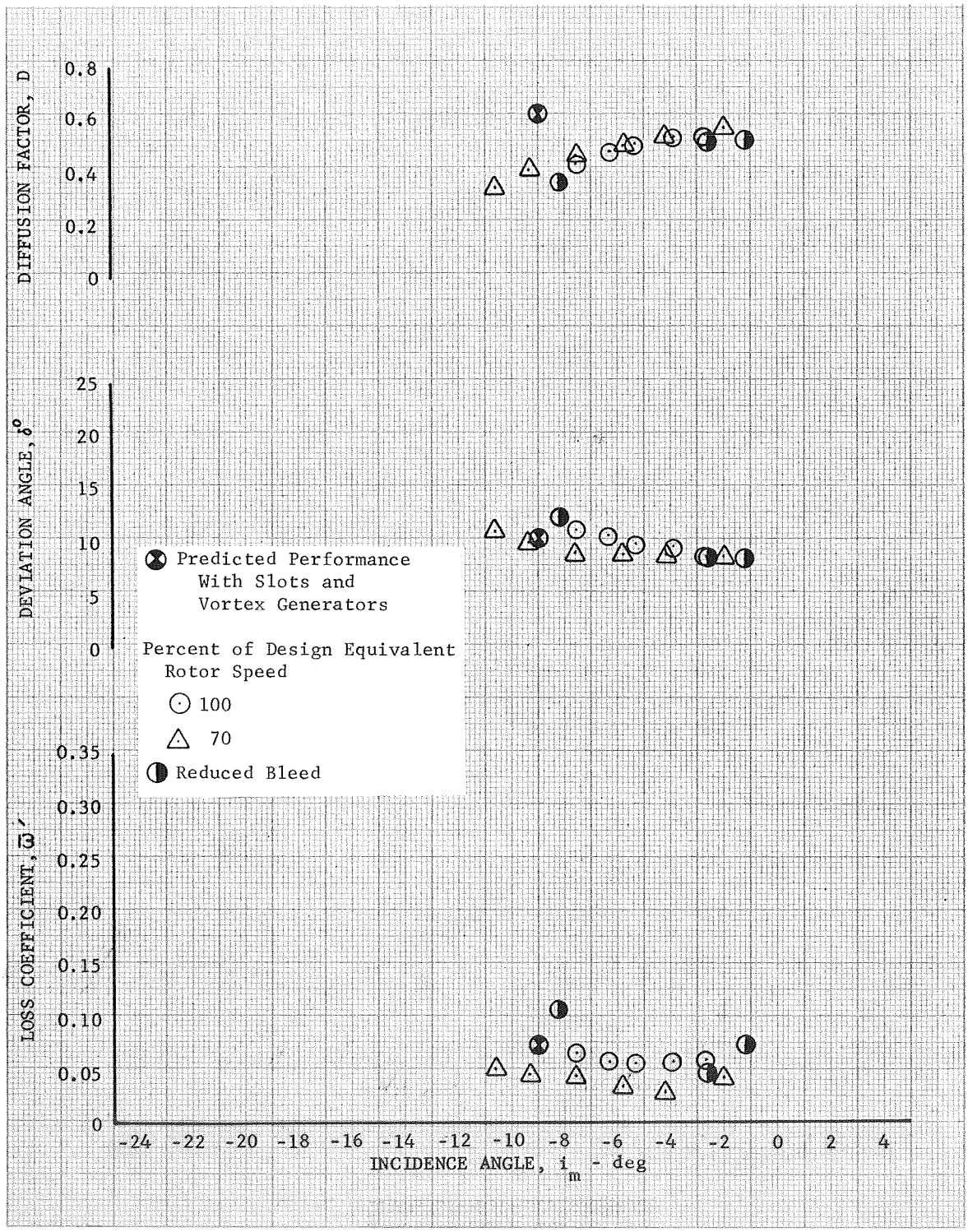

Figure 28e. Slotted Rotor 4 Blade Element Performance, 50% Span From Tip

DF 83336

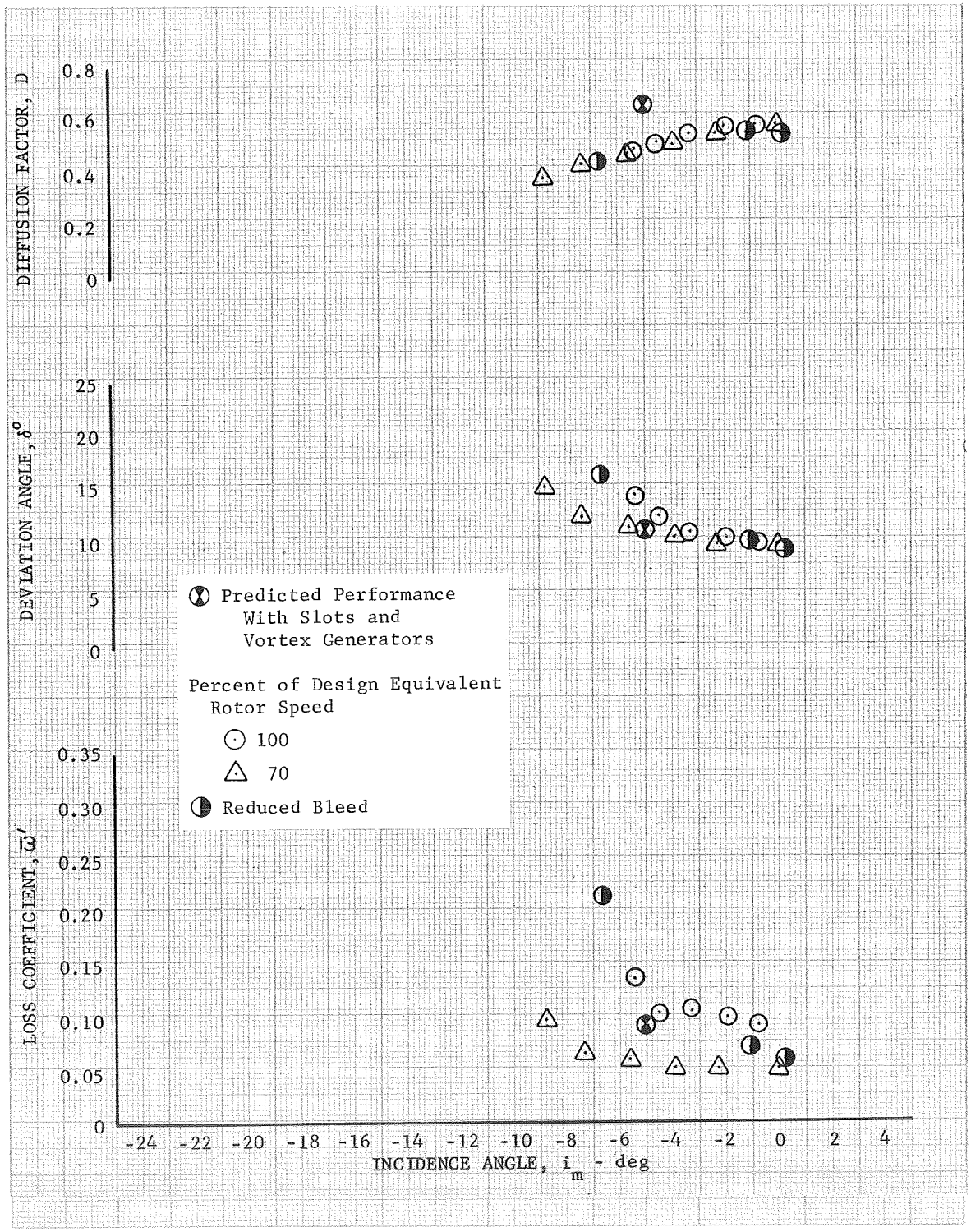

Figure 28f. Slotted Rotor 4 Blade Element Performance, 70% Span From Tip

DF 83337

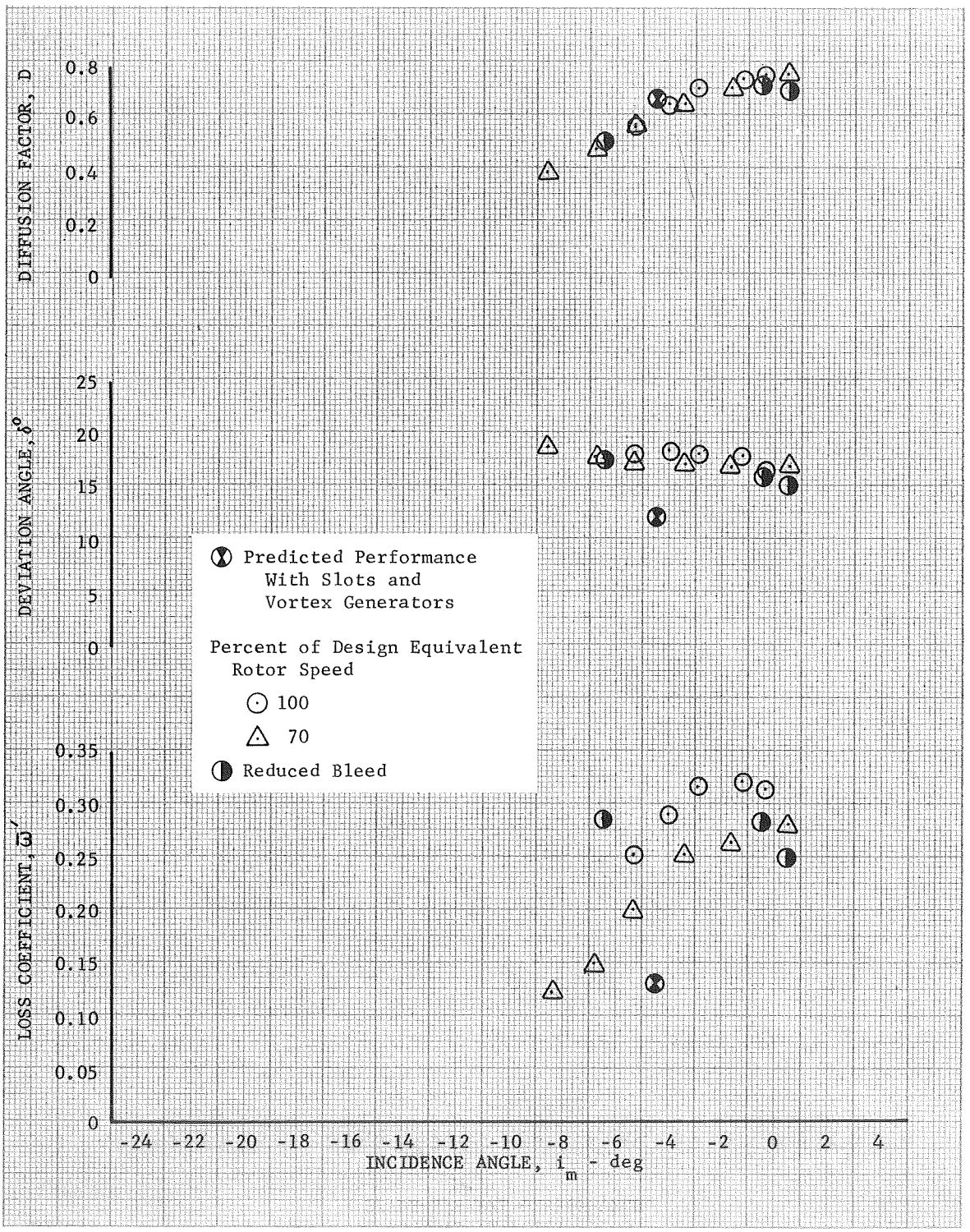

Figure 28g. Slotted Rotor 4 Blade Element Performance, 85% Span From Tip

DF 83338

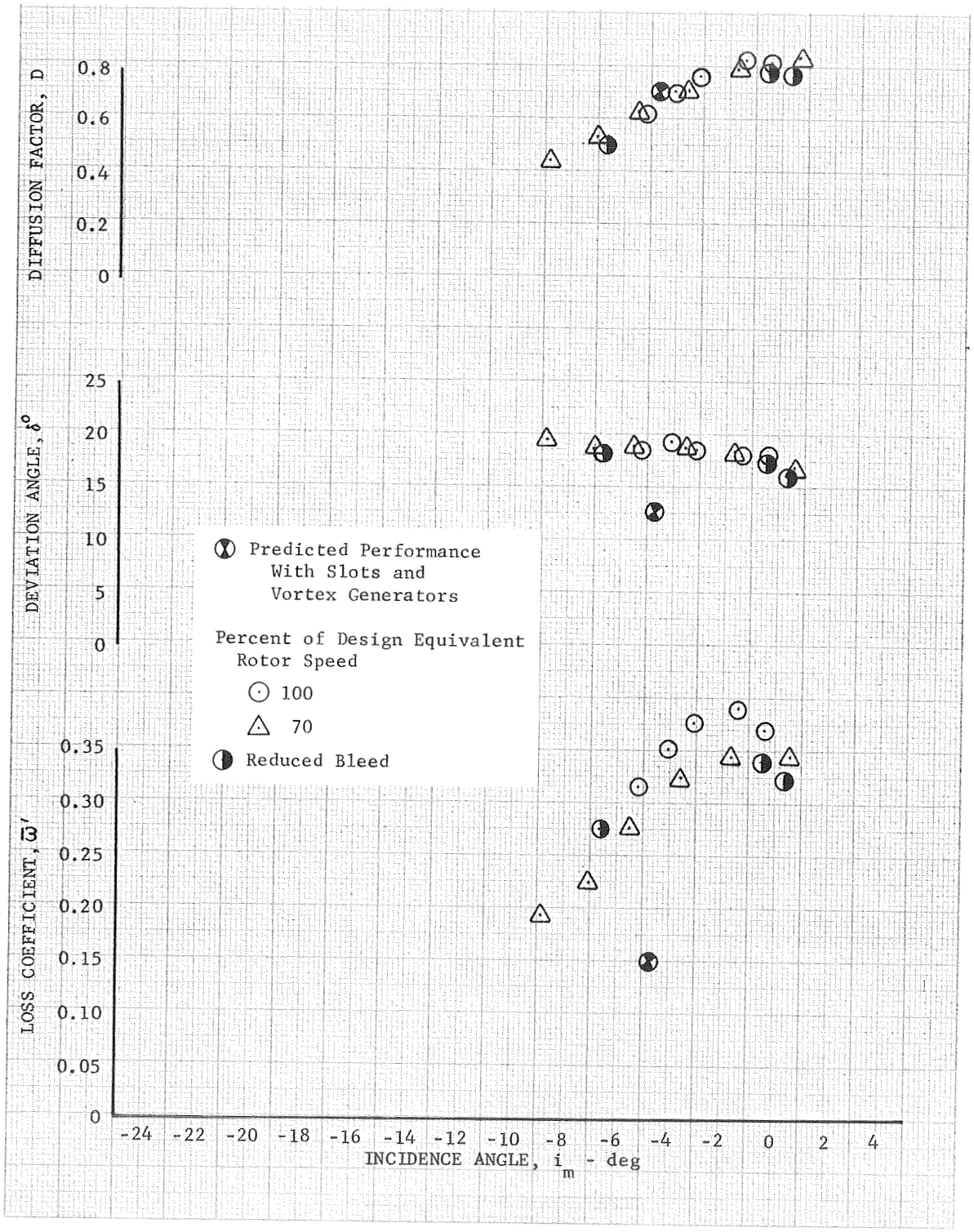

Figure 28h. Slotted Rotor 4 Blade Element Performance, 90% Span From Tip

DF 83339

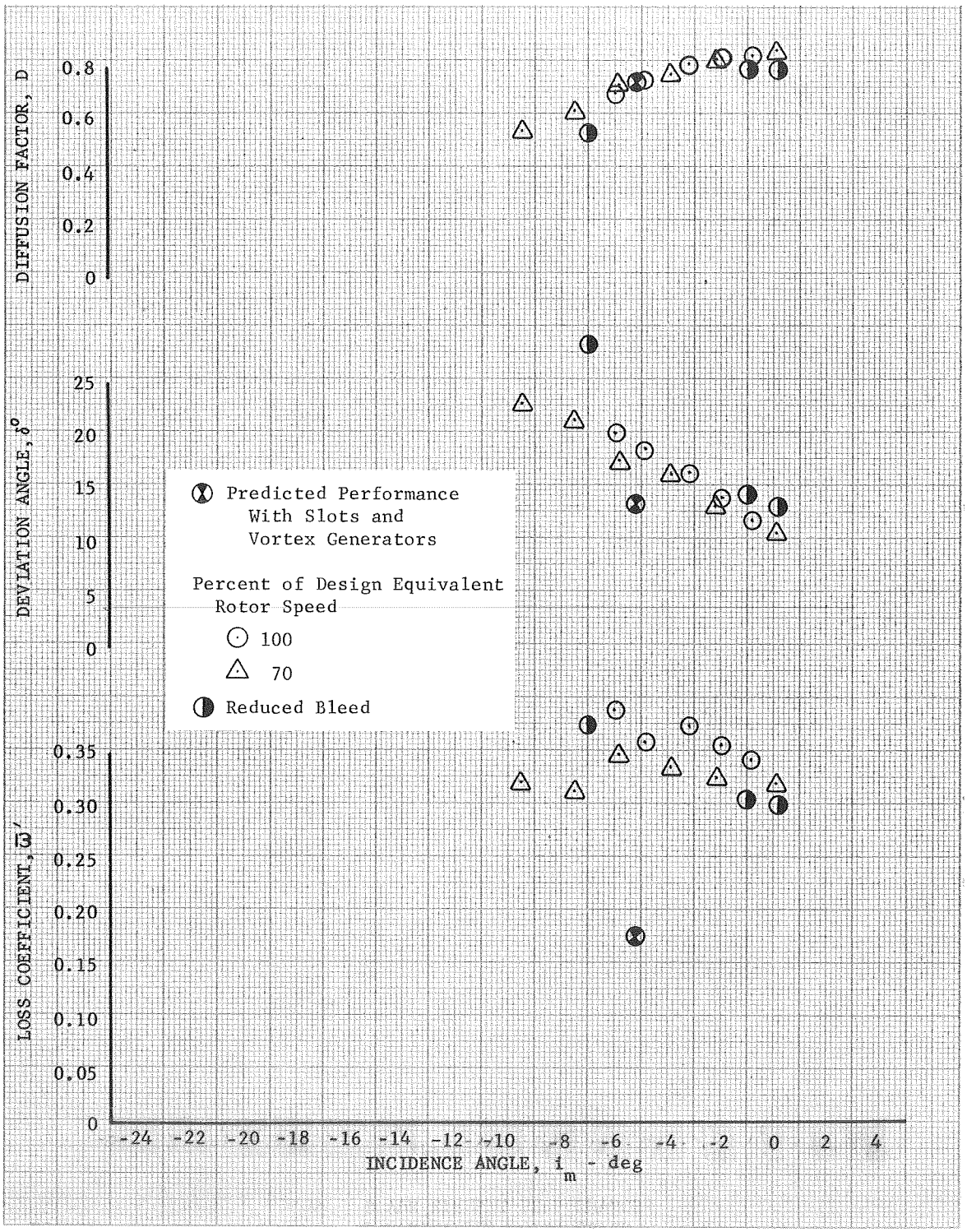

Figure 28i. Slotted Rotor 4 Blade Element Performance, 95% Span From Tip DF 83340

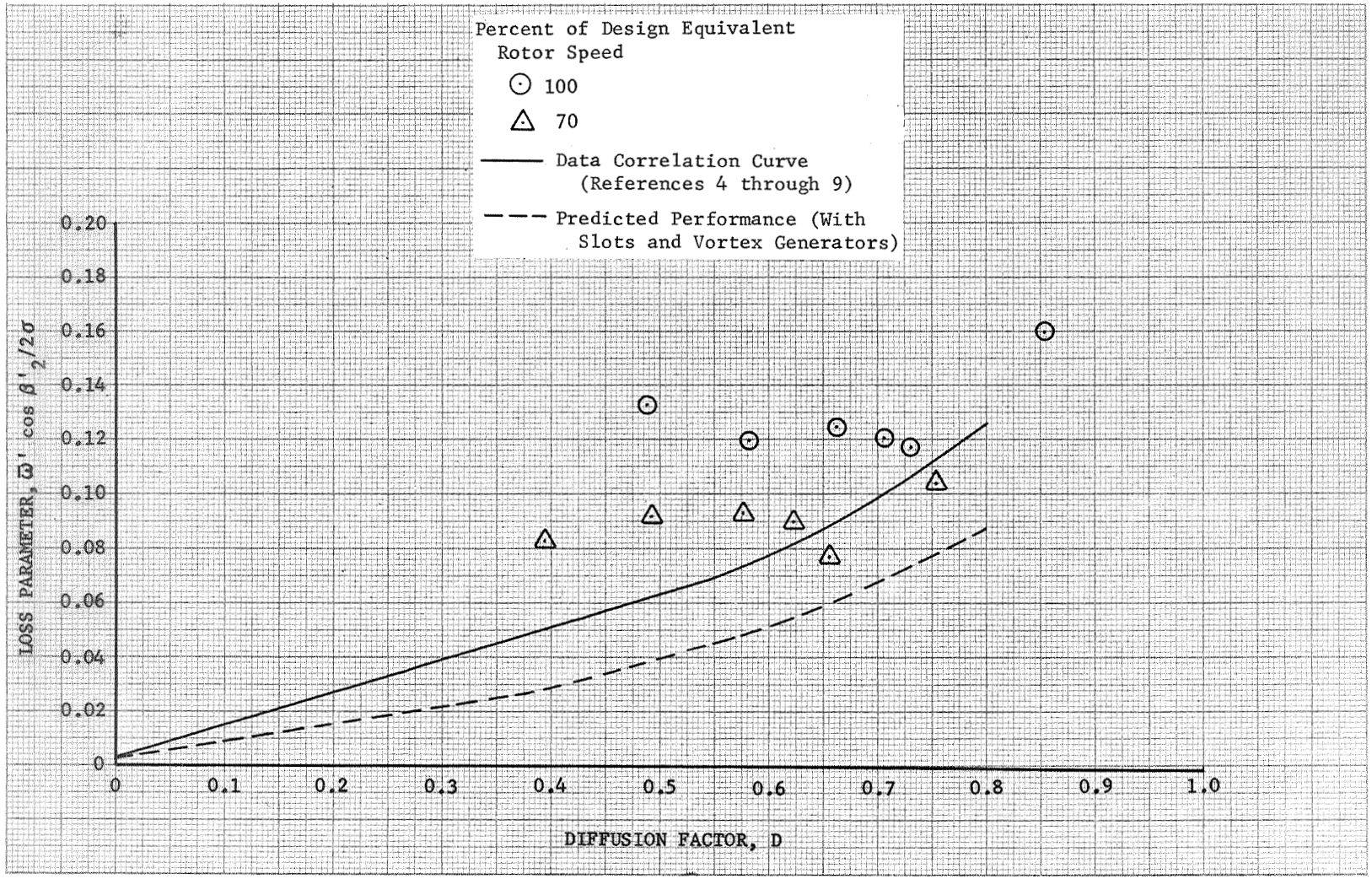

Figure 29a. Slotted Rotor 4 Loss Parameter vs Diffusion Factor, 10% Span From Tip

DF 83341

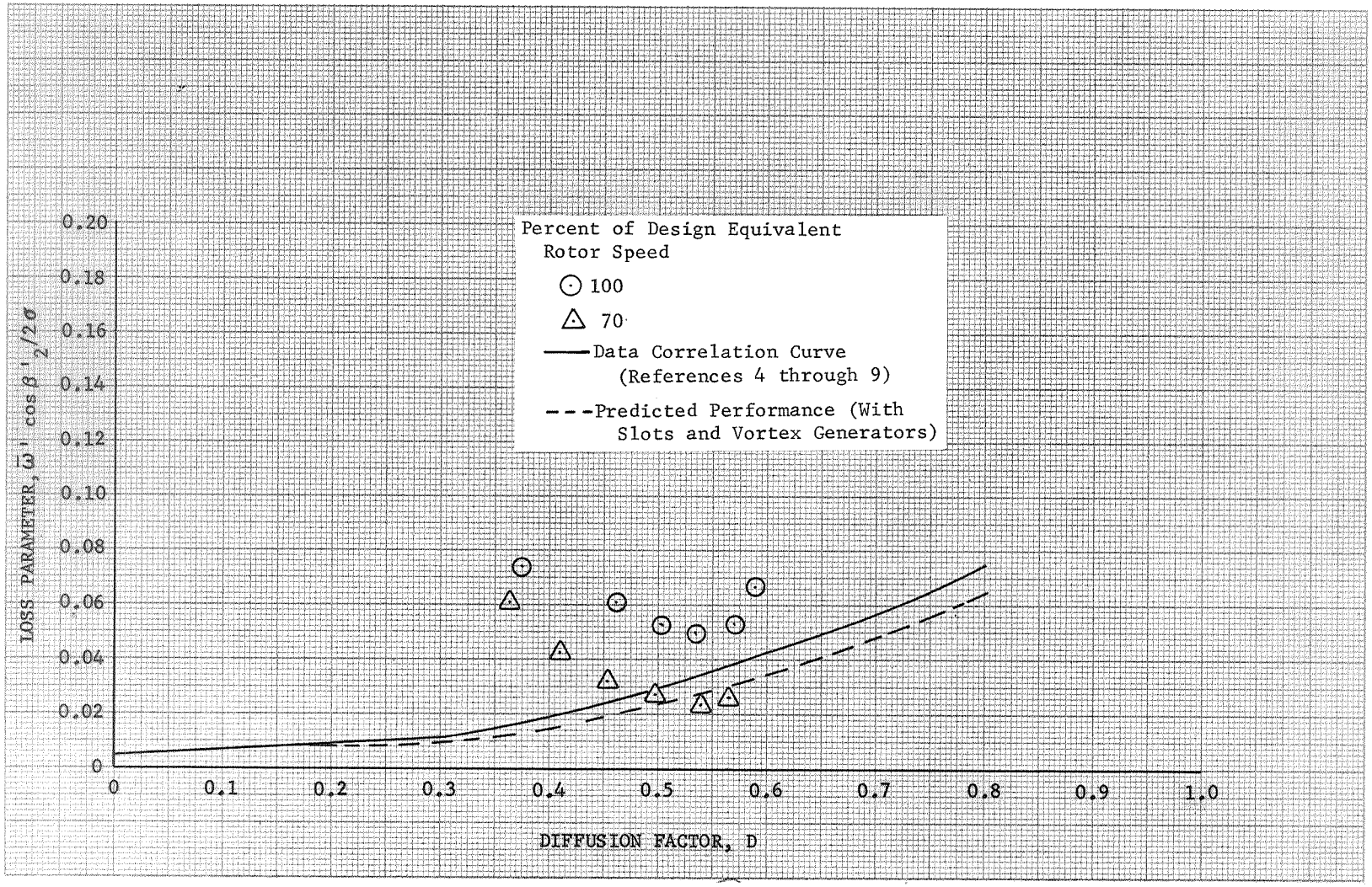

Figure 29b. Slotted Rotor 4 Loss Parameter vs Diffusion Factor, 30% Span From Tip DF 83342

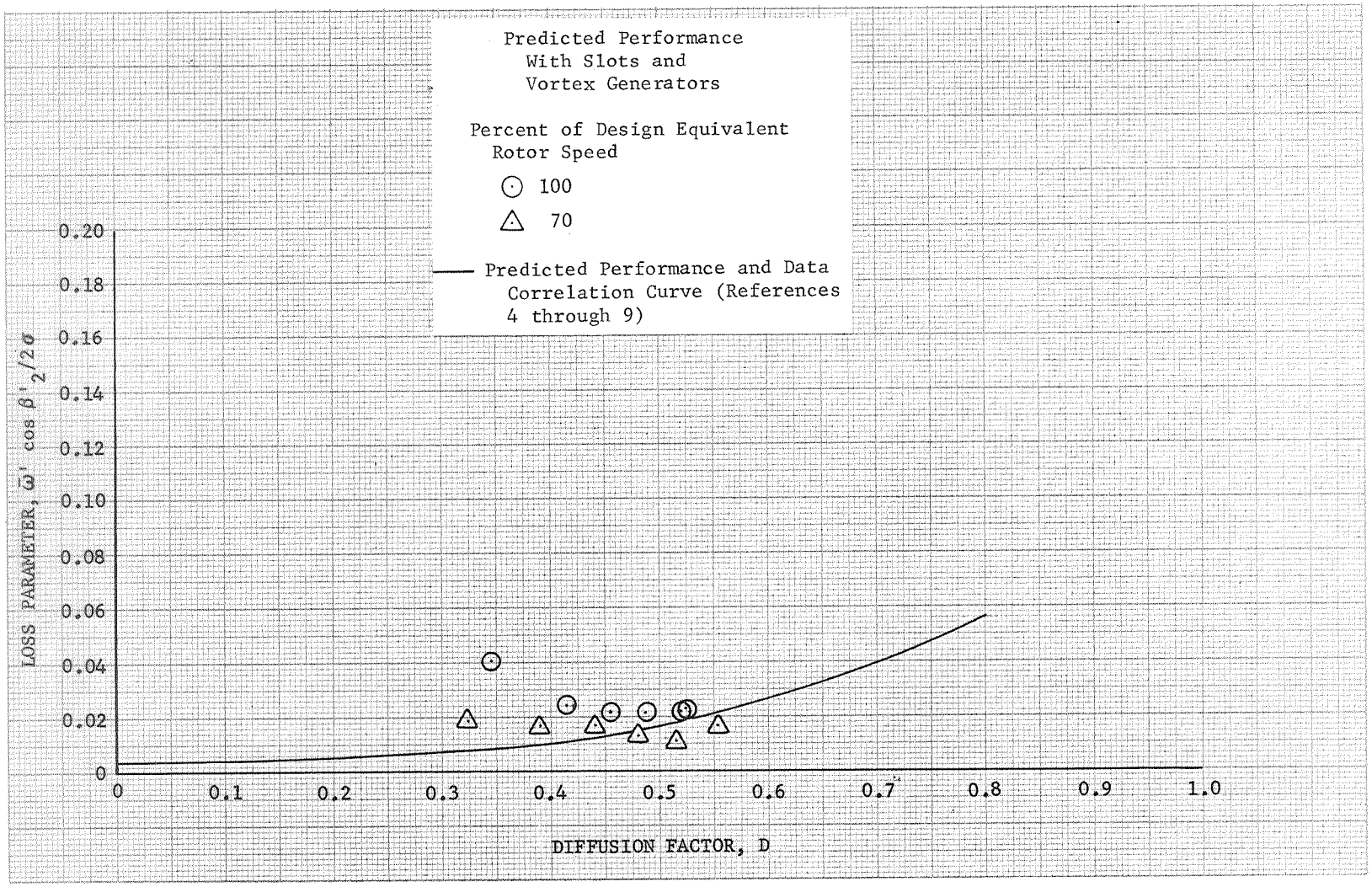

Figure 29c. Slotted Rotor 4 Loss Parameter vs Diffusion Factor, 50% Span From Tip

DF 83343

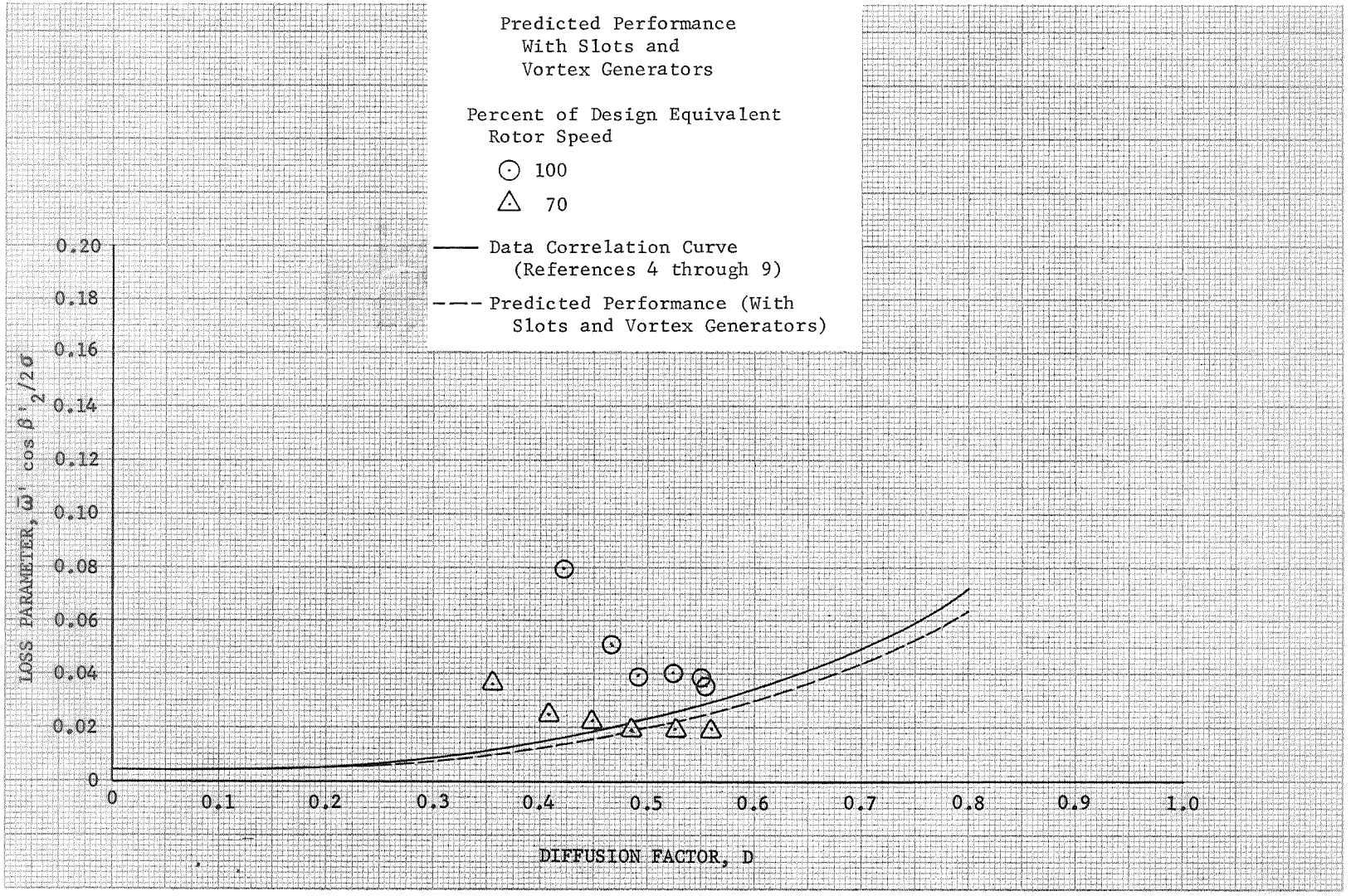

Figure 29d. Slotted Rotor 4 Loss Parameter vs Diffusion Factor, 70% Span From Tip

DF 83344

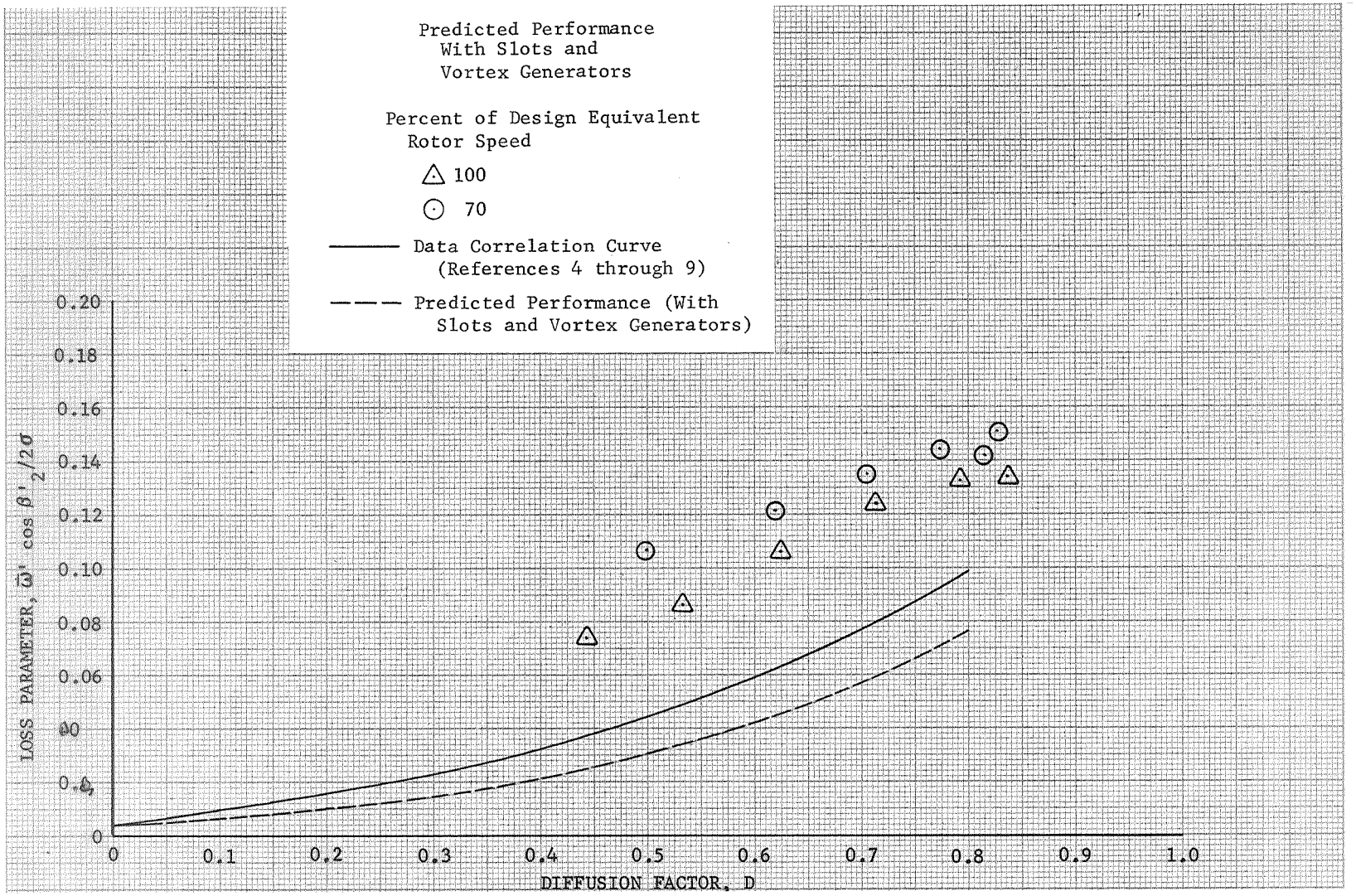

Figure 29e. Slotted Rotor 4 Loss Parameter vs Diffusion Factor, 90% Span From Tip

DF 83345

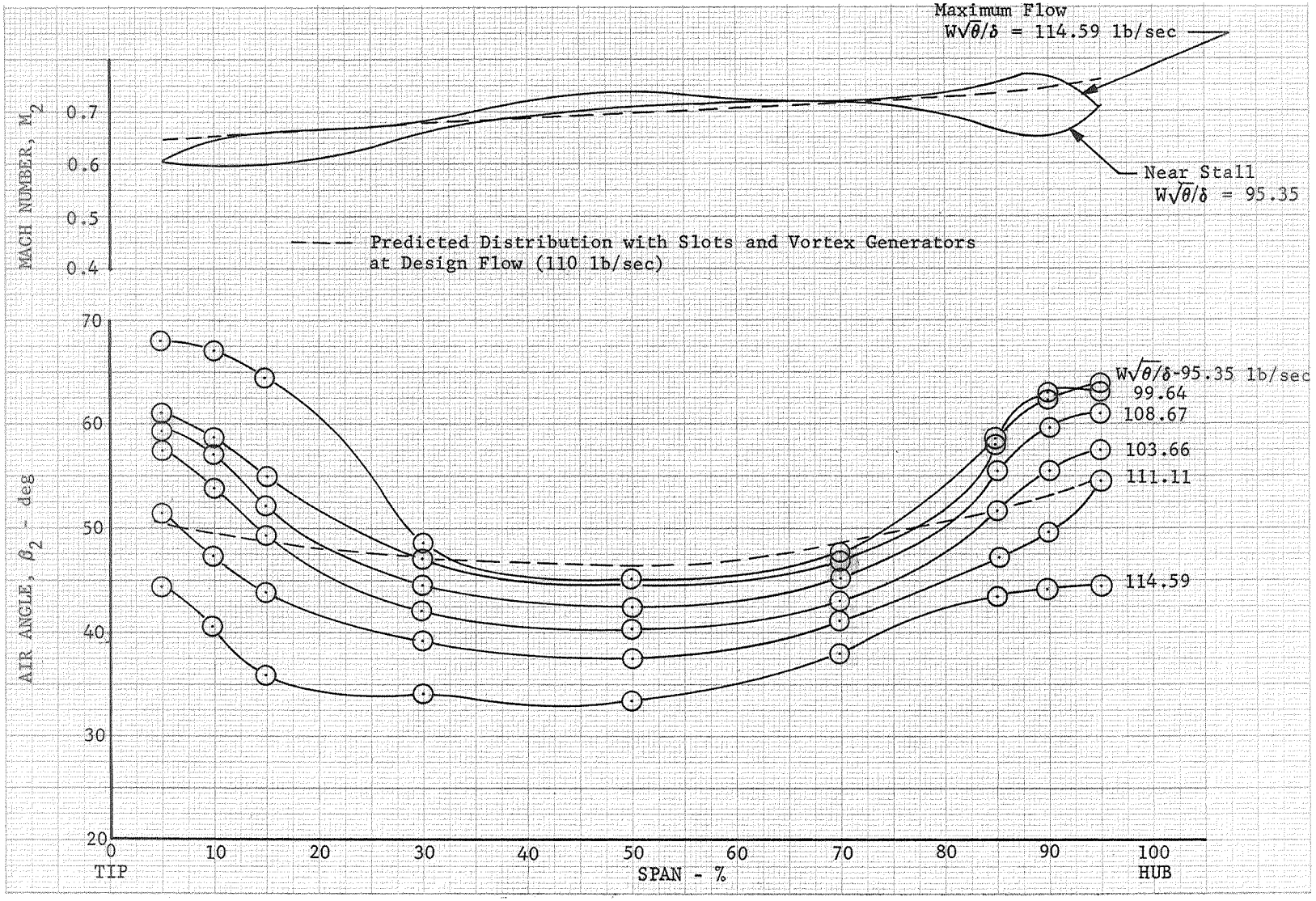

Figure 30. Slotted Stator 4 Inlet Air Angle and Mach Number Distribution, Design Equivalent Rotor Speed DF 83421

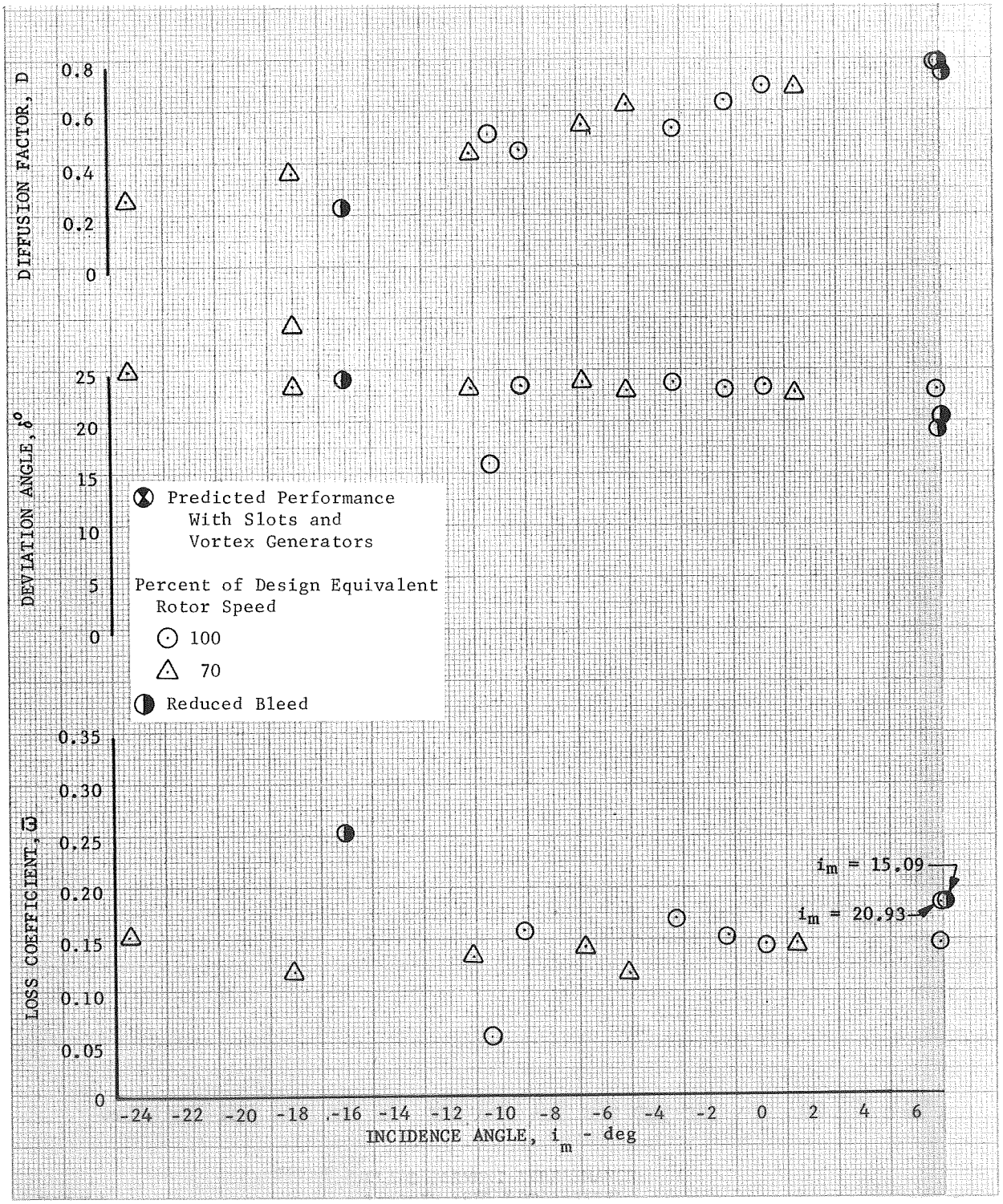

Figure 31a. Slotted Stator 4 Blade Element Performance, 5% Span From Tip

DF 83346

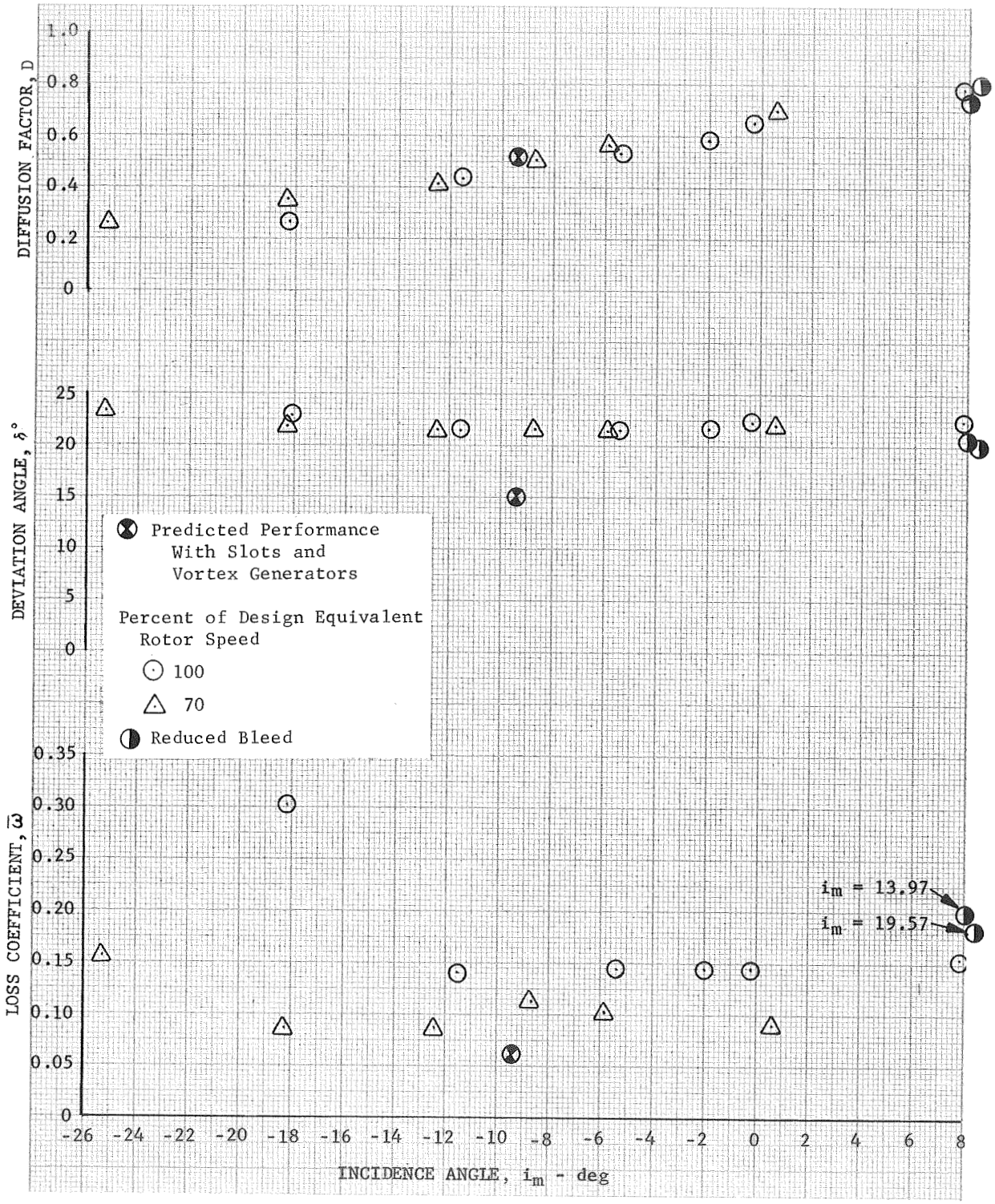

Figure 31b. Slotted Stator 4 Blade Element Performance, 10% Span From Tip

DF 83347

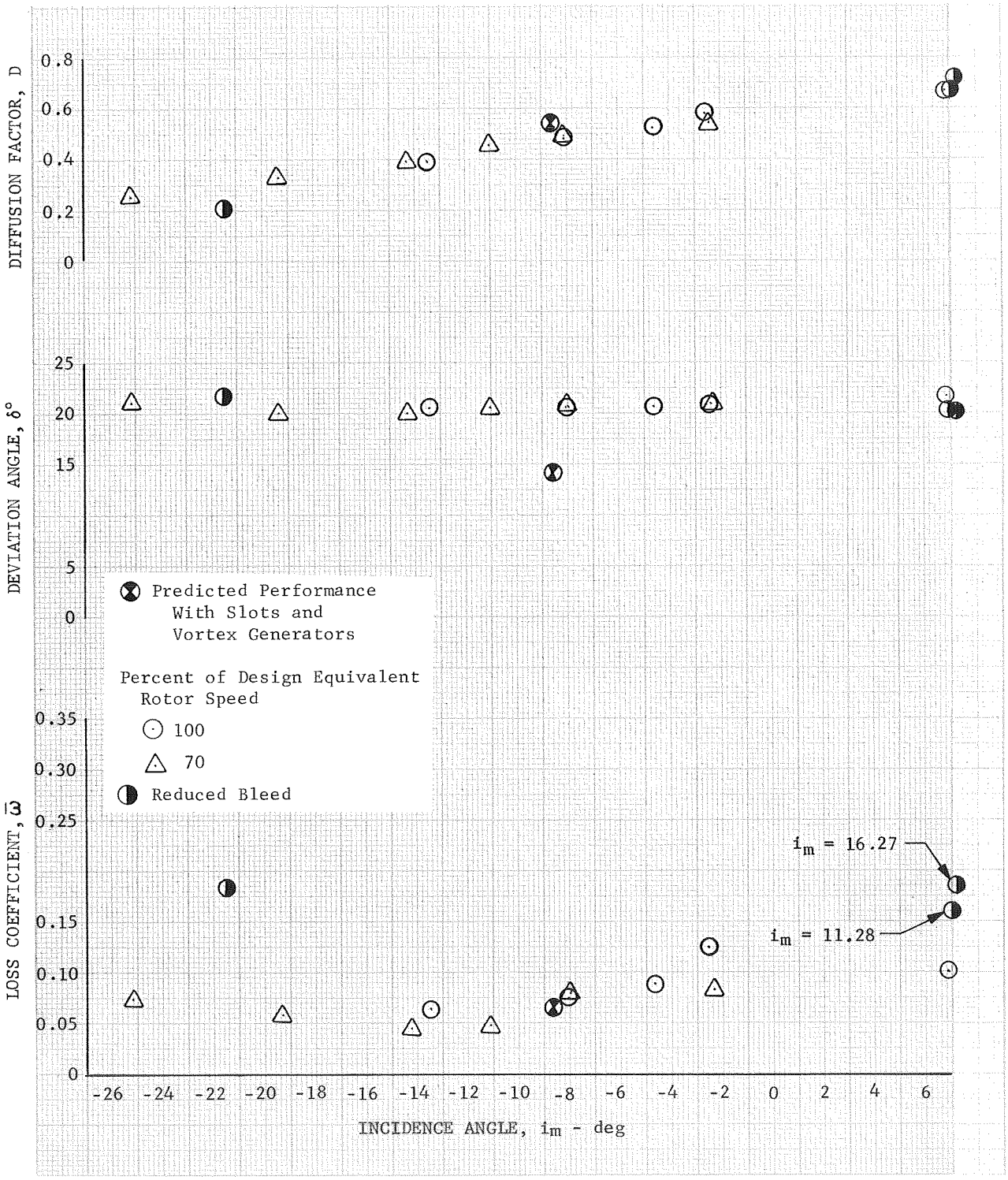

Figure 31c. Slotted Stator 4 Blade Element Performance, 15% Span From Tip

DF 83348

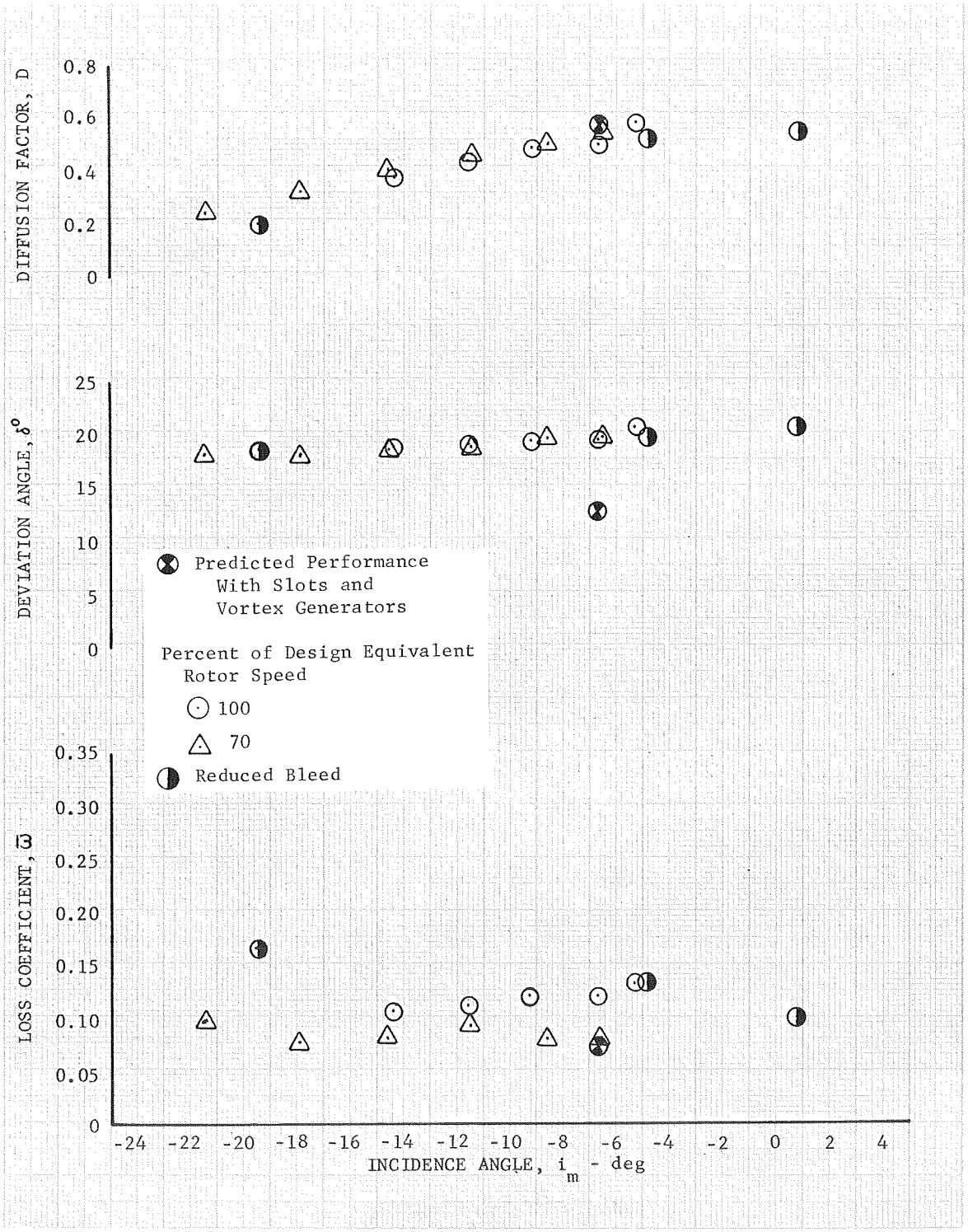

Figure 31d. Slotted Stator 4 Blade Element Performance, 30% Span From Tip

DF 83349

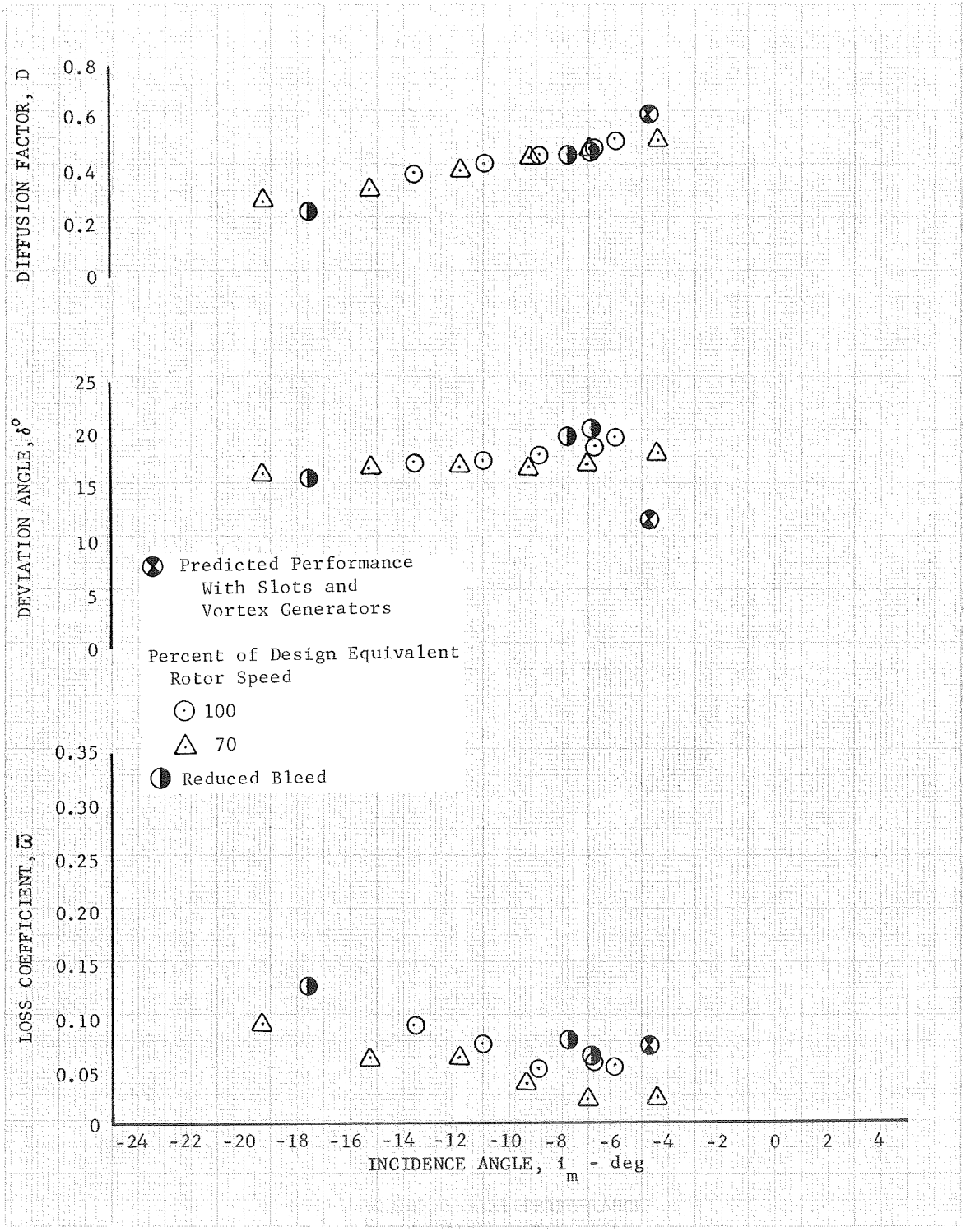

Figure 31e. Slotted Stator 4 and Blade Element Performance, 50% Span From Tip

DF 83350

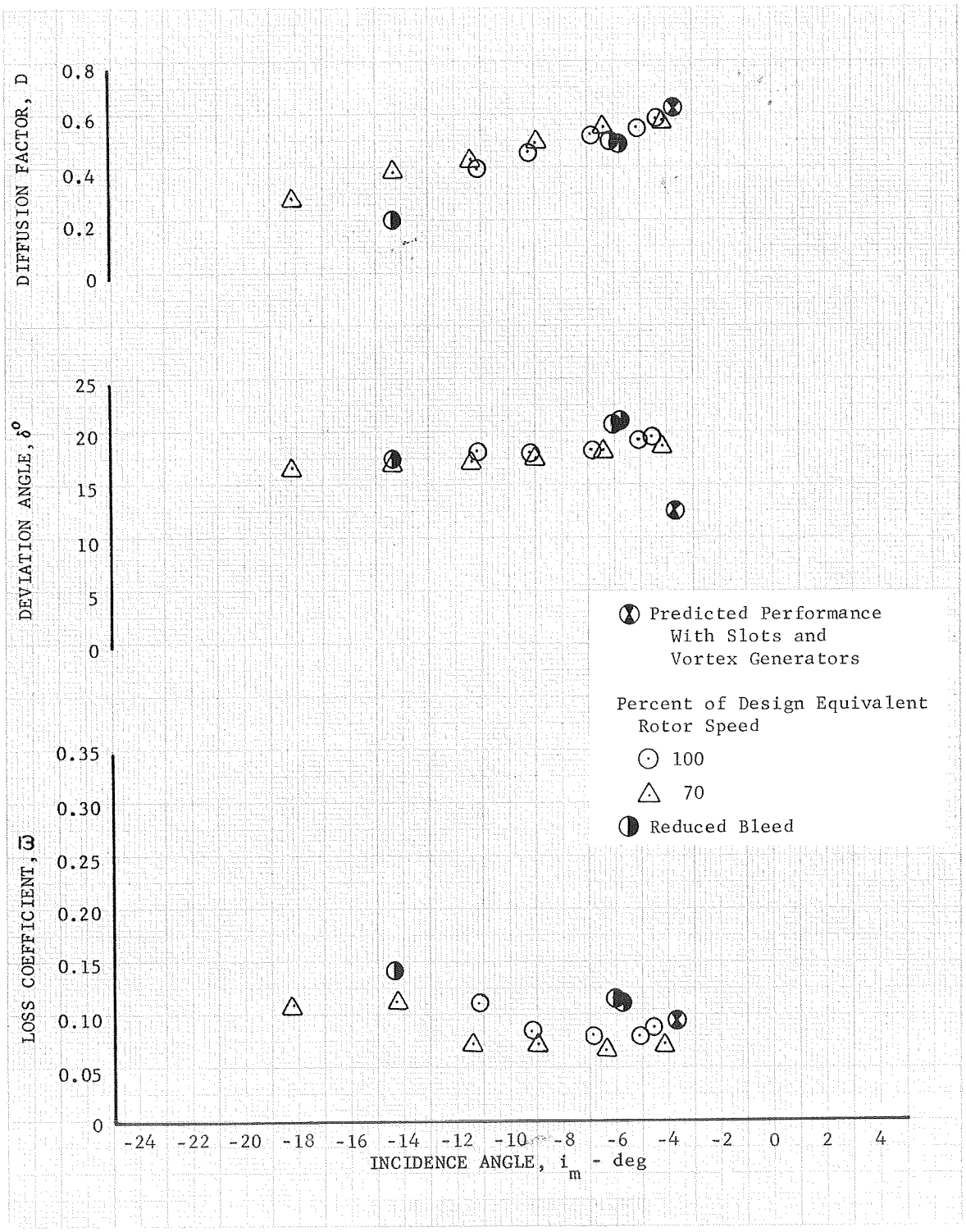

Figure 31f. Slotted Stator 4 Blade Element Performance, 70% Span From Tip

DF 83351

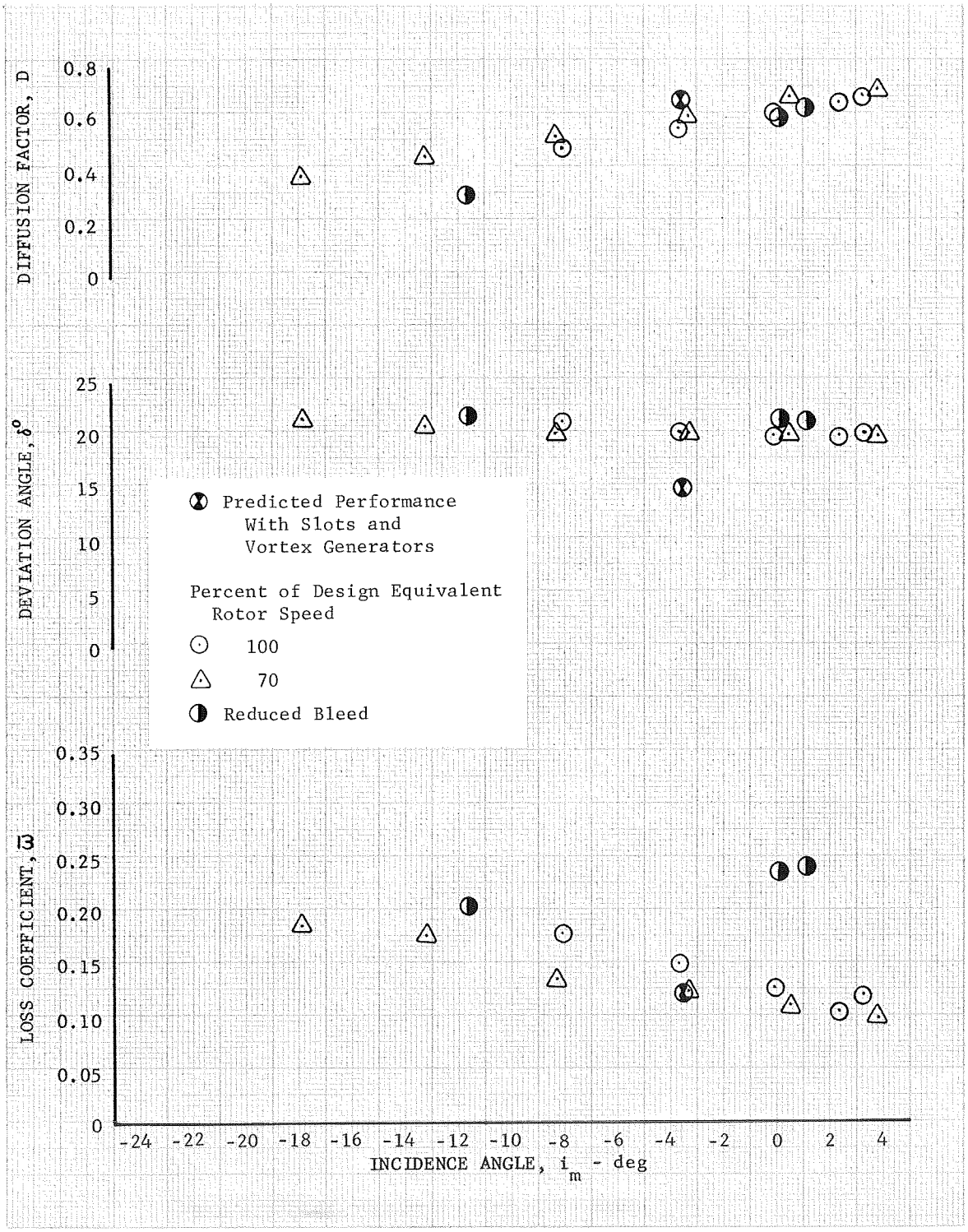

Figure 31g. Slotted Stator 4 Blade Element Performance, 85% Span From Tip

DF 83352

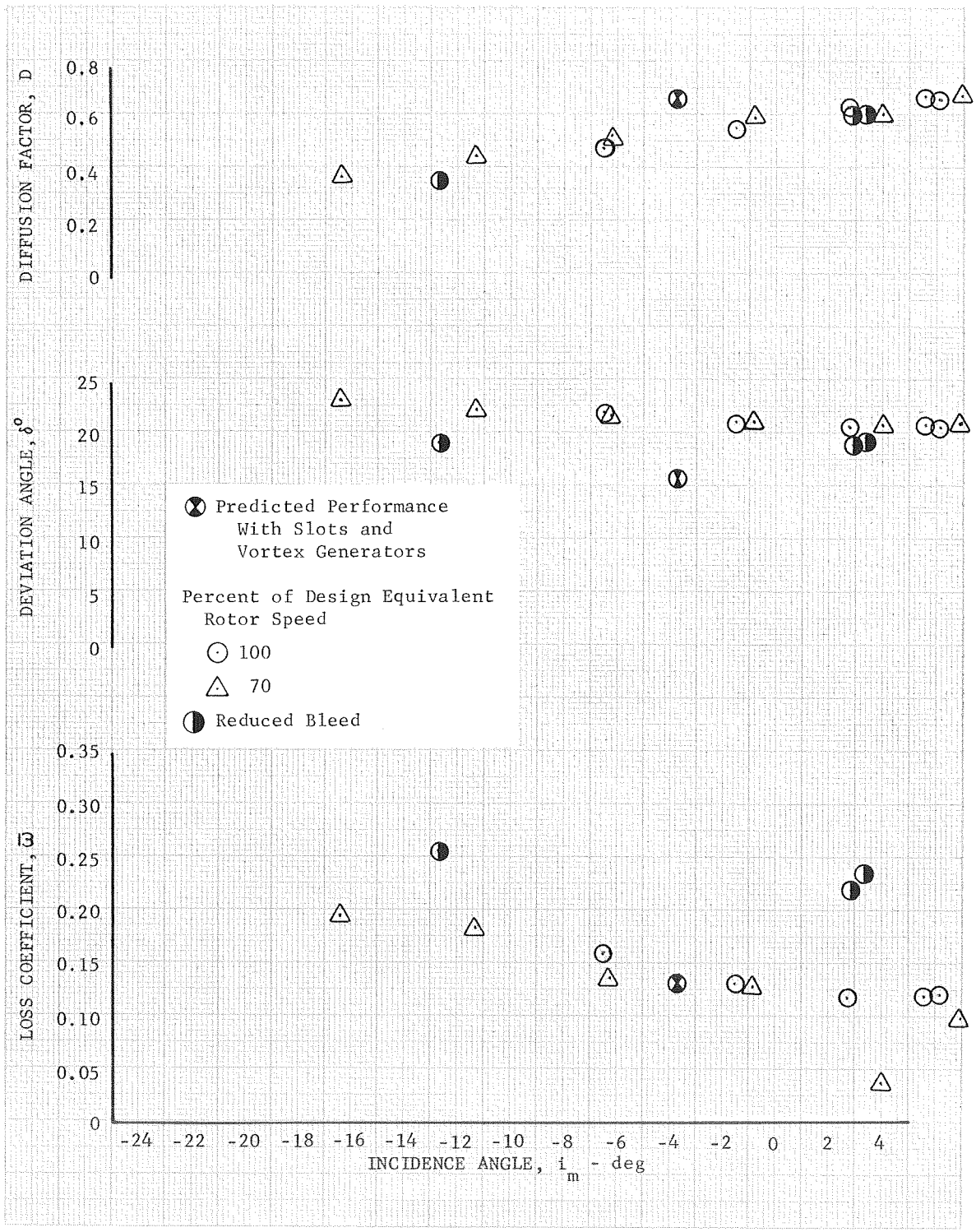

Figure 31h. Slotted Stator 4 Blade Element Performance, 90% Span From Tip

DF 83353

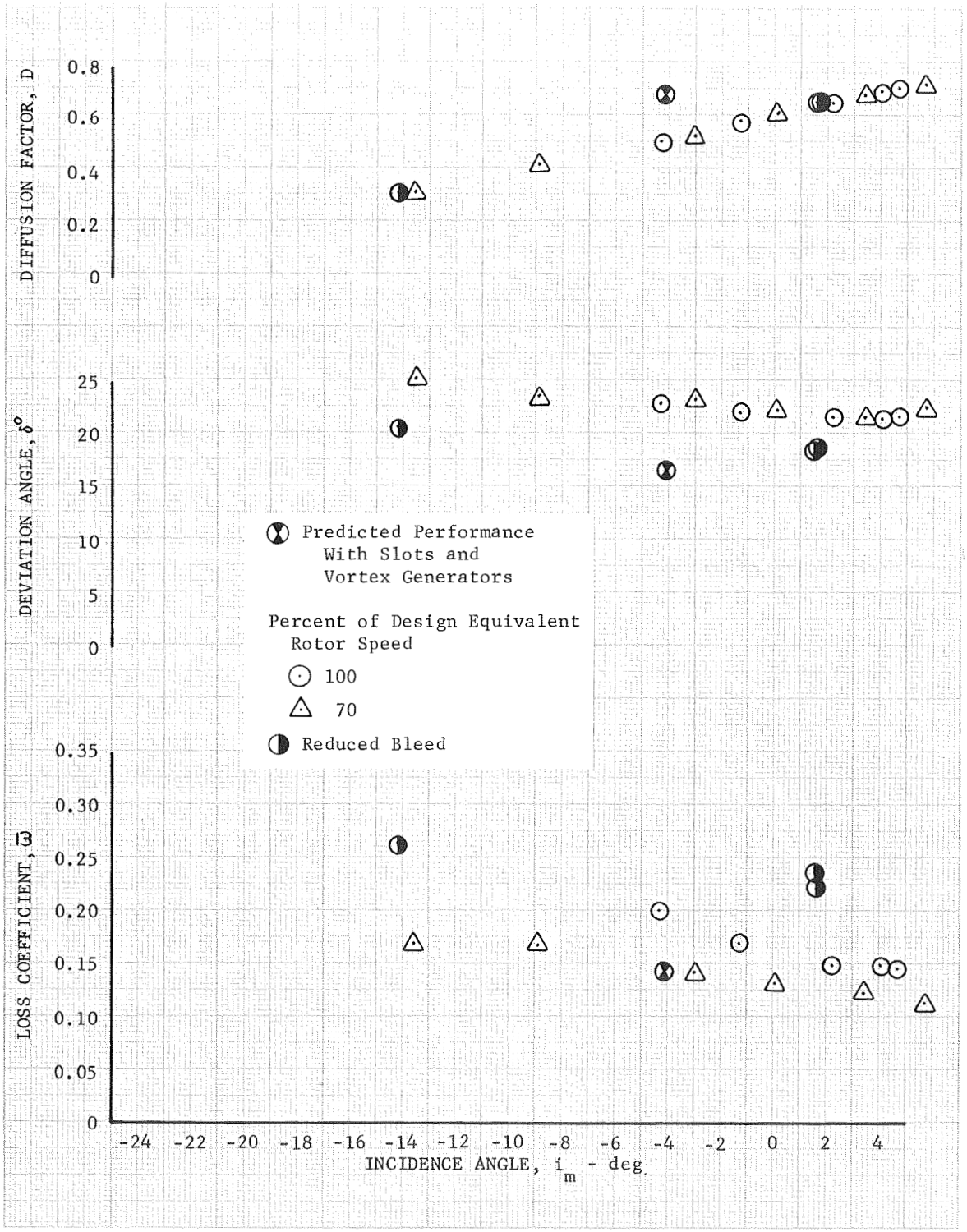

Figure 31i. Slotted Stator 4 Blade Element Performance, 95% Span From Tip

DF 83354

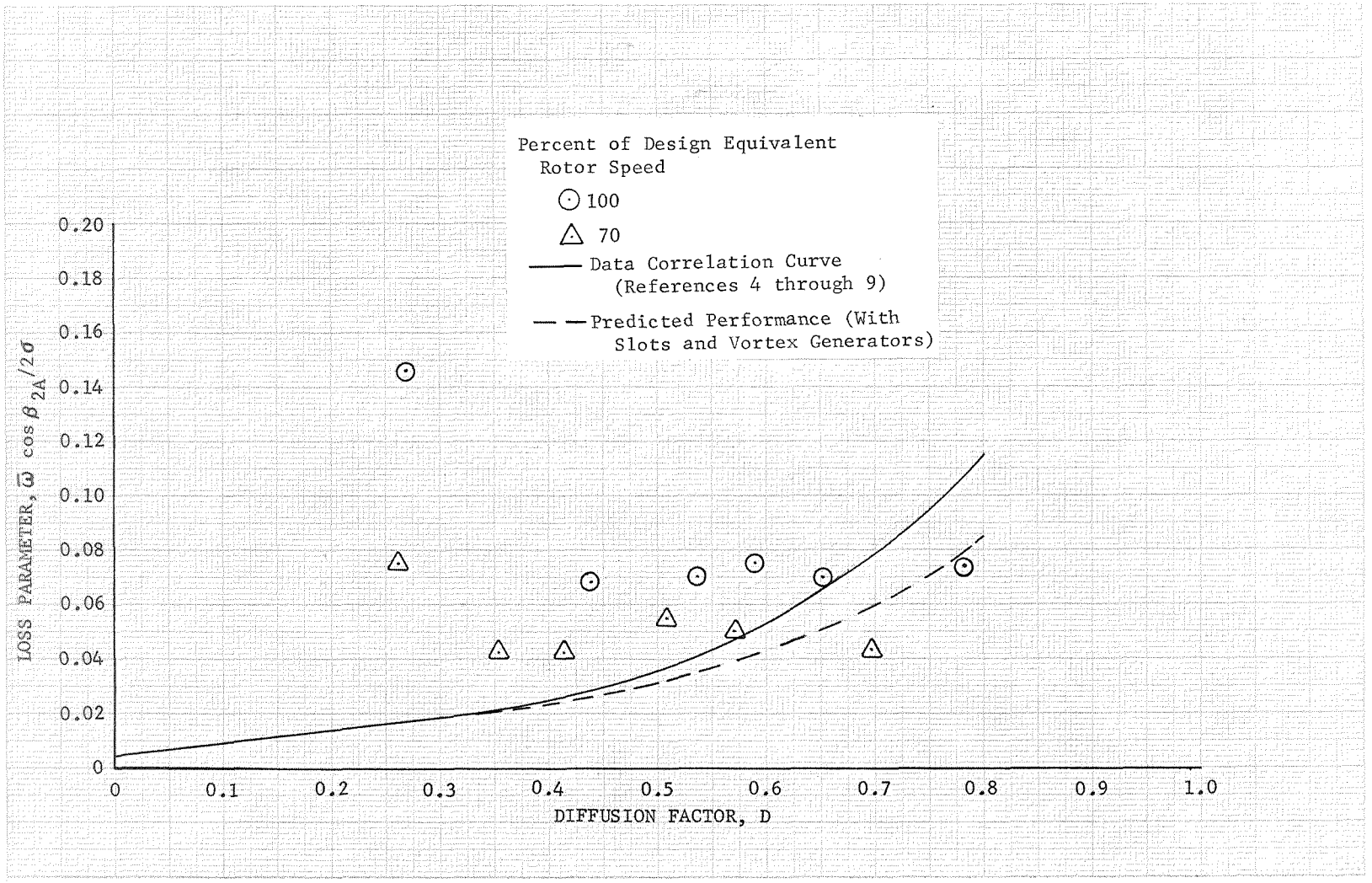

Figure 32a. Slotted Stator 4 Loss Parameter vs Diffusion Factor, 10% Span From Tip

DF 83355

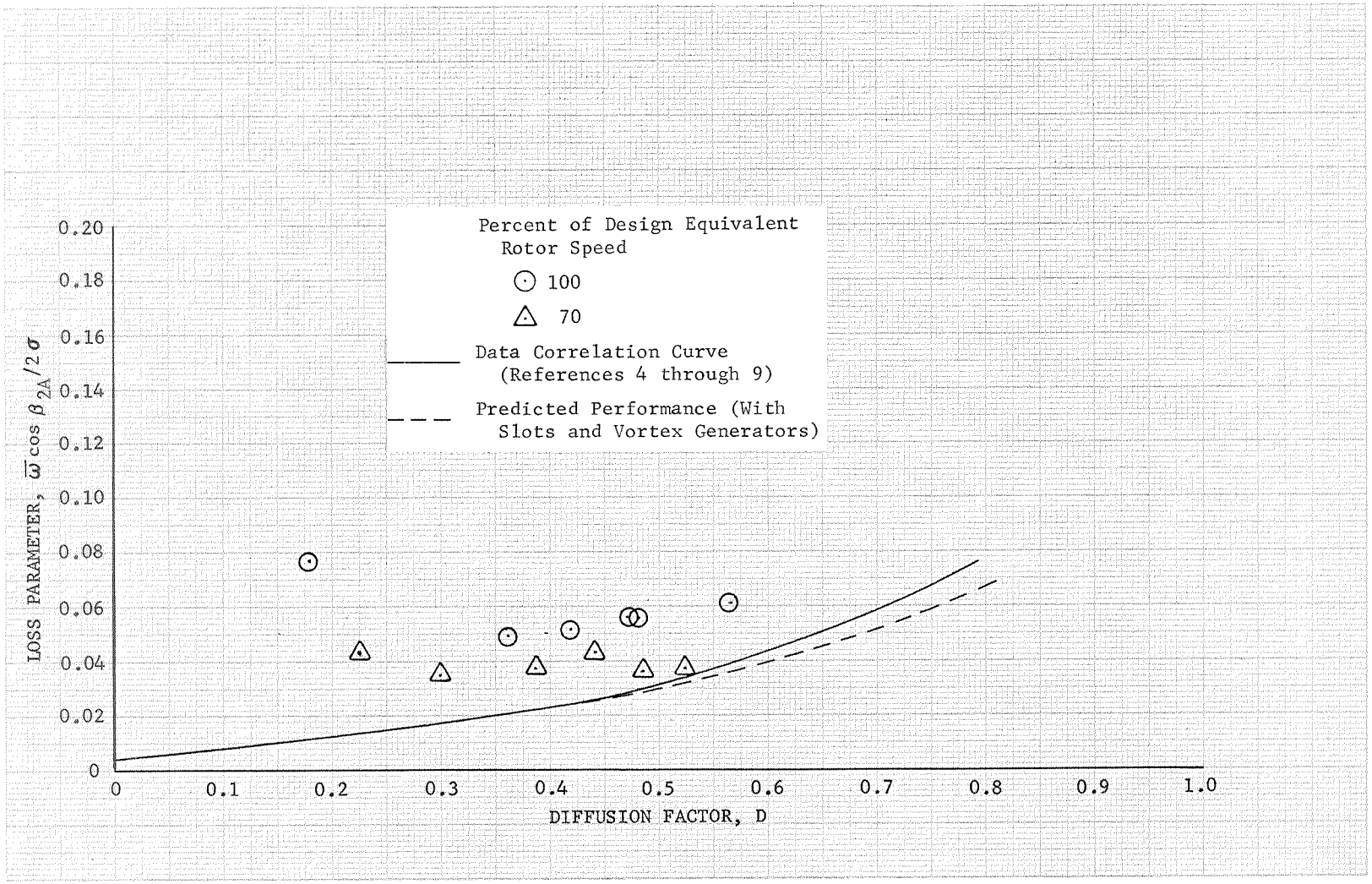

Figure 32b. Slotted Stator 4 Loss Parameter vs Diffusion Factor, 30% Span From Tip

DF 83356

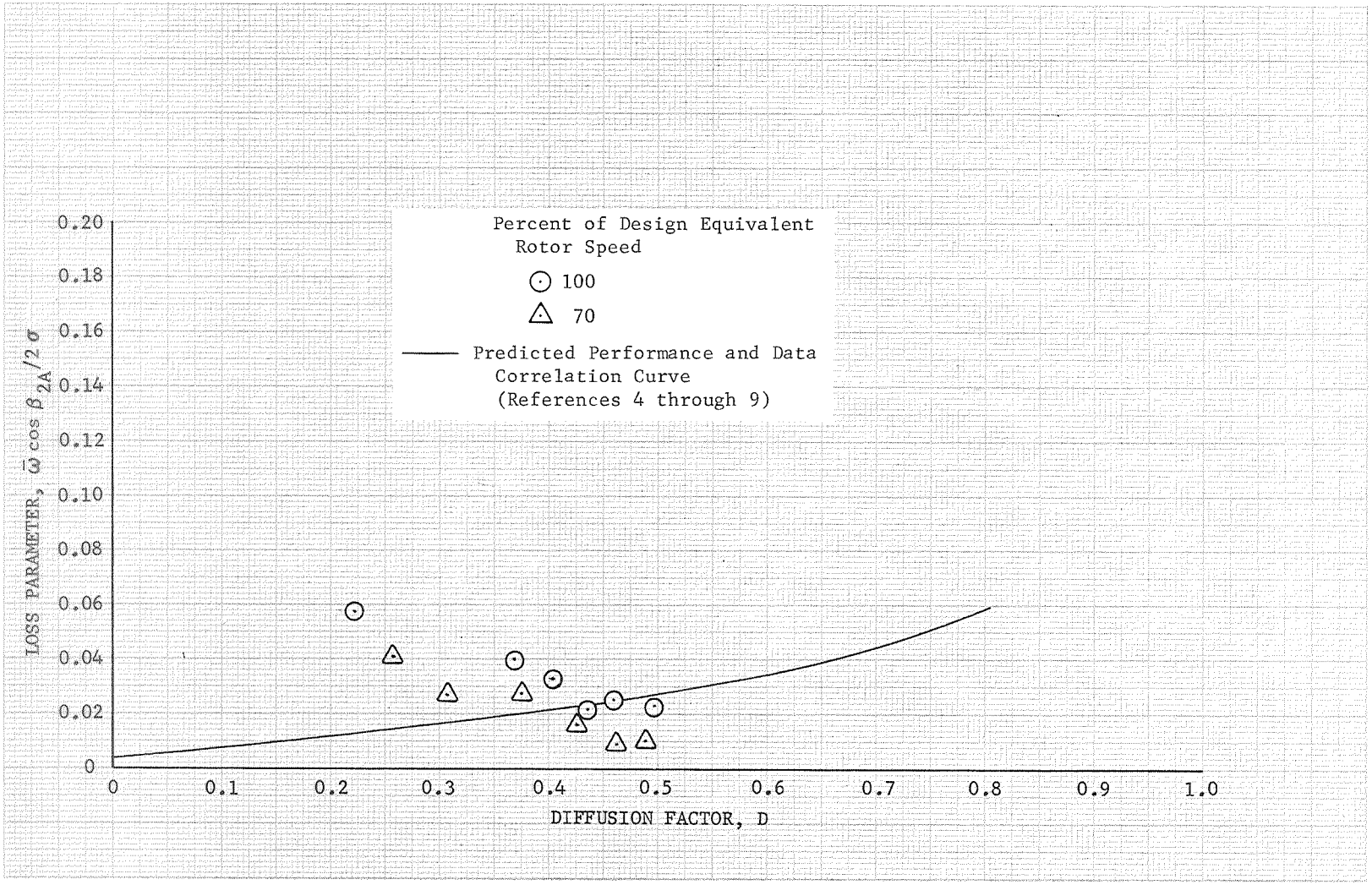

Figure 32c. Slotted Stator 4 Loss Parameter vs Diffusion Factor, 50% Span From Tip

DF 83357

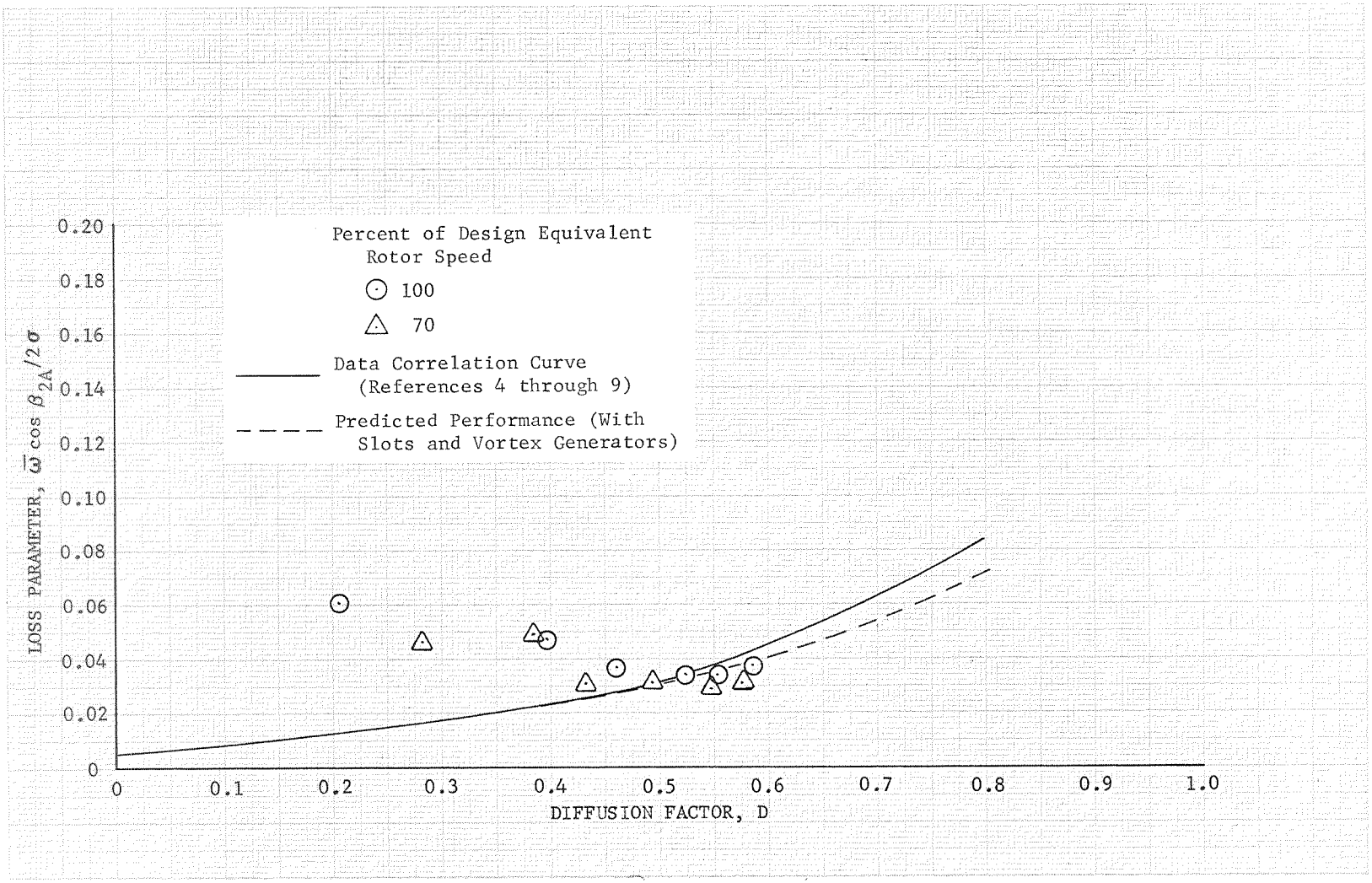

Figure 32d. Slotted Stator 4 Loss Parameter vs Diffusion Factor, 70% Span From Tip

DF 83358

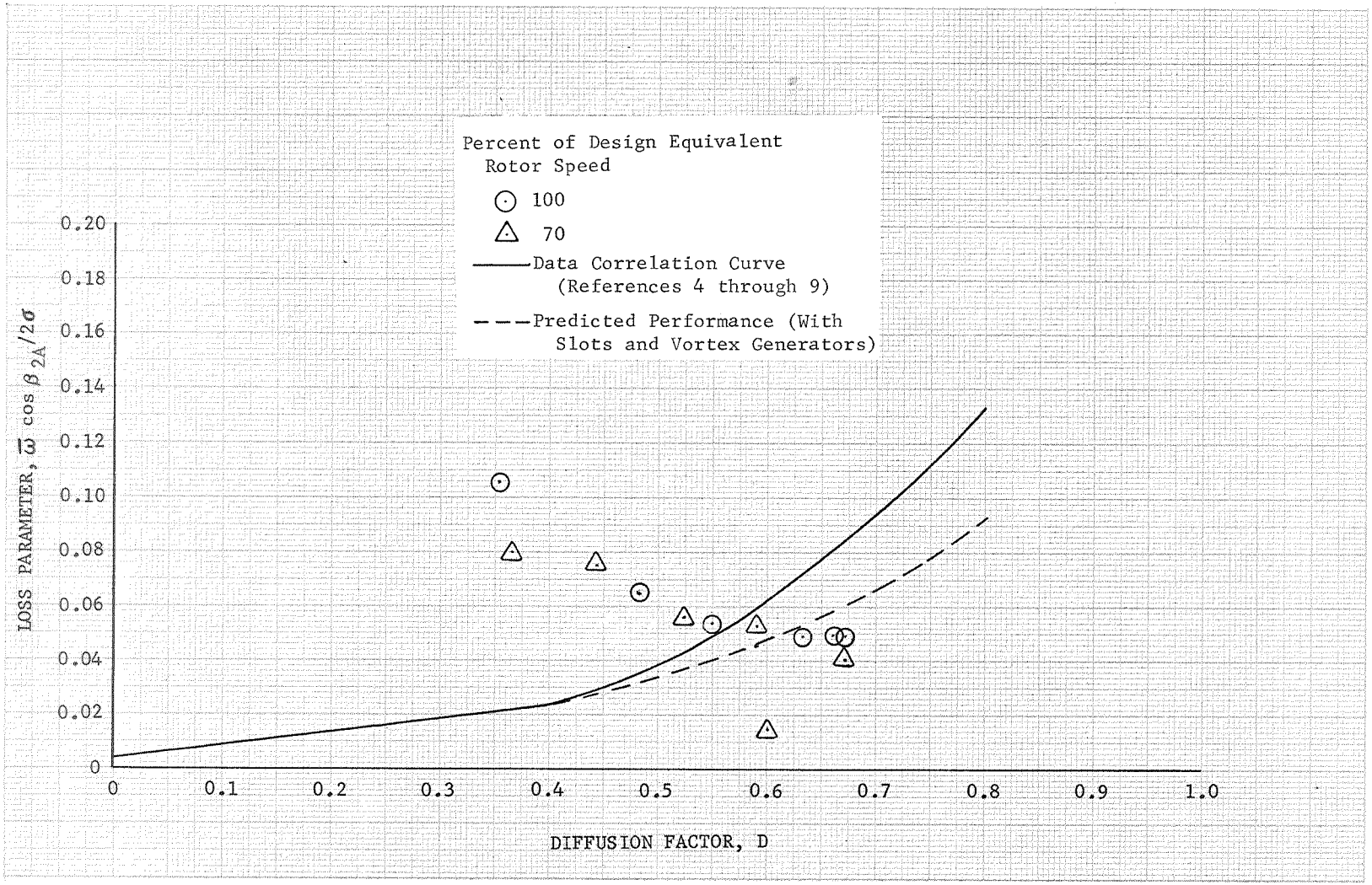

Figure 32e. Slotted Stator 4 Loss Parameter vs Diffusion Factor, 90% Span From Tip

DF 83359

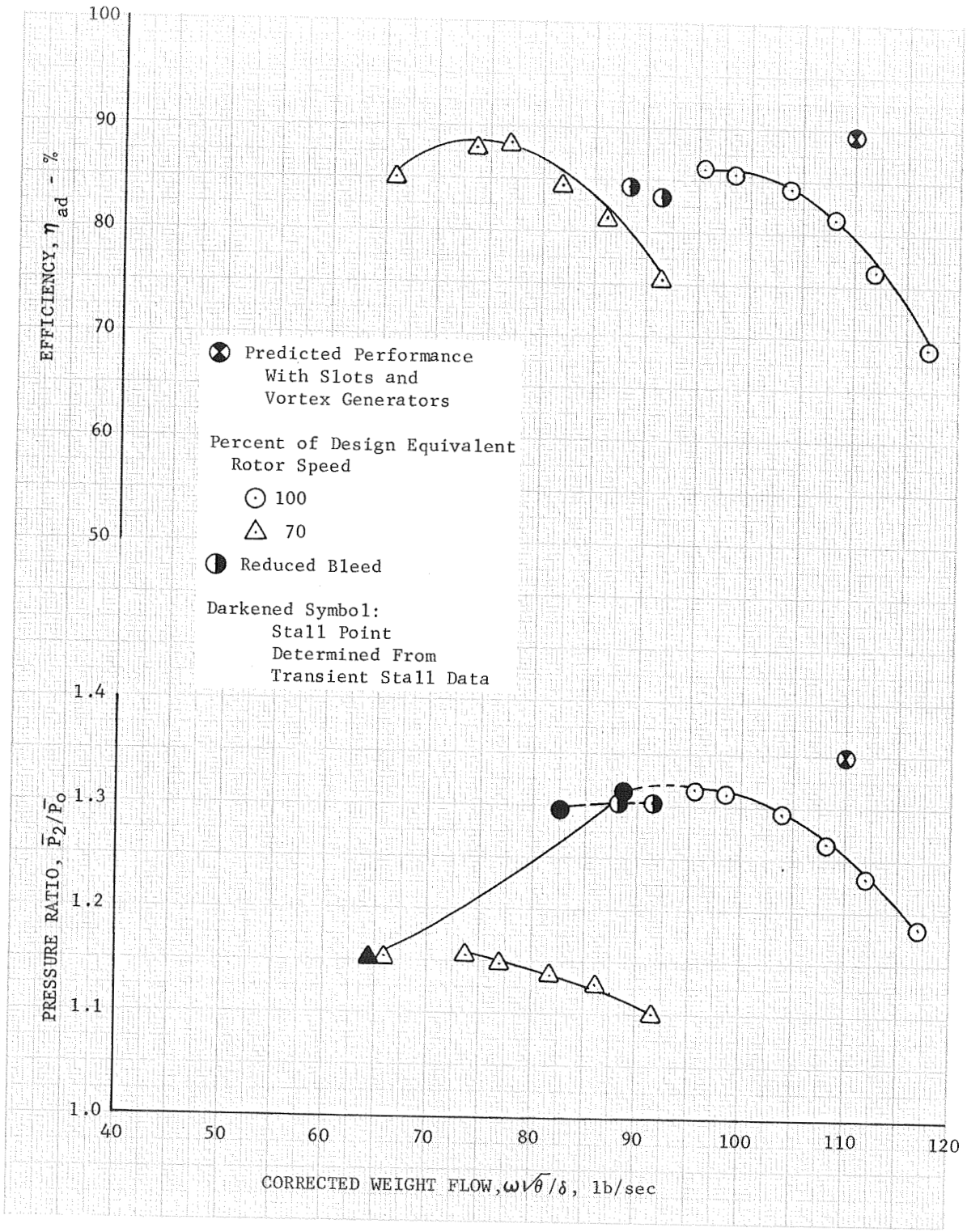

Figure 33. Overall Performance Slotted Rotor 4 (With Vortex Generators Ahead of the Rotor) DF 83360

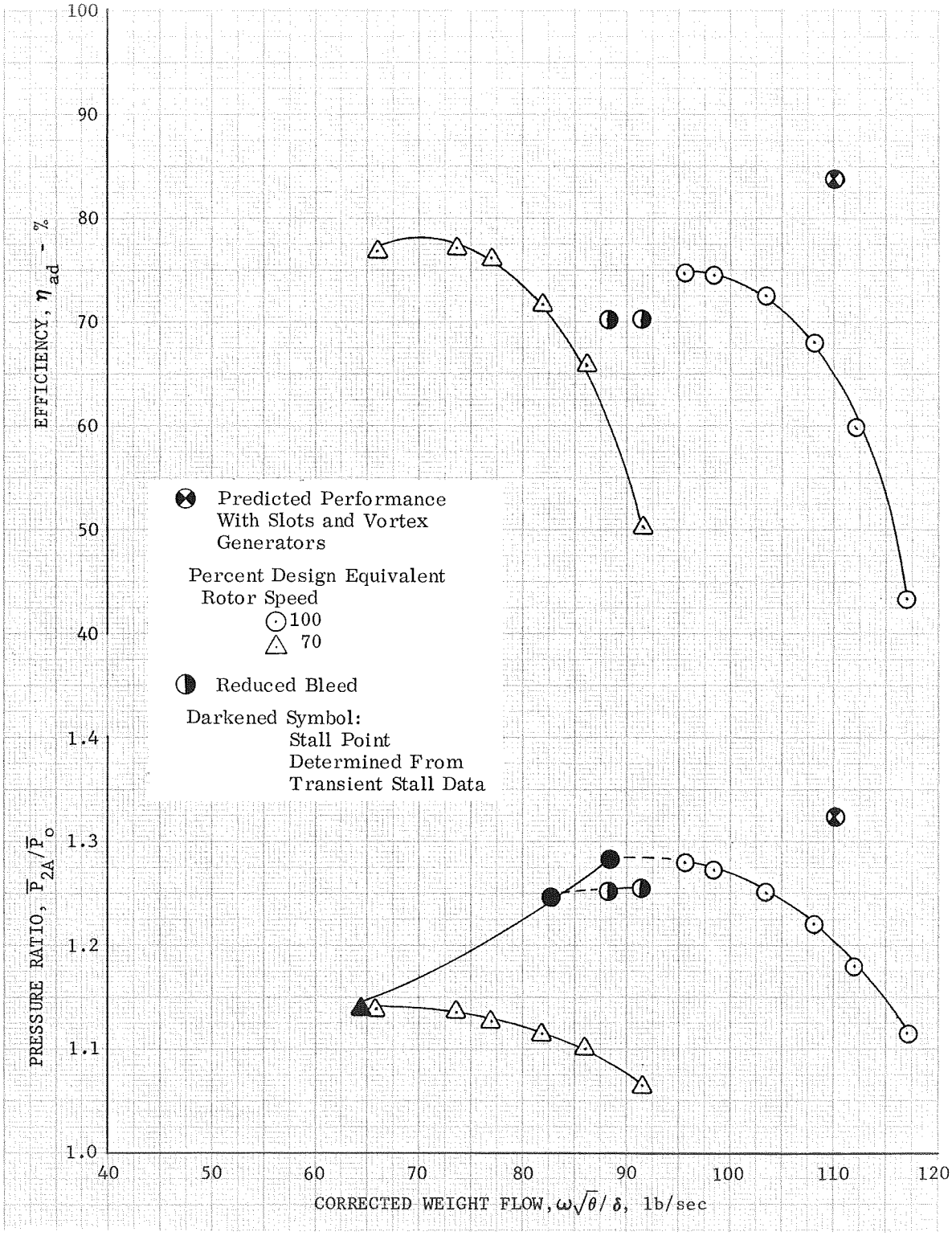

Figure 34. Overall Performance Slotted Stage 4 (With Vortex Generators Ahead of the Rotor) DF 83361

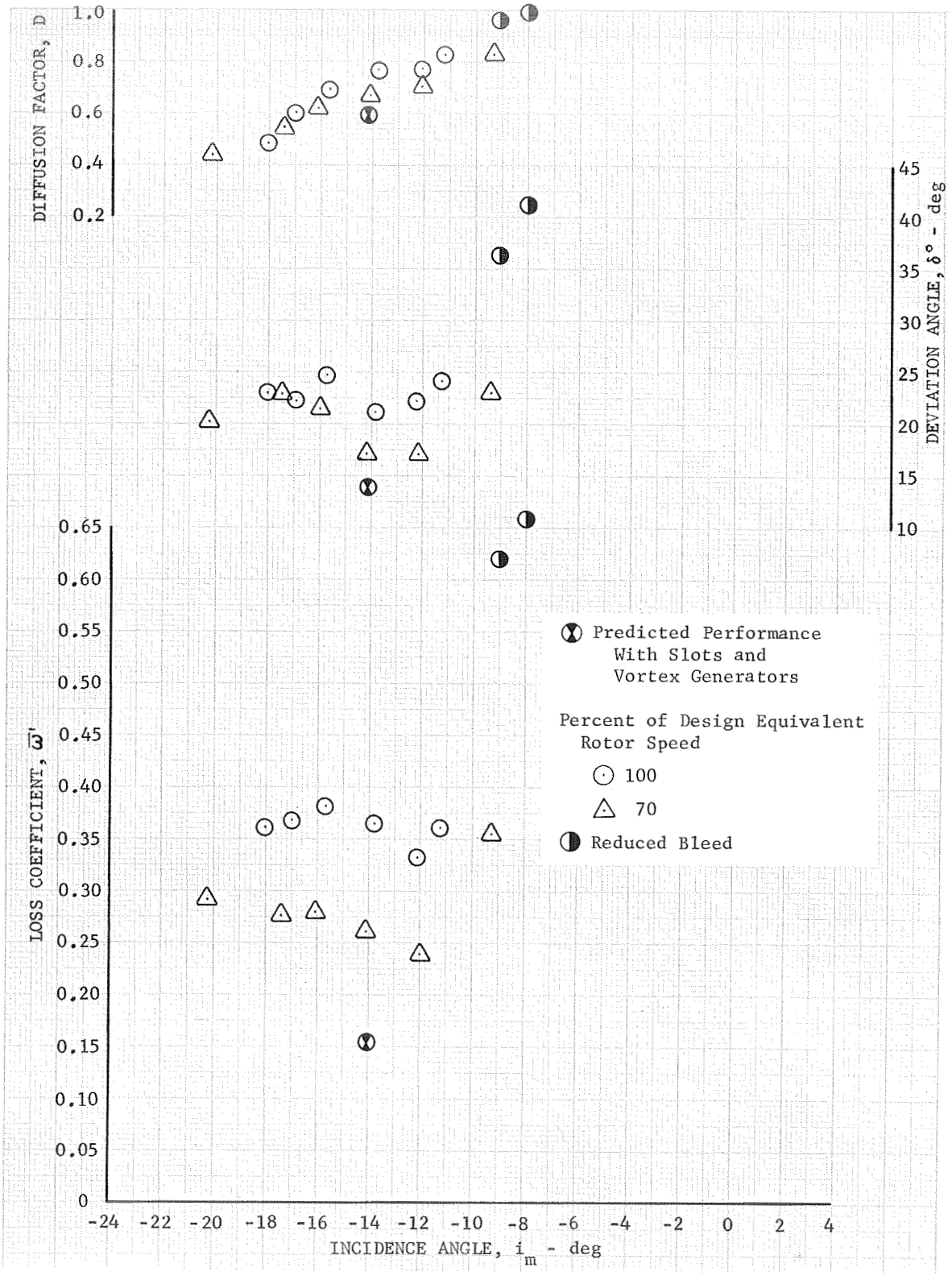

Figure 35a. Slotted Rotor 4 (With Vortex Generators Ahead of the Rotor) Blade Element Performance, 5% Span From Tip

DF 83422

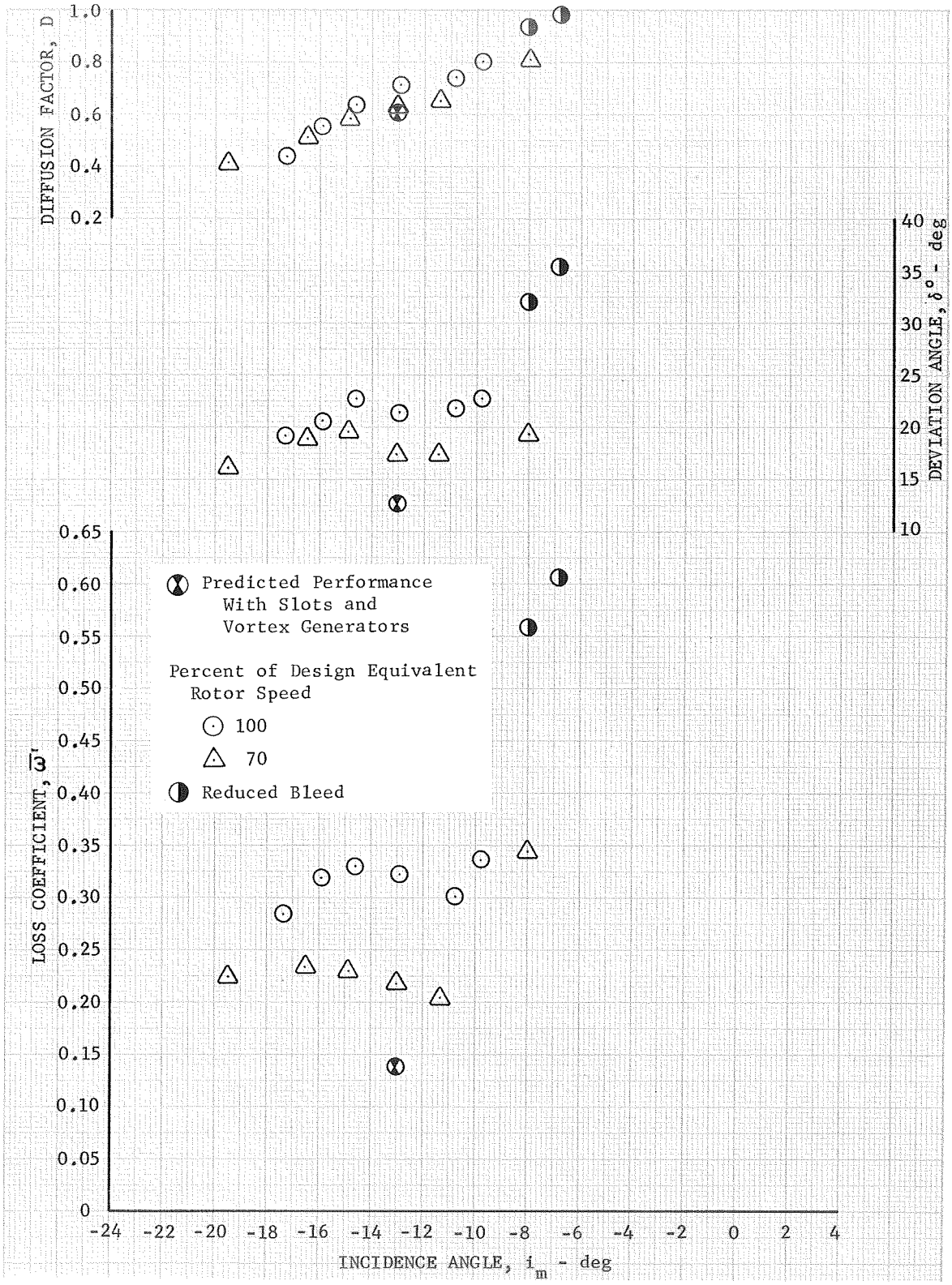

Figure 35b. Slotted Rotor 4 (With Vortex Generators Ahead of the Rotor) Blade Element Performance, 10% Span From Tip

DF 83423

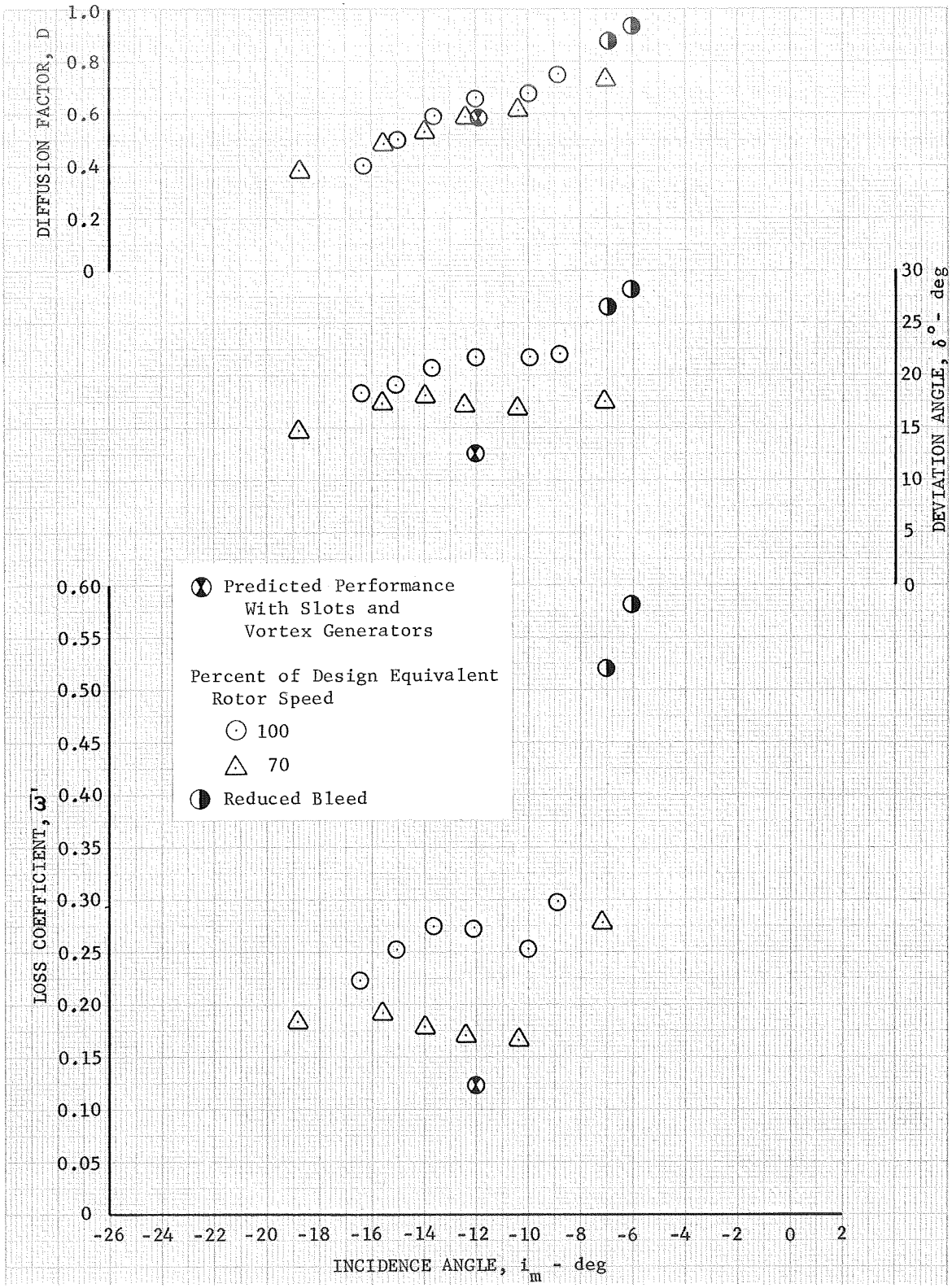

Figure 35c. Slotted Rotor 4 (With Vortex Generators Ahead of the Rotor) Blade Element Performance, 15% Span From Tip DF 83424

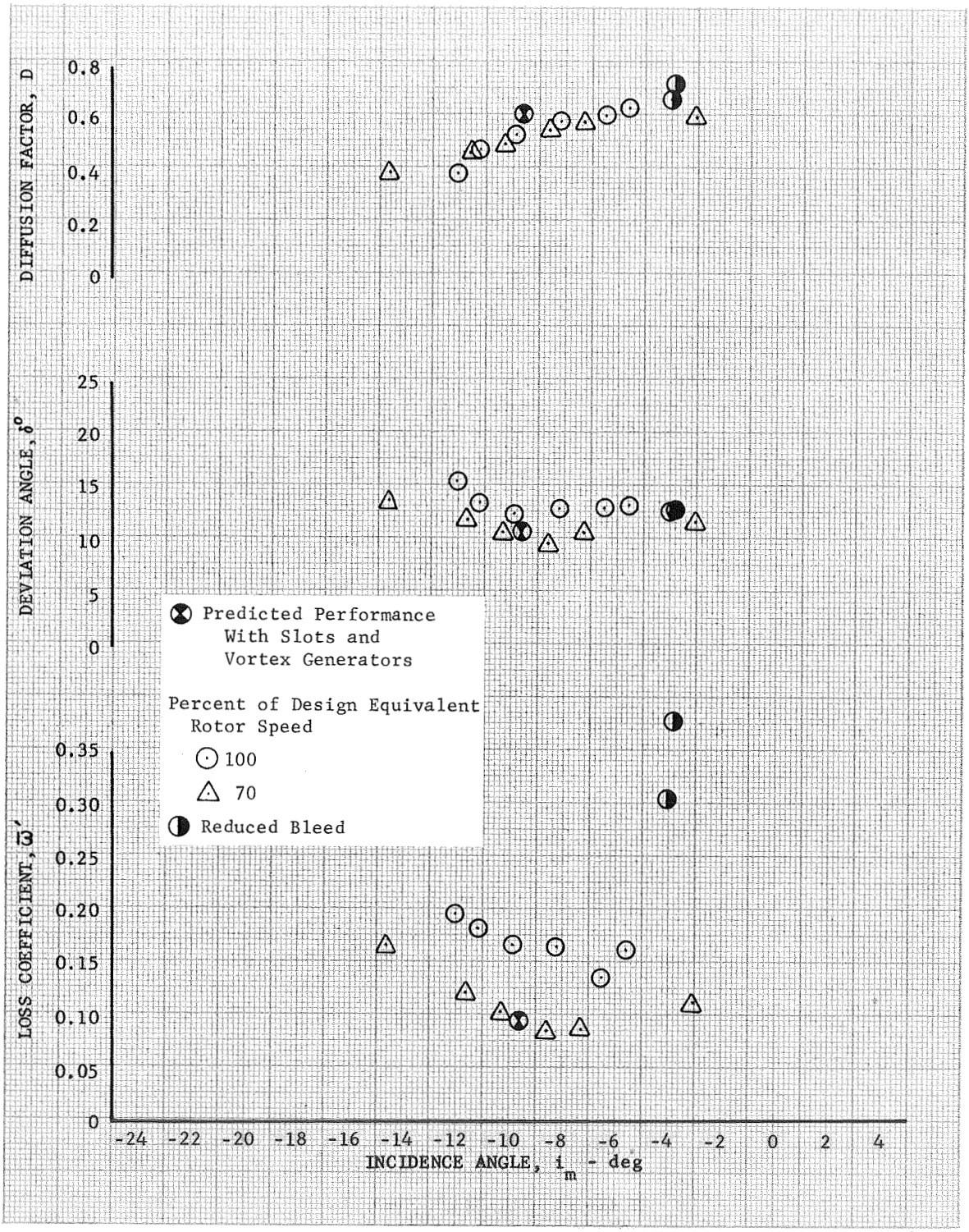

Figure 35d. Slotted Rotor 4 (With Vortex Generators Ahead of the Rotor) Blade Element Performance, 30% Span From Tip

DF 83362

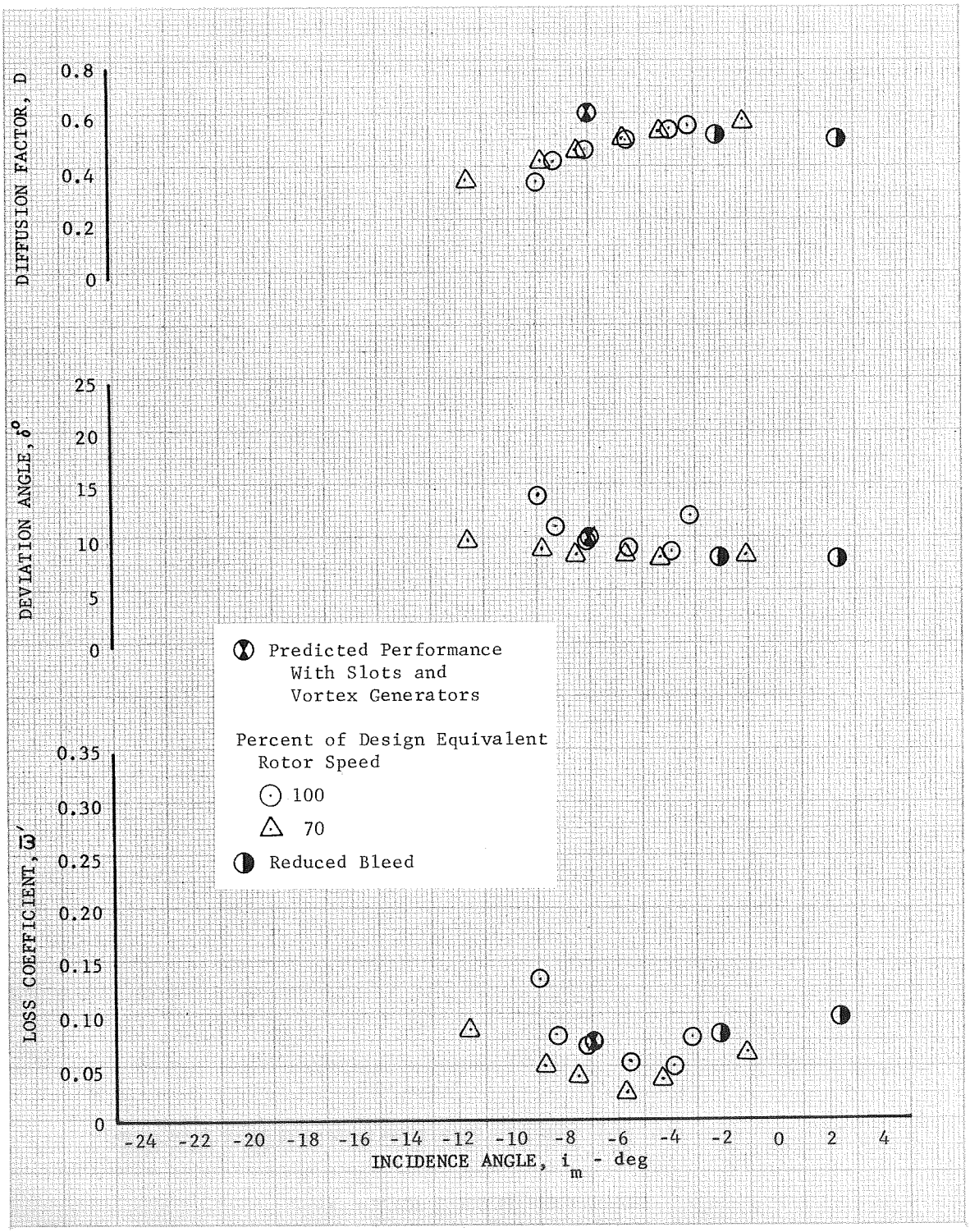

Figure 35e. Slotted Rotor 4 (With Vortex Generators Ahead of the Rotor) Blade Element Performance, 50% Span From Tip DF 83363

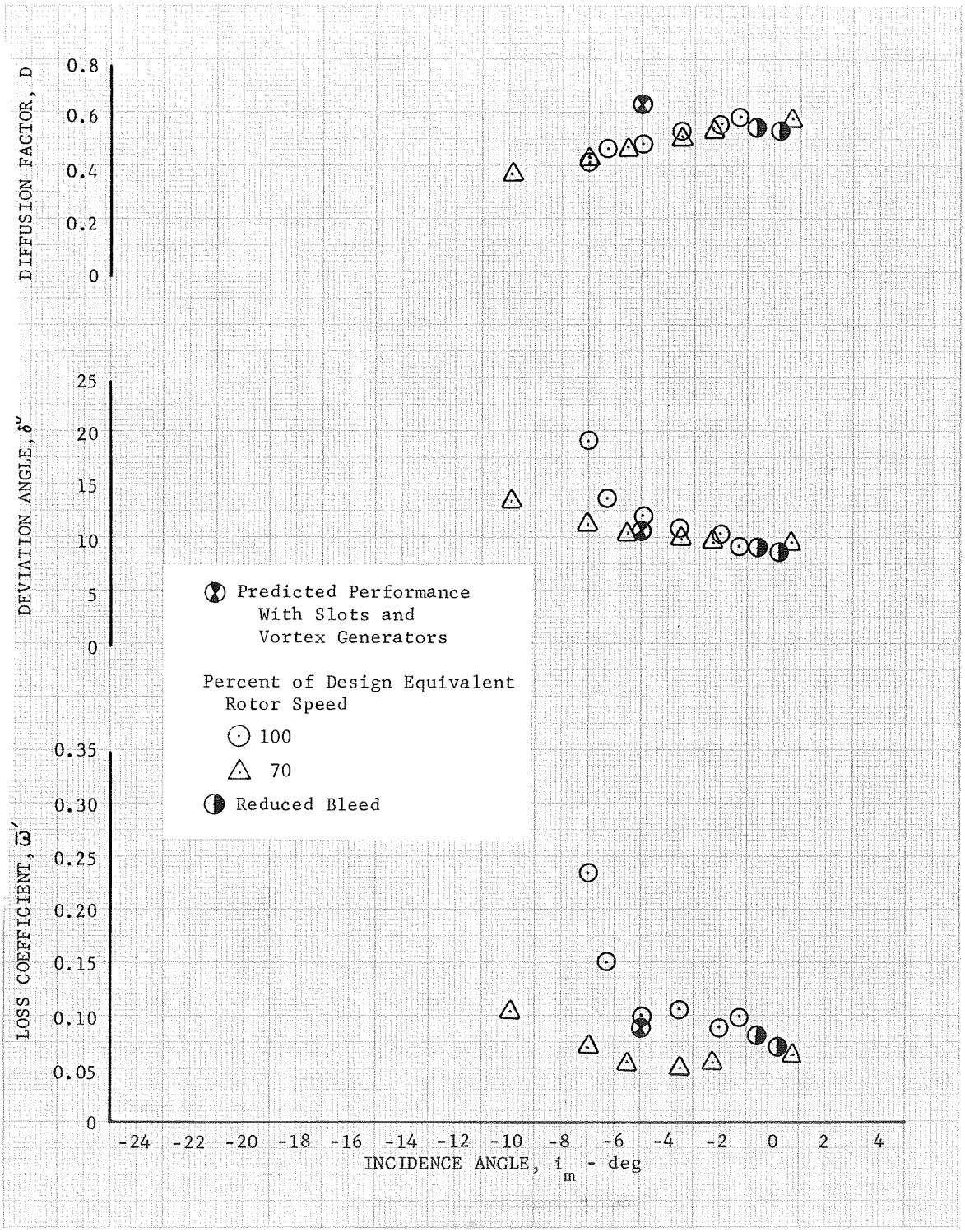

Figure 35f. Slotted Rotor 4 (With Vortex Generators Ahead of the Rotor) Blade Element Performance, 70% Span From Tip

DF 83364

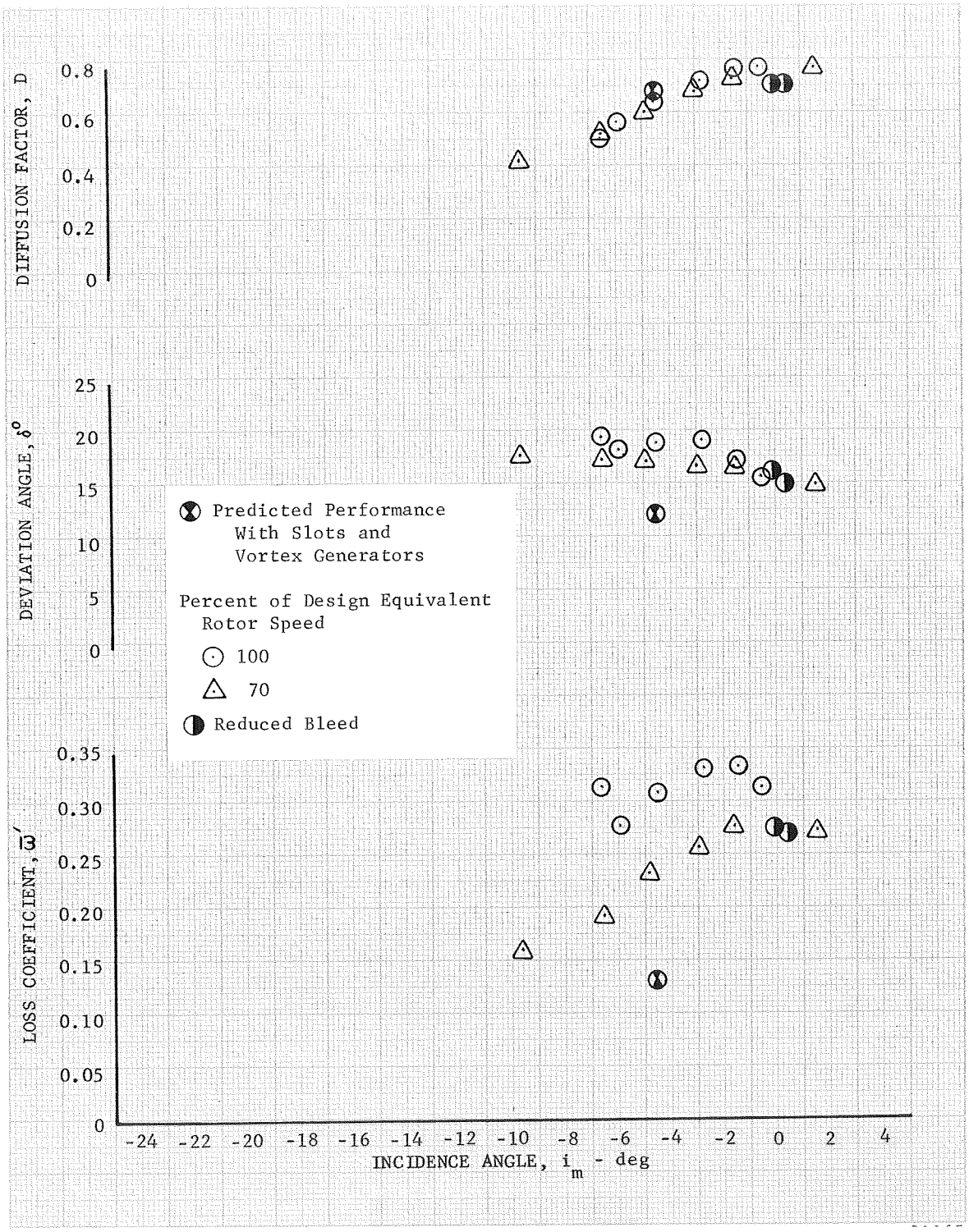

Figure 35g. Slotted Rotor 4 (With Vortex Generators Ahead of the Rotor) Blade Element Performance, 85% Span From Tip DF 83365

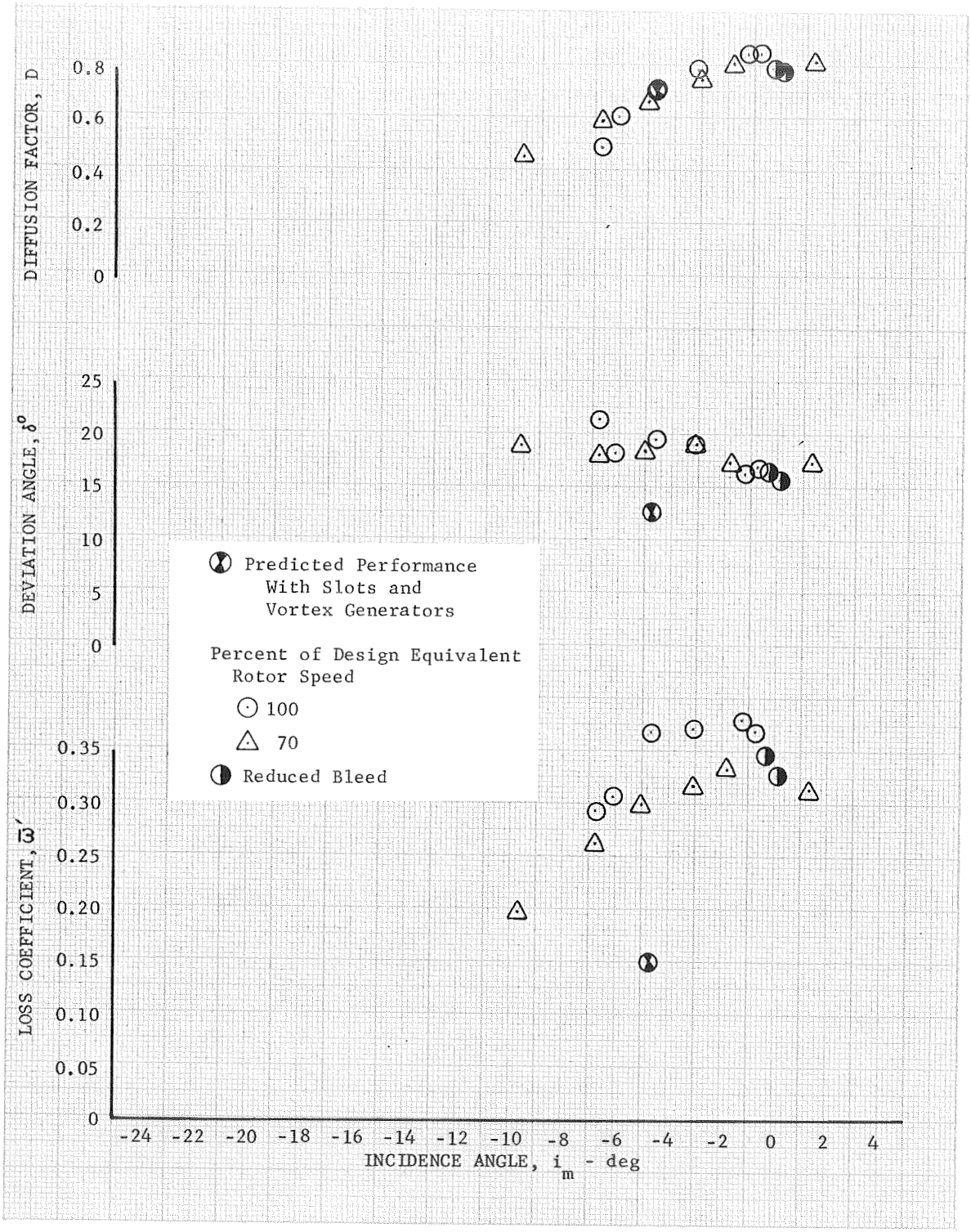

Figure 35h. Slotted Rotor 4 (With Vortex Generators Ahead of the Rotor) Blade Element Performance, 90% Span From Tip DF 83366

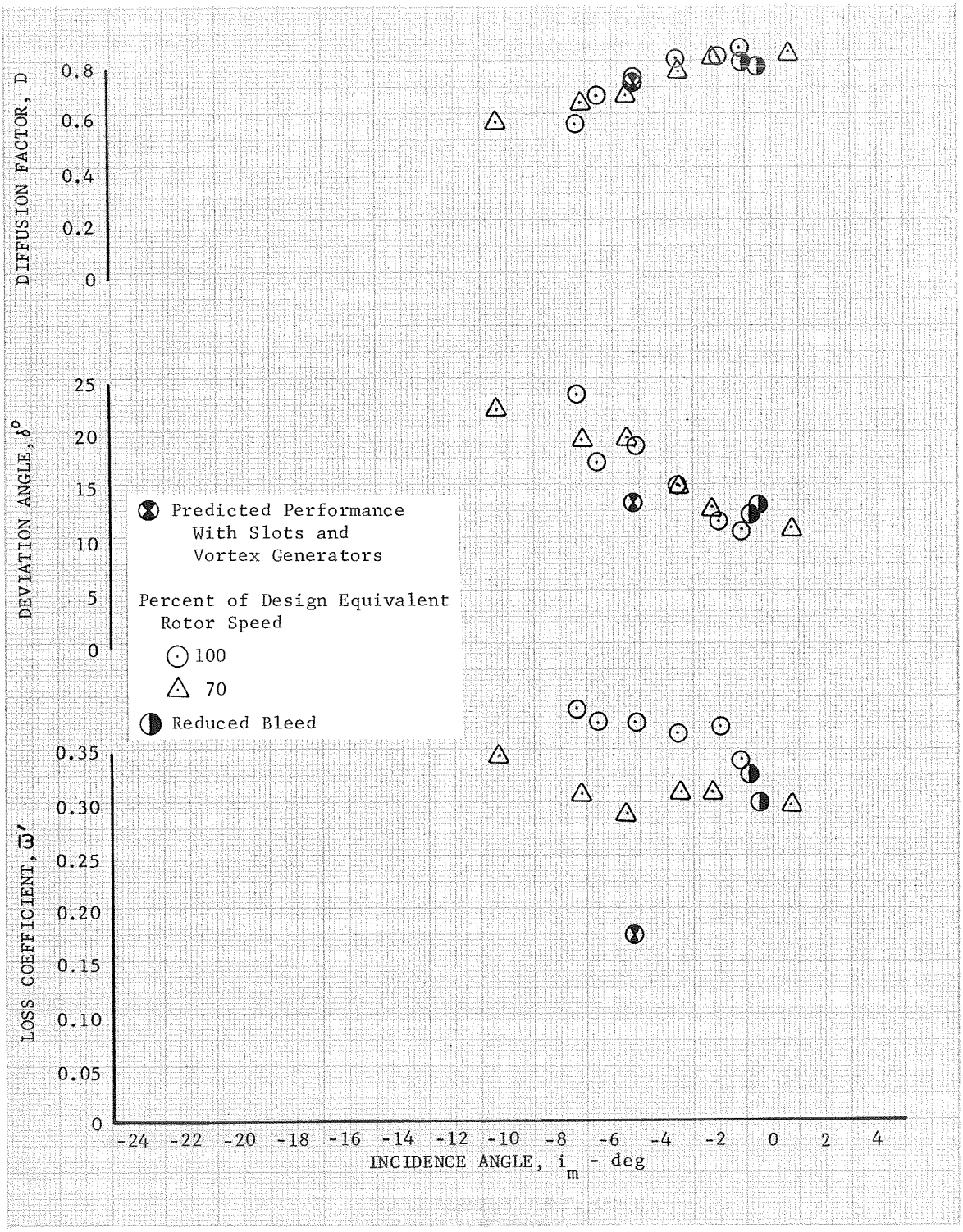

Figure 35i Slotted Rotor 4 (With Vortex Generators Ahead of the Rotor) Blade Element Performance, 95% Span From Tip

DF 83367

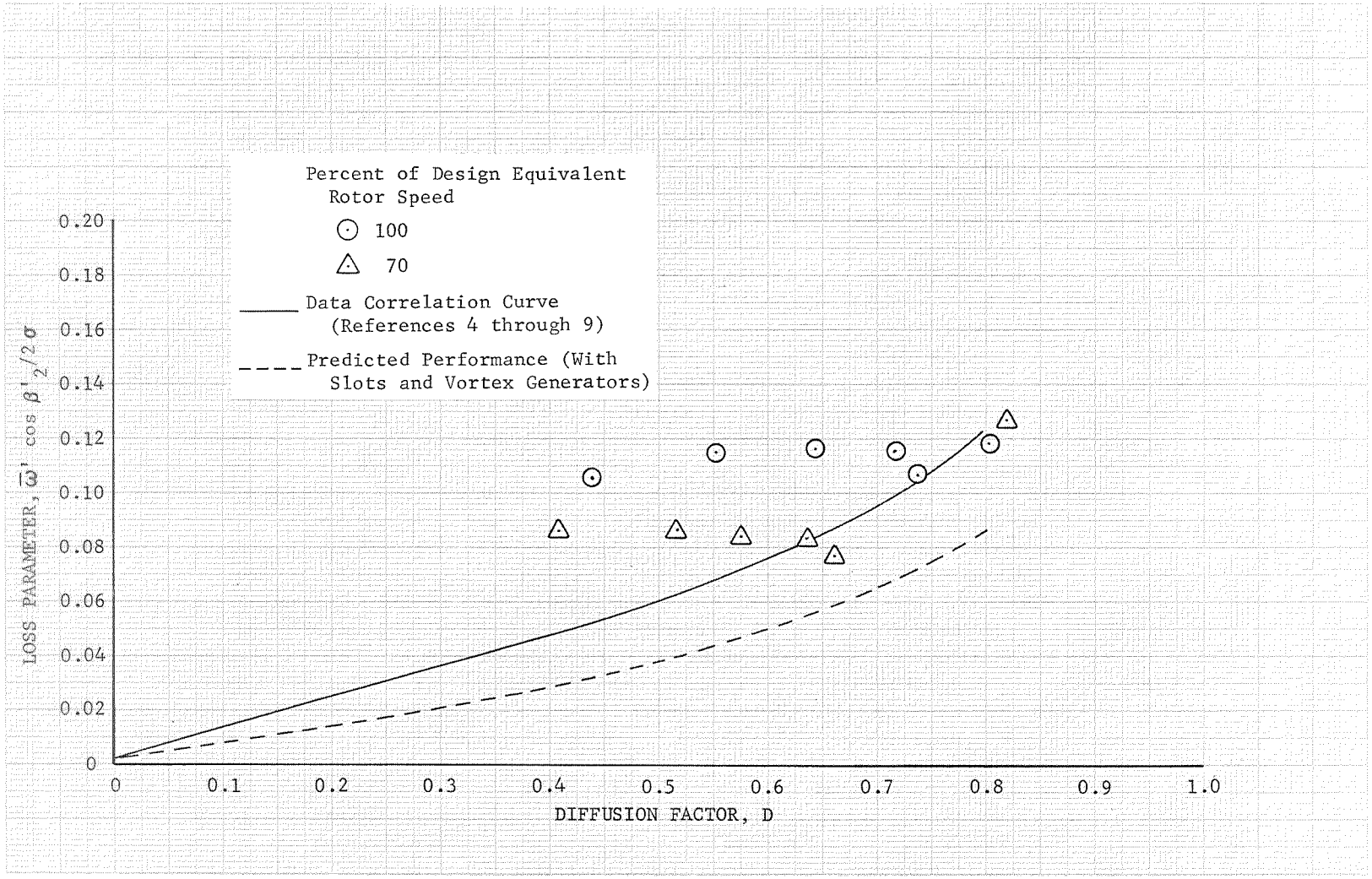

Figure 36a. Slotted Rotor 4 (With Vortex Generators Ahead of the Rotor) Loss Parameter vs Diffusion Factor, 10% Span From Tip

DF 83368

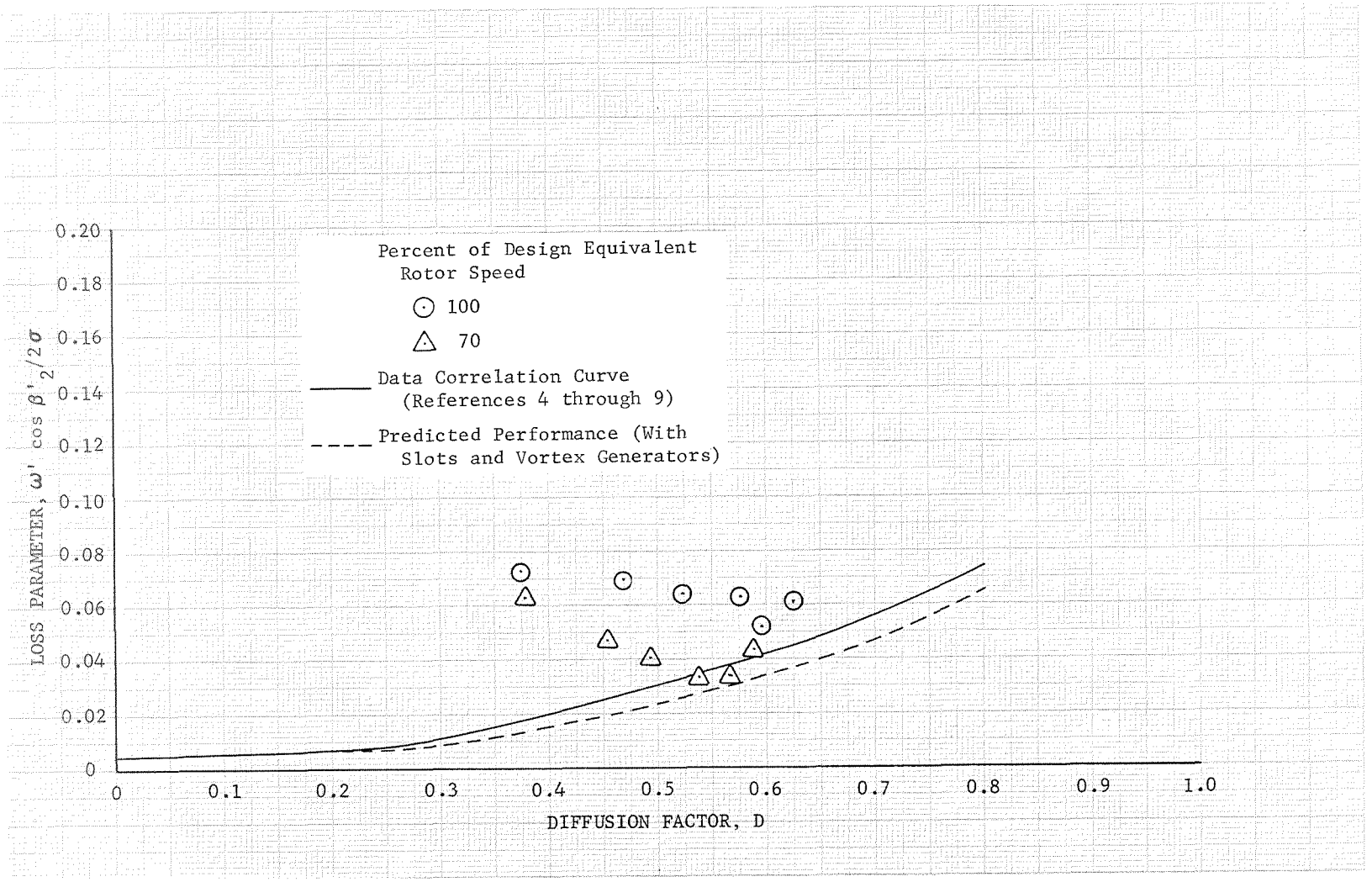

Figure 36b. Slotted Rotor 4 (With Vortex Generators Ahead of the Rotor) Loss Parameter vs Diffusion Factor, 30% Span From Tip

DF 83369

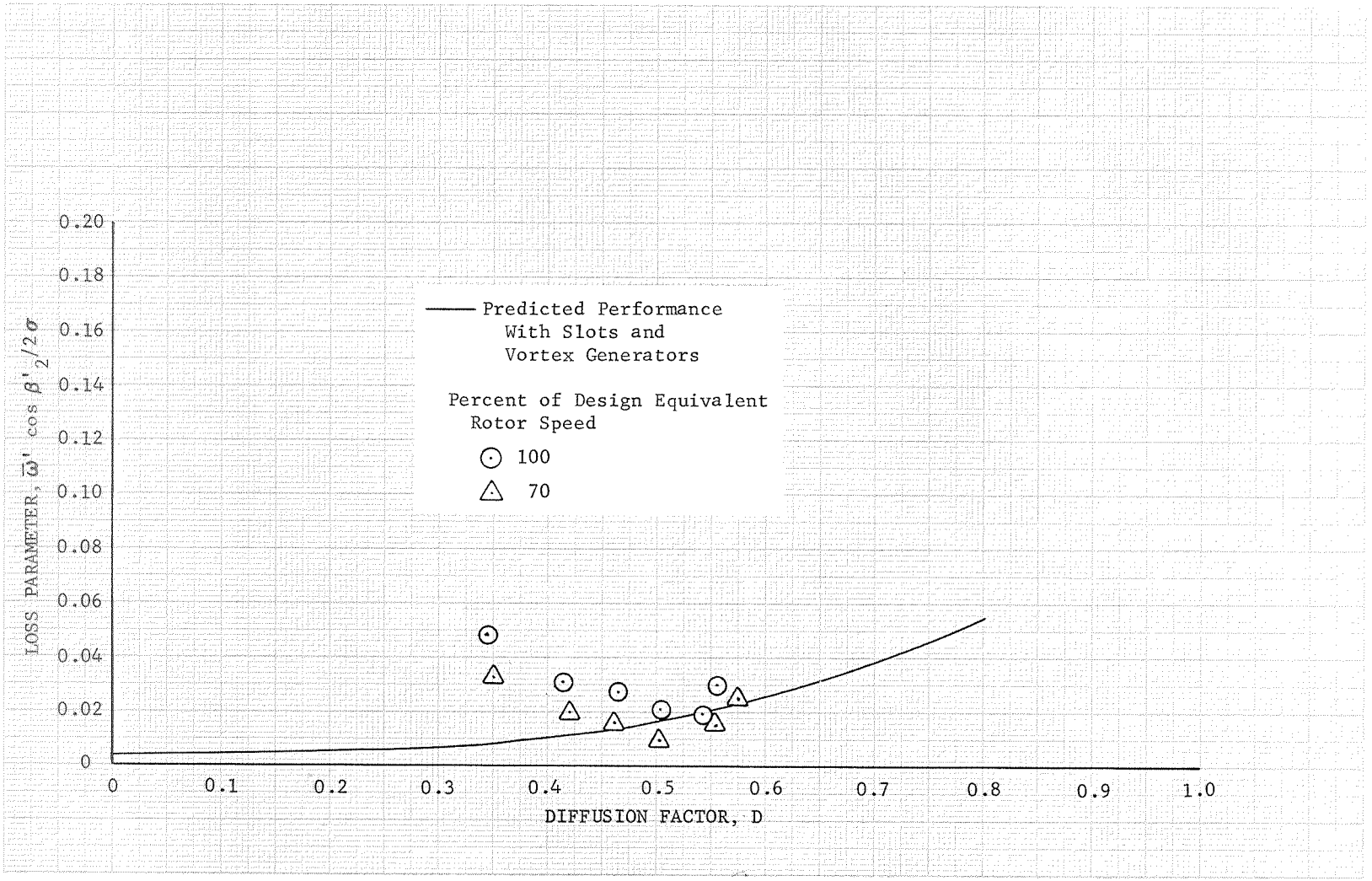

Figure 36c. Slotted Rotor 4 (With Vortex Generators Ahead of the Rotor) Loss Parameter vs Diffusion Factor, 50% Span From Tip

DF 83370

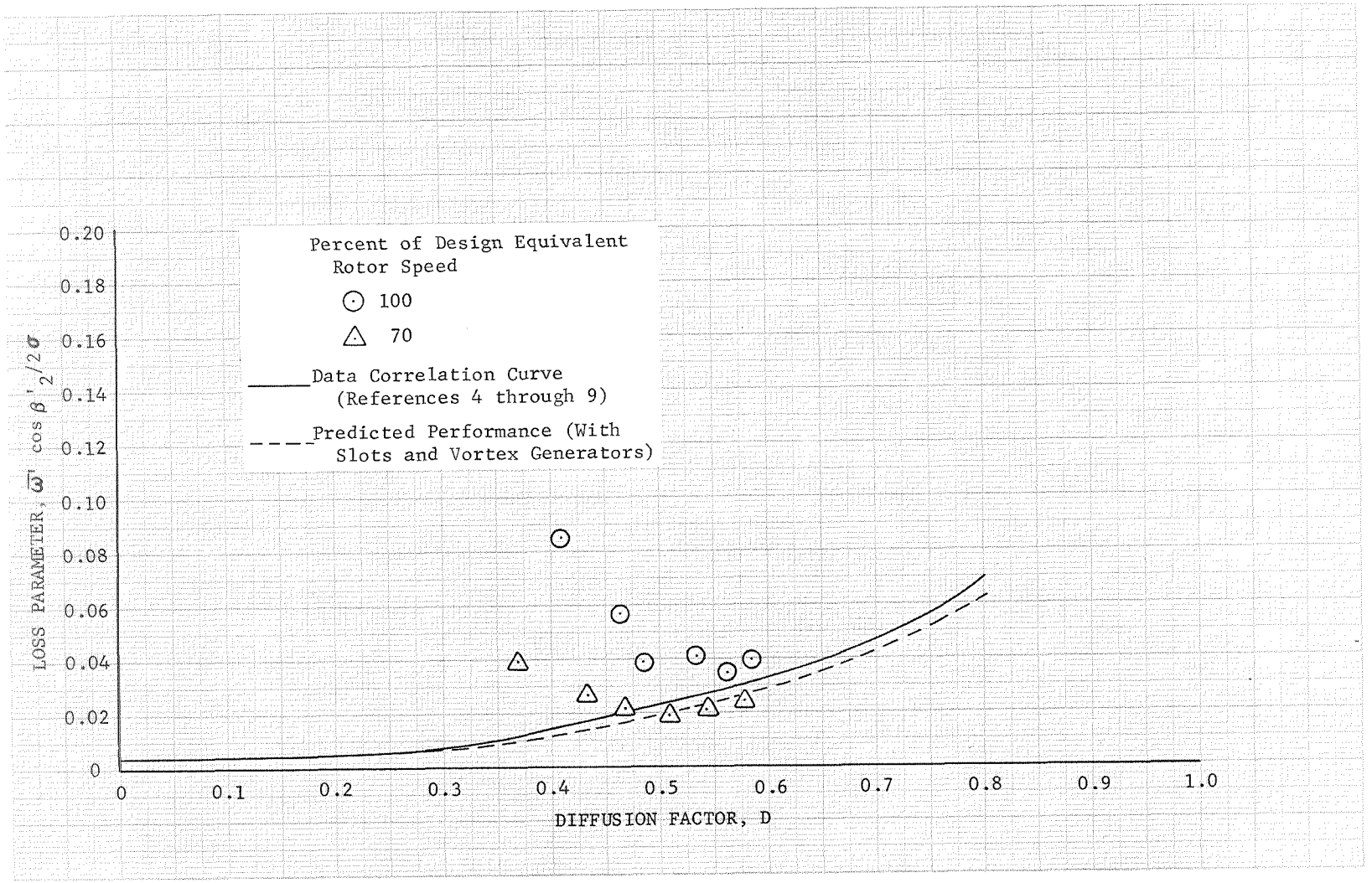

Figure 36d. Slotted Rotor 4 (With Vortex Generators Ahead of the Rotor) Loss Parameter vs Diffusion Factor, 70% Span From Tip

DF 83371

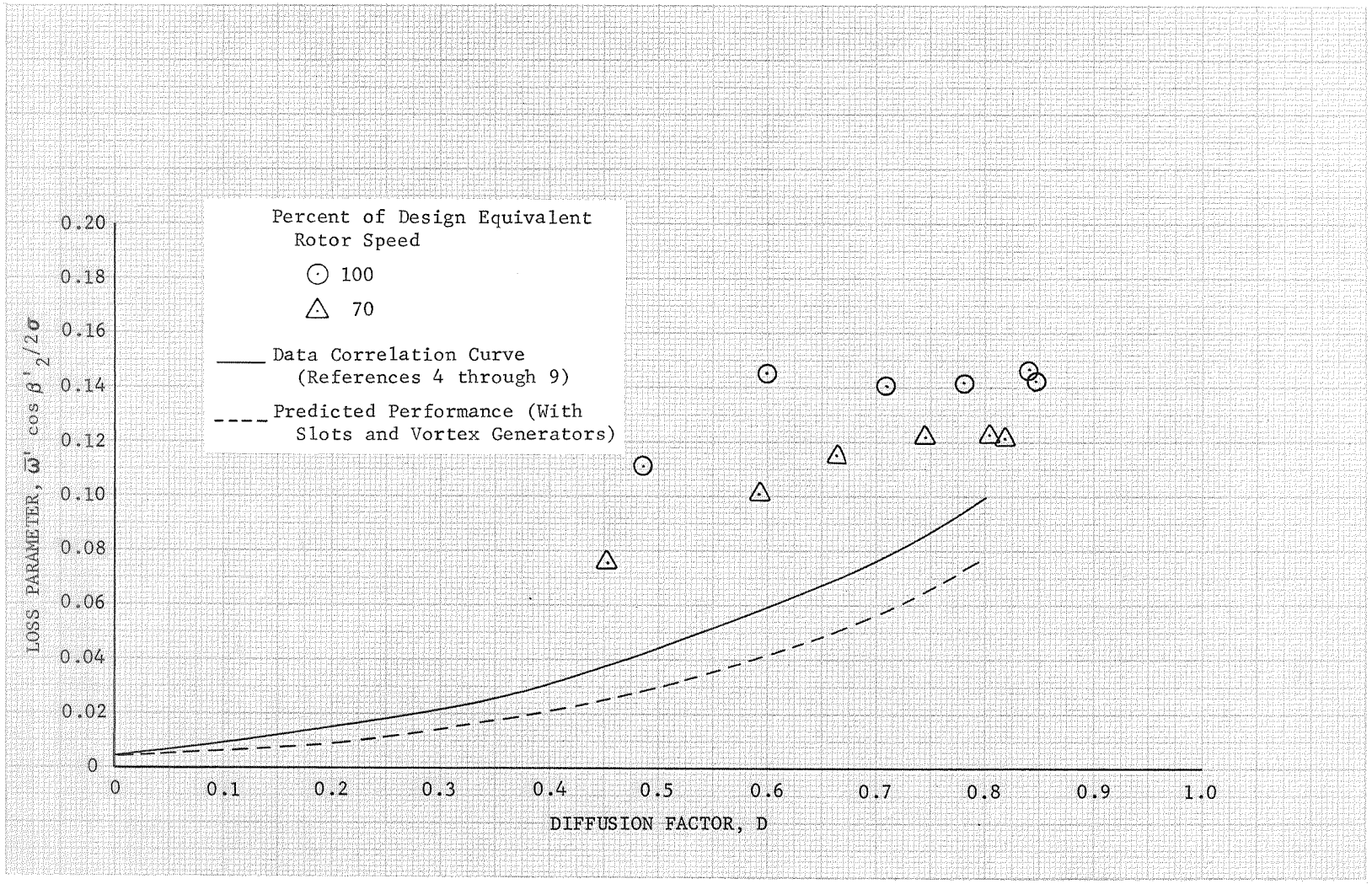

Figure 36e. Slotted Rotor 4 (With Vortex Generators Ahead of the Rotor) Loss Parameter vs Diffusion Factor, 90% Span From Tip

DF 83372

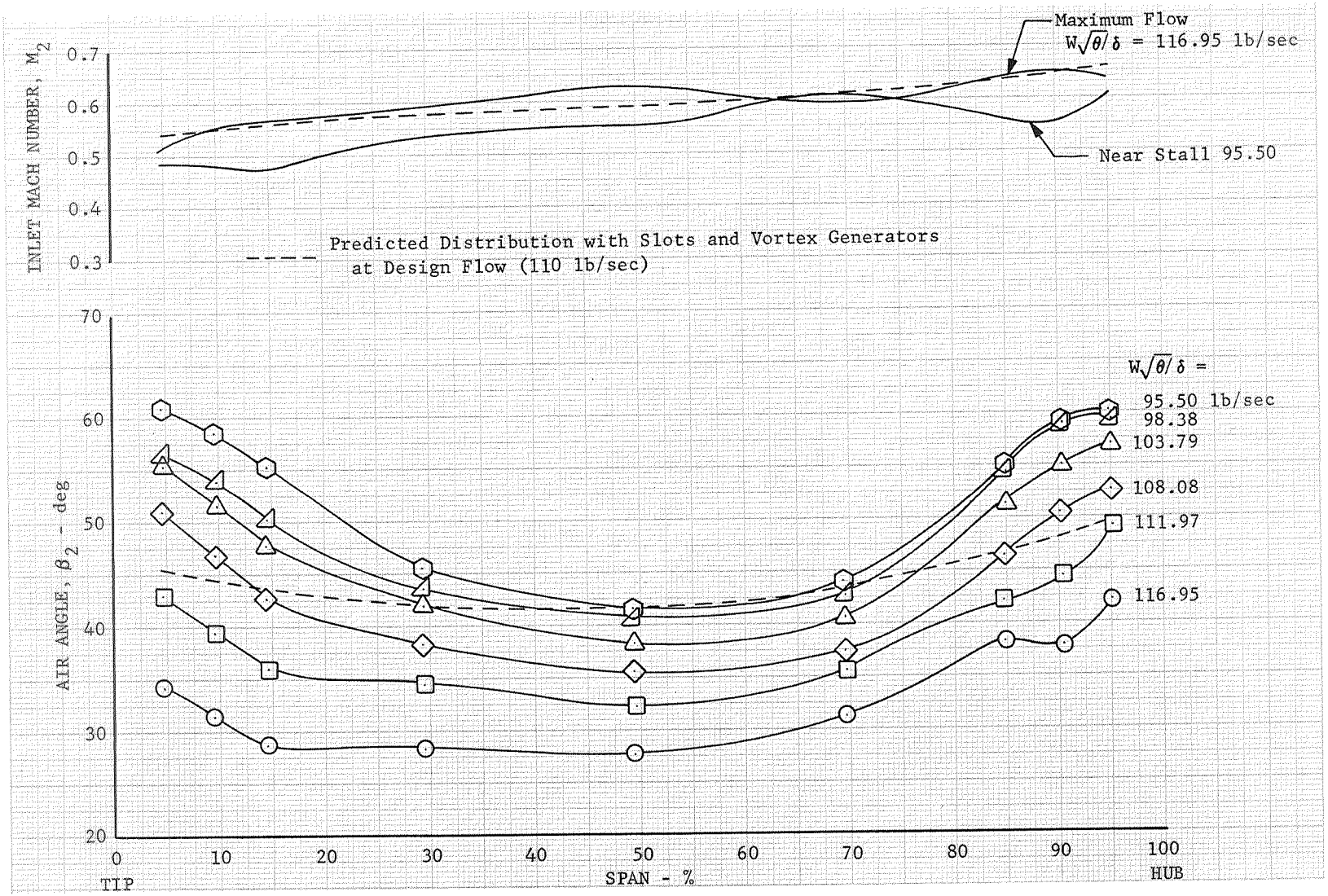

DF 83425

Figure 37. Slotted Stator 4 (With Vortex Generators Ahead of the Rotor) Inlet Air Angle and Mach Number Distribution, Design Equivalent Rotor Speed

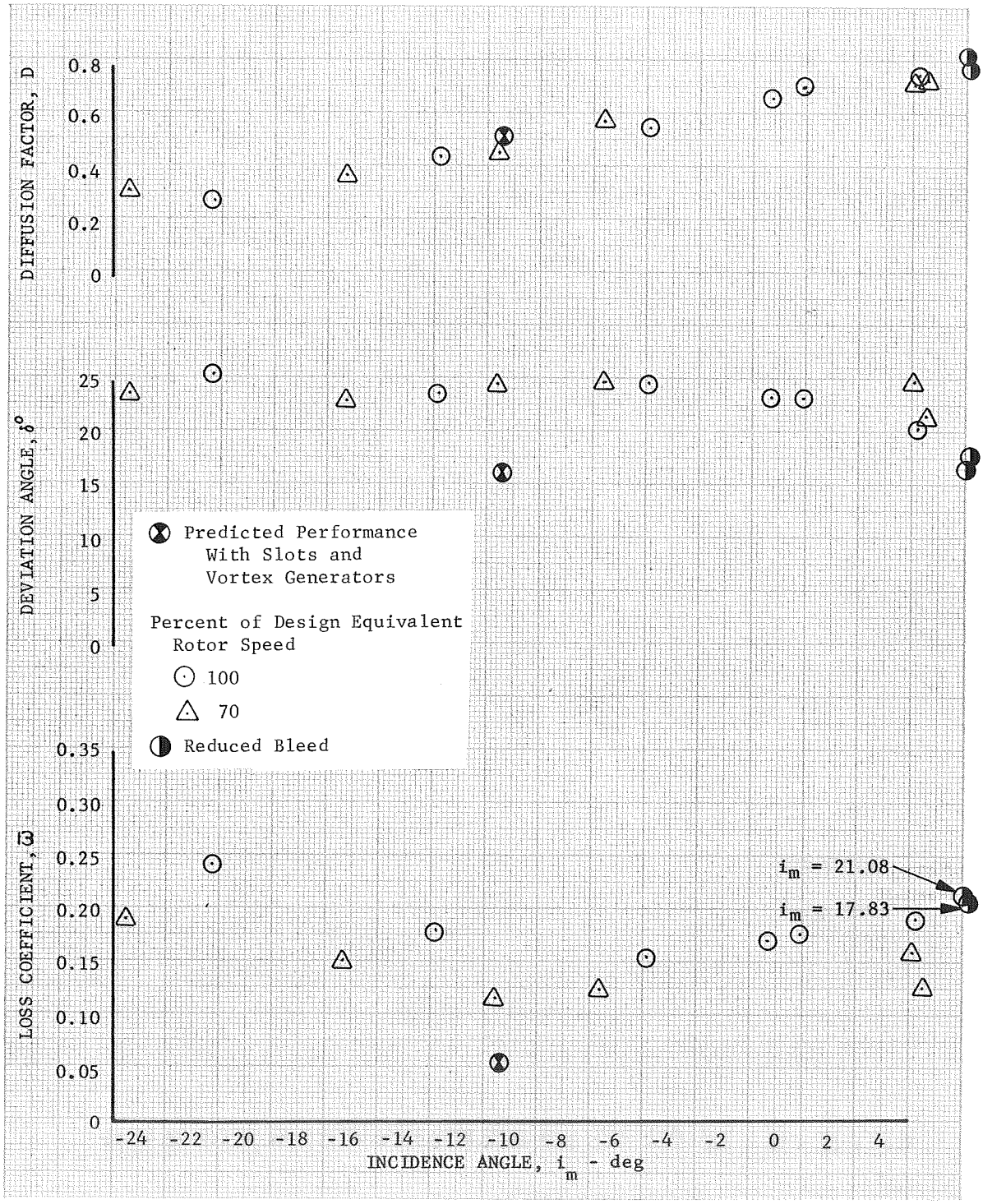

Figure 38a. Slotted Stator 4 (With Vortex Generators Ahead of the Rotor) Blade Element Performance, 5% Span From Tip DF 83373

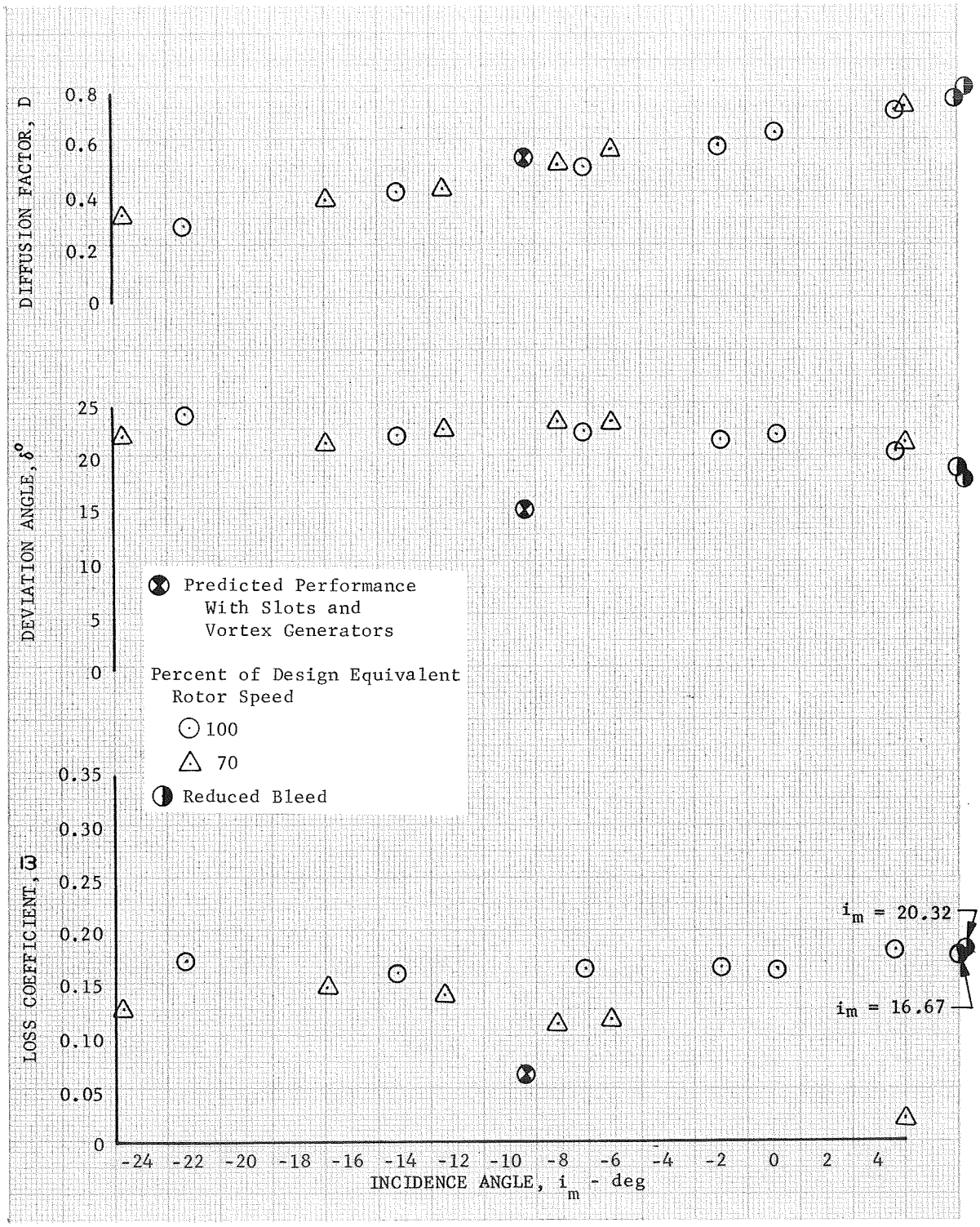

Figure 38b. Slotted Stator 4 (With Vortex Generators Ahead of the Rotor) Blade Element Performance, 10% Span From Tip DF83374

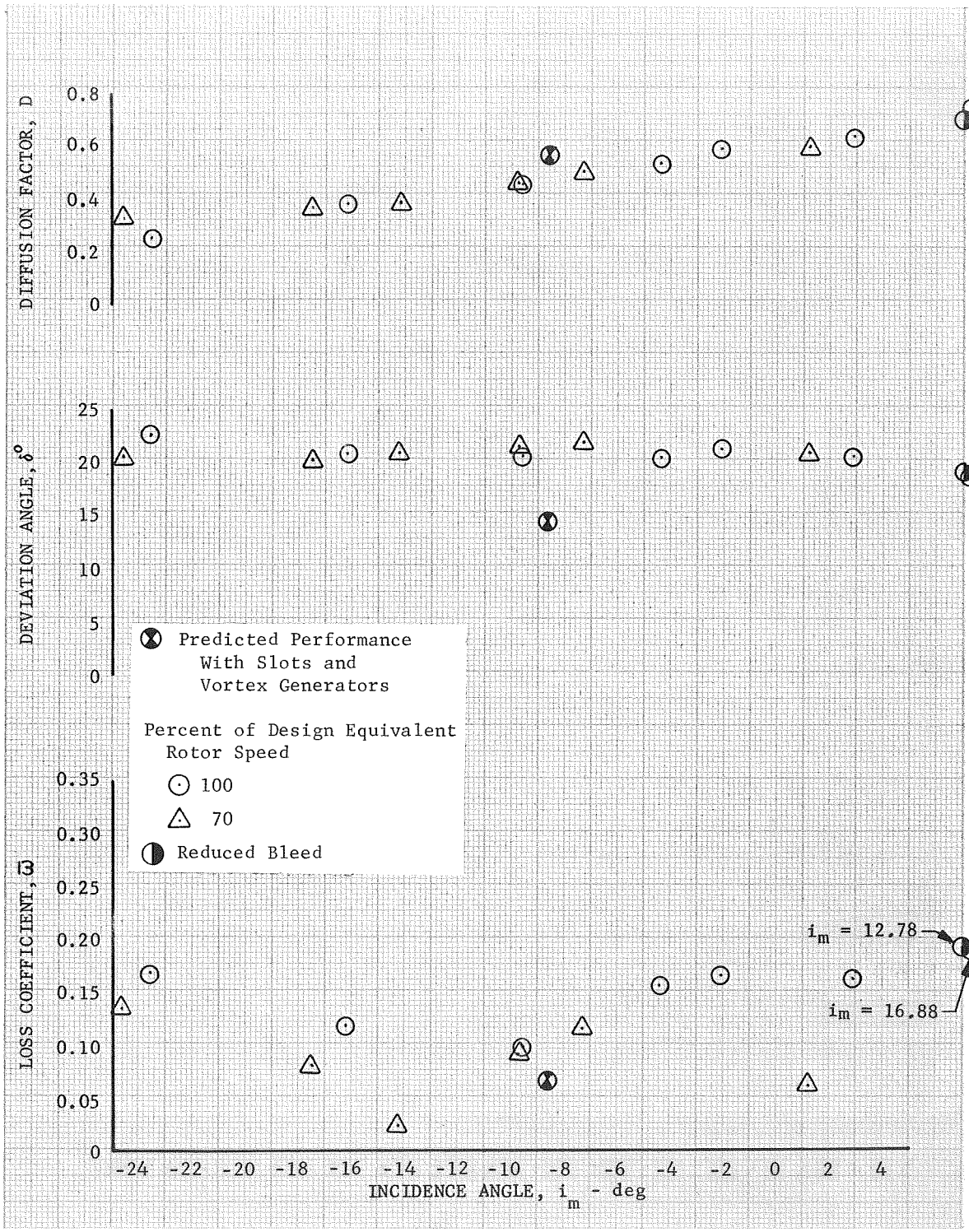

Figure 38c. Slotted Stator 4 (With Vortex Generator Ahead of the Rotor) Blade Element Performance, 15% Span From Tip DF 83375

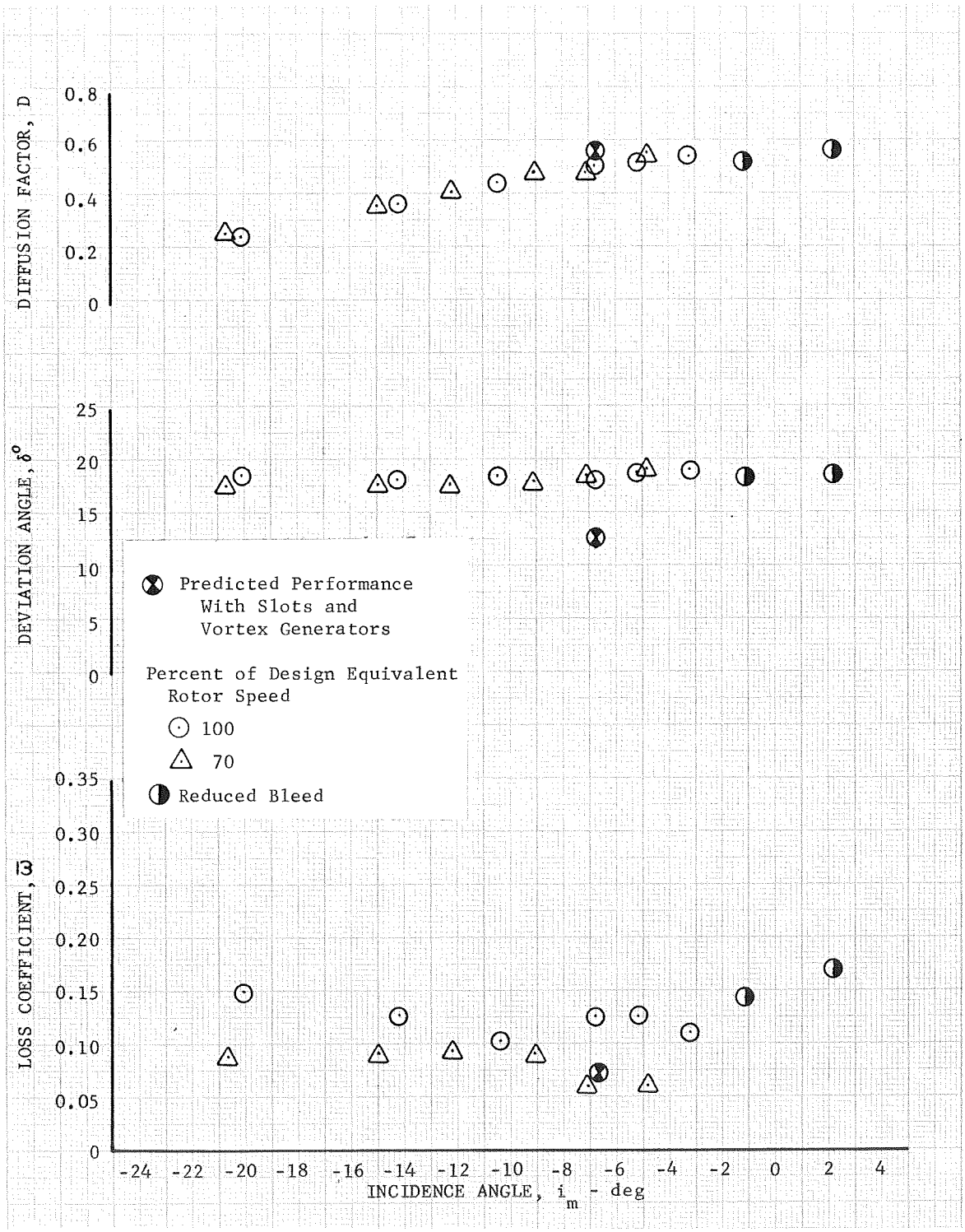

Figure 38d. Slotted Stator 4 (With Vortex Generators Ahead of the Rotor) Blade Element Performance, 30% Span From Tip

DF 83376

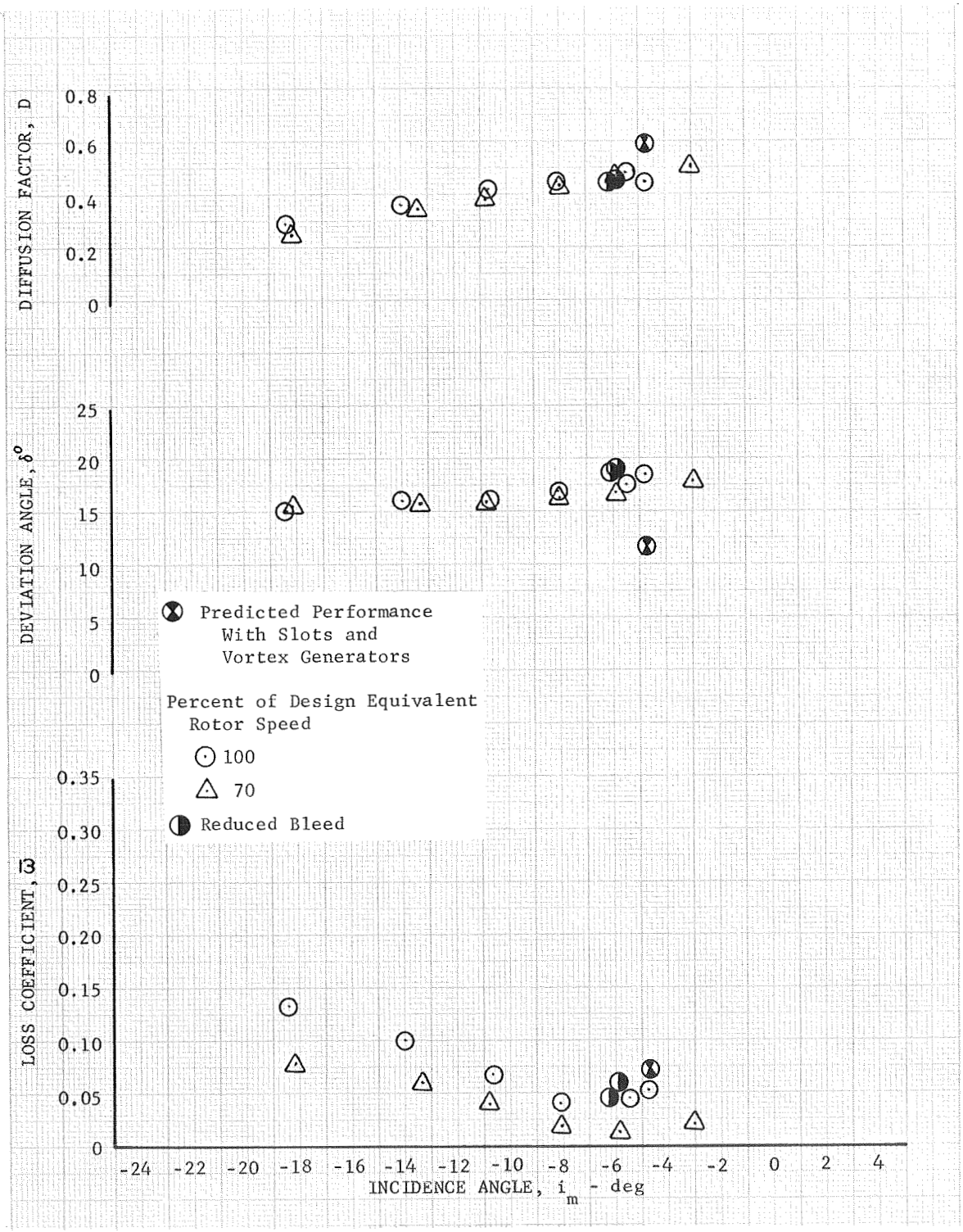

Figure 38e. Slotted Stator 4 (With Vortex Generators Ahead of the Rotor) Blade Element Performance, 50% Span From Tip DF 83377

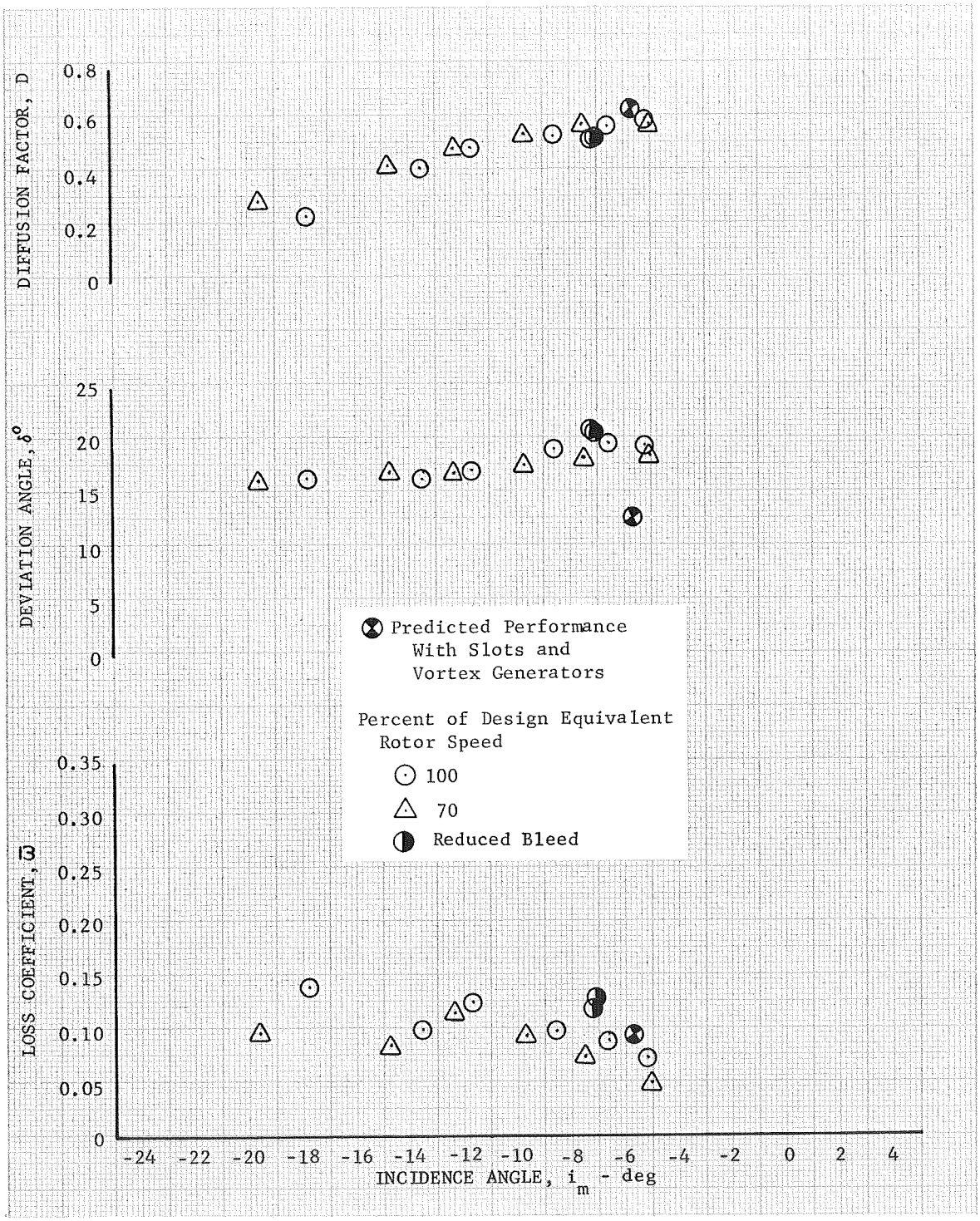

Figure 38f. Slotted Stator 4 (With Vortex Generators Ahead of the Rotor) Blade Element Performance, 70% Span From Tip

DF 83378

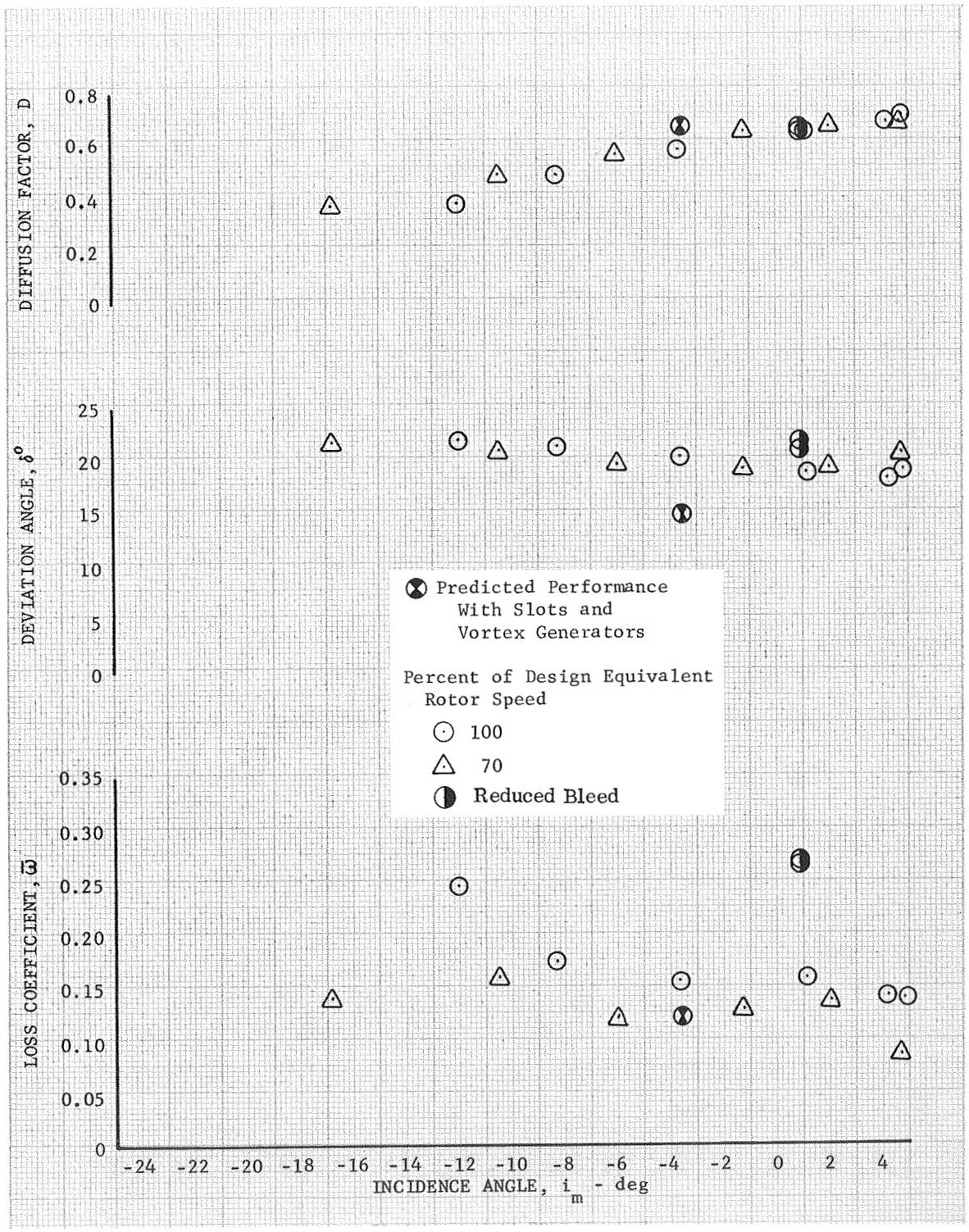

Figure 38g. Slotted Stator 4 (With Vortex Generators Ahead of the Rotor) Blade Element Performance, 85% Span From Tip DF 83379

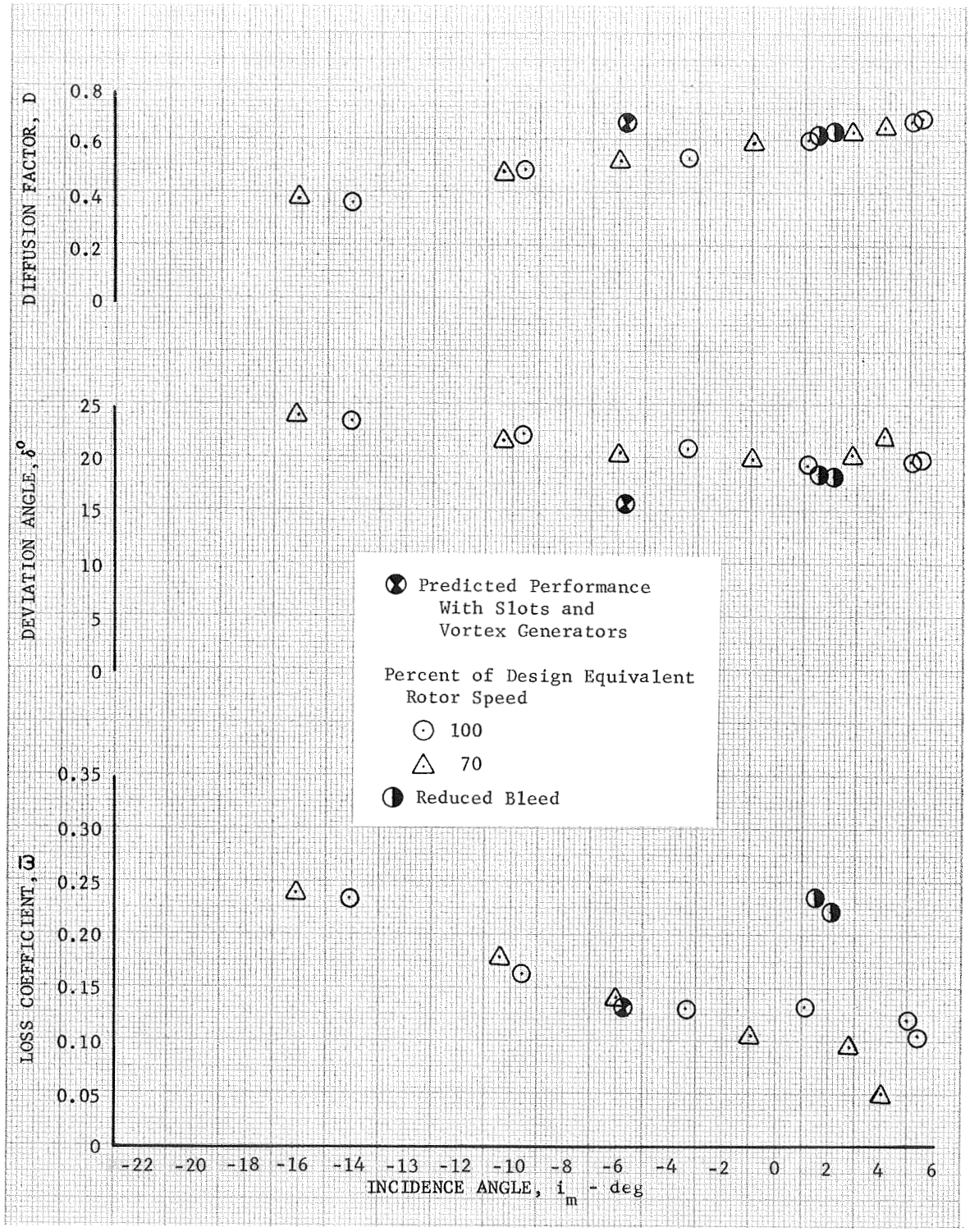

Figure 38h. Slotted Stator 4 (With Vortex Generators Ahead of the Rotor) Blade Element Performance, 90% Span From Tip

DF 83380

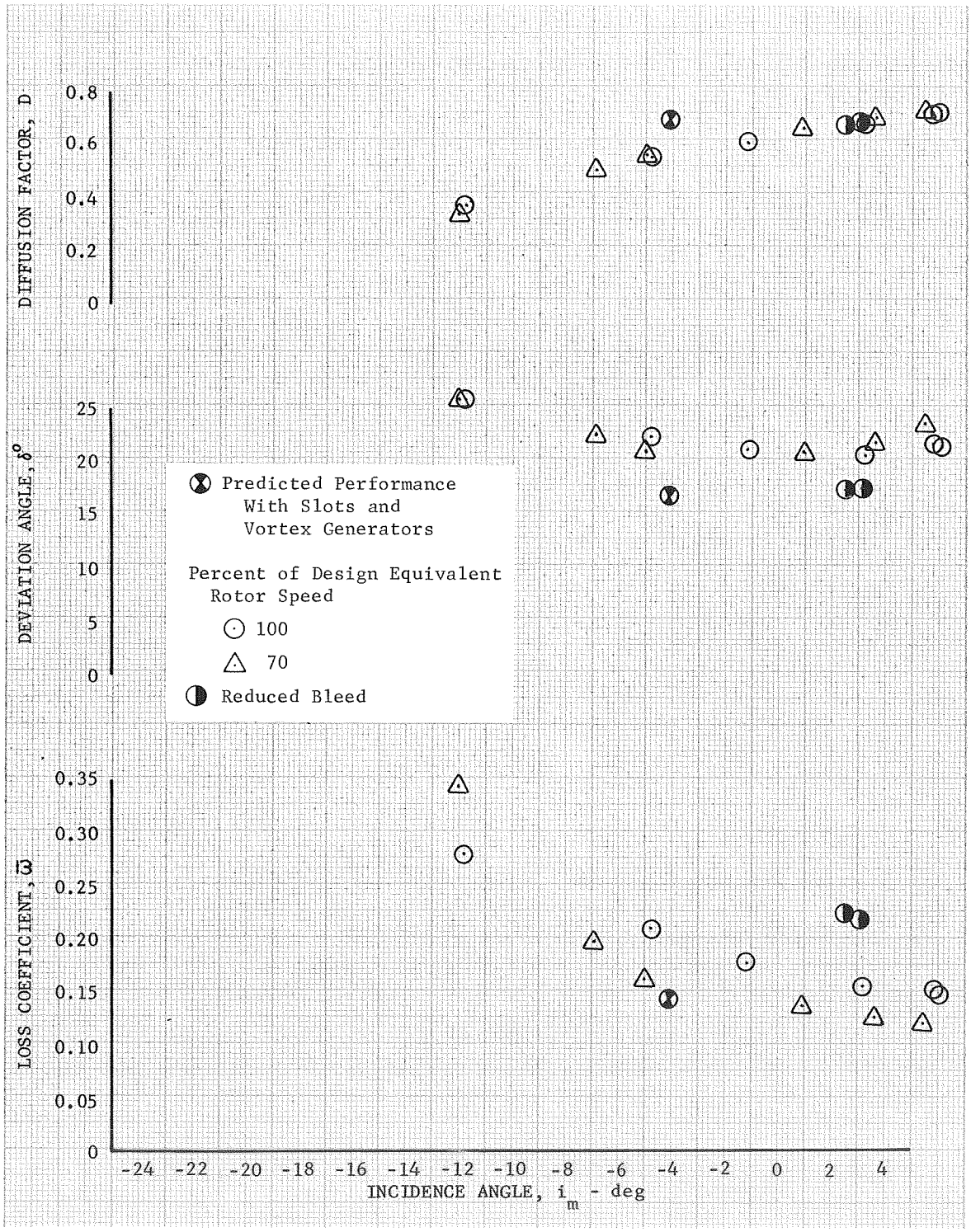

Figure 38i. Slotted Stator 4 (With Vortex Generators Ahead of the Rotor) Blade Element Performance, 95% Span From Tip DF 83301

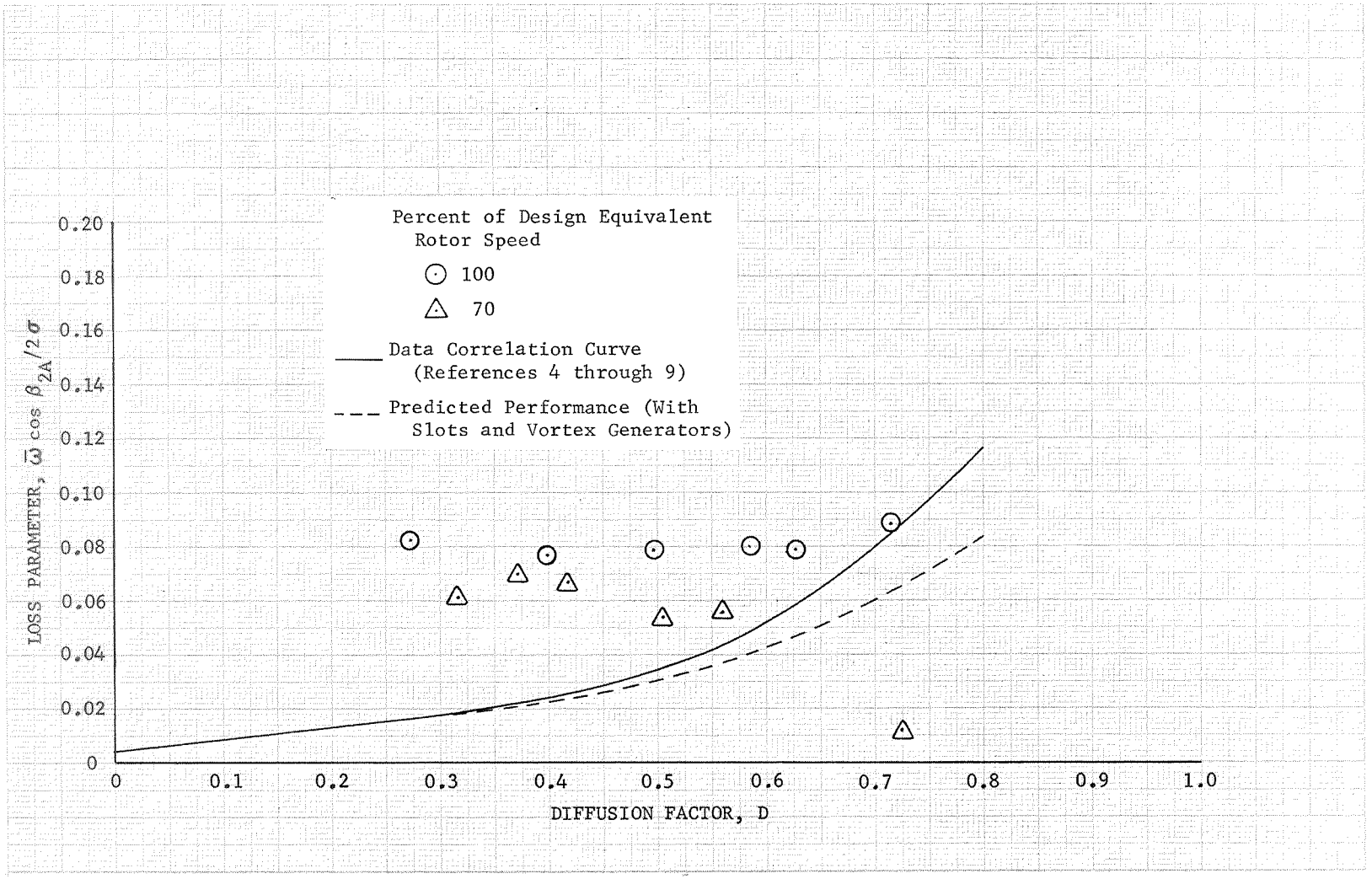

Figure 39a. Slotted Stator 4 (With Vortex Generators Ahead of the Rotor) Loss Parameter vs Diffusion Factor, 10% Span From Tip

DF 83304

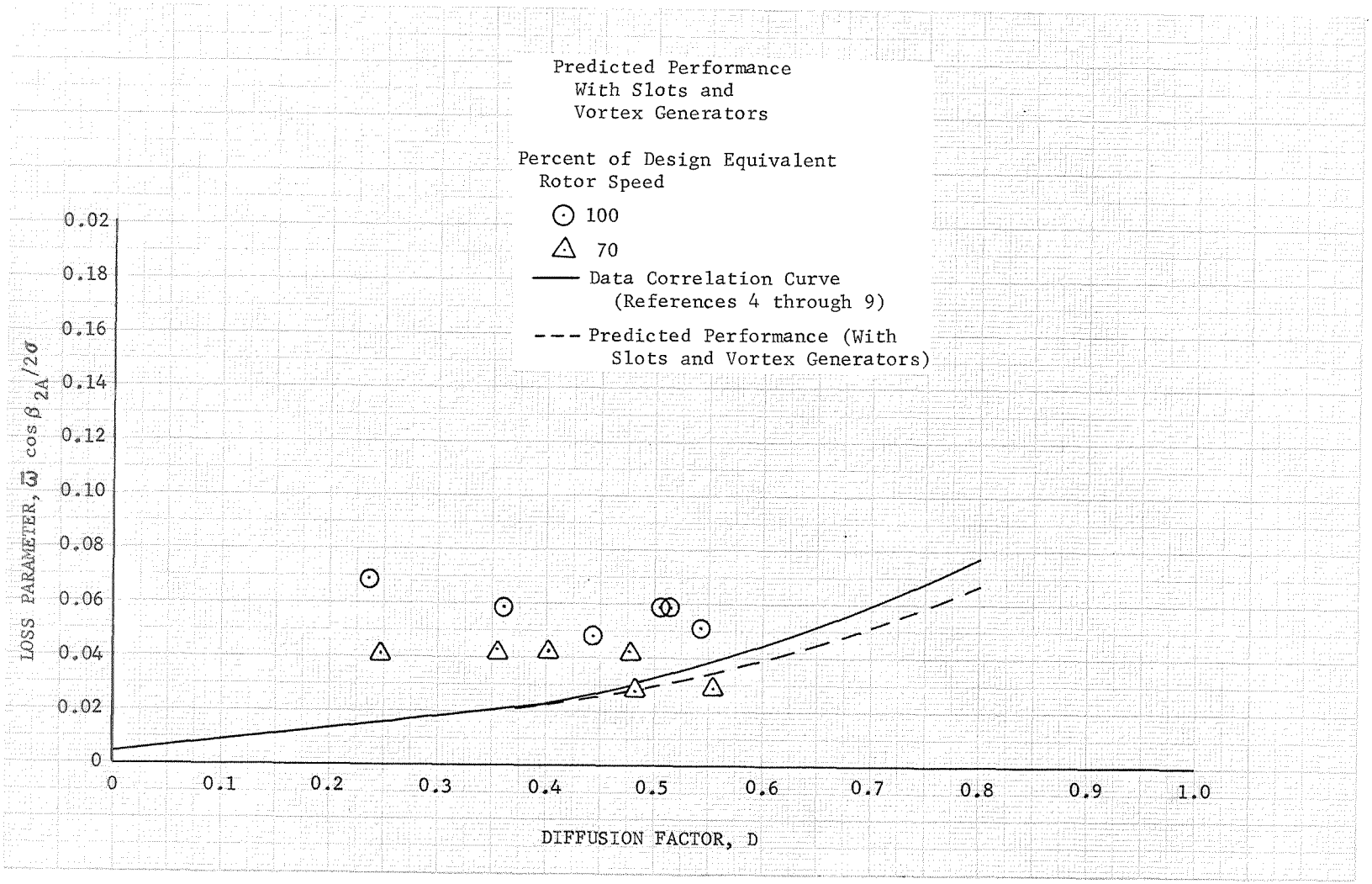

Figure 39b. Slotted Stator 4 (With Vortex Generators Ahead of the Rotor) Loss Parameter vs Diffusion Factor, 30% Span From Tip

DF 83302

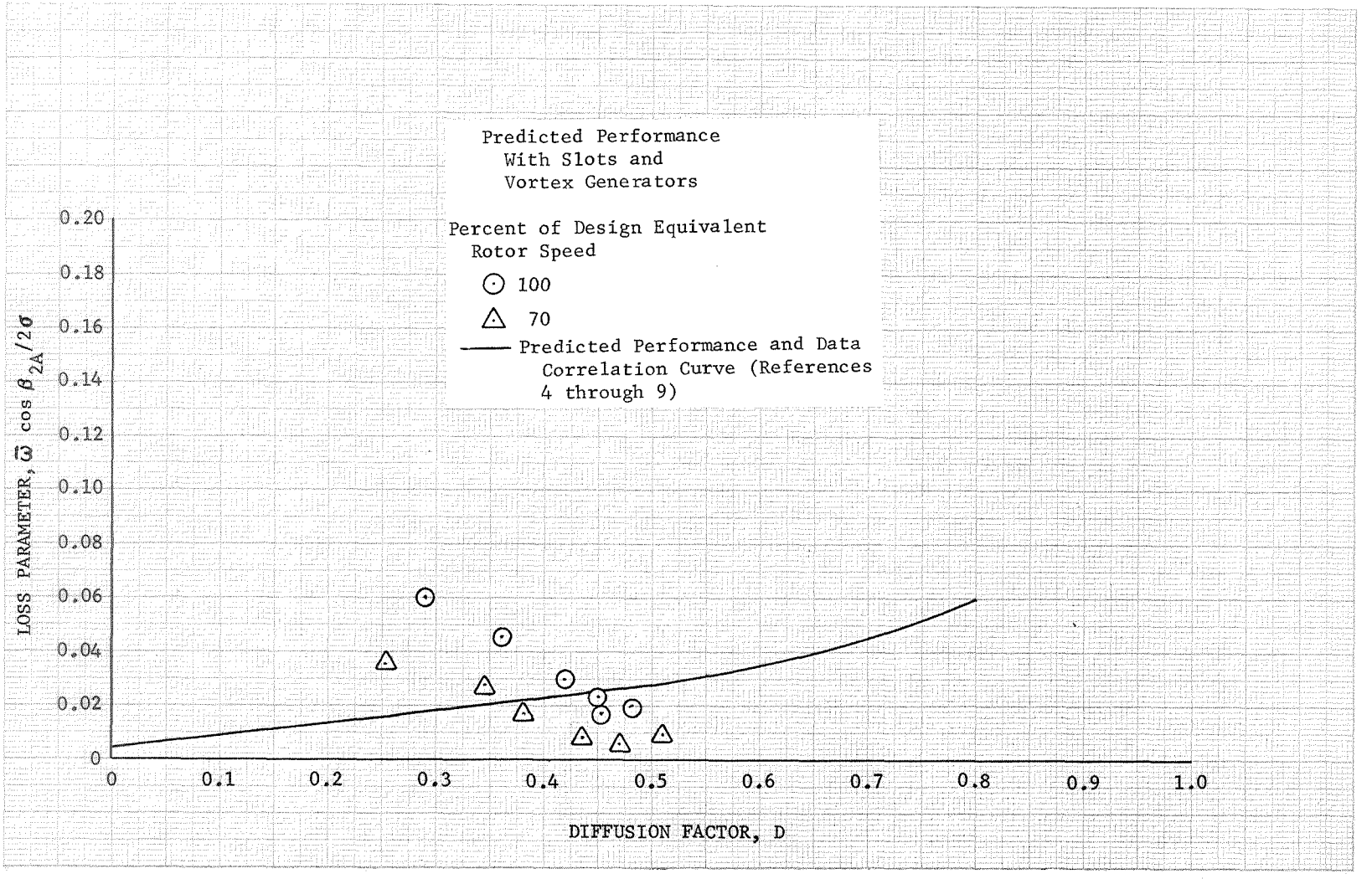

Figure 39c. Slotted Stator 4 (With Vortex Generators Ahead of the Rotor) Loss Parameter vs Diffusion Factor, 50% Span From Tip

DF 83303

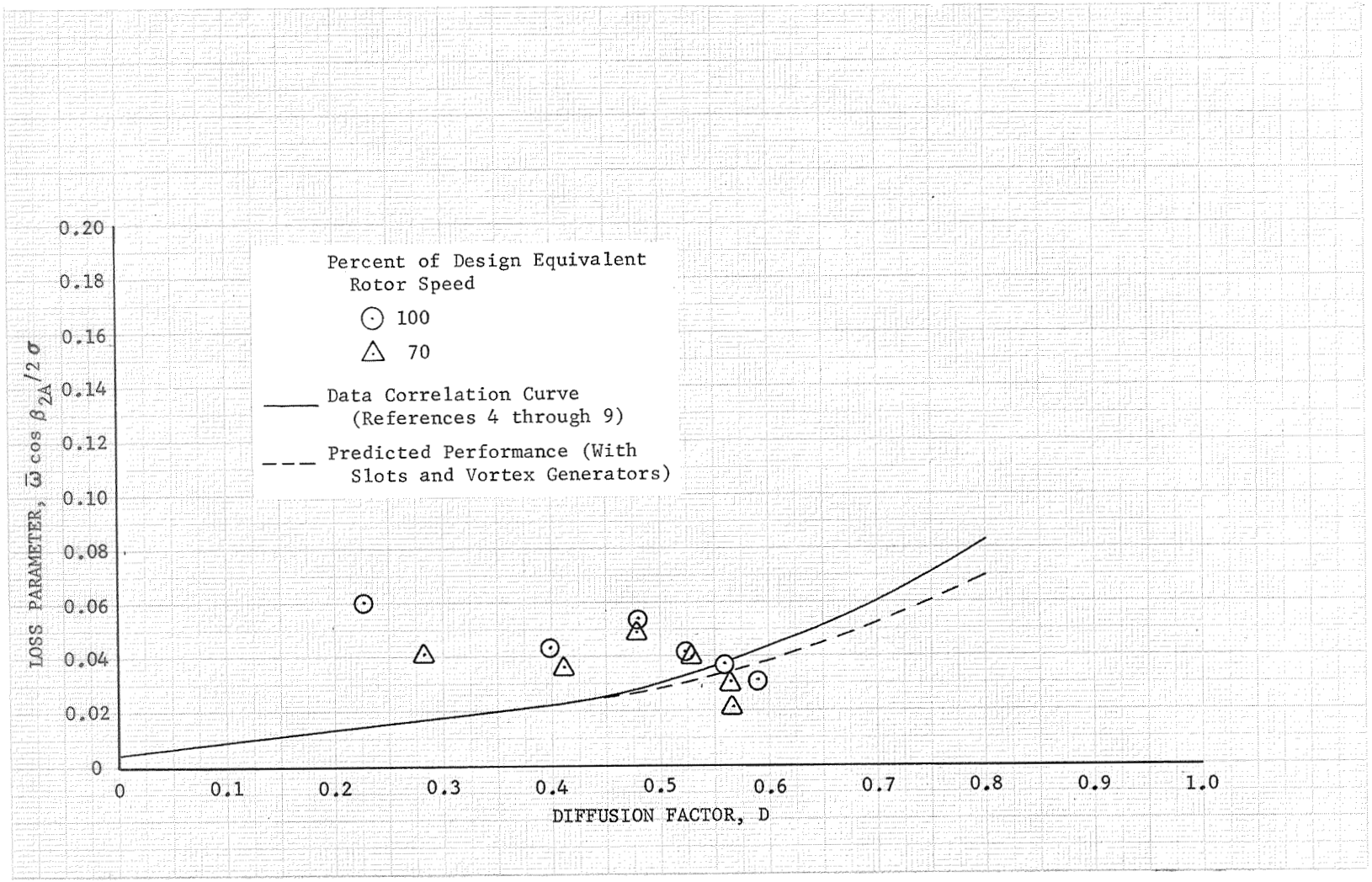

Figure 39d. Slotted Stator 4 (With Vortex Generators Ahead of the Rotor) Loss Parameter vs Diffusion Factor, 70% Span From Tip

DF 83305

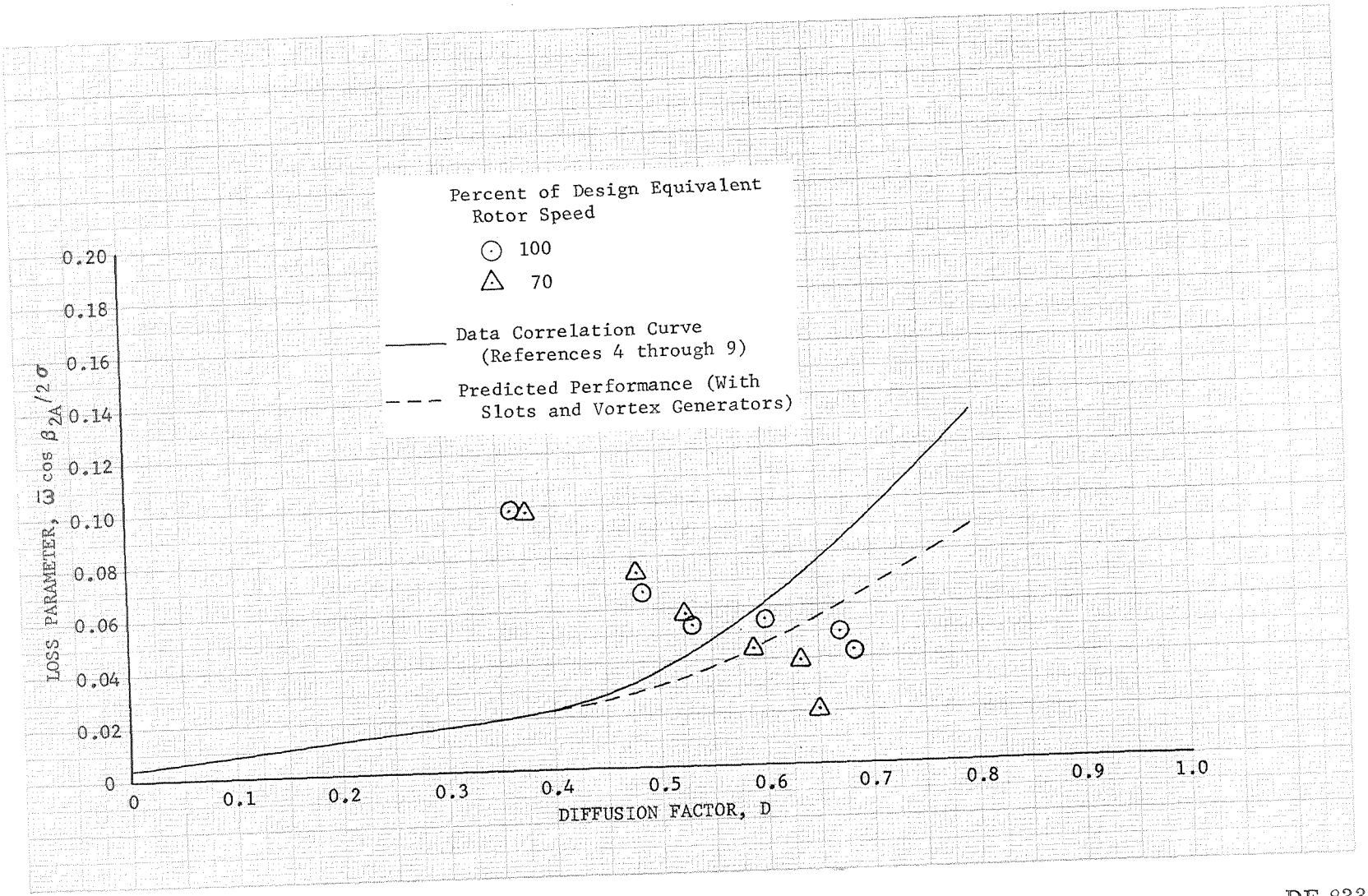

DF 83306

Figure 39e. Slotted Stator 4 (With Vortex Generators Ahead of the Rotor) Loss Parameter vs Diffusion Factor, 90% Span From Tip

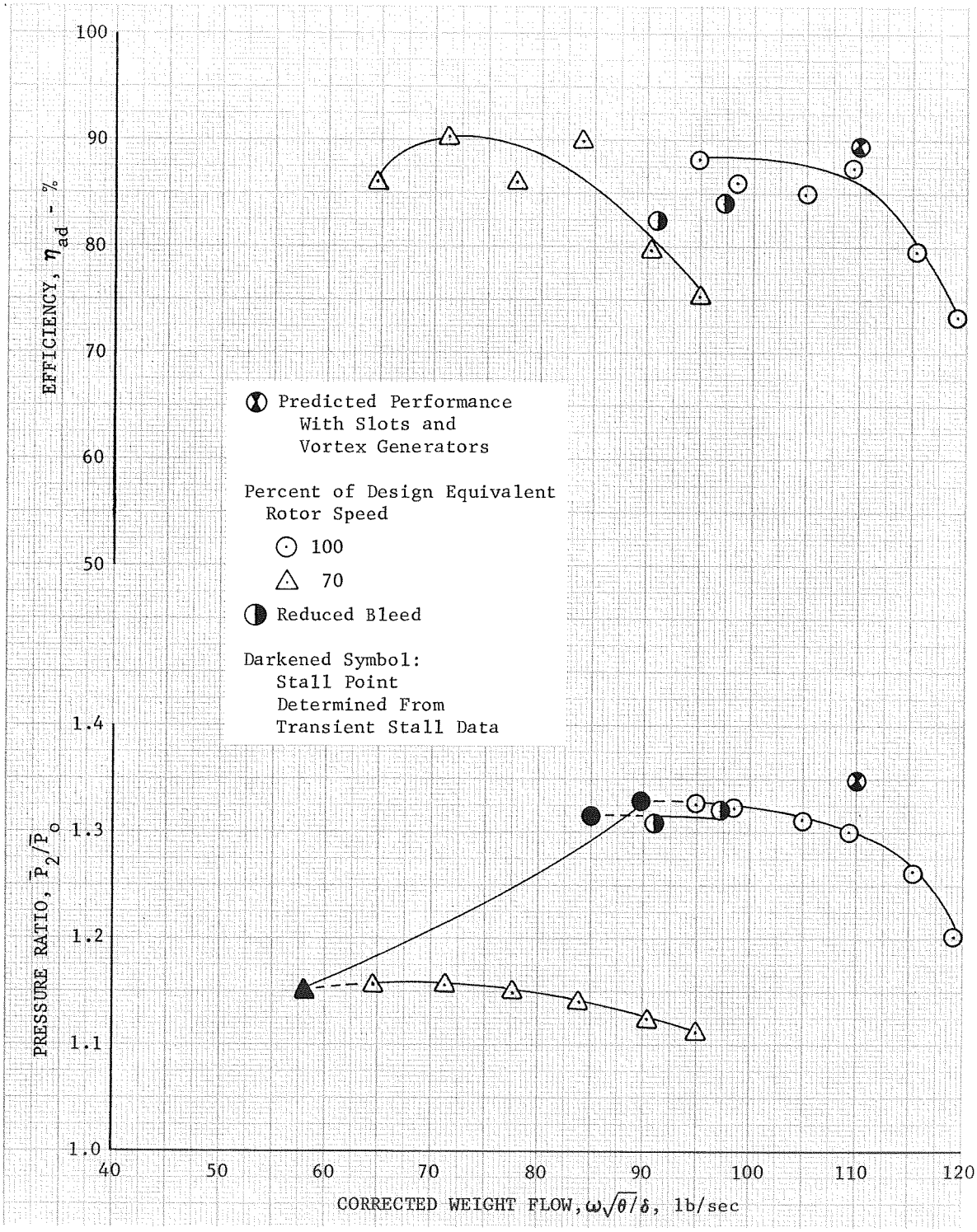

Figure 40. Overall Performance of Unslotted Rotor 4 DF 83307
(With Vortex Generators Ahead of the
Rotor and Between the Rotor and Stator)

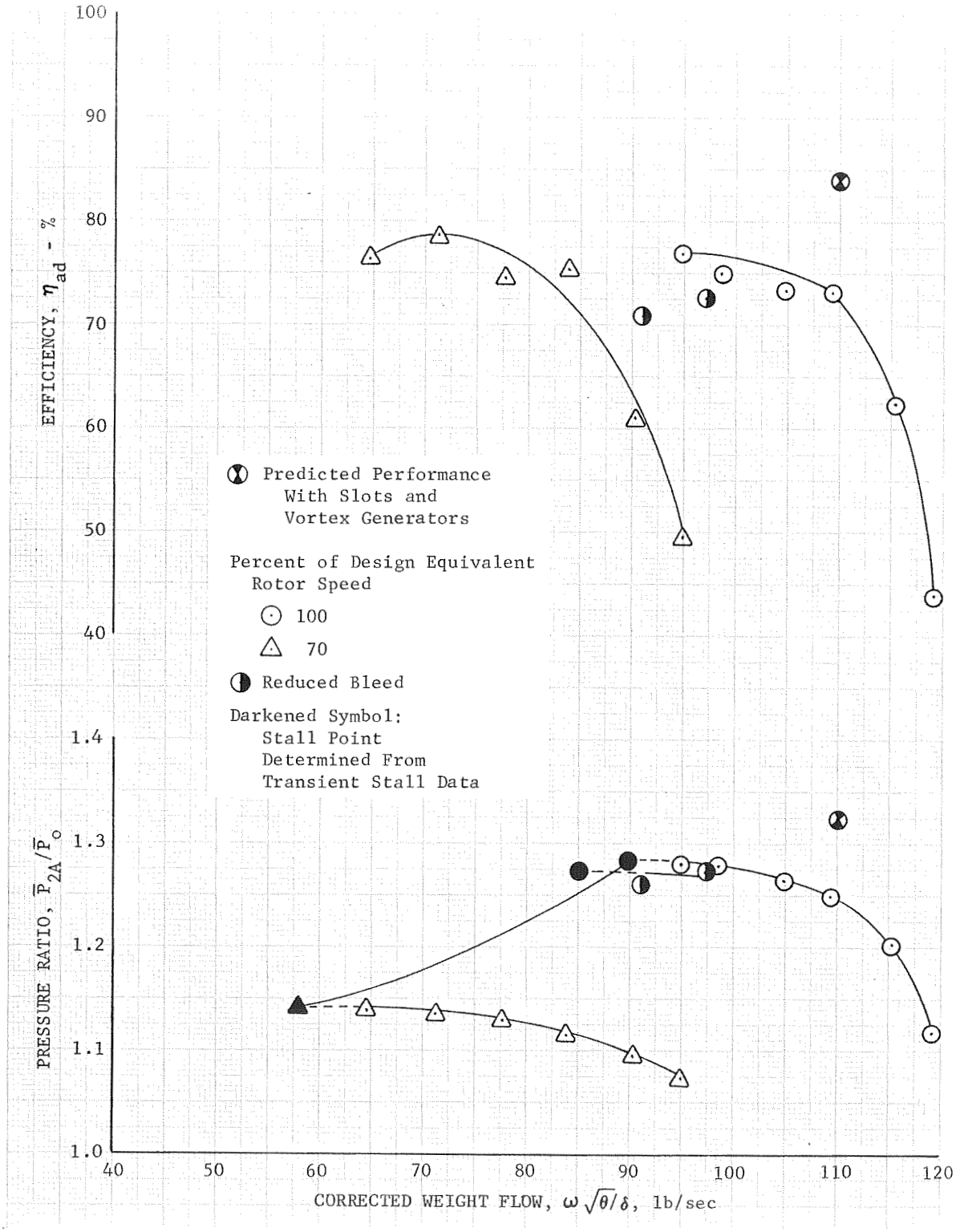

Figure 41. Overall Performance of Unslotted Stage 4 (With Vortex Generators Ahead of the Rotor and Between the Rotor and Stator) DF 83308

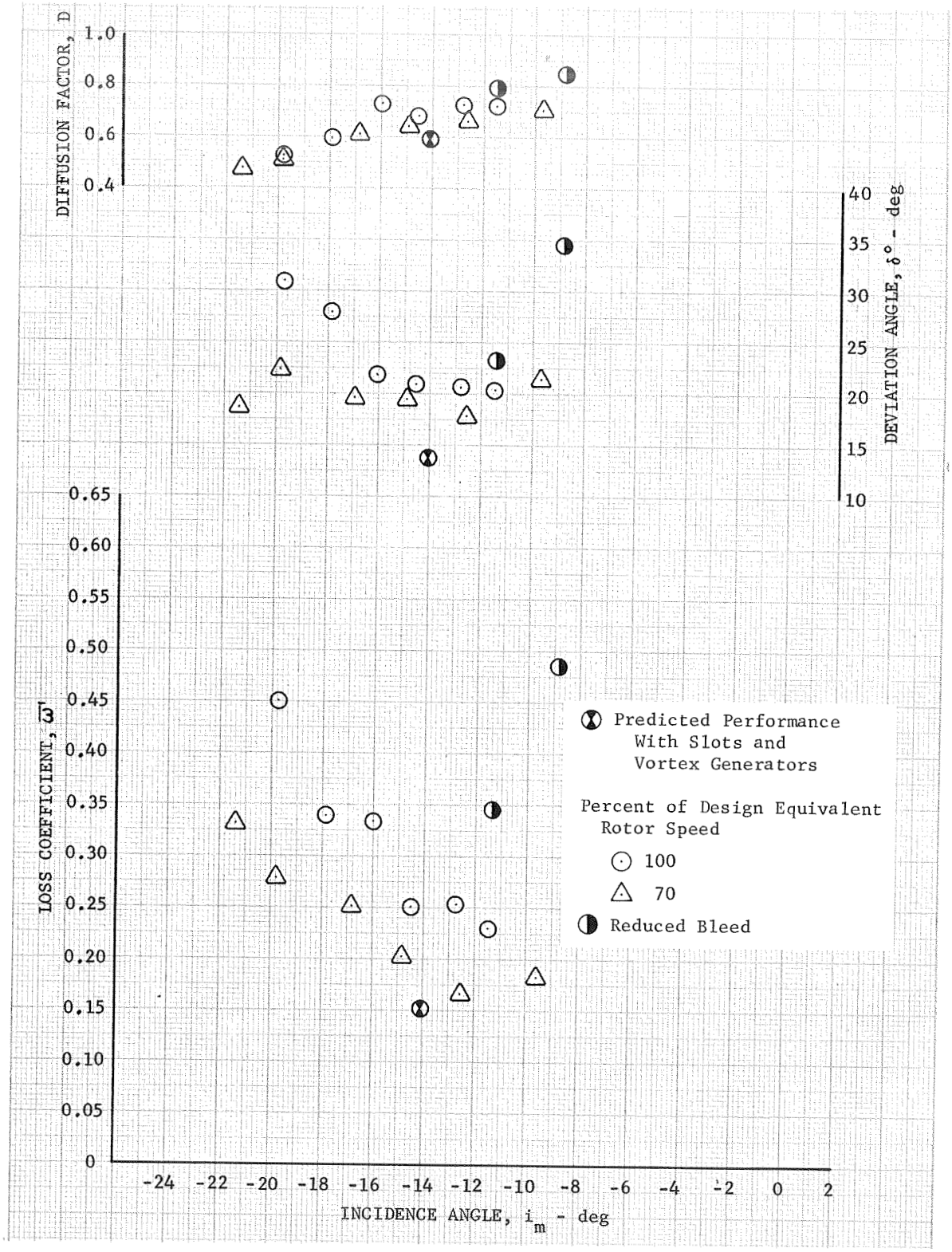

Figure 42a. Unslotted Rotor 4 (With Vortex Generators DF 83426 Ahead of the Rotor and Between the Rotor and Stator) Blade Element Performance, 5% Span From Tip

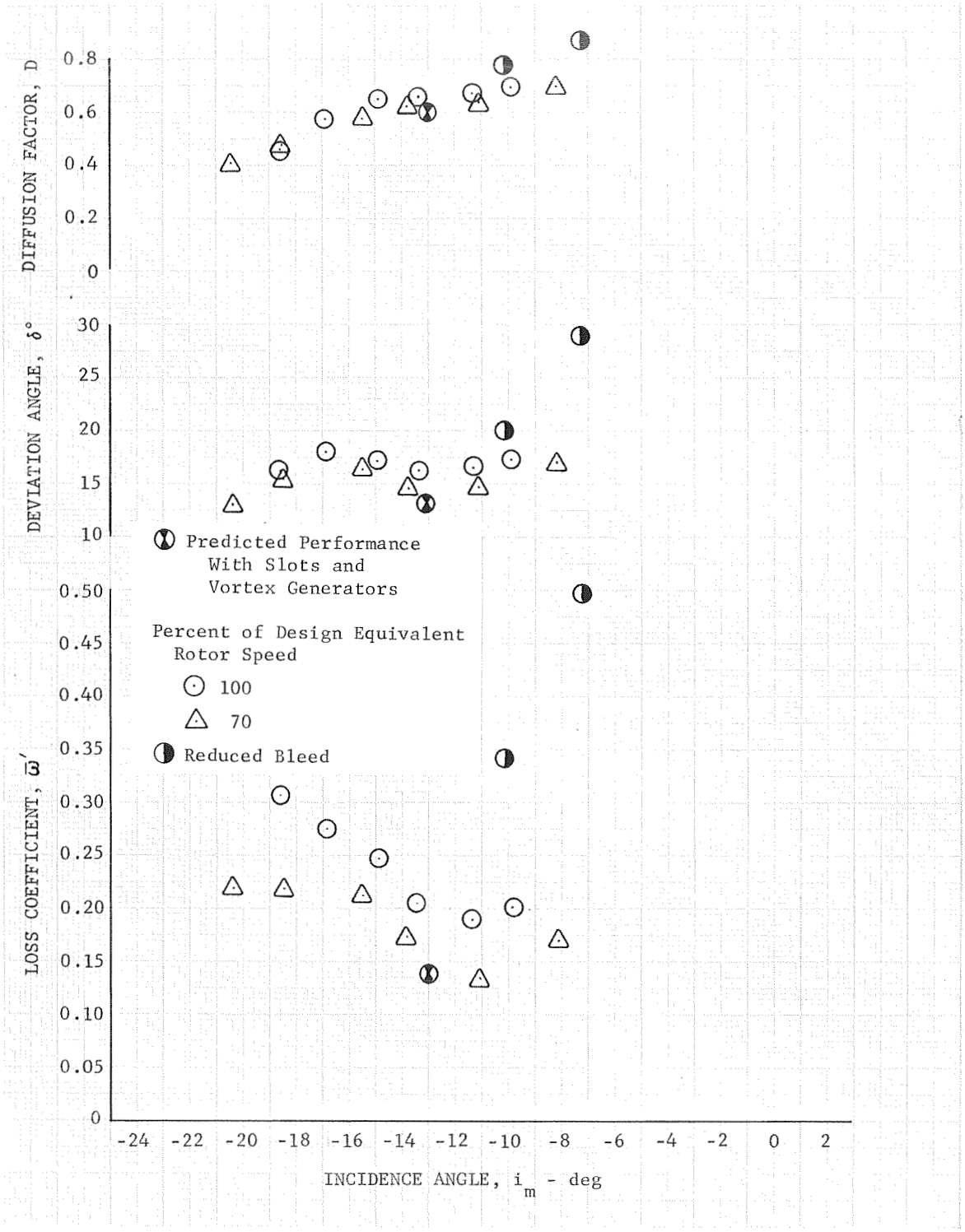

Figure 42b. Unslotted Rotor 4 (With Vortex Generators Ahead of the Rotor and Between the Rotor and Stator) Blade Element Performance, 10% Span From Tip

DF 83309

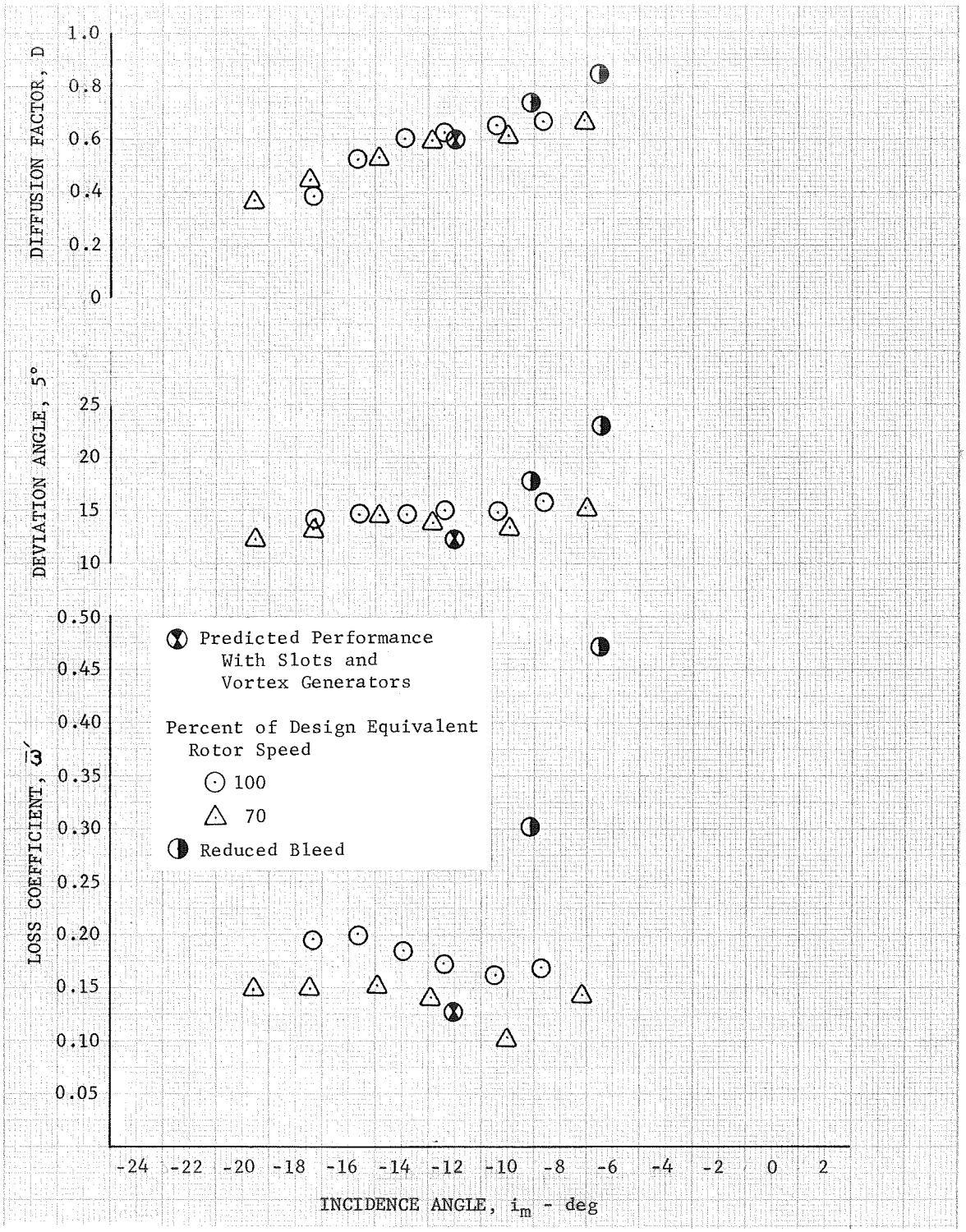

Figure 42c. Unslotted Rotor 4 (With Vortex Generators Ahead of the Rotor and Between the Rotor and Stator) Blade Element Performance, 15% Span From Tip

DF 83310

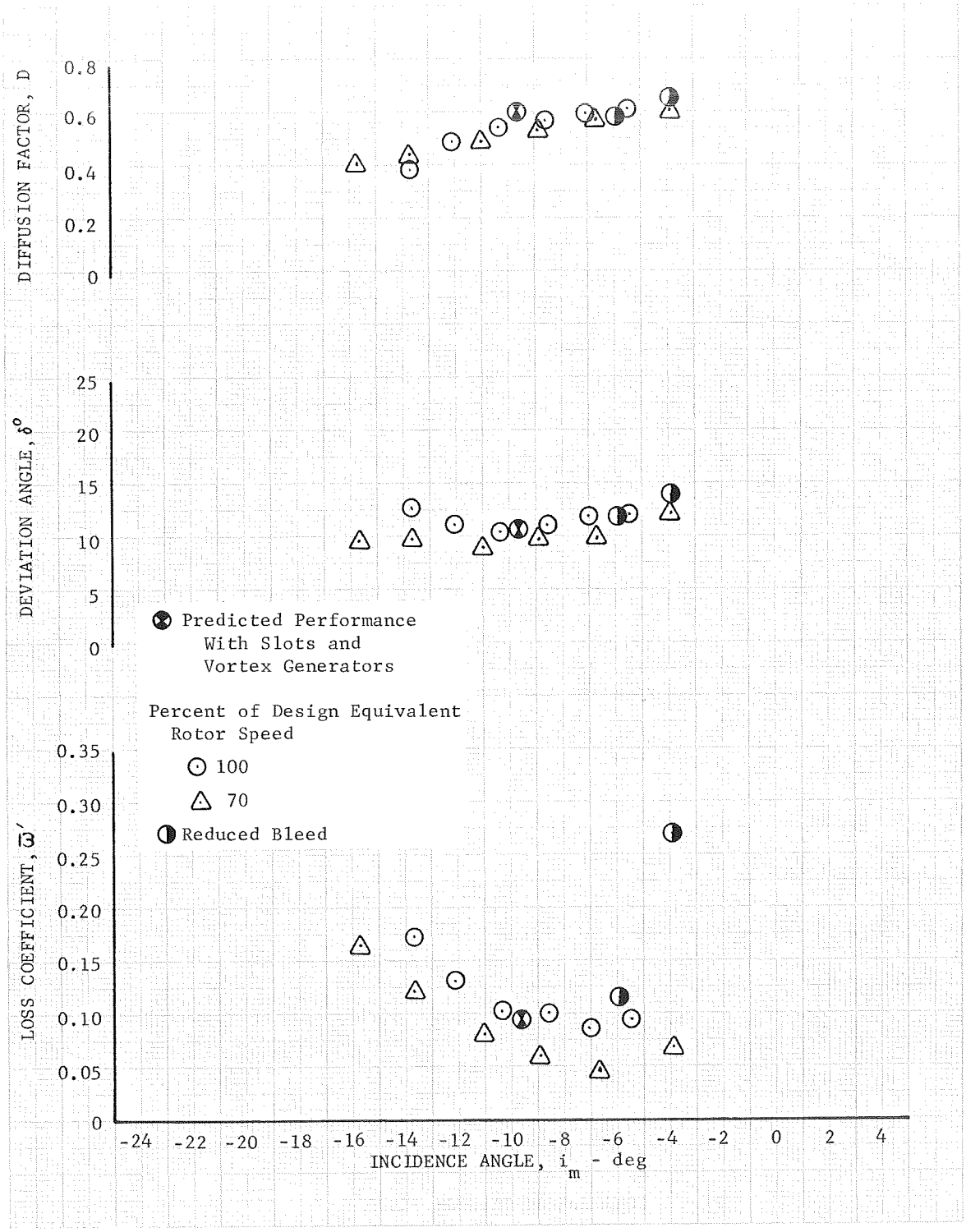

Figure 42d. Unslotted Rotor 4 (With Vortex Generators Ahead of the Rotor and Between the Rotor and Stator) Blade Element Performance, 30% Span From Tip

DF 83311

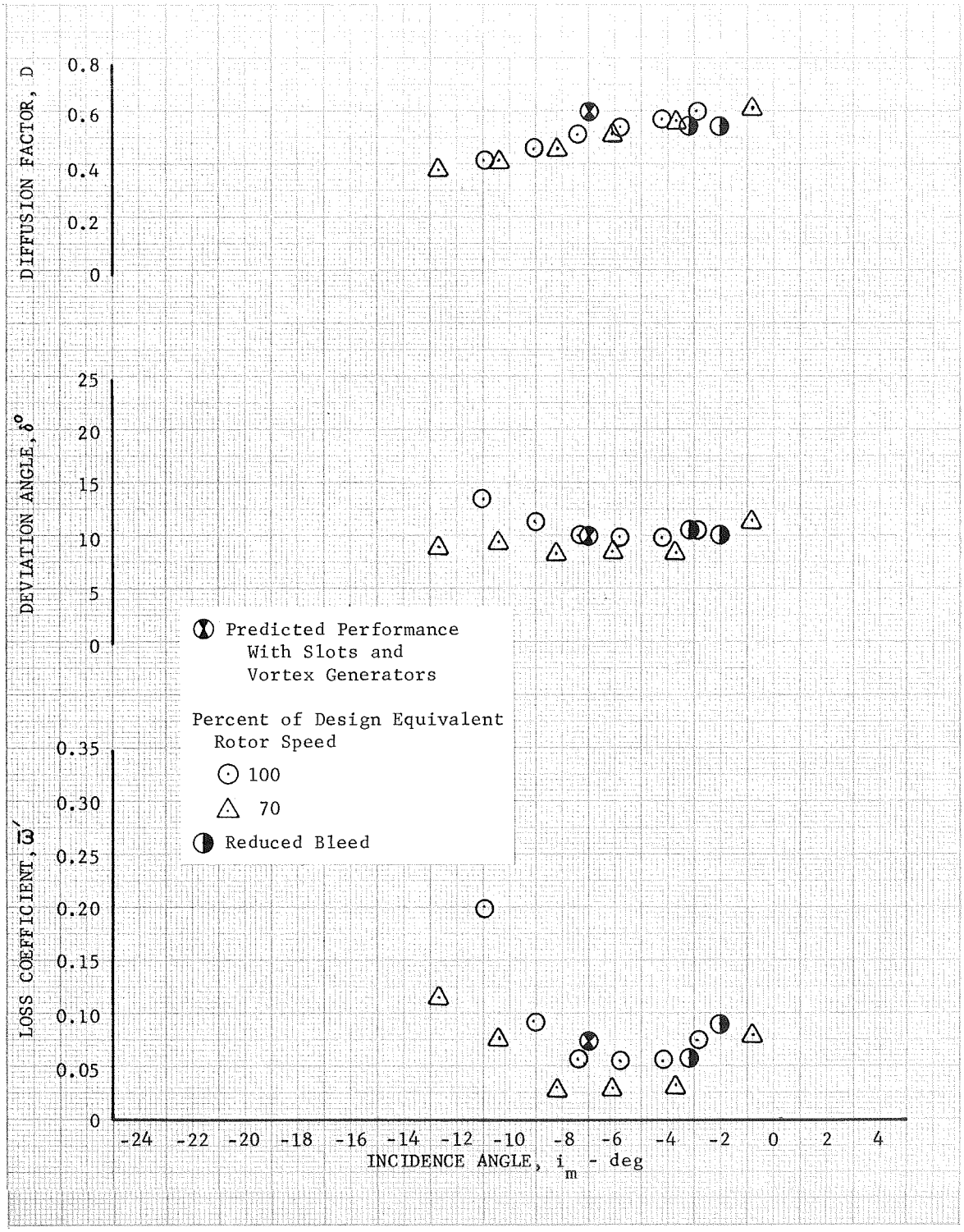

Figure 42e. Unslotted Rotor 4 (With Vortex Generators Ahead of the Rotor and Between the Rotor and Stator) Blade Element Performance, 50% Span From Tip

DF 83312

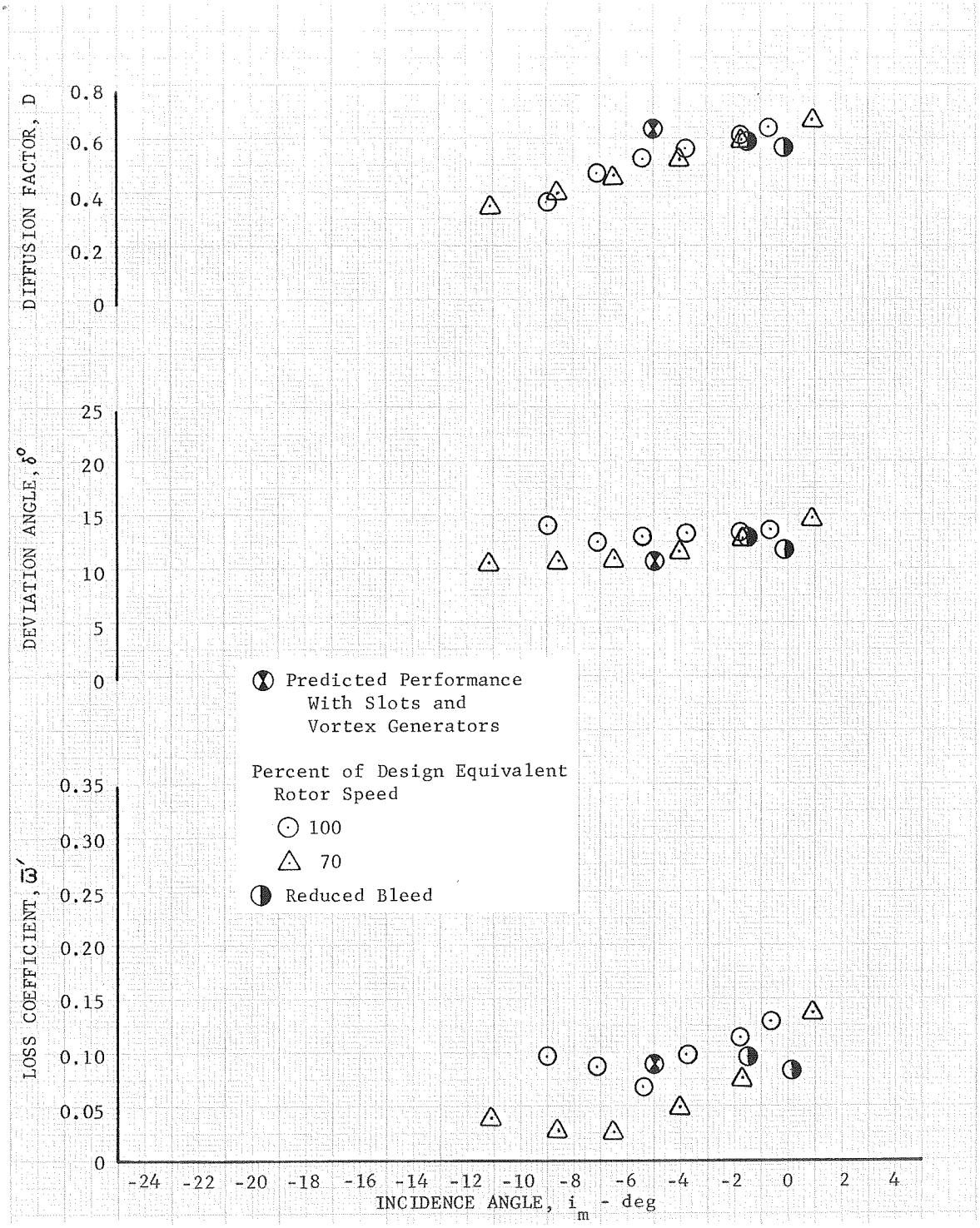

Figure 42f. Unslotted Rotor 4 (With Vortex Generators Ahead of the Rotor and Between the Rotor and Stator) Blade Element Performance, 70% Span From Tip

DF 83313

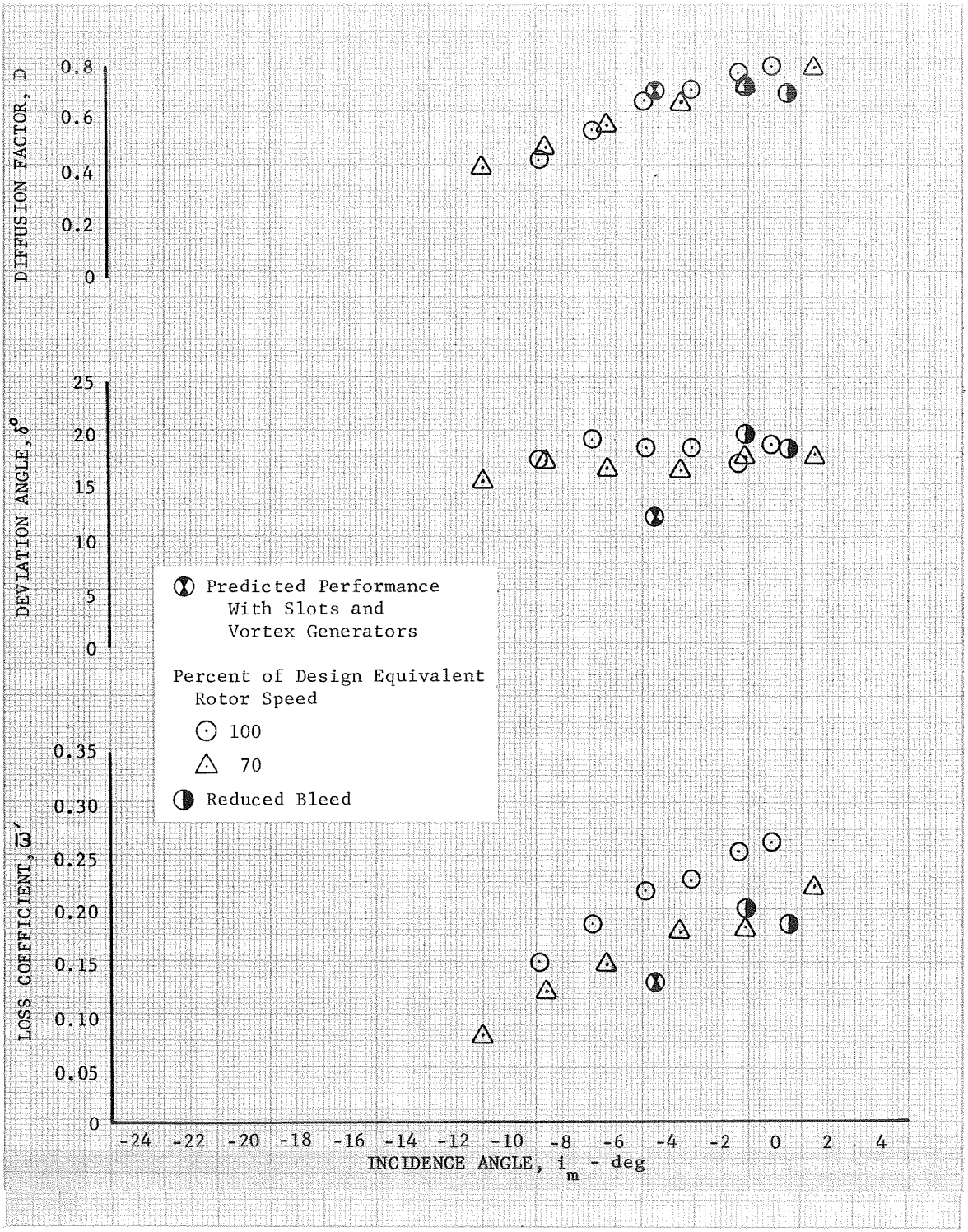

Figure 42g. Unslotted Rotor 4 (With Vortex Generators Ahead of the Rotor and Between the Rotor and Stator) Blade Element Performance, 85% Span From Tip

DF 83314

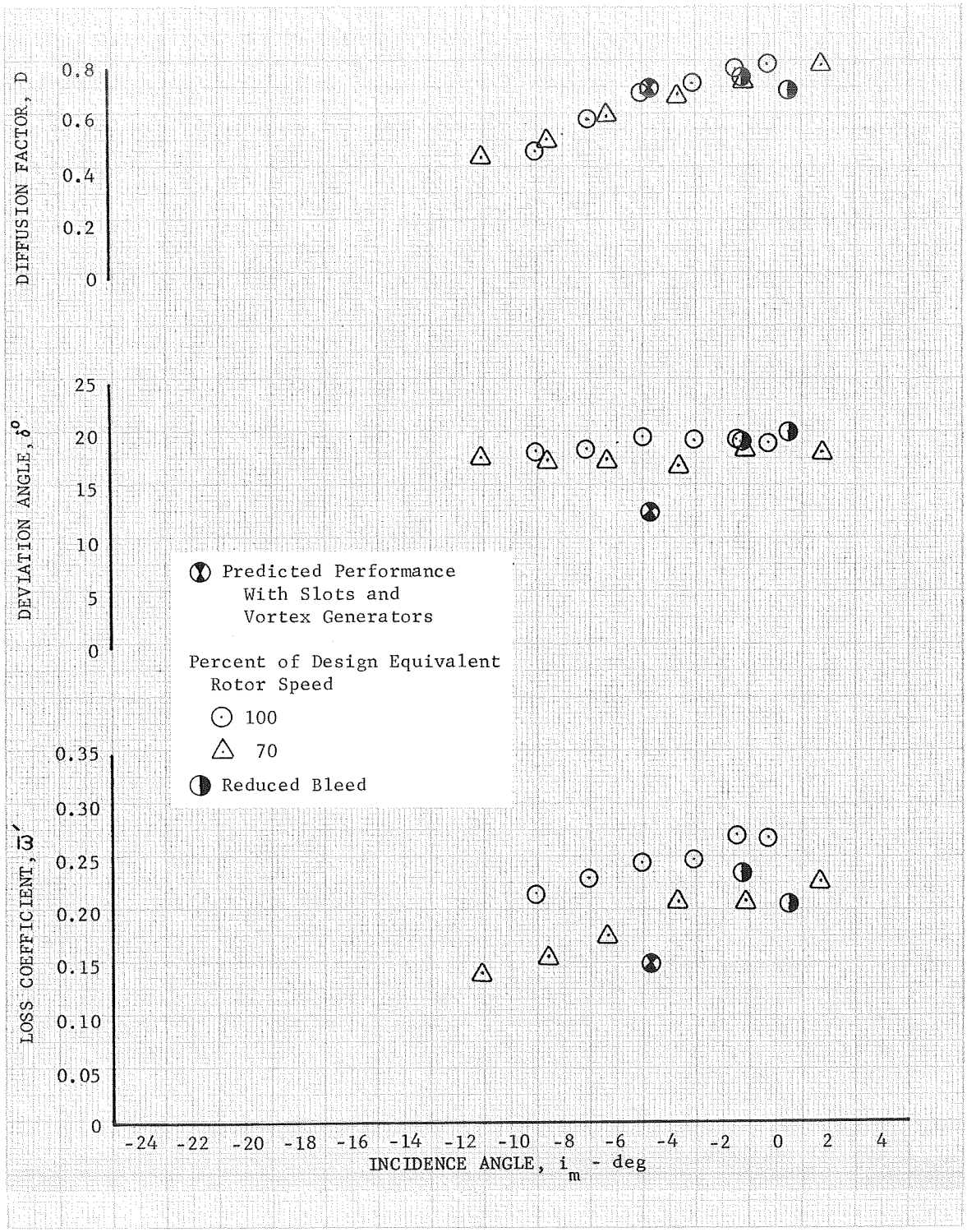

Figure 42h. Unslotted Rotor 4 (With Vortex Generators Ahead of the Rotor and Between the Rotor and Stator) Blade Element Performance, 90% Span From Tip

DF 83315

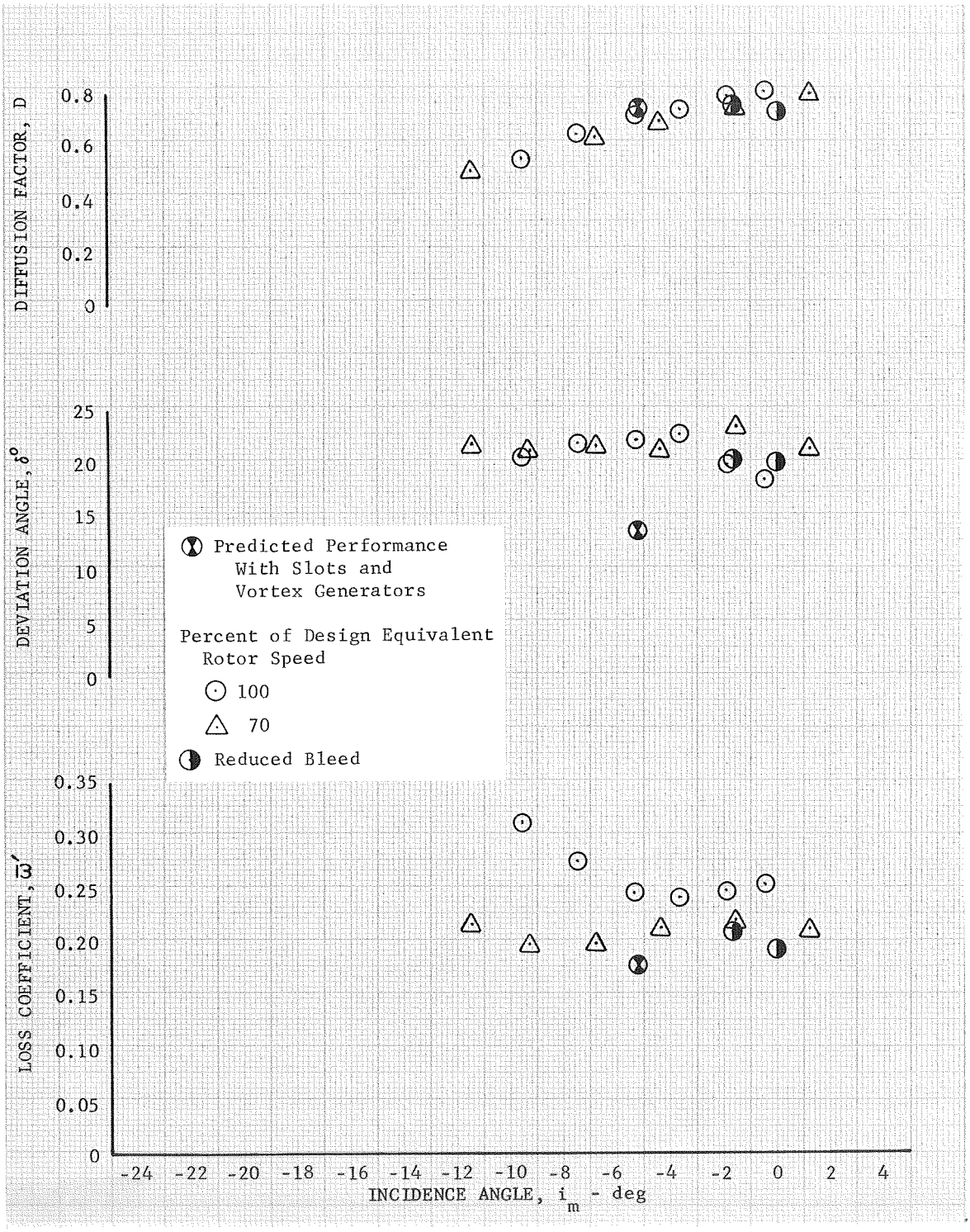

Figure 42i. Unslotted Rotor 4 (With Vortex Generators Ahead of the Rotor and Between the Rotor and Stator) Blade Element Performance 95% Span From Tip

DF 83316

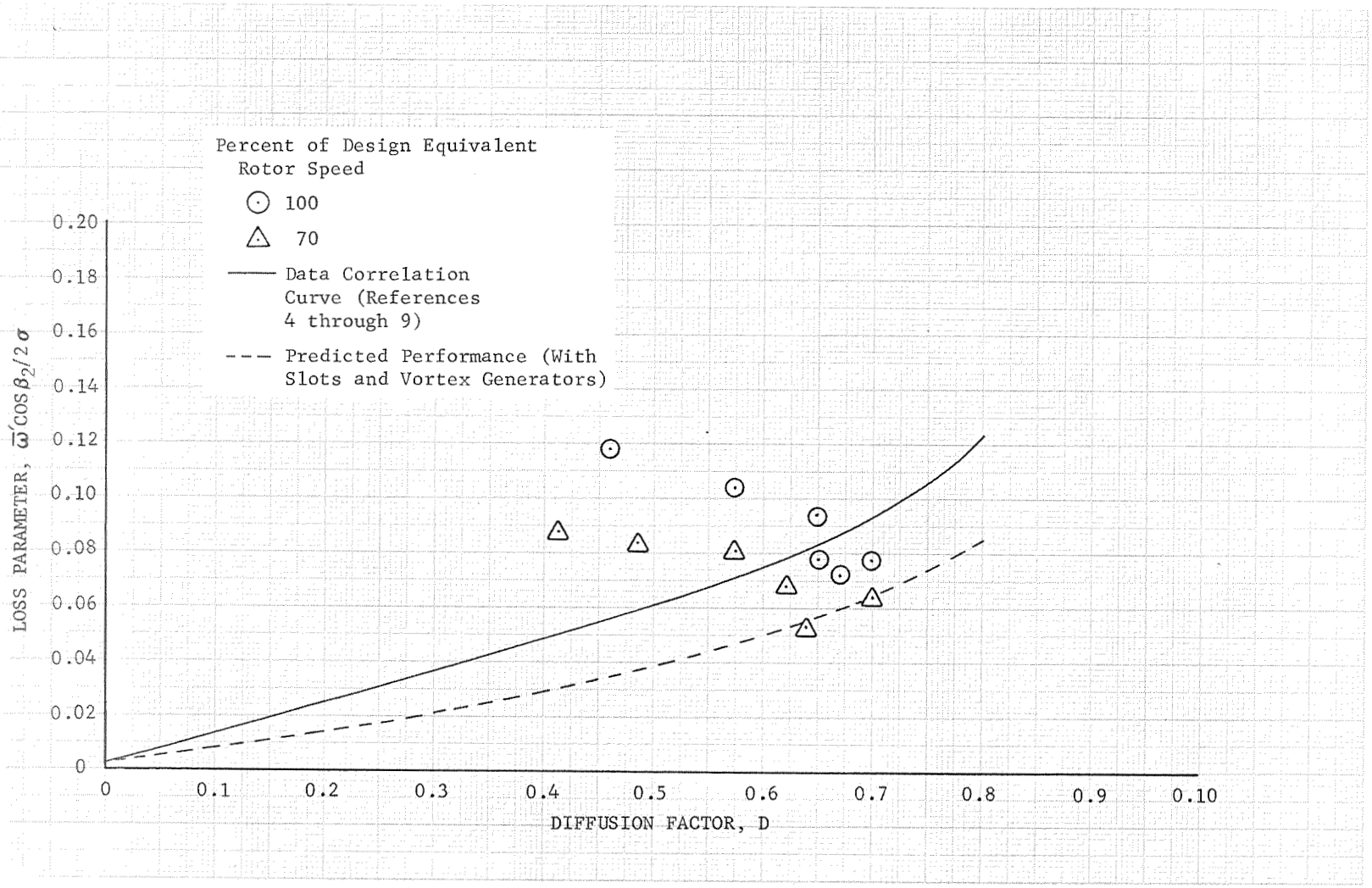

Figure 43a. Unslotted Rotor 4 (With Vortex Generators Ahead of the Rotor and Between the Rotor and Stator) Loss Parameter vs Diffusion Factor, 10% Span From Tip

DF 83317

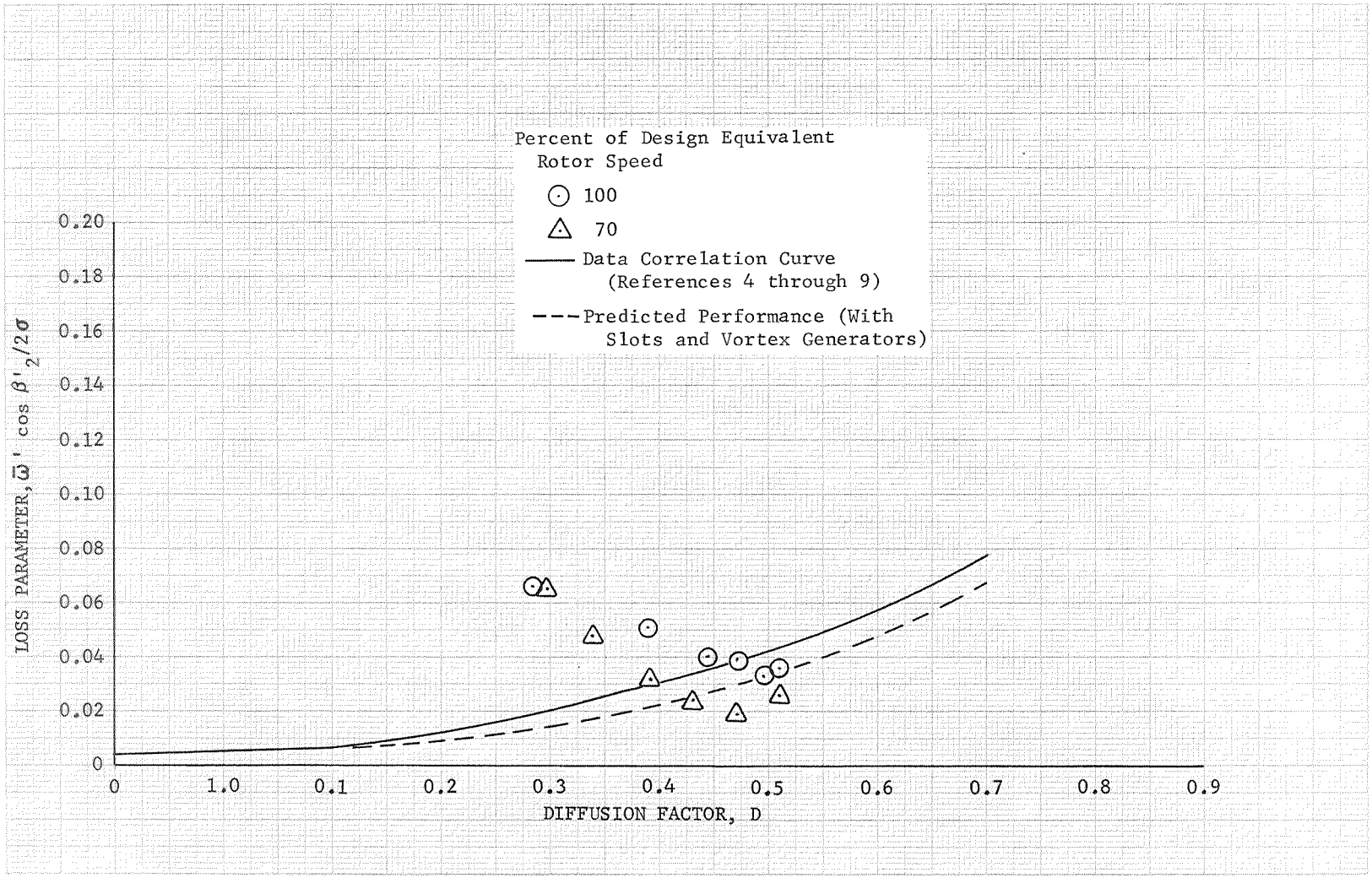

Figure 43b. Unslotted Rotor 4 (With Vortex Generators Ahead of the Rotors and Between the Rotor and Stator) Loss Parameter vs Diffusion Factor, 30% Span From Tip

DF 83318

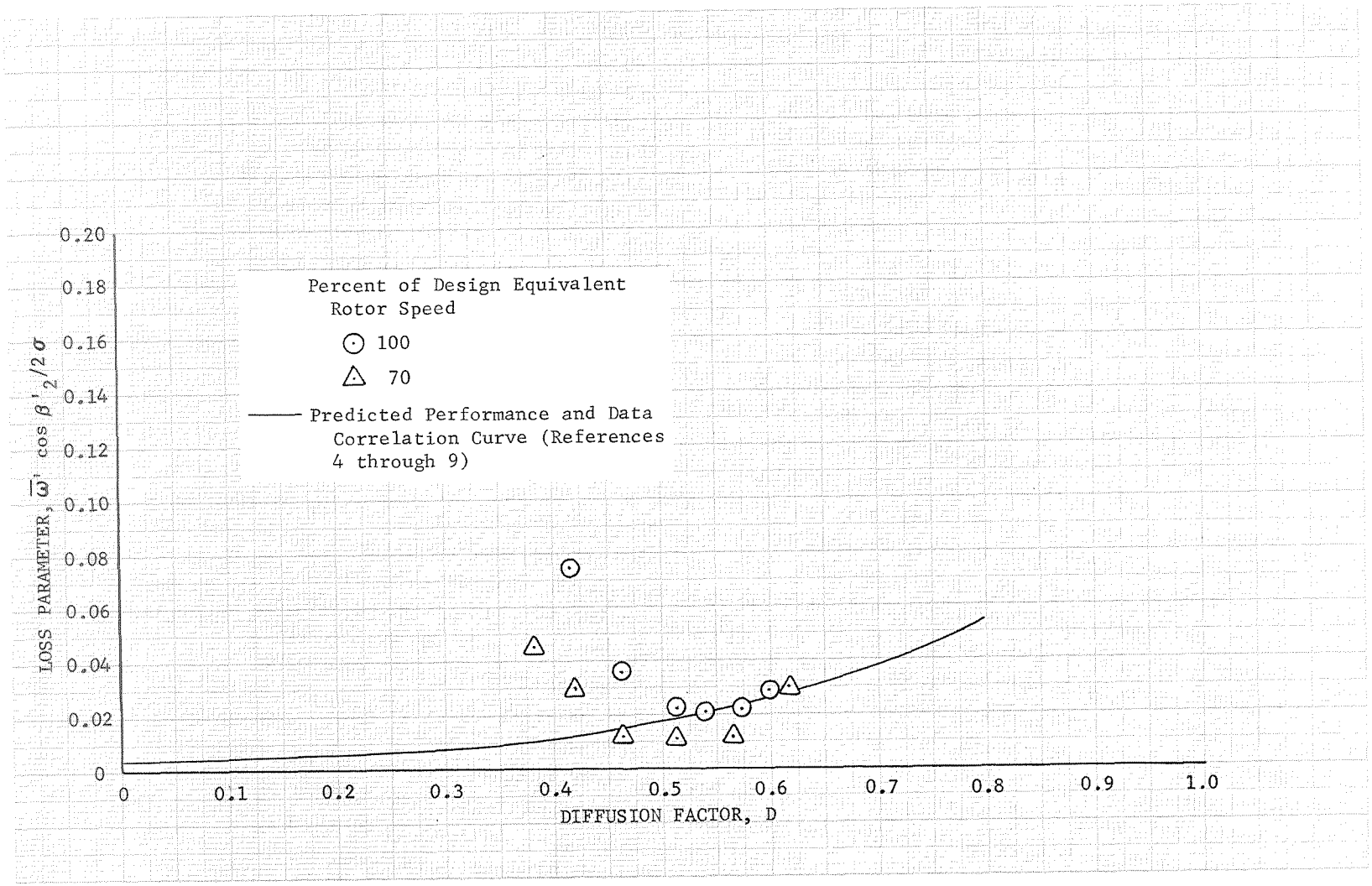

DF 83319

Figure 43c. Unslotted Rotor 4 (With Vortex Generators Ahead of the Rotor and Between the Rotor and Stator) Loss Parameter vs Diffusion Factor, 50% Span From Tip

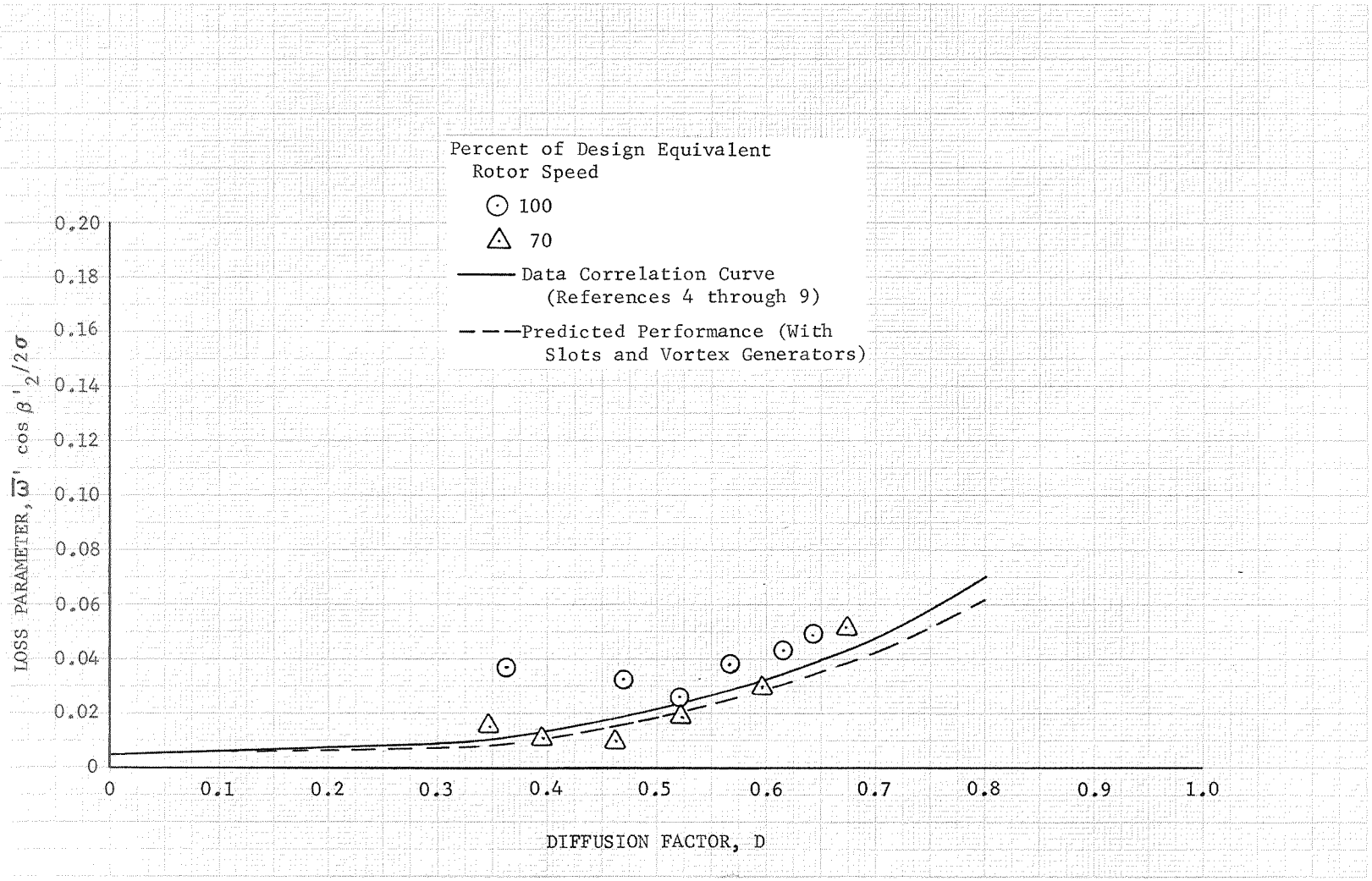

Figure 43d. Unslotted Rotor 4 (With Vortex Generators Ahead of the Rotor and Between the Rotor and Stator) Loss Parameter vs Diffusion Factor, 70% Span From Tip

DF 83320

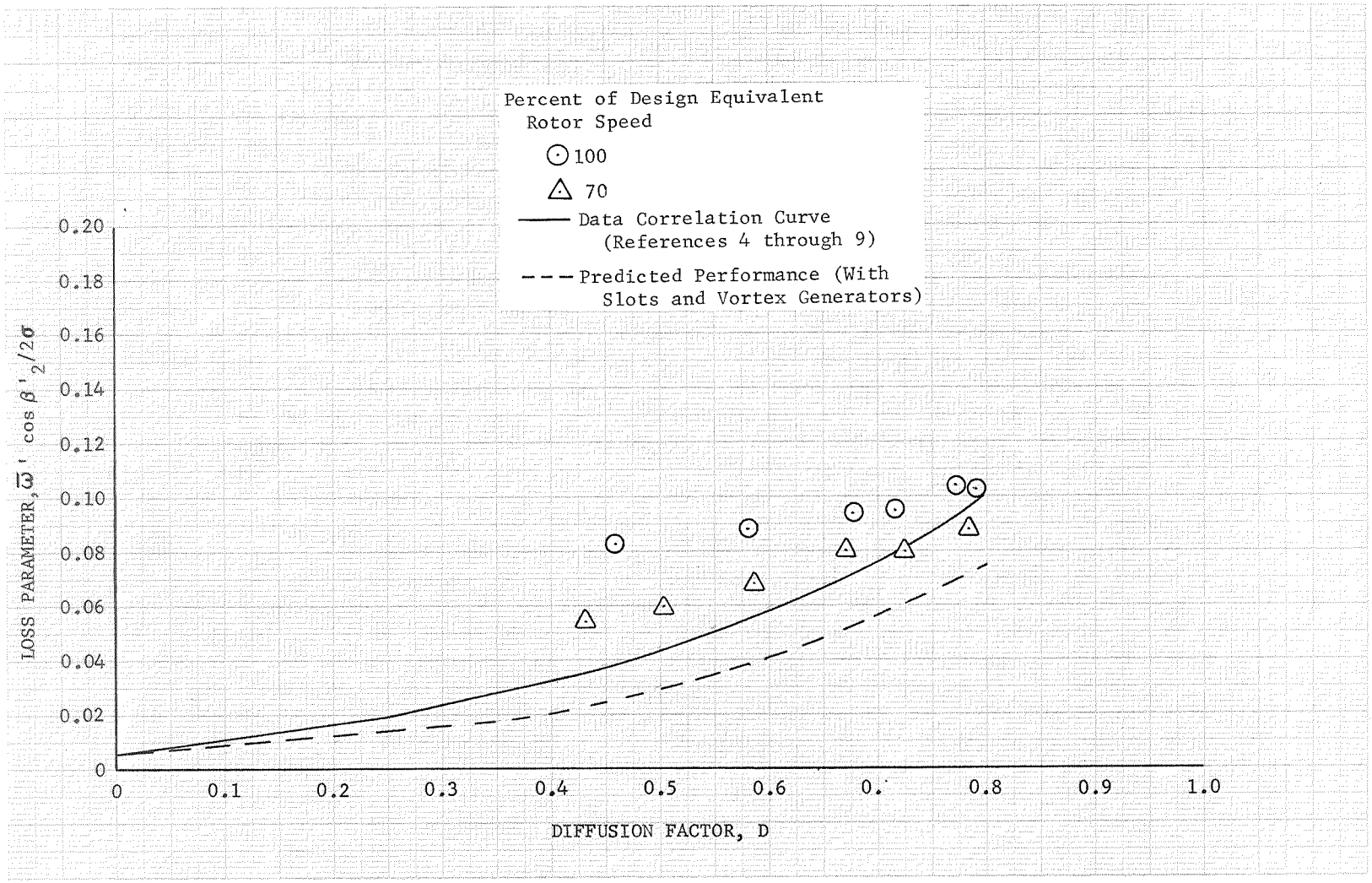

Figure 43e. Unslotted Rotor 4 (With Vortex Generators Ahead of the Rotor and Between the Rotor and Stator) Loss Parameter vs Diffusion Factor, 90% Span From Tip

DF 83321

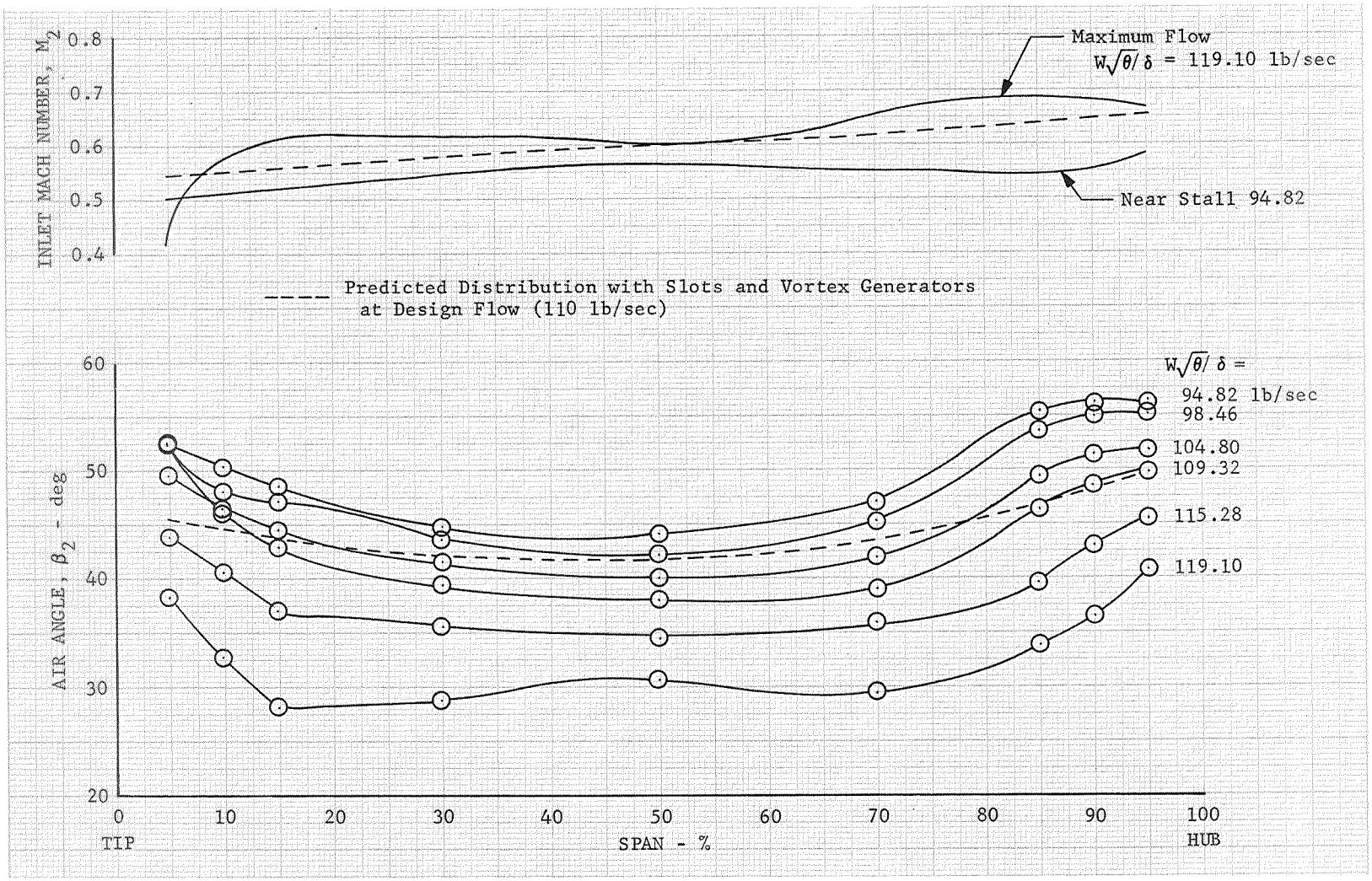

Figure 44. Slotted Stator 4 (With Vartex Generators Ahead of the Rotor and Between the Rotor and Stator) Inlet Air Angle and Mach Number Distribution, Design Equivalent Rotor Speed

DF 83427

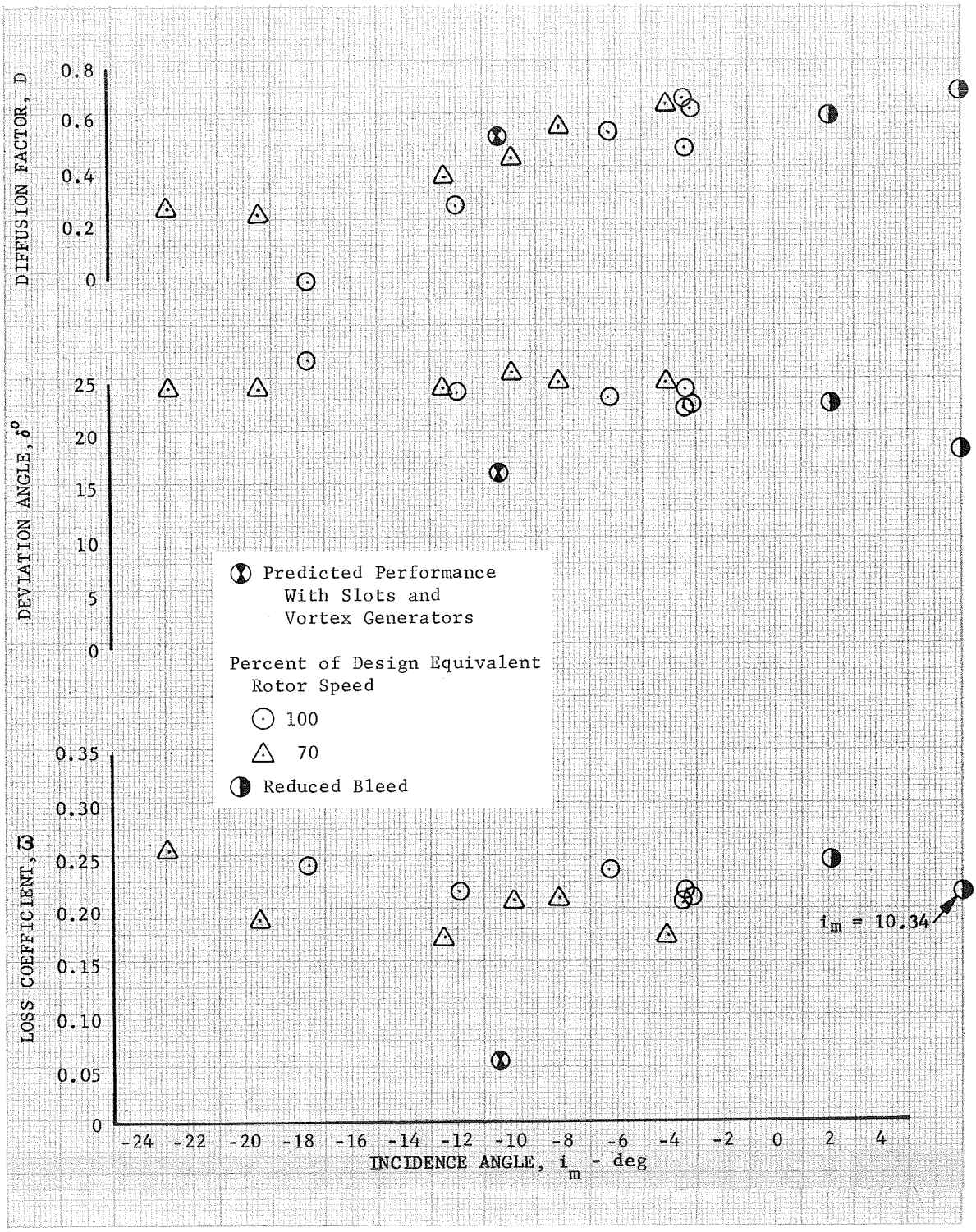

Figure 45a. Slotted Stator 4 (With Vortex Generators Ahead of the Rotor and Between the Rotor and Stator) Blade Element Performance, 5% Span From Tip

DF 83322

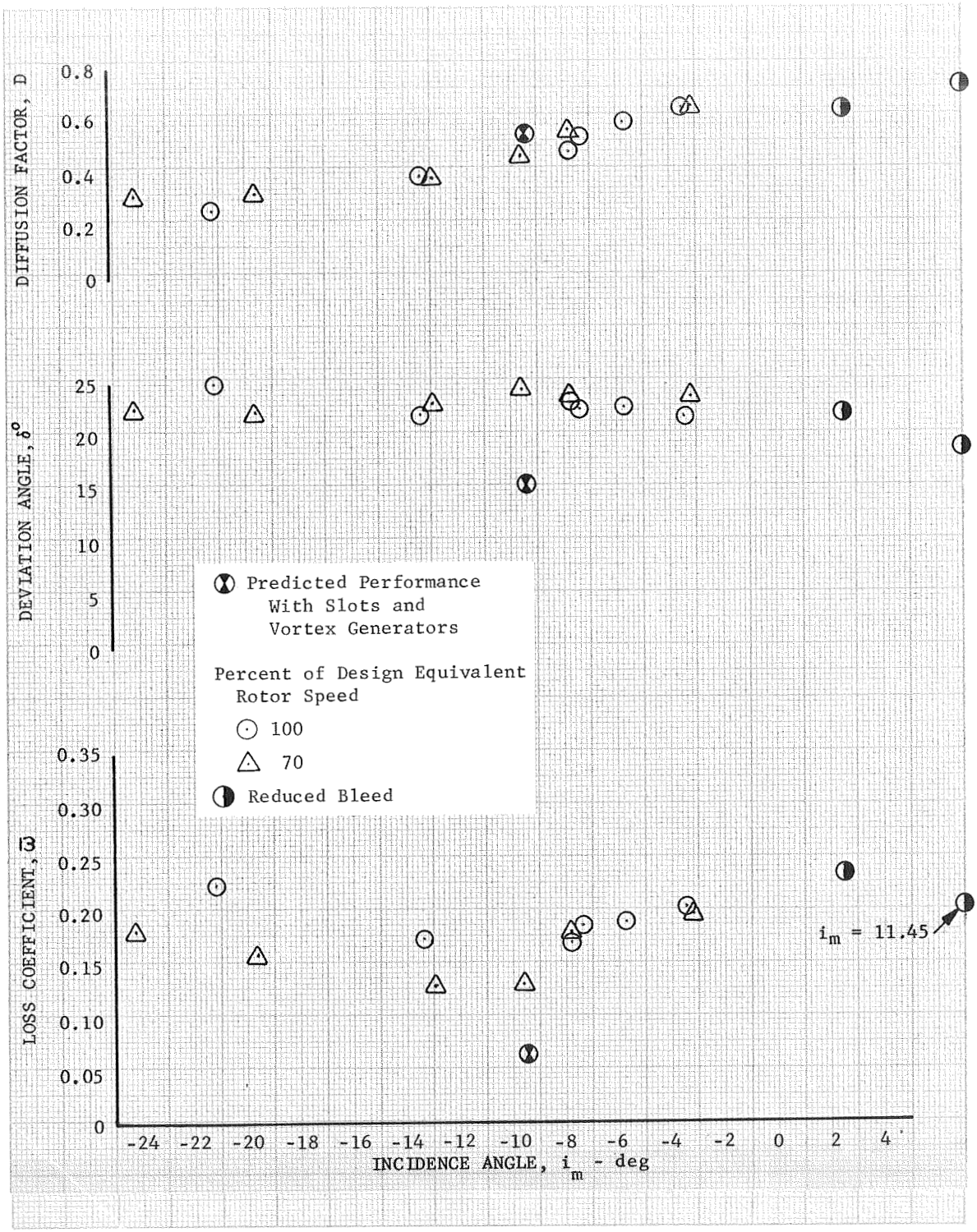

Figure 45b. Slotted Stator 4 (With Vortex Generators Ahead of the Rotor and Between the Rotor and Stator) Blade Element Performance, 10% Span From Tip

DF 83323

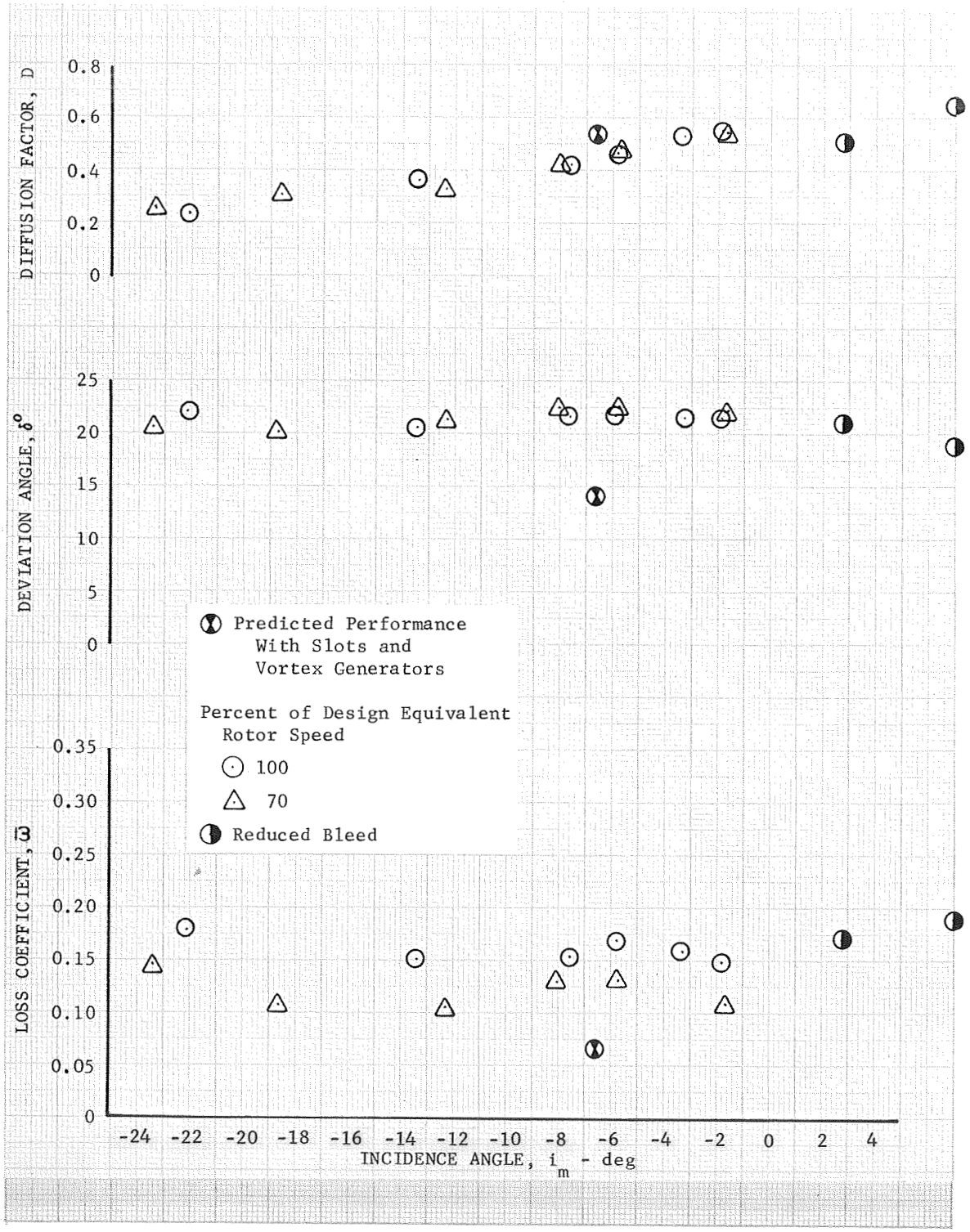

Figure 45c. Slotted Stator 4 (With Vortex Generators Ahead of the Rotor and Between the Rotor and Stator) Blade Element Performance, 15% Span From Tip

DF 83324

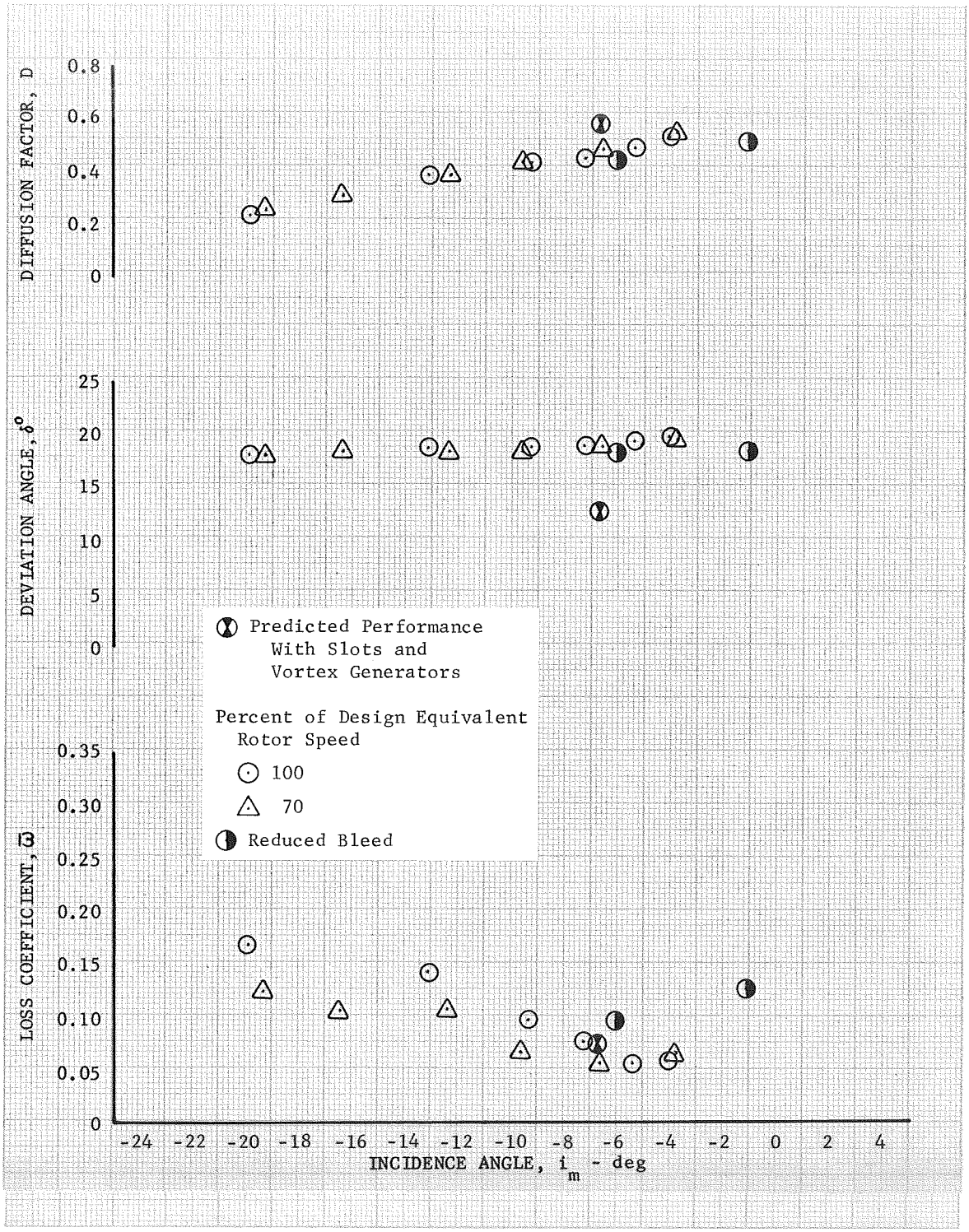

Figure 45d. Slotted Stator 4 (With Vortex Generators Ahead of the Rotor and Between the Rotor and Stator) Blade Element Performance, 30% Span From Tip

DF 83325

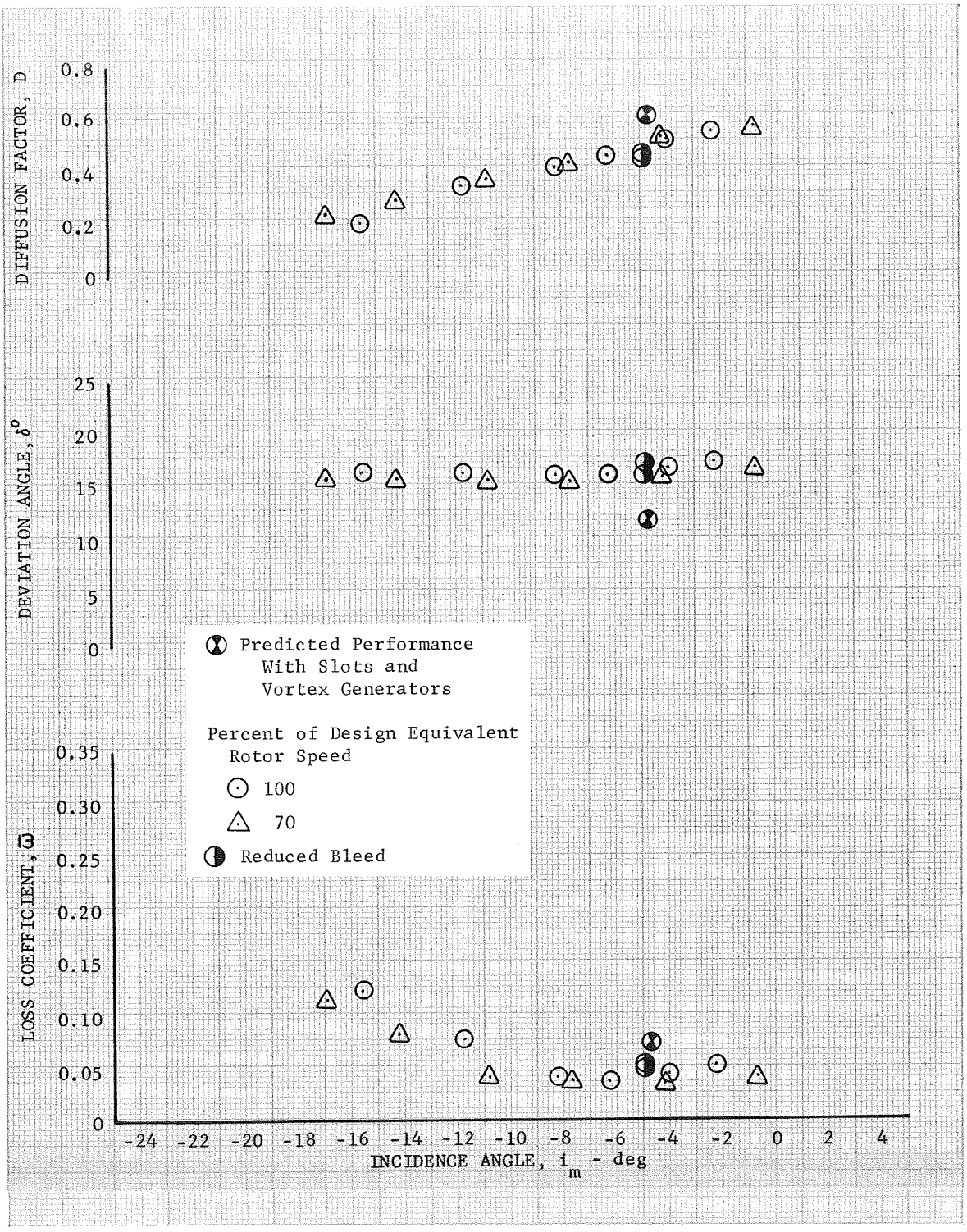

Figure 45e. Slotted Stator 4 (With Vortex Generators Ahead of the Rotor and Between the Rotor and Stator) Blade Element Performance, 50% Span From Tip

DF 83326

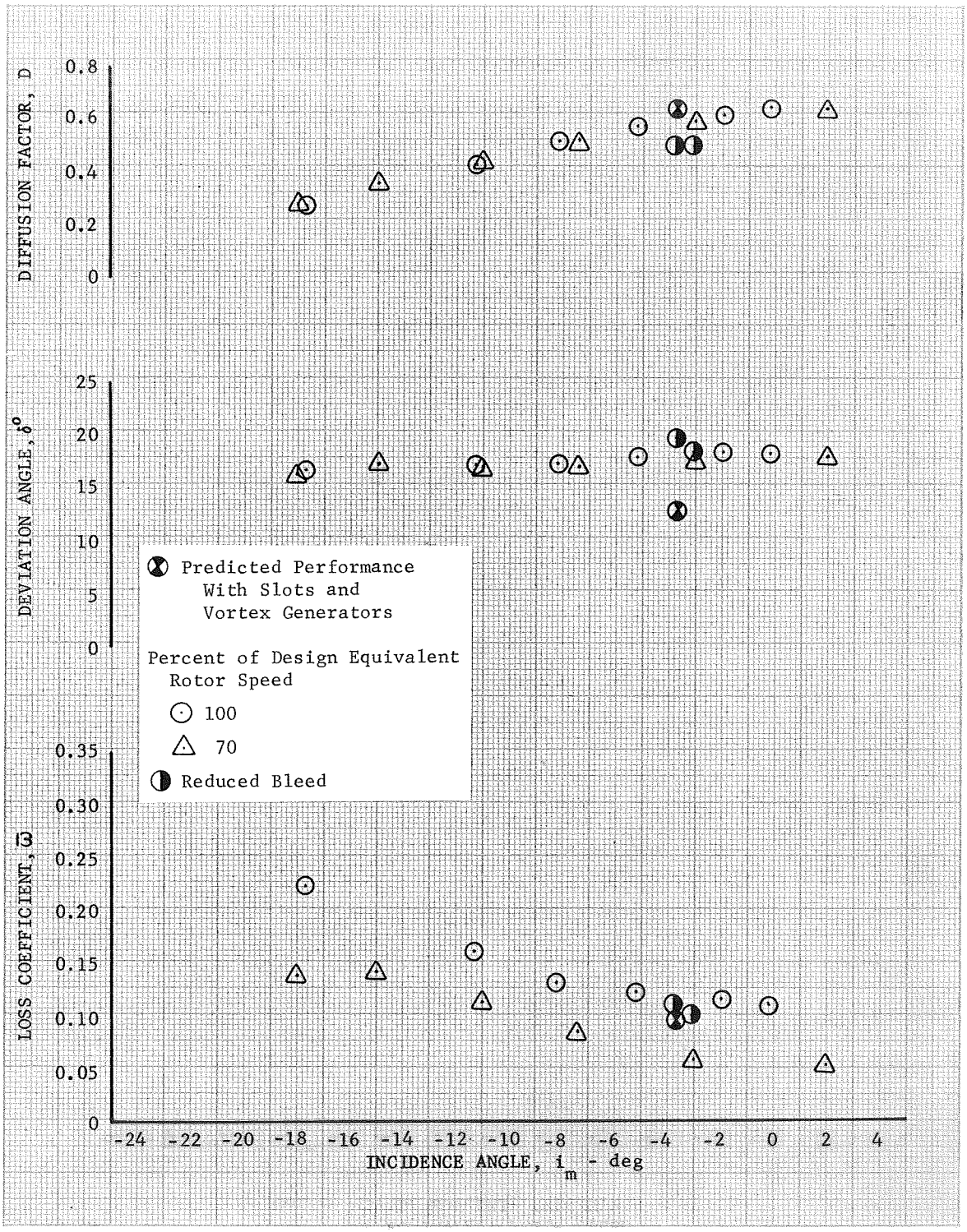

Figure 45f. Slotted Stator 4 (With Vortex Generators Ahead of the Rotor and Between the Rotor and Stator) Blade Element Performance, 70% Span From Tip

DF 83327

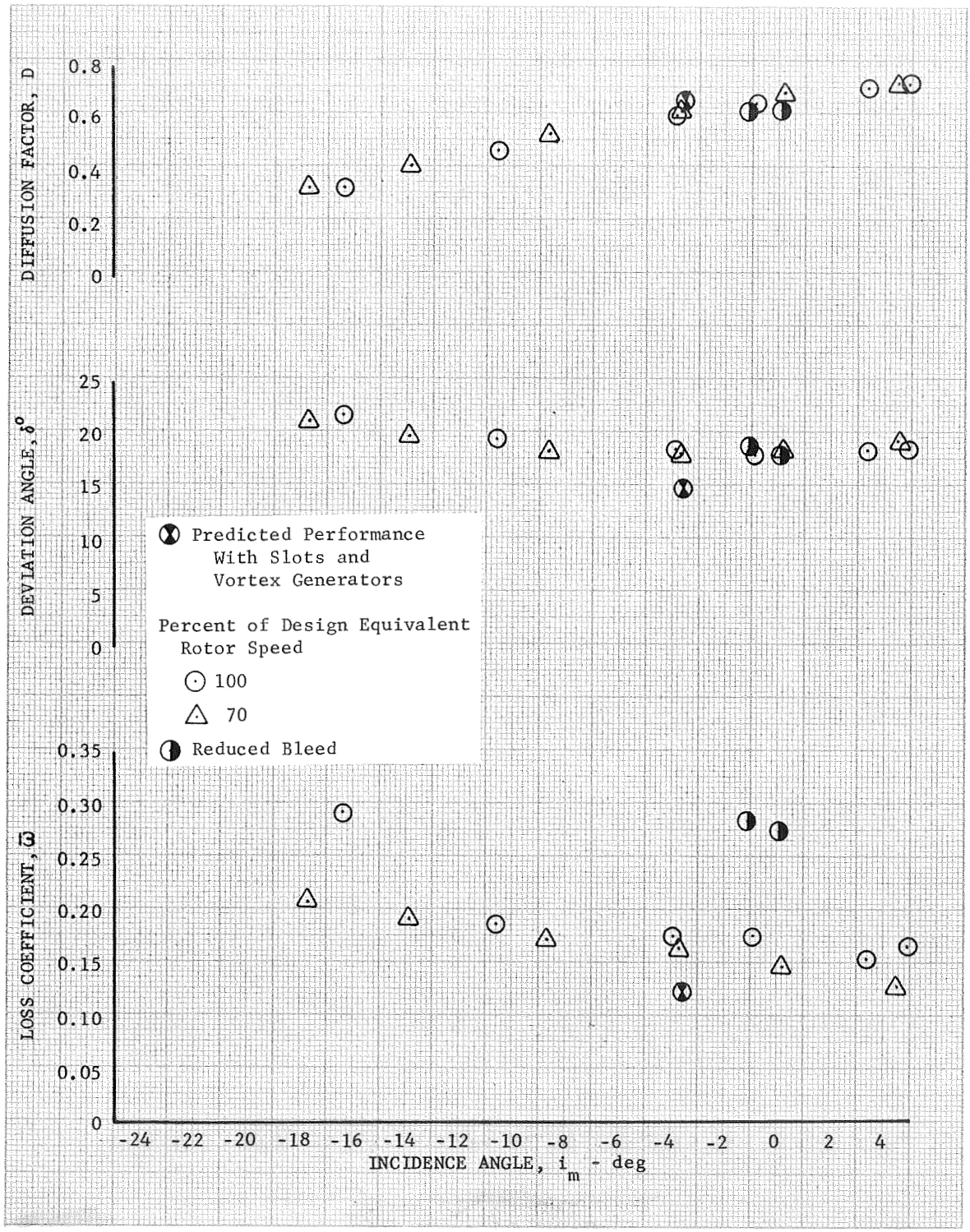

Figure 45g. Slotted Stator 4 (With Vortex Generators Ahead of the Rotor and Between the Rotor and Stator) Blade Element Performance, 85% Span From Tip

DF 83328

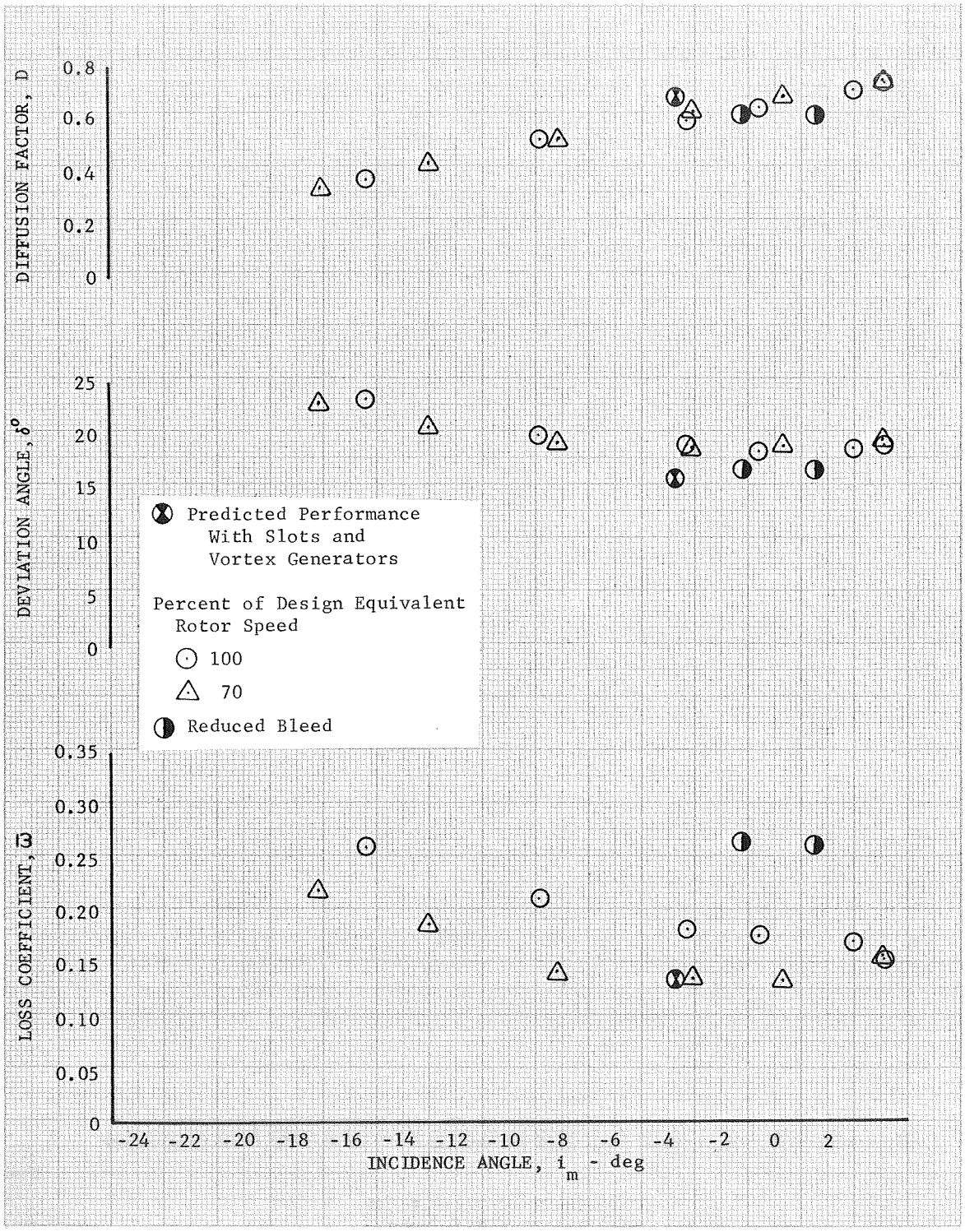

Figure 45h. Slotted Stator 4 (With Vortex Generators Ahead of the Rotor and Between the Rotor and Stator) Blade Element Performance, 90% Span From Tip

DF 83329

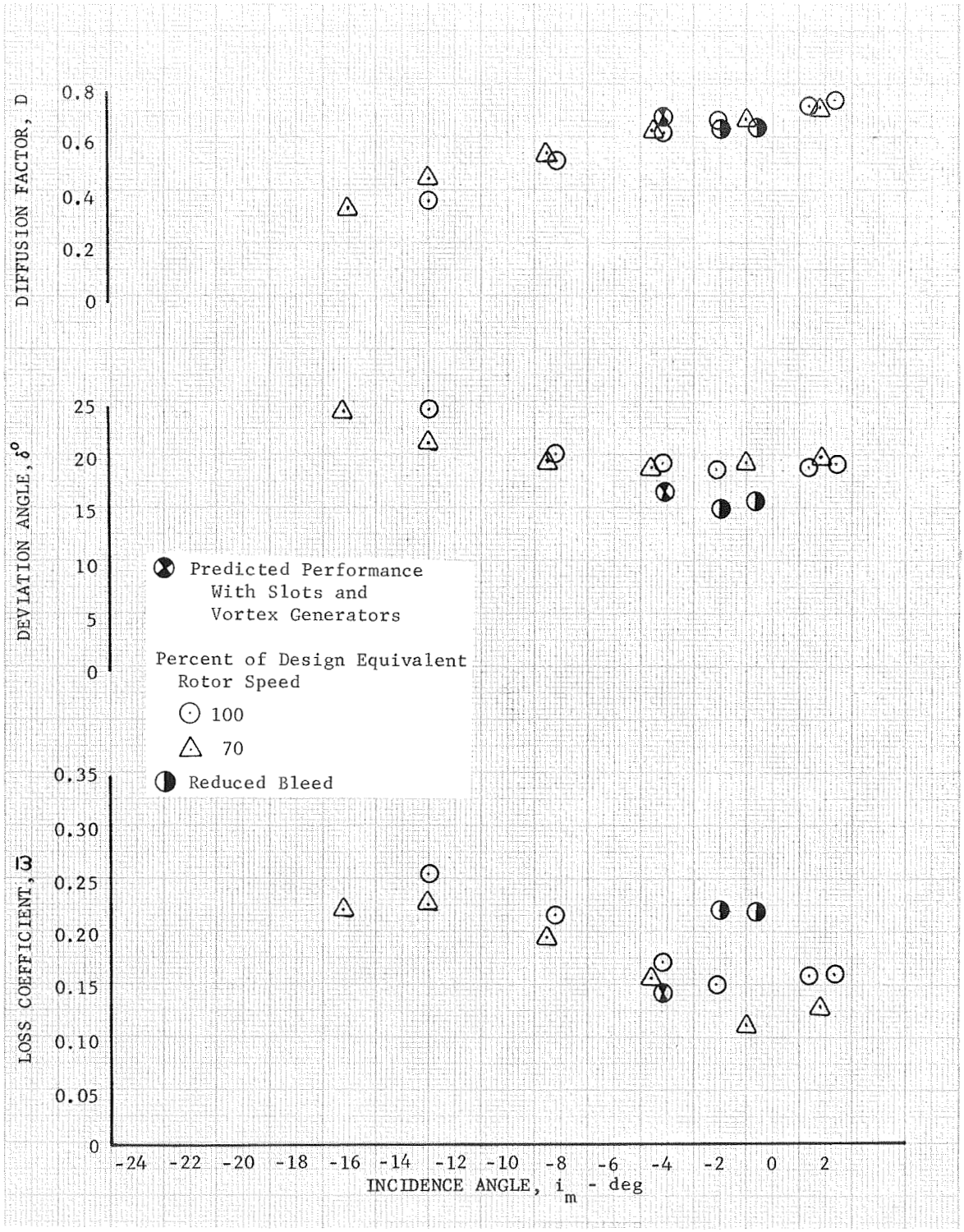

Figure 45i. Slotted Stator 4 (With Vortex Generators Ahead of the Rotor and Between the Rotor and Stator) Blade Element Performance, 95% Span From Tip

DF 83330

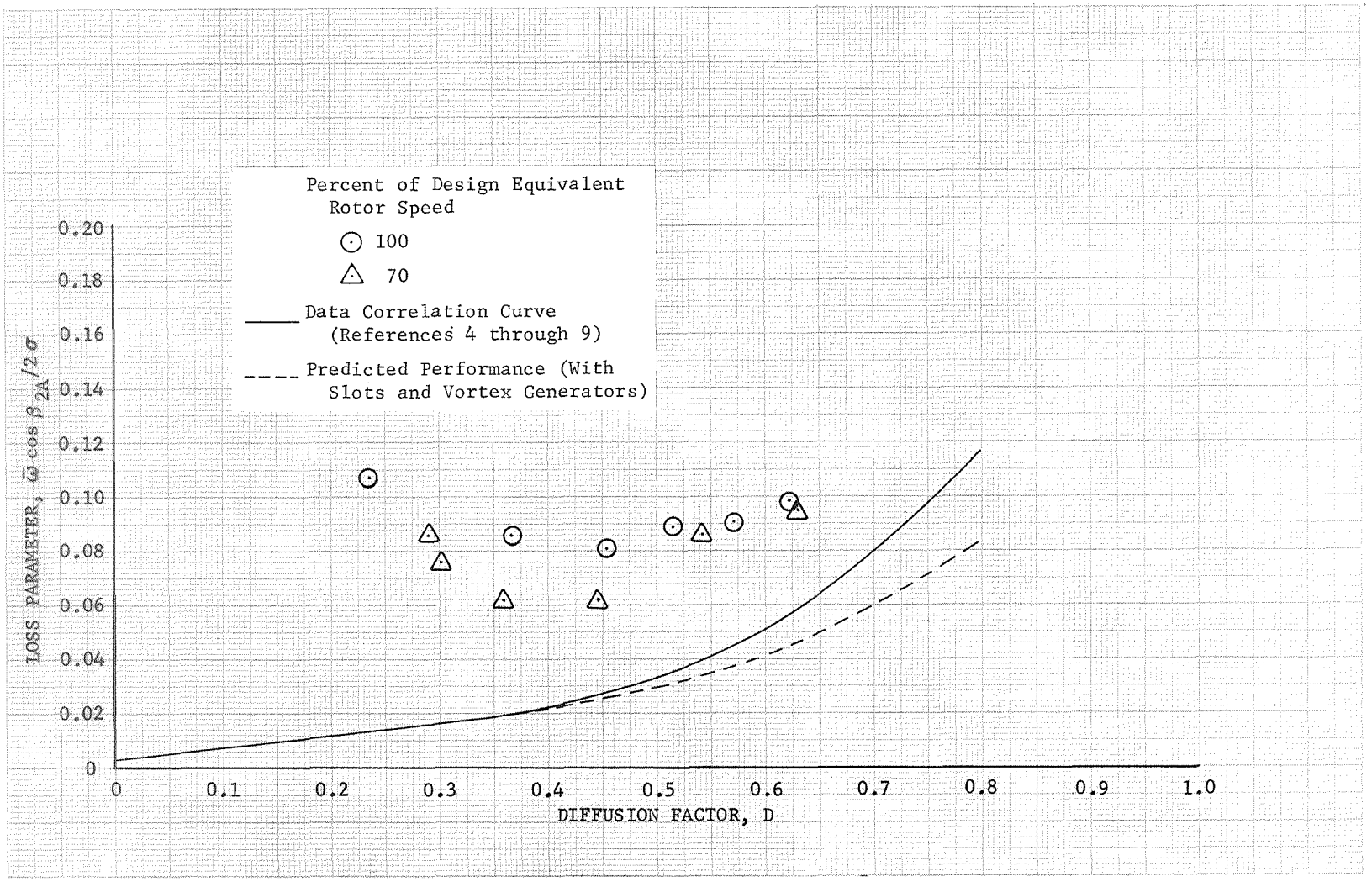

Figure 46a. Slotted Stator 4 (With Vortex Generators Ahead of the Rotor and Between the Rotor and Stator) Loss Parameter vs Diffusion Factor, 10% Span From Tip

DF 83331

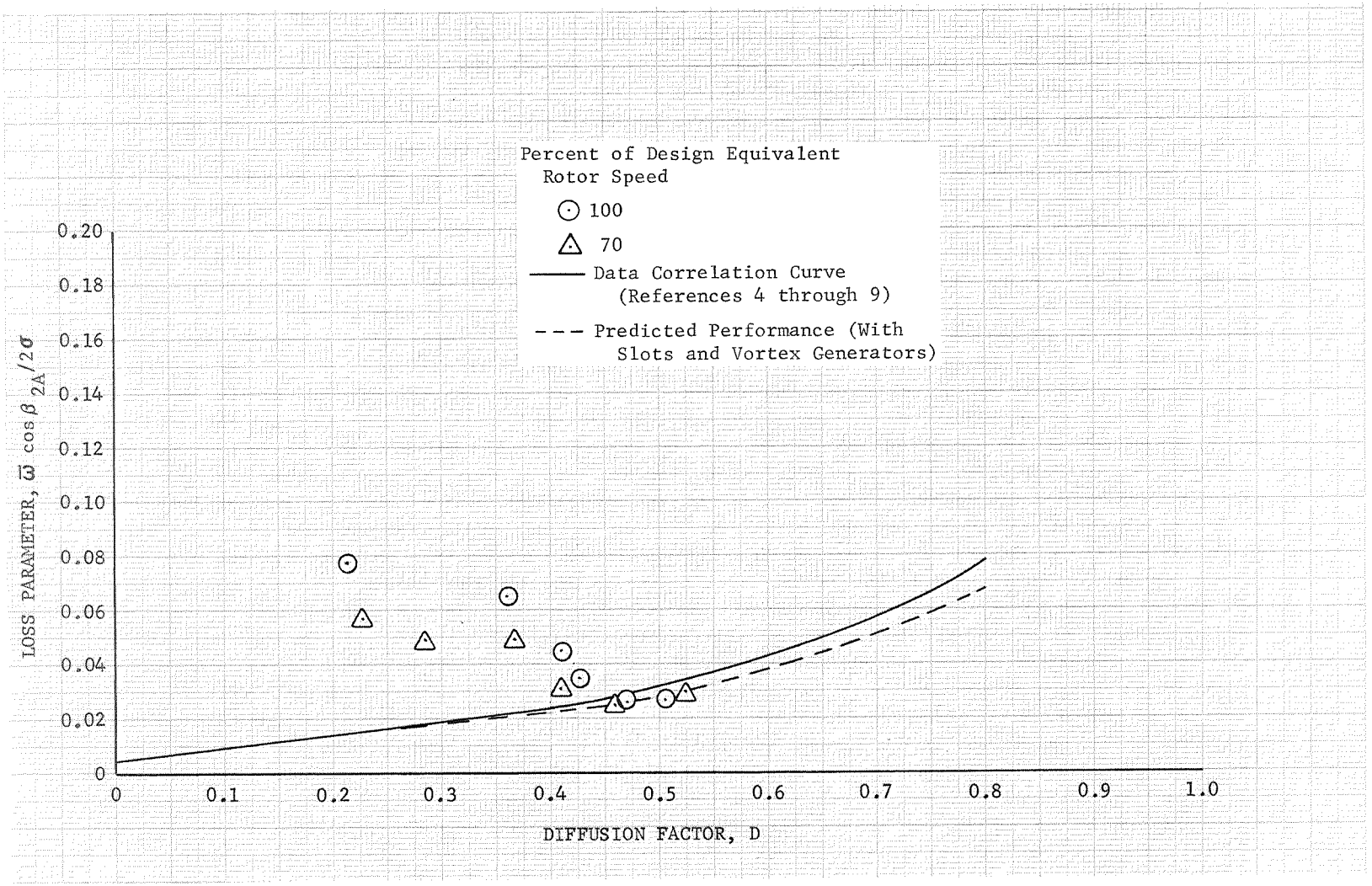

Figure 46b. Slotted Stator 4 (With Vortex Generators Ahead of the Rotor and Between the Rotor and Stator) Loss Parameter vs Diffusion Factor, 30% Span From Tip

DF 83332

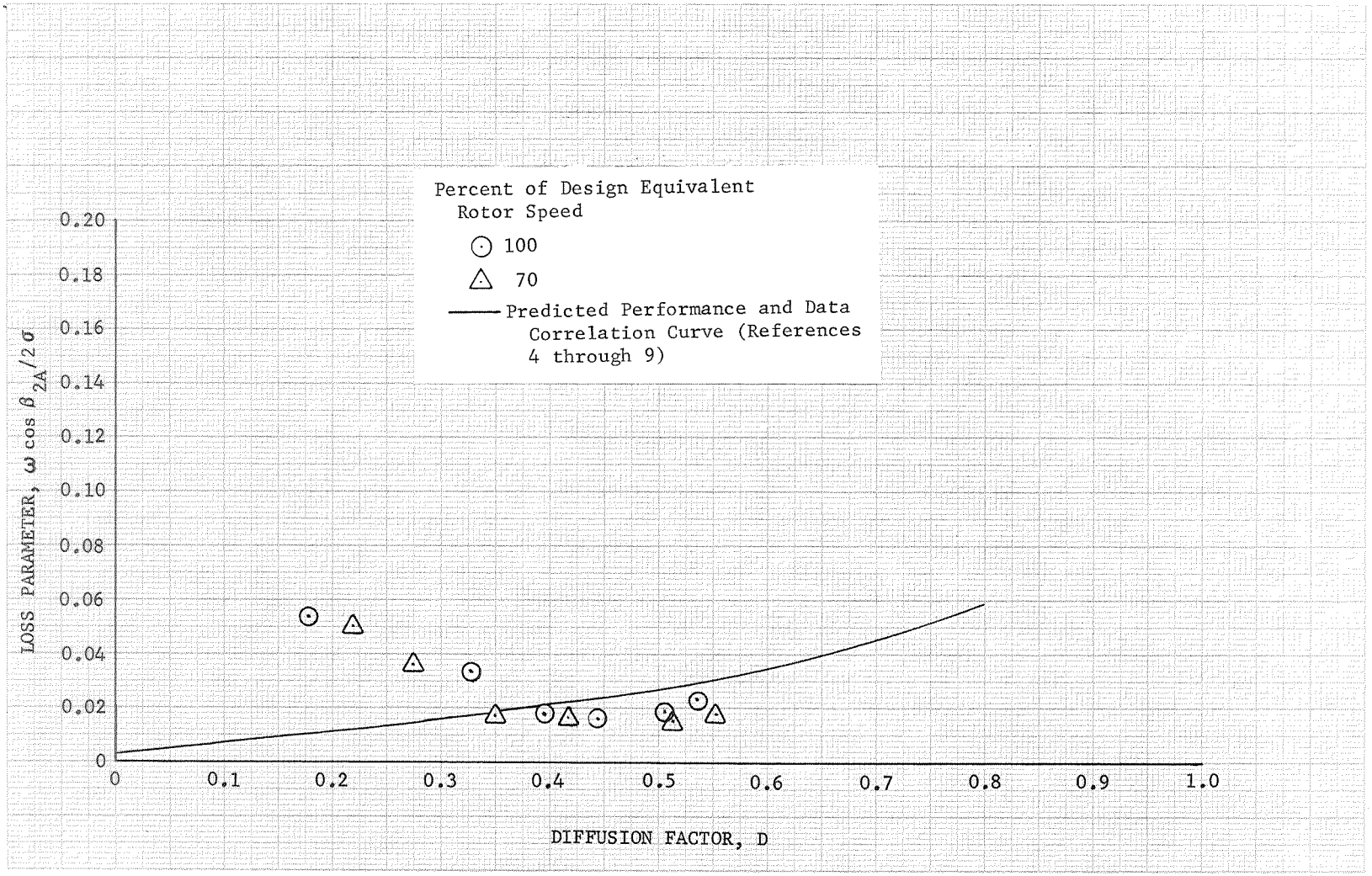

Figure 46c. Slotted Stator 4 (With Vortex Generators Ahead of the Rotor and Between the Rotor and Stator) Loss Parameter vs Diffusion Factor, 50% Span From Tip

DF 83333

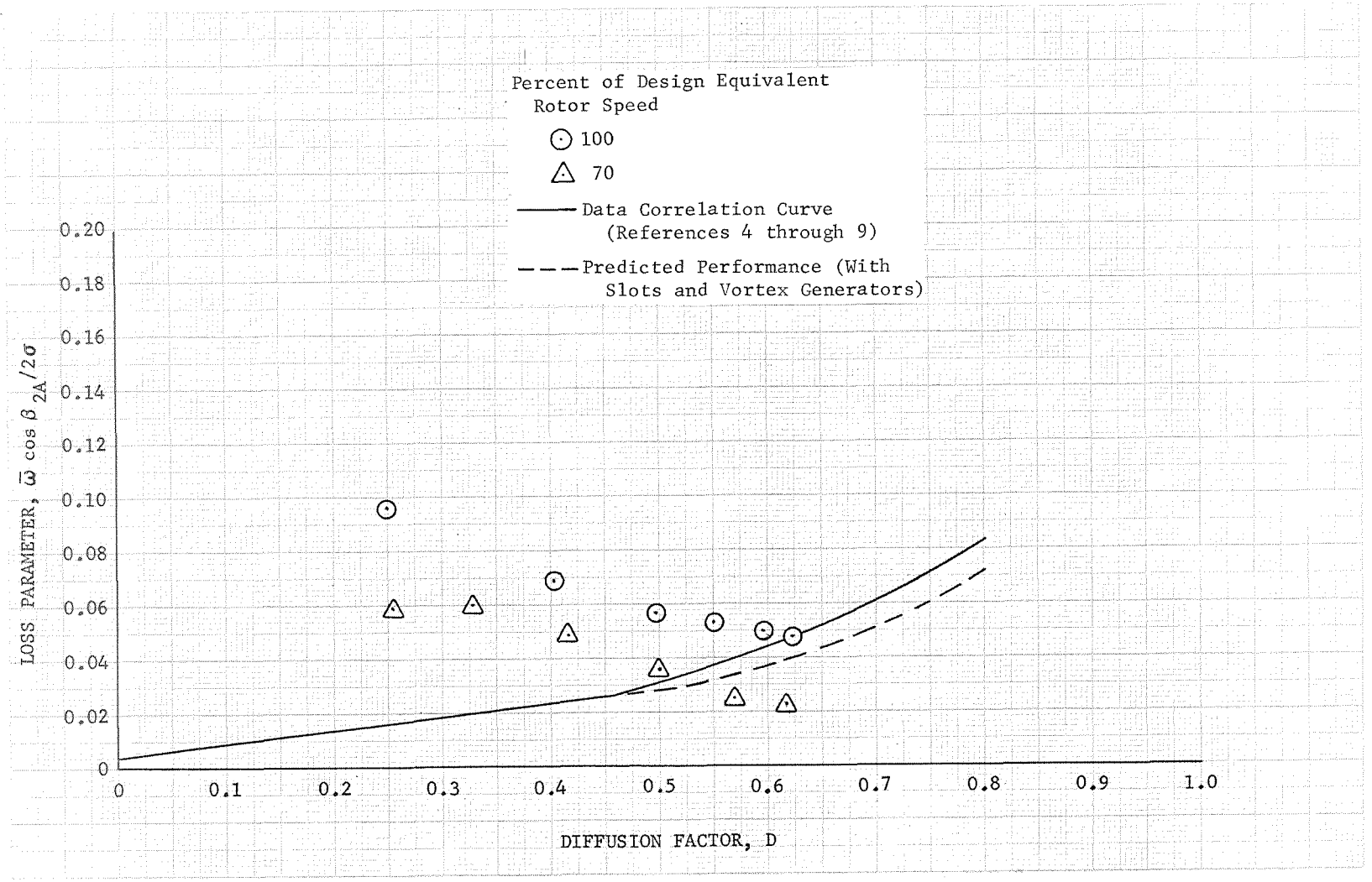

Figure 46d. Slotted Stator 4 (With Vortex Generators Ahead of the Rotor and Between the Rotor and Stator) Loss Parameter vs Diffusion Factor, 70% Span From Tip

DF 83334

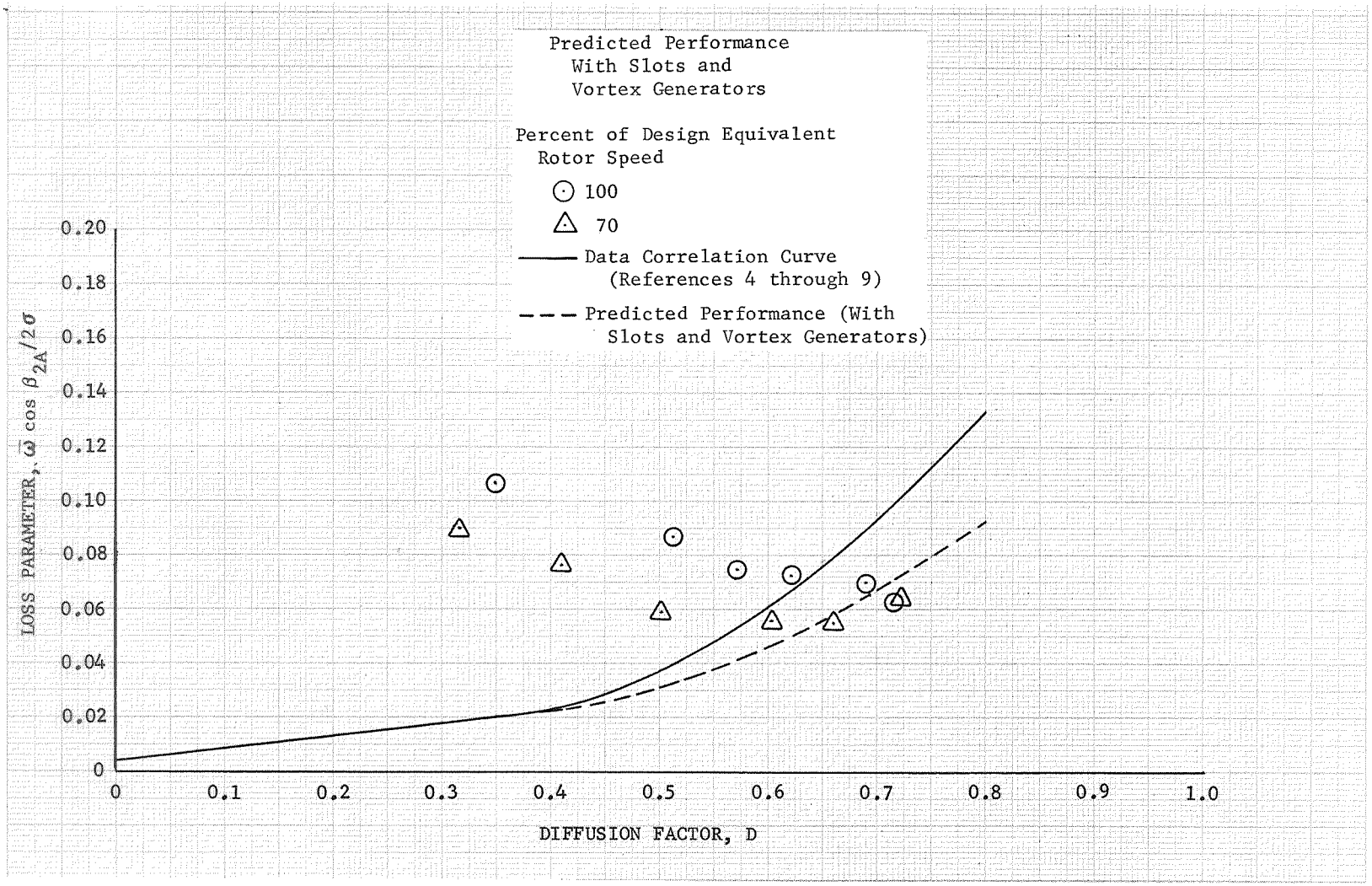

Figure 46e. Slotted Stator 4 (With Vortex Generators Ahead of the Rotor and Between the Rotor and Stator) Loss Parameter vs Diffusion Factor, 90% Span From Tip

DF 83335

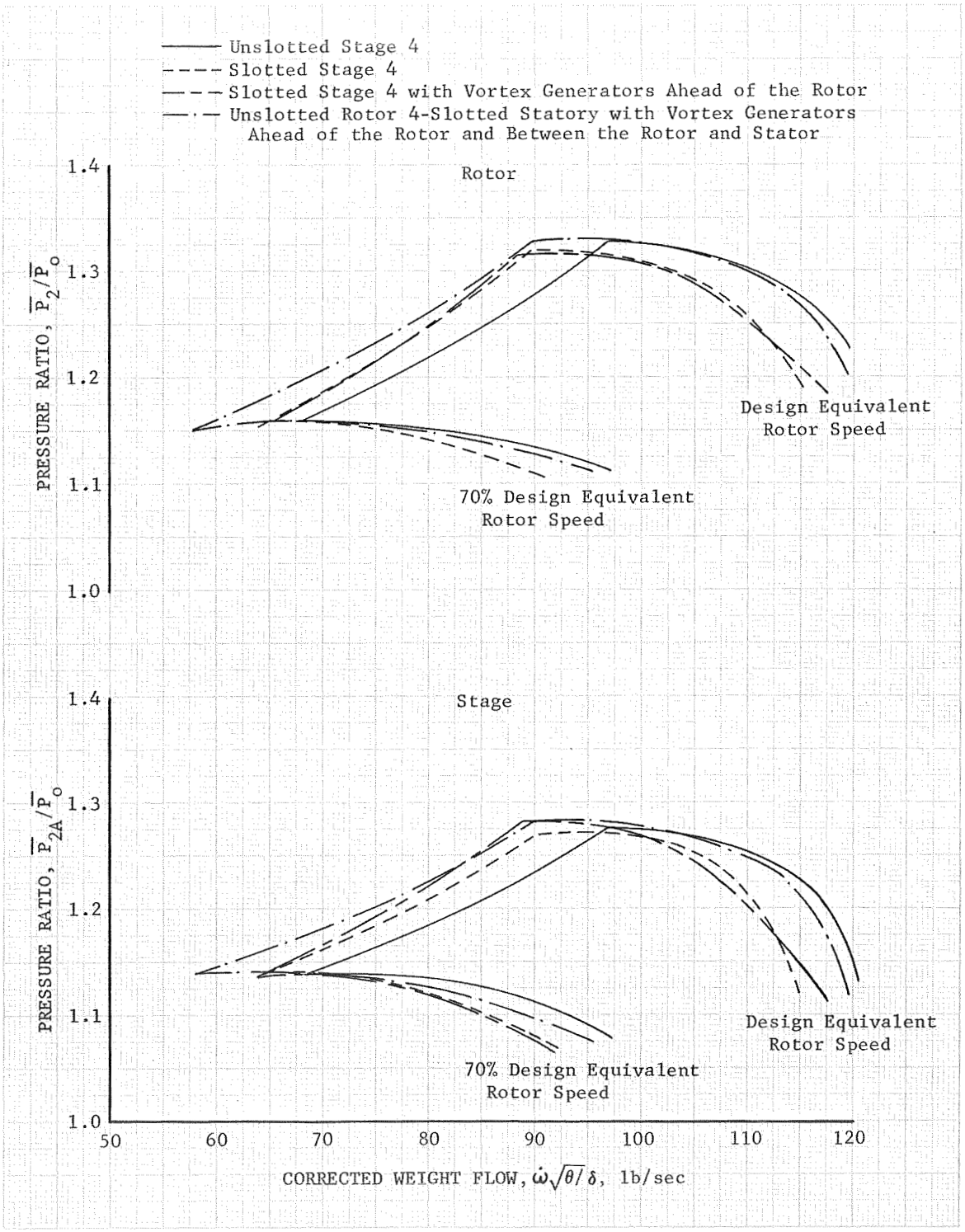

Figure 47. Rotor and Stage Pressure Ratio Comparisons

DF 83428

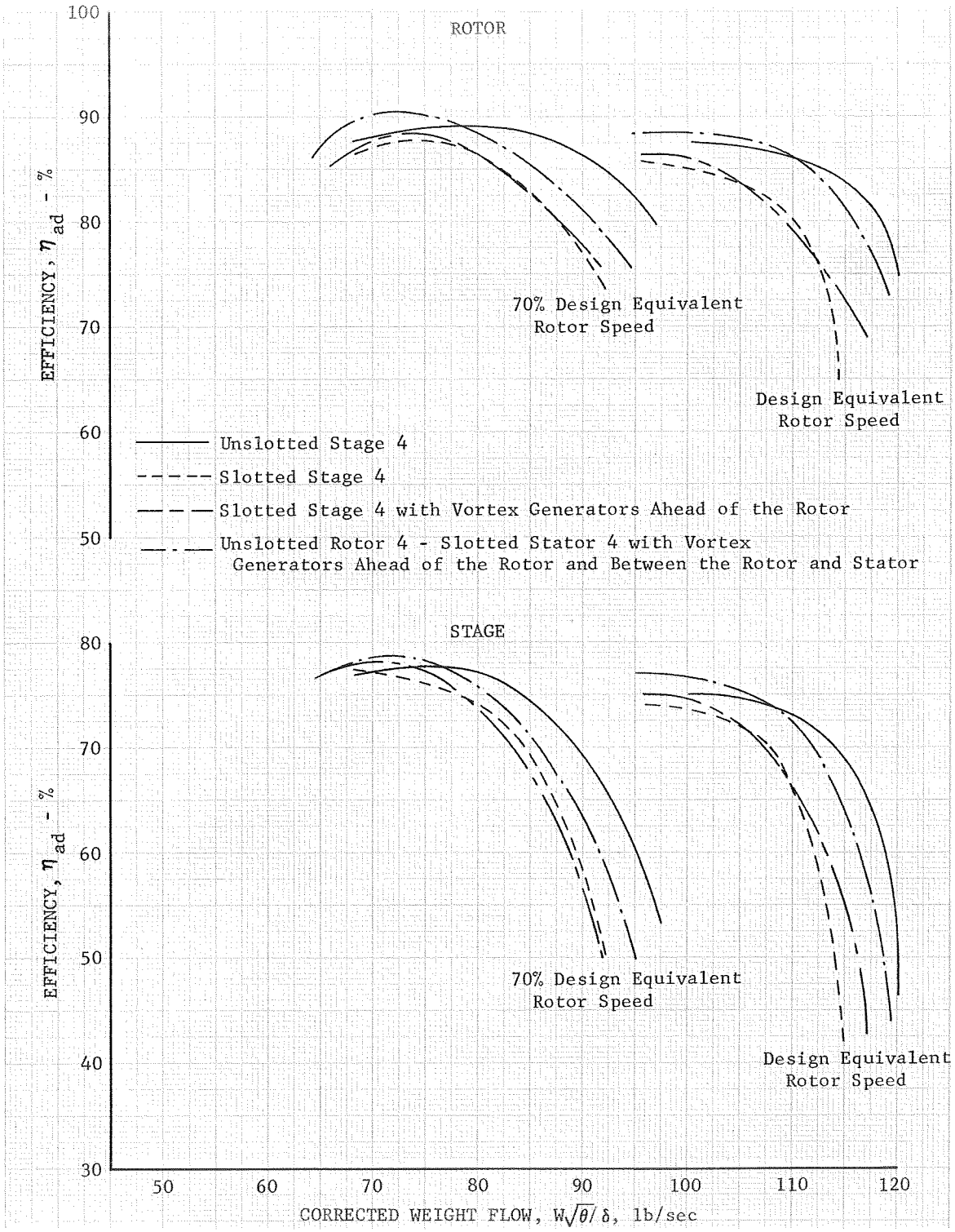

Figure 48. Rotor and Stage Efficiency Comparisons DF 83429

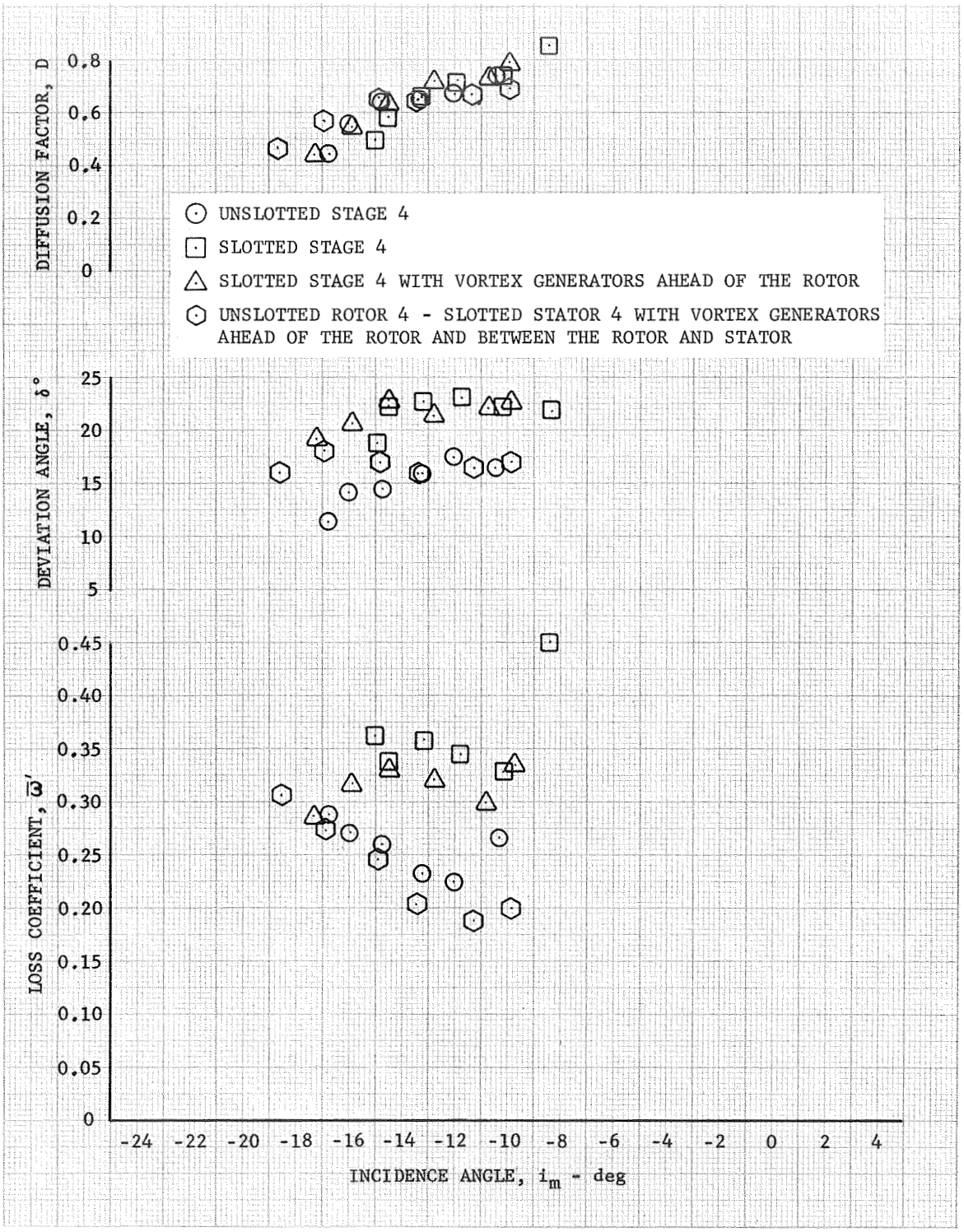

Figure 49a. Rotor Blade Element Performance Comparisons, 10% Span From Tip, 100% Design Equivalent Rotor Speed

DF 83430

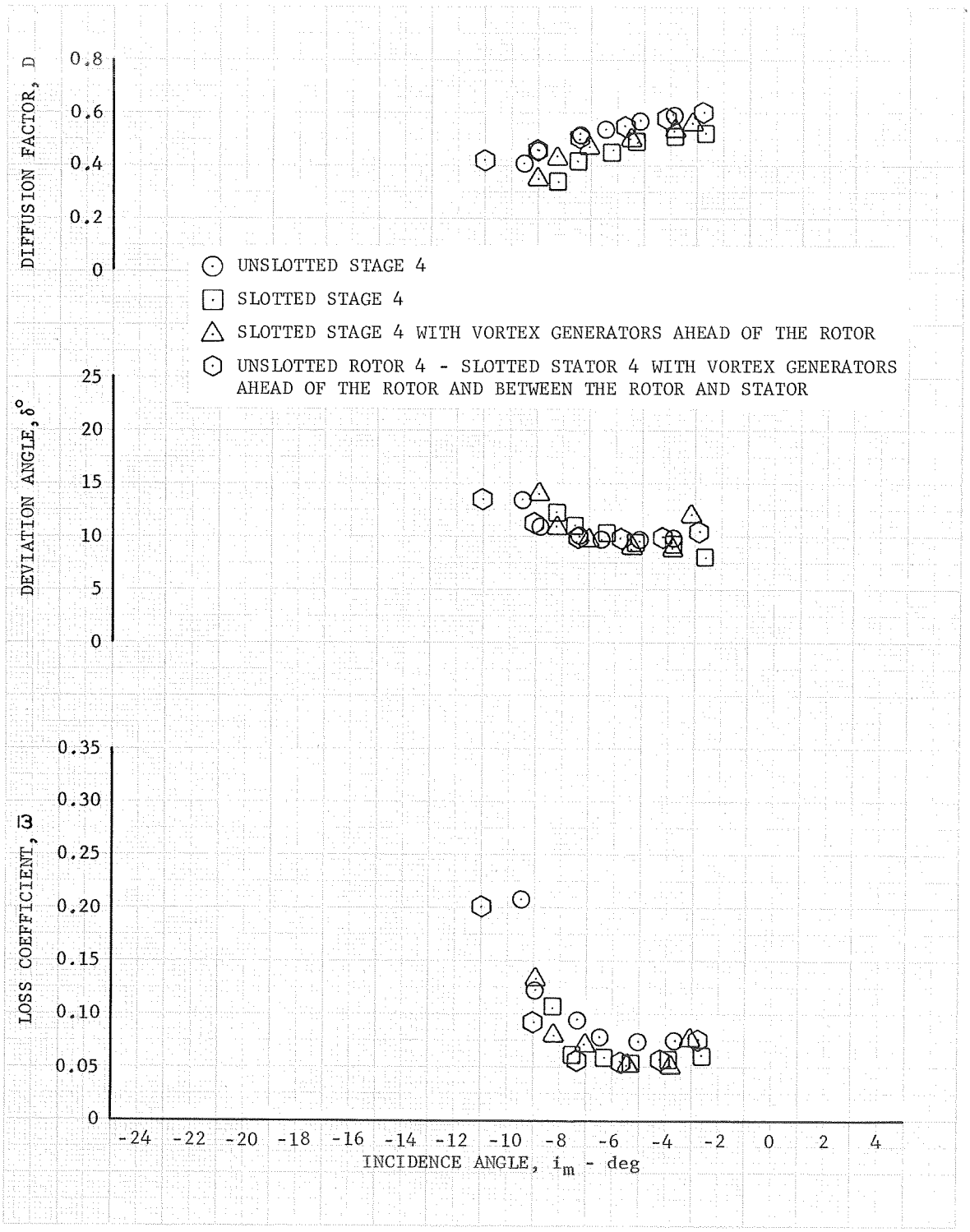

Figure 49b. Rotor Blade Element Performance Comparisons, 50% Span From Tip, 100% Design Equivalent Rotor Speed

DF 83431

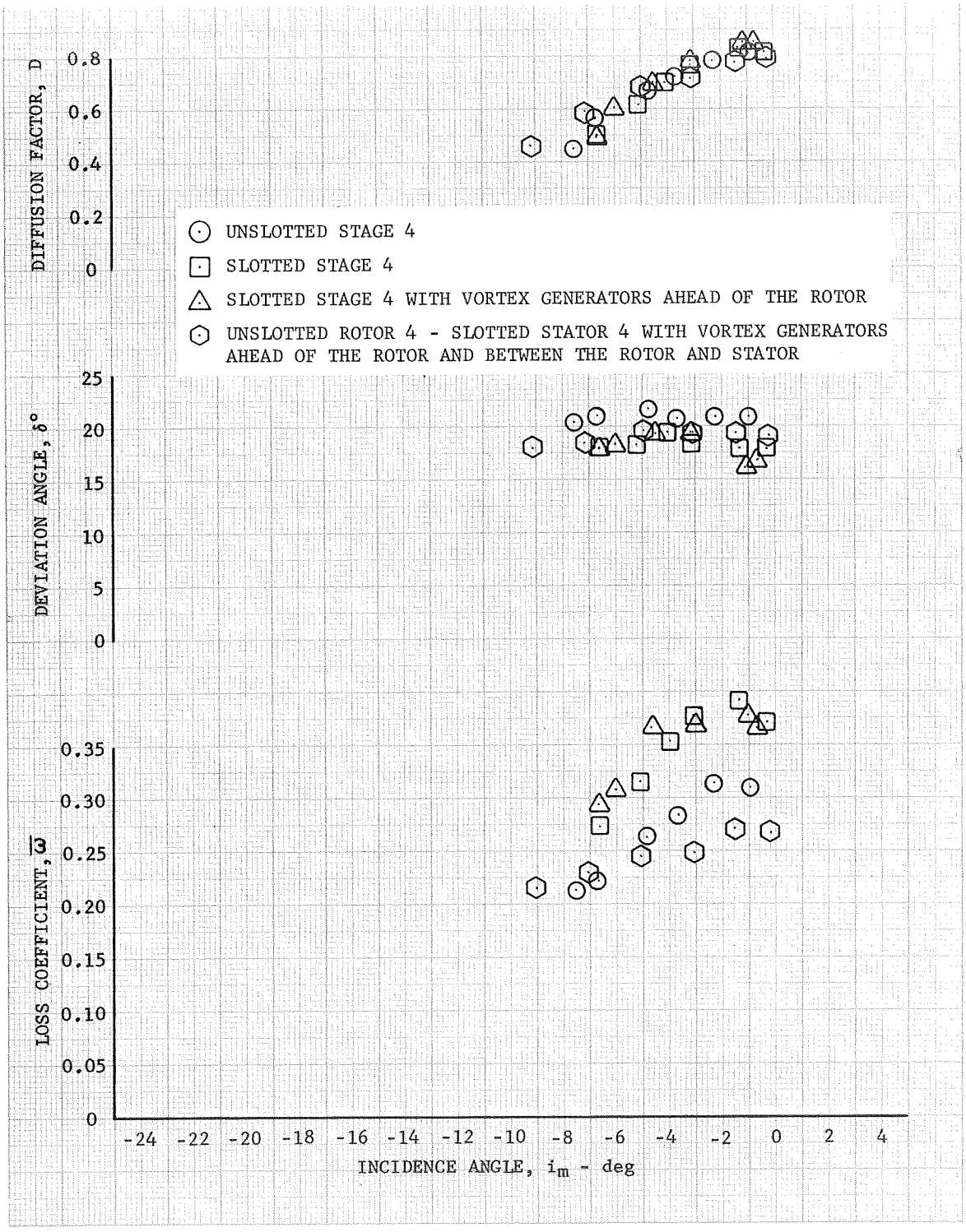

Figure 49c. Rotor Blade Element Performance Comparisons, 90% Span From Tip, 100% Design Equivalent Rotor Speed

DF 83432

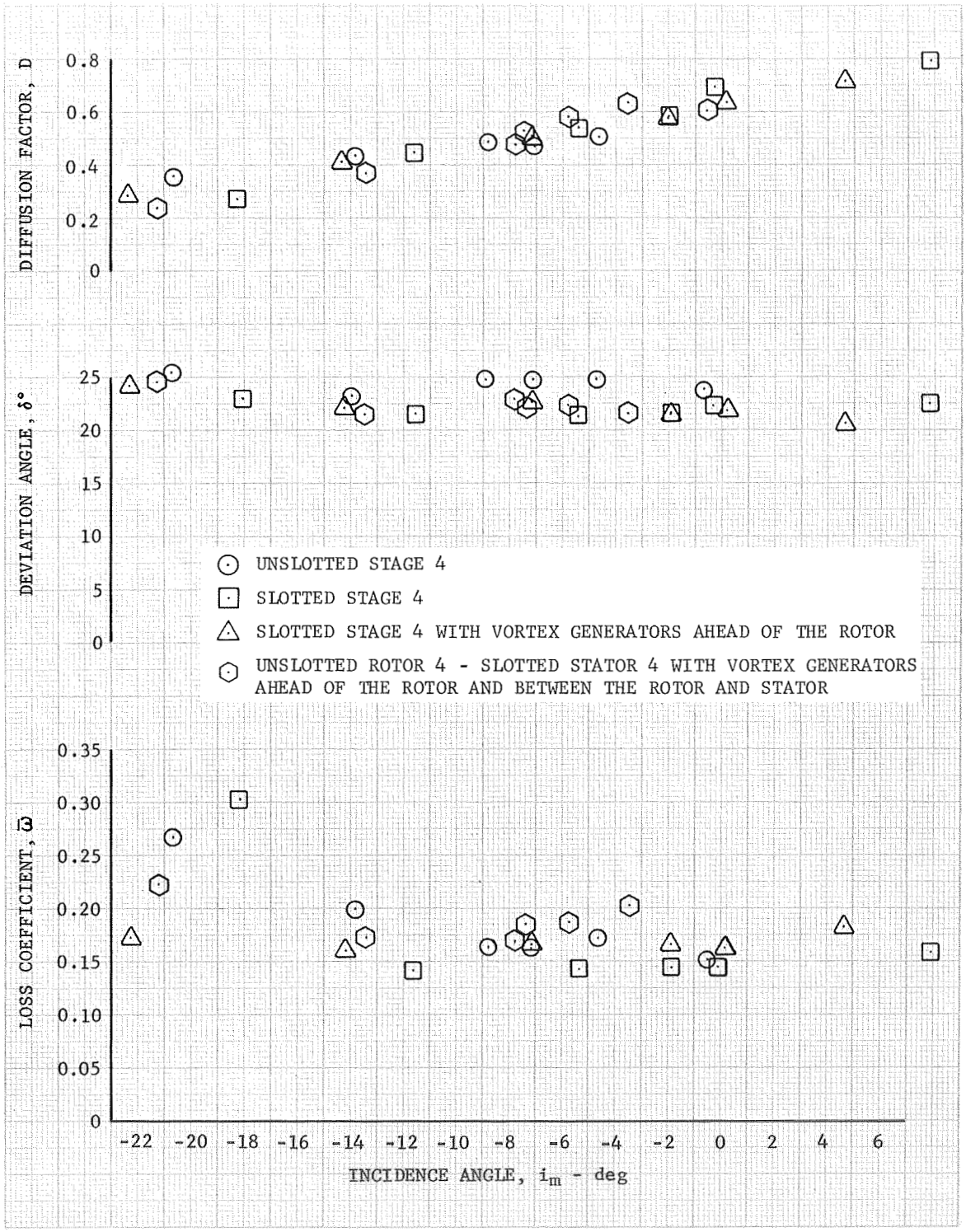

Figure 50a. Stator Blade Element Performance Comparisons, 10% Span From Tip, 100% Design Equivalent Rotor Speed

DF 83433

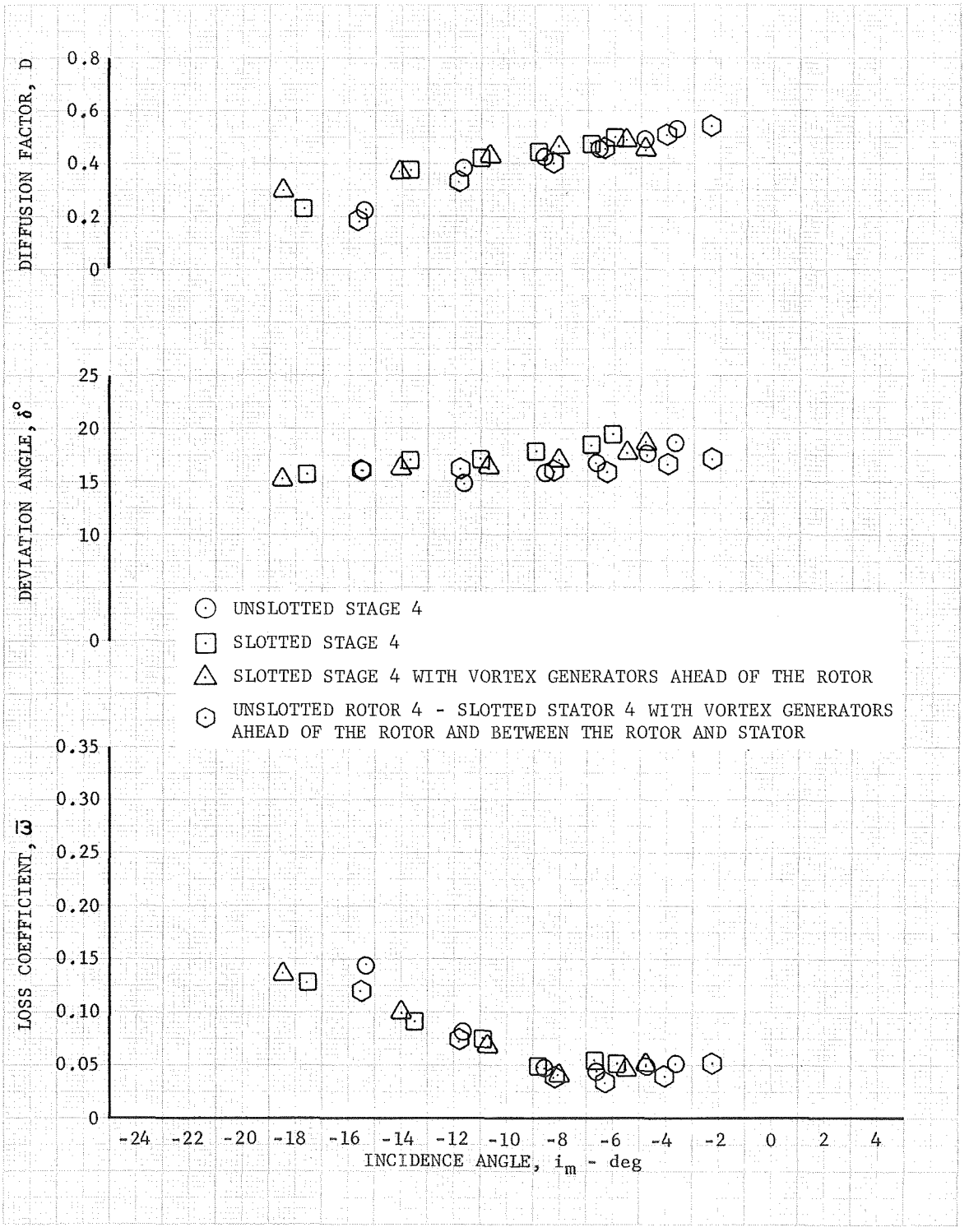

Figure 50b. Stator Blade Element Performance Comparisons, 50% Span From Tip, 100% Design Equivalent Rotor Speed

DF 83434

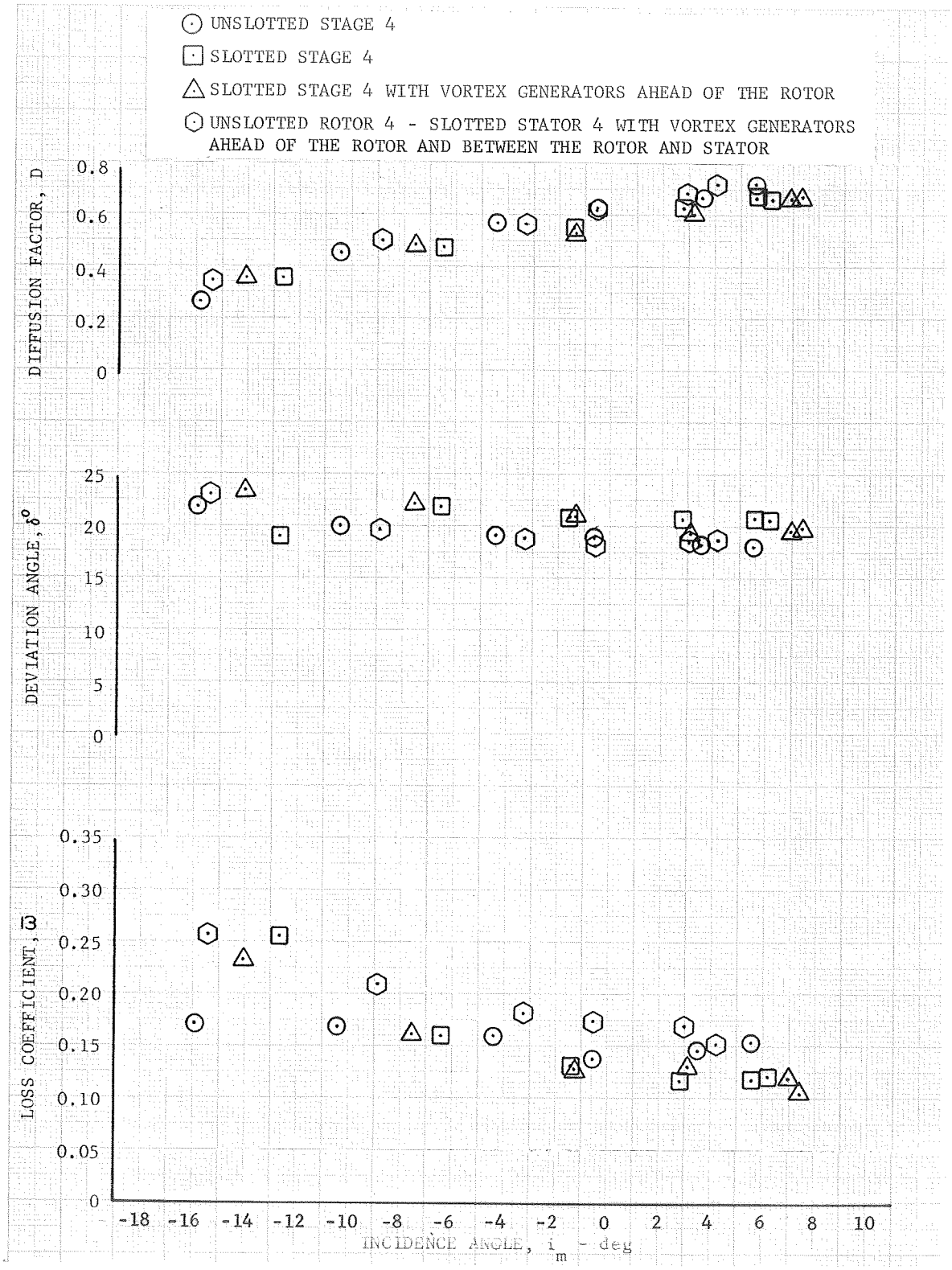

Figure 50c. Stator Blade Element Performance Comparisons, 90% Span From Tip, 100 % Design Rotor Speed

DF 83435

APPENDIX A
DEFINITION OF SYMBOLS AND PERFORMANCE VARIABLES

A_A	Flowpath annular area, ft^2
a'_o	Inlet relative stagnation velocity of sound, ft/sec
c	Chord length, in.
C_p	Static pressure coefficient
d	Diameter
D	Diffusion Factor
i_m	Incidence angle, deg (based on equivalent circular arc meanline)
M	Absolute Mach number
N	Rotor speed, rpm
O	Minimum blade passage gap, in.
O*	Critical blade passage gap, in.
P	Total pressure, psia
p	Static pressure, psia
t	Blade maximum thickness, in.
T	Total temperature, °R
T_s	Static temperature, °R
U	Rotor speed, ft/sec
V	Velocity, ft/sec
W	Actual flowrate, lb_m/sec
β	Air angle, deg from axial direction
γ	Ratio of specific heats
$\gamma°$	Blade-chord angle, deg from axial direction
δ	Ratio of total pressure to NASA standard sea level pressure of 14.694 psia
$\delta°$	Deviation angle, deg
ηad	Adiabatic efficiency
θ	Ratio of total temperature to NASA standard sea level temperature of 518.7°R
κ	Blade metal angle, deg from axial direction (based on equivalent circular arc meanline)
ρ	Density, $lb_f\ sec^2/ft^4$
σ	Solidity, c/S

ϕ	Blade camber angle, $\kappa_1 - \kappa_2$, deg
$\bar{\omega}$	Loss coefficient
$\bar{\omega} \cos \beta/2\sigma$	Loss parameter

Subscripts:

0	Compressor inlet (bellmouth)
1	Rotor inlet
2	Rotor exit
2A	Stator exit
3	Stator exit (1.0 chord length downstream from Station 2A)
f	Force
id	Isentropic condition
L	Local
m	Mean or mass
le	Leading edge
te	Trailing edge
s	Static condition
z	Axial component
θ	Tangential component

Superscripts:

'	Related to rotor blade
-	Mass average value

Definition of Overall Performance Variables

Pressure Ratio:

Rotor: $\dfrac{\overline{P}_2}{\overline{P}_o}$ Stage: $\dfrac{\overline{P}_{2A}}{\overline{P}_o}$

Corrected Flow

$$W\sqrt{\theta}/\delta$$

Corrected Specific Flow:

$$\frac{W\sqrt{\theta}}{\delta A_A}$$

Equivalent Rotor Speed:

$$N/\sqrt{\theta}$$

Adiabatic Efficiency:

Rotor: $\dfrac{(\overline{P}_2/\overline{P}_o)^{\frac{\gamma-1}{\gamma}} - 1}{\overline{T}_{2A}/518.7 - 1}$ Stage: $\dfrac{(\overline{P}_{2A}/\overline{P}_o)^{\frac{\gamma-1}{\gamma}} - 1}{\overline{T}_{2A}/518.7 - 1}$

Polytropic Efficiency:

Rotor: $\eta_P = \dfrac{\frac{\gamma-1}{\gamma}\ln(P_2/P_1)}{\ln(T_2/518.7)}$ Stator: $\eta_P = \dfrac{\frac{\gamma-1}{\gamma}\ln(p_{2A}/p_2)}{\ln\left(T_{s_{2A}}/T_{s_2}\right)}$

Stall Margin:

$$\frac{\left(\dfrac{\overline{P}_2/\overline{P}_1}{W\sqrt{\theta}/\delta}\right)_{\text{stall}} - \left(\dfrac{\overline{P}_2/\overline{P}_1}{W\sqrt{\theta}/\delta}\right)_{\text{design}}}{\left(\dfrac{\overline{P}_2/\overline{P}_1}{W\sqrt{\theta}/\delta}\right)_{\text{design}}}$$

Definition of Blade Element Performance Variables

Incidence Angle:

Rotor: $i_m = \beta'_1 - \kappa_{le}$ Stator: $i_m = \beta_2 - \kappa_{le}$

Diffusion Factor:

$$\text{Rotor: } D = 1 - \frac{V'_2}{V'_1} + \frac{d_2 V_{\theta 2} - d_1 V_{\theta 1}}{(d_1 + d_2) V'_1 \sigma}$$

$$\text{Stator: } D = 1 - \frac{V_{2A}}{V_2} + \frac{d_2 V_{\theta 2} - d_{2A} V_{\theta 2A}}{(d_2 + d_{2A}) V_2 \sigma}$$

Deviation Angle:

Rotor: $\delta^\circ = \beta'_2 - \kappa_{te}$ Stator: $\delta^\circ = \beta_{2A} - \kappa_{te}$

Loss Coefficient:

$$\text{Rotor: } \bar{\omega} = \frac{\bar{P}'_{2id} - P'_2}{\bar{P}'_1 - p_1}$$

where:

$$P'_{2id} = P'_1 \left\{ 1 + \frac{\gamma - 1}{2} \left(\frac{U_2^2}{a'^2_{o_1}} \right) \left[1 - \left(\frac{d_1}{d_2} \right)^2 \right] \right\}^{\frac{\gamma}{\gamma - 1}}$$

P' is found from $p/P' = \left[1 + \frac{\gamma - 1}{2} M'^2 \right]^{\frac{\gamma}{\gamma - 1}}$

and M' is calculated using trigonometric functions and the measurements of U, β, P, and p.

$$\text{Stator: } \bar{\omega} = \frac{P_{2_1} - P_{2A}}{P_{2_1} - p_2}$$

where:

P_{2_1} = the wake rake freestream total pressure

Stator Static Pressure Coefficient:

$$C_P = \frac{p_L - p_2}{1/2 \rho_2 V_2^2}$$

APPENDIX B

BLADE ELEMENT DESIGN DATA

Rotor and stator design velocity diagram data, blade element geometry data and predicted performance for Stage 4 designed on the assumption that there would be reduced losses due to slots and vortex generators are presented in tables B-1 and B-2. Velocity diagram and predicted performance for the Stage 4 blading without assuming reduced losses due to slots and vortex generators are given in tables B-3 and B-4. The rotor and stator design geometry from tables B-1 and B-2 are repeated in tables B-3 and B-4. Symbols are performance variables are defined in Appendix A.

Table B-1. Slotted Rotor 4 Blade Element Design Data Along Design Streamlines

Geometry Data

Airfoil: NACA 65 (A = 1.0)
No. of Blades: 60

Aspect Ratio: 1.820
Chord Length: 2.21 in.

% Span from Tip Leading Edge	% Span from Tip Trailing Edge	κ_{le}	κ_{te}	ϕ	γ	0/0*	σ	t/c
97.01	96.90	56.43	-8.50	64.93	23.97	1.286	1.276	0.078
91.02	91.02	56.22	-3.50	59.72	26.36	1.270	1.258	0.076
86.71	86.60	56.28	-0.20	56.48	28.04	1.259	1.243	0.074
71.02	69.60	57.70	9.75	47.95	33.73	1.224	1.197	0.068
50.06	49.10	61.29	16.40	44.89	38.85	1.194	1.143	0.060
29.59	28.40	65.85	19.10	46.75	42.48	1.177	1.093	0.052
14.02	13.50	70.18	19.28	50.90	44.73	1.147	1.060	0.046
9.23	8.80	71.89	19.05	52.84	45.47	1.134	1.050	0.044
3.36	3.36	73.85	18.65	55.20	46.25	1.119	1.040	0.042

Velocity Diagram Data

Corrected Rotor Speed 4210

% Span From Tip Leading Edge	% Span From Tip Trailing Edge	V'_{le}	V_{zle}	$V'_{\theta le}$	β'_{le}	U_{le}	V'_{te}	V_{zte}	$V'_{\theta te}$	β'_{te}	U_{te}
97.01	96.90	780.00	489.20	605.10	51.23	604.9	438.80	437.50	37.9	4.82	607.9
91.02	91.02	788.35	490.09	616.70	51.53	615.7	453.25	447.70	71.2	8.95	616.2
86.71	86.60	794.20	492.80	623.60	51.78	624.2	463.90	454.20	95.9	11.75	622.6
71.02	69.60	814.30	496.00	647.80	52.74	647.7	498.40	466.75	174.9	20.40	645.5
50.06	49.10	837.40	488.25	679.80	54.30	680.0	527.25	471.65	234.9	26.47	675.8
29.59	28.40	855.20	473.70	711.30	56.28	711.7	546.75	472.70	272.3	29.83	705.3
14.02	13.50	865.10	454.60	735.00	58.17	735.0	556.80	472.05	292.3	31.55	726.3
9.23	8.80	867.50	446.65	742.65	58.85	742.5	560.30	472.20	297.9	32.05	733.1
3.36	3.36	870.05	436.25	751.80	59.72	751.7	565.75	473.75	303.8	32.58	740.2

Table B-1. Slotted Rotor 4 Blade Element Design Data Along Design Streamlines (Continued)

Pressure Ratio: 1.349 Efficiency: 89.5%

% Span From Tip Leading Edge	% Span From Tip Trailing Edge	$\Delta\beta'$	M'_{le}	i_m	D_f	$\bar{\omega}'$	Loss Parameter	$\delta°$	P_{te}	T_{te}
97.01	96.90	46.41	0.713	- 5.20	0.722	0.176	0.069	13.32	20.197	576.59
91.02	91.02	42.58	0.720	- 4.69	0.697	0.149	0.058	12.45	20.116	574.41
86.71	86.60	40.03	0.726	- 4.50	0.681	0.131	0.052	11.95	20.057	573.16
71.02	69.60	28.64	0.744	- 4.96	0.632	0.089	0.034	10.65	19.834	569.53
50.06	49.10	27.83	0.765	- 6.99	0.603	0.073	0.029	10.07	19.766	568.50
29.59	28.40	26.45	0.780	- 9.57	0.598	0.094	0.037	10.73	19.762	569.58
14.02	13.50	26.62	0.789	-12.01	0.600	0.127	0.051	12.27	19.719	571.30
9.23	8.80	26.80	0.790	-13.04	0.600	0.139	0.056	13.00	19.714	571.87
3.36	3.36	27.14	0.792	-14.13	0.599	0.155	0.063	13.93	19.683	572.54

Table B-2. Slotted Stator 4 Blade Element Design Data Along Design Streamlines

Geometry Data

Airfoil: NACA 65 (A = 1.0)
No. of Vanes: 58

Aspect Ratio: 1.689
Chord Length: 2.182 in.
Thickness Ratio, t/c: 0.090

% Span From Tip Leading Edge	% Span From Tip Trailing Edge	κ_{le}	κ_{te}	ϕ	$\gamma°$	0/0*	σ
94.87	94.87	53.81	-16.48	70.29	18.67	1.324	1.214
90.07	90.07	51.87	-15.59	67.46	18.14	1.310	1.200
85.0	84.85	50.23	-14.62	64.85	17.81	1.297	1.187
70.27	69.98	47.18	-12.52	59.70	17.33	1.265	1.151
50.40	49.95	46.30	-11.67	57.97	17.32	1.236	1.105
30.27	29.25	48.75	-12.52	61.27	18.12	1.216	1.063
15.27	14.60	52.40	-14.12	66.52	19.14	1.196	1.032
10.27	9.70	53.92	-14.95	68.87	19.49	1.194	1.021
5.0	4.60	55.80	-15.95	71.75	19.93	1.199	1.010

Velocity Diagram Data

% Span From Tip Leading Edge	% Span From Tip Trailing Edge	V_{le}	V_{zle}	$V_{\theta le}$	β_{le}	V_{te}	V_{zte}	$V_{\theta te}$	β_{te}
94.87	94.87	735.2	474.2	561.2	49.71	469.0	468.9	0.0	0.0
90.07	90.07	725.0	482.9	540.2	48.15	468.9	468.8	0.0	0.0
85.0	84.85	715.2	491.2	520.4	46.68	468.7	468.7	0.0	0.0
70.27	69.98	690.0	501.1	474.3	43.45	468.9	468.8	0.0	0.0
50.40	49.95	667.9	498.9	443.2	41.59	477.0	476.4	0.0	0.0
30.27	29.25	649.6	481.0	435.2	42.07	489.9	489.9	0.0	0.0
15.27	14.60	631.2	454.8	436.8	43.77	504.9	503.7	0.0	0.0
10.27	9.70	623.8	443.5	437.8	44.52	511.1	510.2	0.0	0.0
5.0	4.60	615.3	429.9	438.5	45.40	518.7	517.5	0.0	0.0

Table B-2. Slotted Stator 4 Blade Element Design Data Along Design Streamlines English Units (Continued)

Stage Pressure Ratio: 1.324 Stage Efficiency: 83.8%

% Span From Tip Leading Edge	% Span From Tip Trailing Edge	$\Delta\beta$	M_{le}	i_m	D_f	$\bar{\omega}$	Loss Parameter	$\delta°$	P_{te}
94.87	94.87	49.71	0.652	- 4.105	0.676	0.142	0.058	16.48	19.455
90.07	90.07	48.15	0.644	- 3.730	0.663	0.132	0.055	15.59	19.455
85.0	84.85	46.68	0.634	- 3.555	0.652	0.121	0.051	14.62	19.455
70.27	69.98	43.45	0.612	- 3.730	0.620	0.094	0.041	12.52	19.418
50.40	49.95	41.59	0.591	- 4.710	0.588	0.072	0.033	11.67	19.440
30.27	29.25	42.07	0.574	- 6.680	0.563	0.073	0.034	12.52	19.469
15.27	14.60	43.77	0.557	- 8.630	0.537	0.066	0.032	14.12	19.484
10.27	9.70	44.52	0.549	- 9.400	0.526	0.062	0.030	14.95	19.484
5.0	4.60	45.40	0.541	-10.405	0.511	0.056	0.028	15.95	19.492

Table B-3. Unslotted Rotor 4 Blade Element Design Data Along Design Streamlines

Geometry Data

Airfoil: NACA 65 (A = 1.0)
No. of Blades: 60

Aspect Ratio: 1.820
Chord Length: 2.21 in.

% Span from Tip Leading Edge	% Span from Tip Trailing Edge	κ_{le}	κ_{te}	ϕ	$\gamma°$	0/0*	σ	t/c
97.01	96.90	56.43	-8.50	64.93	23.97	1.286	1.276	0.078
91.02	91.02	56.22	-3.50	59.72	26.36	1.270	1.258	0.076
86.71	86.60	56.28	-0.20	56.48	28.04	1.259	1.243	0.074
71.02	69.60	57.70	9.75	47.95	33.73	1.224	1.197	0.068
50.06	49.10	61.29	16.40	44.89	38.85	1.194	1.143	0.060
29.59	28.40	65.85	19.10	46.75	42.48	1.177	1.093	0.052
14.02	13.50	70.18	19.28	50.90	44.73	1.147	1.060	0.046
9.23	8.80	71.89	19.05	52.84	45.47	1.134	1.050	0.044
3.36	3.36	73.85	18.65	55.20	46.25	1.119	1.040	0.042

Velocity Diagram Data

Corrected Rotor Speed 4210 rpm

Corrected Weight Flow: 110 lb/sec

% Span from Tip Leading Edge	% Span from Tip Trailing Edge	V'_{le}	V_{zle}	$V'_{\theta le}$	β'_{le}	U_{le}	V'_{te}	V_{zte}	$V'_{\theta te}$	β'_{te}	U_{te}
96.8	94.9	780.1	488.3	608.3	51.25	608.3	413.8	411.4	44.3	6.14	610.7
92.2	89.8	786.4	489.6	615.4	51.49	615.4	437.1	430.9	73.4	9.67	618.0
87.4	84.6	793.0	491.0	622.8	51.75	622.8	459.6	448.0	102.5	12.89	625.3
72.0	69.3	812.7	492.7	646.3	52.68	646.3	519.7	487.1	181.3	20.41	647.2
50.5	49.1	836.8	488.5	679.4	54.28	679.4	560.3	501.6	249.6	26.45	676.1
28.9	29.1	855.8	474.1	712.4	56.36	712.4	561.7	487.2	279.5	29.84	704.5
13.4	14.4	865.4	454.8	736.3	58.30	736.3	545.6	464.7	286.0	31.61	725.4
8.4	9.6	867.9	446.9	744.0	59.01	744.0	540.0	457.5	287.0	32.11	732.3
3.4	4.9	870.0	438.2	751.6	59.76	751.6	535.0	450.9	287.9	32.56	739.1

Table B-3. Unslotted Rotor 4 Blade Element Design Data Along Design Streamlines (Continued)

Design Performance Data

Pressure Ratio: 1.335 Efficiency: 86.8%

%Span from Tip Leading	%Span from Tip Trailing	$\Delta\beta'$	M'_{le}	i_m	D_f	$\bar{\omega}'$	Loss Parameter	$\delta°$	P_{te}	T_{te}
96.8	94.9	45.11	0.712	-5.15	0.754	0.261	0.102	14.44	19.65	576.3
92.2	89.8	41.82	0.718	-4.76	0.718	0.222	0.087	14.17	19.67	574.7
87.4	84.6	38.86	0.724	-4.50	0.684	0.186	0.073	13.69	19.69	573.1
72.0	69.3	32.27	0.742	-4.92	0.599	0.097	0.038	11.11	19.70	568.9
50.5	49.1	30.83	0.764	-6.97	0.555	0.057	0.022	10.15	19.66	566.7
28.9	29.1	26.52	0.781	-9.44	0.575	0.106	0.042	10.69	19.54	568.5
13.4	14.4	26.69	0.788	-12.15	0.615	0.184	0.074	12.36	19.38	571.8
8.4	9.6	26.90	0.790	-13.09	0.628	0.211	0.085	13.11	19.33	573.0
3.4	4.9	27.20	0.791	-14.24	0.641	0.238	0.097	13.88	19.28	574.2

Table B-4. Unslotted Stator 4 Blade Element Design Data Along Design Streamlines

Geometry Data

Airfoil: NACA 65 (A = 1.0)
No. of Vanes: 58

Aspect Ratio: 1.689
Chord Length: 2.182 in.
Thickness Ratio, t/c: 0.090

% Span from Tip Leading Edge	% Span from Tip Trailing Edge	κ_{le}	κ_{te}	ϕ	$\gamma°$	0/0*	σ
94.87	94.87	53.81	-16.48	70.29	18.67	1.324	1.214
90.07	90.07	51.87	-15.59	67.46	18.14	1.310	1.200
85.0	84.85	50.23	-14.62	64.85	17.81	1.297	1.187
70.27	69.98	47.18	-12.52	59.70	17.33	1.265	1.151
50.40	49.95	46.30	-11.67	57.97	17.32	1.236	1.105
30.27	29.25	48.75	-12.52	61.27	18.12	1.216	1.063
15.27	14.60	52.40	-14.12	66.52	19.14	1.196	1.032
10.27	9.70	53.92	-14.95	68.87	19.49	1.194	1.021
5.0	4.60	55.80	-15.95	71.75	19.93	1.199	1.010

Velocity Diagram Data

% Span from Tip Leading Edge	% Span from Tip Trailing Edge	V_{le}	V_{zle}	$V_{\theta le}$	β_{le}	V_{te}	V_{zte}	$V_{\theta te}$	β_{te}
95.1	94.5	723.3	449.4	566.7	51.59	371.1	371.1	0.0	0.0
90.2	88.8	719.0	468.6	545.3	49.33	410.1	410.1	0.0	0.0
85.3	83.4	714.2	485.3	523.9	47.19	442.7	442.7	0.0	0.0
70.4	67.8	700.9	521.9	467.8	41.87	505.7	505.7	0.0	0.0
50.7	47.6	681.4	529.5	428.9	39.01	520.3	520.3	0.0	0.0
30.8	27.7	656.3	497.8	427.6	40.66	518.7	518.7	0.0	0.0
15.6	13.5	629.5	448.2	442.0	44.60	520.0	520.0	0.0	0.0
10.4	9.0	619.4	428.2	447.6	46.27	521.9	521.9	0.0	0.0
5.2	4.6	608.2	405.6	453.2	48.17	524.7	524.7	0.0	0.0

Table B-4. Unslotted Stator 4 Blade Element Design Data Along Design Streamlines (Continued)

Design Performance Data

Stage Pressure Ratio: 1.305 Stage Efficiency: 79.7%

% Span from Tip Leading Edge	% Span from Tip Trailing Edge	$\Delta\beta$	M_{le}	i_m	D_f	$\bar{\omega}$	Loss Parameter	$\delta°$	P_{te}
95.1	94.5	51.59	0.639	-2.41	0.810	0.318	0.131	16.55	18.15
90.2	88.8	49.33	0.636	-2.54	0.746	0.264	0.110	15.52	18.44
85.3	83.4	47.19	0.632	-3.12	0.690	0.211	0.089	14.70	18.71
70.4	67.8	41.87	0.622	-5.33	0.569	0.094	0.041	12.50	19.28
50.7	47.6	39.01	0.605	-7.29	0.522	0.063	0.029	11.57	19.39
30.8	27.7	40.66	0.580	-8.06	0.517	0.075	0.035	12.51	19.24
15.6	13.5	44.60	0.553	-7.70	0.515	0.075	0.036	14.14	19.11
10.4	9.0	46.27	0.543	-7.63	0.512	0.074	0.036	14.93	19.07
5.2	4.6	48.17	0.532	-7.58	0.506	0.072	0.036	15.90	19.03

Distribution List
NAS3 - 10481

		Copies
NASA-Lewis Research Center		
21000 Brookpark Road		
Cleveland, Ohio 44135		
Attention:		
Report Control Office	MS 5-5	1
Technical Utilization Office	MS 3-19	1
Library	MS 60-3	2
Fluid System Components Division	MS 5-3	1
Pump and Compressor Branch	MS 5-9	6
Dr. B. Lubarsky	MS 3-3	1
A. Ginsburg	MS 5-3	1
M. J. Hartmann	MS 5-9	1
W. A. Benser	MS 5-9	1
D. M. Sandercock	MS 5-9	1
L. J. Herrig	MS 7-1	1
T. F. Gelder	MS 5-9	1
C. L. Ball	MS 5-9	1
L. Reid	MS 5-9	1
J. E. Dilley	MS 500-309	1
S. Lieblein	MS 100-1	1
C. L. Meyer	MS 60-4	1
J. H. Povolny	MS 60-4	1
A. W. Goldstein	MS 7-1	1
J. J. Kramer	MS 7-1	1
W. L. Beede	MS 5-3	1
C. H. Voit	MS 5-3	1
E. E. Bailey	MS 5-9	1
NASA Scientific and Technical Information Facility		
P. O. Box 33		
College Park, Maryland 20740		
Attention: NASA Representative		6
FAA Headquarters		
800 Independence Ave., S. W.		
Washington, D. C. 20553		
Attention: Brig. General J. C. Maxwell		1
F. B. Howard		1
NASA Headquarters		
Washington, D. C. 20546		
Attention: N. F. Rekos (RAP)		1
U.S. Army Aviation Material Laboratory		
Fort Eustes, Virginia		
Attention: John White		1

	Copies
Headquarters Wright Patterson AFB, Ohio 45433	
Attention: J. L. Wilkins, SESOS	1
S. Kobelak, APTP	1
R. P. Carmichael, SESSP	1
Department of Navy Bureau of Weapons Washington, D. C. 20525	
Attention: Robert Brown, RAPP14	1
Department of Navy Bureau of Ships Washington, D. C. 20360	
Attention: G. L. Graves	1
NASA-Langley Research Center Technical Library Hampton, Virginia 23365	
Attention: Mark R. Nichols	1
John V. Becker	1
The Boeing Company Commercial Airplane Group	
Attention: G. J. Schott	
Organization: G-8410, M.S. 73-24	
P. O. Box 3707 Seattle, Washington 98124	1
Douglas Aircraft Company 3855 Lakewood Boulevard Long Beach, California 90801	
Attention: J. E. Merriman	1
Technical Information Center C1-250	
Pratt & Whitney Aircraft Florida Research & Development Center P. O. Box 2691 West Palm Beach, Florida 33402	
Attention: R. A. Schmidtke	1
H. D. Stetson	1
J. M. Silk	1
W. R. Alley	
R. W. Rockenbach	1
B. A. Jones	1
B. S. Savin	1
J. A. Fligg	1

			Copies
Pratt & Whitney Aircraft			
400 Main Street			
East Harford, Connecticut			
Attention:	R. E. Palatine		1
	T. G. Slaiby		
	H. V. Marman		
	M. J. Keenan		1
	B. B. Smyth		
	A. A. Mikolajczak		1
	Library (UARL)		1
Allison Division, GMC			
Department 8894, Plant 8			
P. O. Box 894			
Indianapolis, Indiana 46206			
Attention:	J. N. Barney		1
	G. E. Holbrook		
	B. A. Hopkins		
	R. J. Loughery		1
	Library		1
	J. L. Dillard		1
	P. Tramm		1
Northern Research and Engineering			
219 Vassar Street			
Cambridge 39, Massachusetts			
Attention:	K. Ginwala		1
General Electric Company			
Flight Propulsion Division			
Cincinnati 15, Ohio			
Attention:	J. W. Blanton	J-19	
	W. G. Cornell	K-49	
	D. Prince	H-79	1
	E. E. Hood/J. C. Pirtle	J-165	
	J. F. Klapproth	H-42	
	J. W. McBride	H-44	
	L. H. Smith	H-50	1
	S. N. Suciu	H-32	
	J. B. Taylor	J-168	
	Technical Information Center	N-32	1
	Marlen Miller	H-50	1
General Electric Company			
1000 Western Avenue			
West Lynn, Massachusetts			
Attention:	D. P. Edkins	Bldg. 2-40	
	F. F. Ehrich	Bldg. 2-40	
	L. H. King	Bldg. 2-40	1
	R. E. Neitzel	Bldg. 2-40	
	Dr. C. W. Smith Library	Bldg. 2-40M	1

		Copies
Curtiss-Wright Corporation Wright Aeronautical Woodridge, New Jersey Attention: S. Lombardo G. Provenzale		1
Air Research Manufacturing Company 402 South 36th Street Phoenix, Arizona 85034 Attention: Robert O. Bullock John H. Deman		1
Air Research Manufacturing Company 8951 Sepulveda Boulevard Los Angeles, California 90009 Attention: Linwood C. Wright		1
Union Carbide Corporation Nuclear Division Oak Ridge Gaseous Diffusion Plant P. O. Box "P" Oak Ridge, Tennessee 37830 Attention: R. G. Jordan D. W. Burton,	 K-1001, K-25	 1 1
Avco Corporation Lycoming Division 550 South Main Street Stratford, Connecticut Attention: Clause W. Bolton		1
Teledyne Cae 1330 Laskey Road Toledo, Ohio 43601 Attention: Eli H. Benstein Howard C. Walch		1
Solar San Diego, California 92112 Attention: P. A. Pitt Mrs. L. Walper		1
Goodyear Atomic Corporation Box 628 Piketon, Ohio Attention: C. O. Langebrake		1
Iowa State University of Science and Technology Ames, Iowa 50010 Attention: Professor George K. Serovy Dept. of Mechanical Engineering		1

	Copies
Hamilton Standard Division of United Aircraft Corporation Windsor Locks, Connecticut Attention: Mr. Carl Rohrbach Head of Aerodynamics and Hydrodynamics	1
Westinghouse Electric Corporation Small Steam and Gas Turbine Engineering B-4 Lester Branch P. O. Box 9175 Philadelphia, Pennsylvania 19113 Attention: Mr. S. M. DeCorso	1
J. Richard Joy Supervisor, Analytical Section Williams Research Corporation P. O. Box 95 Walled Lake, Michigan	1
Raymond S. Poppe Building 541, Dept. 80-91 Lockheed Missile and Space Company P. O. Box 879 Mountain View, California 94040	1
James D. Raisbeck The Boeing Company 224 N. Wilkinson Dayton, Ohio 45402	1
James Furlong Chrysler Corporation Research Office Dept. 9000 P. O. Box 1118 Detroit, Michigan 48231	1
Elliott Company Jeannette, Pennsylvania 15644 Attention: J. Rodger Schields Director-Engineering	1
R. H. Carmody Dresser Industries Inc. Clark Gas Turbine Division 16530 Peninsula Boulevard P. O. Box 9989 Houston, Texas 77015	1

	Copies
California Institute of Technology Pasadena, California 91109 Attention: Professor Duncan Rannie	1
Massachusetts Institute of Technology Cambridge, Massachusetts 02139 Attention: Dr. J. L. Kerrebrock	1
Caterpillar Tractor Company Peoria, Illinois 61601 J. Wiggins	1